

The Effects of Macrocyclic Constraints on Electron Transfer in Peptides

A thesis submitted in the total fulfillment
of the requirements for the degree of
Doctor of Philosophy in Chemistry

by

John R. Horsley



Dept. of Chemistry
University of Adelaide
February 2015

Table of Contents

Abstract.....	v
Declaration and published works.....	vii
Publications generated from thesis.....	viii
Acknowledgements.....	ix
Abbreviations.....	x
Statements of authorship.....	xii

Chapter 1

1.1 Electron transfer in proteins.....	1
1.2 Protein secondary structure.....	4
1.2.1 3_{10} -helix.....	5
1.2.2 β -strand.....	7
1.2.3 Constrained peptides.....	8
1.3 Techniques for intramolecular macrocyclization in peptides.....	9
1.3.1 Click chemistry.....	10
1.3.2 Ring closing metathesis (RCM).....	12
1.3.3 Lactamization.....	14
1.4 Characterization of peptide secondary structure.....	15
1.4.1 Nuclear magnetic resonance (NMR) spectroscopy.....	15
1.4.2 Fourier transform infrared (FTIR) spectroscopy.....	17
1.4.3 Circular dichroism (CD).....	17
1.5 Self-assembled monolayers (SAMs).....	17
1.6 Cyclic voltammetry.....	20

1.7 Determination of electron transfer rate constant (k_{ET}) and significant parameters.....	21
1.8. Electron transfer in peptides	25
1.9. Molecular electronics.....	31
1.10 References.....	33

Chapter 2

2.1 Abstract.....	42
2.2 Introduction.....	43
2.3 Results and discussion	43
2.3.1 Conformational analysis of peptides	43
2.3.2 Electrochemical analysis of intramolecular electron transfer	47
2.3.3 Computational study of intramolecular electron transfer	50
2.4 Acknowledgements.....	54
2.5 Experimental methods	54
2.5.1 Preparation of Au/SWCNT/ferrocene-derivatised peptide electrode.....	54
2.5.2 Chemicals	54
2.5.3 NMR spectroscopy	55
2.5.4 Mass spectroscopy.....	55
2.5.5 Circular dichroism (CD).....	55
2.5.6 FTIR spectroscopy.....	56
2.5.7 High-performance liquid chromatography (HPLC)	56
2.5.8 Peptide synthesis	57
2.6 References.....	71

Chapter 3

3.1 Abstract.....	74
3.2 Introduction.....	75

3.3 Results and discussion	77
3.3.1 Peptide design.....	77
3.3.2 Conformational analysis of peptides	78
3.3.3 Electrochemical analysis of intramolecular electron transfer	84
3.3.4 Computational study of intramolecular electron transfer	90
3.4 Conclusion	95
3.5 Acknowledgements.....	96
3.6 Experimental methods	97
3.6.1 Chemicals	97
3.6.2 High-performance liquid chromatography (HPLC)	97
3.6.3 NMR spectroscopy	97
3.6.4 Mass spectroscopy.....	98
3.6.5 FTIR Spectroscopy.....	98
3.6.6 Electrochemistry.....	98
3.6.7 Computational methods.....	98
3.6.8 General procedure for <i>N</i> -Boc cleavage	99
3.6.9 Peptide synthesis	99
3.7 References.....	123

Chapter 4

4.1 Abstract.....	127
4.2 Introduction.....	128
4.3 Results and discussion	130
4.3.1 Peptide design.....	130
4.3.2 Conformational analysis of peptides	130
4.3.3 Electrochemical analysis of intramolecular electron transfer	135
4.3.4 Molecular junction conductance simulations	138
4.4 Conclusion	144
4.5 Experimental section	146

4.5.1 Chemicals	146
4.5.2 Instrumentation and methods	146
4.5.3 Peptide synthesis	147
4.6 Acknowledgements.....	158
4.7 References.....	159

Chapter 5

5.1 Abstract.....	163
5.2 Introduction.....	164
5.3 Results and discussion	166
5.3.1 Peptide design.....	166
5.3.2 Conformational analysis of peptides	167
5.3.3 Electrochemical analysis of intramolecular electron transfer	171
5.3.4 Computational study of intramolecular electron transfer	178
5.4 Conclusion	182
5.5 Acknowledgements.....	182
5.6 Experimental methods	183
5.6.1 Chemicals	183
5.6.2 High-performance liquid chromatography (HPLC)	183
5.6.3 NMR spectroscopy	183
5.6.4 Mass spectroscopy.....	184
5.6.5 FTIR spectroscopy.....	184
5.6.6 Peptide synthesis	185
5.7 References.....	218

Abstract

Research undertaken in this thesis focuses on electron transfer in peptides constrained into either a 3_{10} -helical or a β -strand conformation in order to progress the field of molecular electronics.

Chapter One

Natural proteins have evolved to promote electron transfer in many biological processes. However, their complex conformational nature inhibits a thorough investigation, so in order to study electron transfer in proteins, simple peptide models containing redox active moieties present as ideal candidates. Chapter One introduces the importance of secondary structure characteristic to proteins/peptides, and its relevance to electron transfer. The proposed mechanisms responsible for such electron transfer are discussed, along with the various approaches used to further constrain the peptides into their geometric conformations. The methods used to characterize the conformation of all peptides synthesized throughout this thesis are outlined, as are details of the electrochemical techniques used to investigate their electronic properties. A literature review describing several factors that have been shown to influence electron transfer in peptides, and a brief summary of molecular electronics follows.

Chapter Two

Two 3_{10} -helical peptides were synthesized, one constrained via a covalent side-chain staple using Huisgencycloaddition, and the other a linear analogue. Both peptides contain a redox active terminal ferrocene moiety, and were separately attached to a single walled carbon nanotube (SWCNT)/gold electrode array for electrochemical analysis. The effect of backbone rigidity imparted by the side-bridge constraint was revealed, which was shown to restrict the necessary torsional motions that lead to facile intramolecular electron transfer along the peptide backbone. High level calculations were used to support the electrochemical observations.

Chapter Three

A series of peptides constrained into either a 3_{10} -helix or β -strand conformation were synthesized, each containing a varied number of electron rich alkene side chains. The ability of the alkene(s) to facilitate electron transfer through the peptides by exploiting a hopping mechanism, and thus act as a “stepping stone” was investigated. Ring closing metathesis was used to further rigidify the backbones of a helical and a β -strand peptide via side chain tethers. The ensuing saturated and unsaturated compounds were electrochemically interrogated in order to explore any possible interplay between the effects of the alkene side-chains and backbone rigidity. High level calculations were conducted to verify the observed electrochemical data.

Chapter Four

Two β -strand peptides were synthesized, one constrained via a covalent side-chain staple using Huisgen cycloaddition, and the other a linear analogue. Both peptides contain a redox active terminal ferrocene moiety, and were separately attached to a SWCNT/gold electrode array for electrochemical analysis. The charge transfer pathway was determined to be intramolecular by measuring the electron transfer rate at various concentrations of the constrained peptidebound to the electrode. This pathway is analogous to charge transfer through a molecular junction involving a single peptide. Theoretical conductance simulations were then undertaken using two peptide analogues in order to establish a link between the electrochemical observations and conductance measurements through a molecular junction.

Chapter Five

Two macrocyclic peptides were synthesized, one constrained into a 3_{10} -helical conformation by linking its i to $i+3$ residues to form a lactam bridge, and the other constrained into a β -strand geometry via a lactam-bridge tether, linking its i to $i+2$ residues. These peptides were chosen in order to define the role of the amide bond in a lactam bridge constraint. Direct linear analogues of each were used to establish the effect on electron transfer from a terminal amide bond located in an untethered side-chain. High level calculations were also conducted in order to elucidate the mechanism(s) responsible for electron transfer in each of the linear and macrocyclic helical peptides.

Declaration and published works

I certify that this work contains no material which has been accepted for the award of any other degree or diploma in any university or other tertiary institution and, to the best of my knowledge and belief contains no material previously published or written by another person, except where due reference has been made in the text. In addition, I certify that no part of this work will, in the future, be used in a submission for any other degree or diploma in any university or other tertiary institution without the prior approval of the University of Adelaide and where applicable, any partner institution responsible for the joint-award of this degree.

I give consent to this copy of my thesis when deposited in the University Library, to be made available for loan and photocopying, subject to the provisions of the Copyright Act 1968.

The author that copyright of published works contained within this thesis resides with the copyright holder(s) of those works.

I also give permission for the digital version of my thesis to be made available on the web, via the University's digital research repository, the Library catalogue and also through web search engines, unless permission has been granted by the University to restrict access for a period of time.

.....

John Horsley

.....

Date

Publications generated from this thesis:

- (1) Yu, J.; Horsley, J. R.; Abell, A. D. *Australian Journal of Chemistry*, **2013**, *66*, 848.
- (2) Yu, J.; Horsley, J. R.; Moore, K. E.; Shapter, J. G.; Abell, A. D. *Chemical Communications*, **2014**, *50*, 1652.
- (3) Horsley, J. R.; Yu, J.; Moore, K. E.; Shapter, J. G.; Abell, A. D. *Journal of the American Chemical Society*, **2014**, *136*, 12479.
- (4) Horsley, J. R., Yu, J., Abell, A. D. “The Correlation of Electrochemical Measurements and Molecular Junction Conductance Simulations in β -Strand Peptides” *Chemistry A European Journal*, **2015**, *21*, 5926-5933.
- (5) Horsley, J. R., Yu, J., Abell, A. D. “Understanding the Role of the Amide Bond and Electron Transfer Mechanisms in Macrocyclic Peptides” (Prepared in publication format “text in manuscript”).

Acknowledgements

Firstly, I would like to thank my supervisor Professor Andrew Abell for his guidance, support and encouragement throughout the duration of my studies. I am greatly appreciative of the freedom afforded me to take ownership of, and control the destiny of my PhD. To be able to publish my work in high-impact chemistry journals is a credit to his drive and foresight. I am indebted to him for making my time as a PhD student so enjoyable, and for preparing me for a potential career in academia. Secondly, I would like to thank my co-supervisor Dr. Jingxian Yu, who taught me nearly everything I know about electrochemistry. His vast knowledge, great work ethic and helpful nature has really inspired my research in this field, and made this a truly rewarding journey.

I would like to thank the members of the Abell group for their friendship and support over the years. Thanks also to Katherine Moore for her work in preparing the electrodes used in the studies described hereafter, and to Professor Joe Shapter for allowing the use of his laboratory and instrumentation. Thanks also to the technical staff at the University of Adelaide for all their help.

I am also grateful to the University of Adelaide for allowing me the opportunity to undertake research at this revered facility, and for providing the doctoral scholarship for me to do so.

Abbreviations

<u>Abbreviation</u>	<u>Full Name</u>
Å	angstrom
Aib	amino isobutyric acid
Ala	alanine
Boc	<i>tert</i> -butoxycarbonyl
br	broad (spectroscopic)
calcd	calculated
conc	concentrated
DBU	1,8-diazabicyclo[5.4.0]undec-7-ene
DCM	dicloromethane
DIPEA	<i>N,N</i> -diisopropylethylamine
DMF	dimethylformamide
DMSO	dimethyl sulphoxide
EDC.HCl	1-ethyl-3-(3-(dimethylamino)propyl)carbodiimide hydrochloride
ESI	electrospray ionization
equiv	equivalents
eV	electron volt
FTIR	Fourier transform infrared
h	hour
HATU	2-(7-aza-1 <i>H</i> -benzotriazol-1-yl)-1,1,3,3- tetramethyluroniumhexafluorophosphate
HOAt	1-hydroxy-7-azabenzotriazole
HOBt	1-hydroxybenzotriazole
HPLC	high performance liquid chromatography
IR	infrared
Leu	leucine
LRMS	low resolution mass spectroscopy

HRMS	high resolution mass spectroscopy
MeOH	methanol
min	minute
nm	nanometre
NMR	nuclear magnetic resonance
quant	quantitative
RCM	ring closing metathesis
rt	room temperature
TFA	trifluoroacetic acid
THF	tetrahydrofuran
TNBS	trinitrobenzene sulfonic acid
v/v	volume per unit volume
w/w	weight per unit weight

Statements of authorship

Statements of authorship preface each chapter of this thesis where such chapter relates to published work.

CHAPTER 1

1.1 Electron transfer in proteins

Electron transfer in proteins plays an important role in a wide range of processes at the cellular level, including photosynthesis.¹ The associated movement of an electron from one species (donor) to another (acceptor) results in a change of oxidation states for both components. The precise mechanisms for this are at present in dispute, however two main modes are widely accepted, i.e. superexchange (also known as tunneling) and hopping (see Figure 1). Superexchange is explained in simple terms if one imagines an electron situated on a donor in a narrow potential well that is separated by a distance from an electron acceptor. The area between the donor and the acceptor is an electrically insulating region and therefore acts as an obstacle for electron transfer. Classical physics states that the electron cannot overcome this hurdle, but quantum mechanics indicates the possibility that the wave function of the electron infiltrates the insulating region to reach the potential well of an electron acceptor.^{1a} The peptide bridge therefore takes on a virtual role, with a high probability that only an extremely small number of electrons occupy the bridge during the electron transport procedure.² With respect to the superexchange mechanism, the electron transport rate decreases exponentially with increased distance between the redox active moieties situated along the peptide chain.³ This means that tunneling is not an efficient method of electron transfer over long distances, i.e. greater than approx. 20 Å.⁴

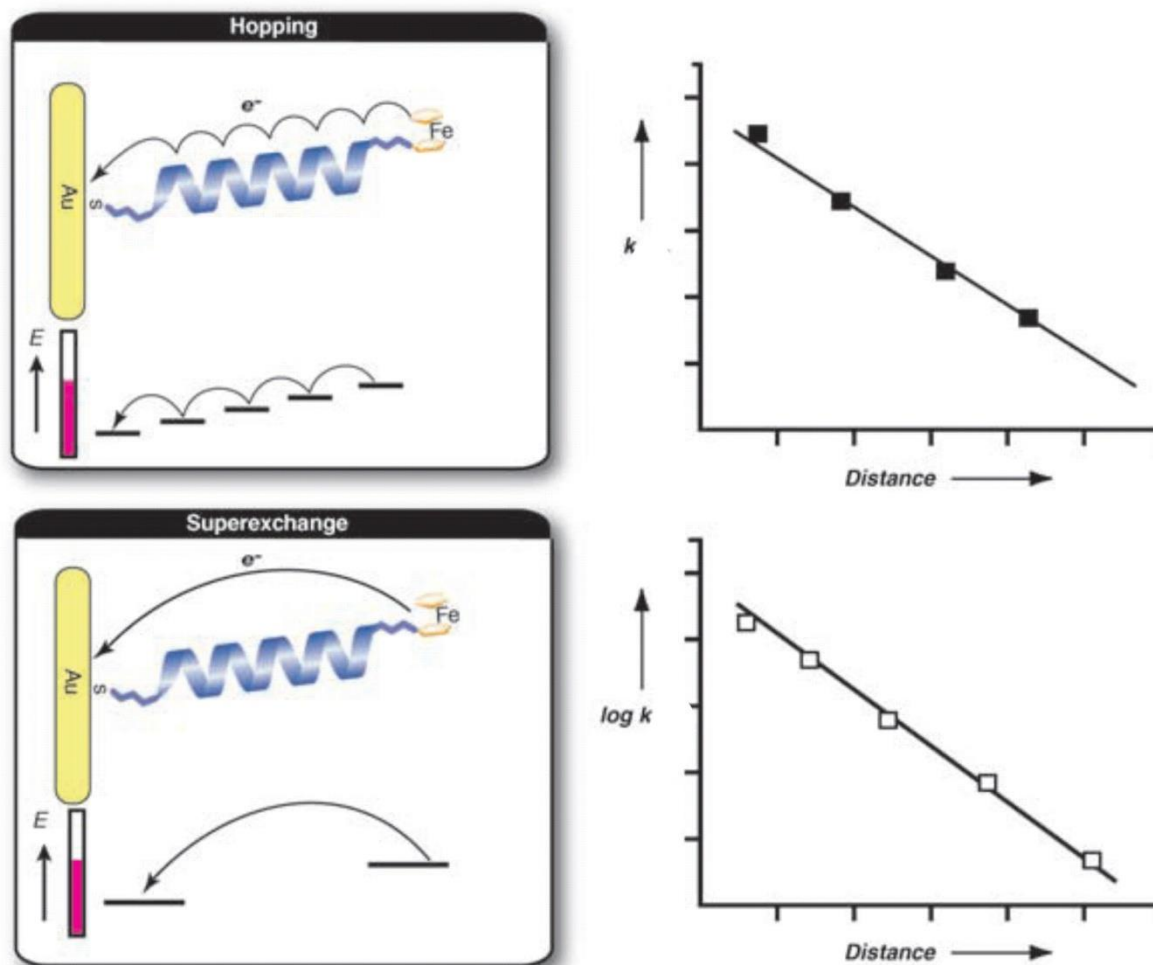


Figure 1. Electron transfer across a helical peptide showing the two widely recognized mechanisms, superexchange (tunneling) and hopping (top).⁵ (Note the electron transfer rate constant decreases exponentially with increasing distance between donor and acceptor, as evidenced by the logarithmic scale on the Y-axis of the graph representative of the superexchange mechanism).

Electron transfer can also occur via a hopping mechanism, whereby an electron “hops” between the redox active moieties, using sites on the peptide chain that are coupled to each other electronically.⁶ For this to occur, the difference in the energy levels of the donor and the bridge separating donor and acceptor, must be negligible.⁷ Recent theoretical studies have found that low-frequency rotation between neighbouring amino acids in a peptide brings adjacent carbonyl groups into alignment, and hence into close proximity to one another. When the backbone dihedral angles reach this critical point, the energy barrier becomes almost negligible, and efficient charge transfer from one amino acid to the next can occur via a hopping mechanism.⁷⁻⁸ A weak distance dependence is reported for the

Chapter 1

hopping mechanism, whereby the electron transfer rate decreases with a linear relationship when the distance between electron donor and acceptor is increased.⁹ In general, this mechanism is reported to occur over longer distances, i.e. greater than approx. 20 Å.⁴ As the rate of electron transfer decreases non-exponentially with distance, this long-range mechanism is thought to occur when the distance between the electron donor and acceptor is separated into shorter and therefore faster steps.¹⁰ It is widely believed that electron transfer utilizes both superexchange and hopping mechanisms, depending on factors such as the specific peptide architecture involved.²

Many proteins have evolved specifically for electron transfer from one redox active site to another.⁵ In nature, a number of cofactors facilitate this electron transfer. However, some metal cofactors are separated by distances too great to promote efficient electron transfer via a superexchange mechanism.¹¹ Situated between these electron donors and acceptors are well placed redox active amino acids, which are fundamental to charge separation and can act as “stepping stones” for electron transfer by exploiting a hopping mechanism. These electron transfer pathways in naturally occurring proteins require a sophisticated framework or architecture that is provided by well-defined secondary structures, such as helices and β -sheets, in order to locate the electron donors/acceptors in a precise and systematic manner.¹² Just as these well-defined secondary structures are responsible for the biological activity in a protein, function and conformation are inextricably linked when it comes to electron transfer in proteins. Nature has optimized the design of electron transfer pathways in proteins, for instance enzymes such as cytochrome c oxidase, so that damage by free radicals and short-circuiting are prevented.¹³ The mechanism of electron transfer in amino isobutyric acid (Aib) homoligomers has been shown to be defined by the extent of secondary structure.¹⁴ Hence, to further our fundamental understanding of electron transfer in proteins, it is important to consider systems that incorporate a well-defined secondary structure. The conformation of even the simplest protein can be labyrinthine, and as such, model peptides containing redox active moieties present as an ideal platform to investigate electron transfer in proteins.

1.2 Protein secondary structure

The primary structure of a protein is determined by its sequence of amino acids. This then folds into secondary, tertiary, and in some cases quaternary structure on the basis of a series of well-defined non-covalent interactions. The resulting three dimensional structures define the overall functionality of the protein.^{1a} There are two main secondary structures known as α -helices and β -pleated sheets, the structures of which are defined by a specific network of hydrogen bonds between the amide backbone carbonyl oxygen and amide hydrogens.^{1a} The conformational freedom of a peptide is determined by the torsion angles of the backbone. Also known as the dihedral angles, these are defined by the atoms N-C α -C(O) and N (see Figure 2). Phi (ϕ) describes the rotation around the N-C α bond, psi (ψ) describes the rotation around the C α -C(O) bond, and omega (ω) describes the rotation around the C(O)-N bond. A Ramachandran plot is used to determine the allowed conformations in the ϕ - ψ plane for all secondary structures¹⁵ (see Figure 3).

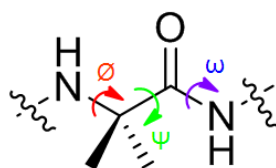


Figure 2. Schematic diagram showing the position of dihedral angles in a peptide backbone. Phi (ϕ) describes the rotation around the N-C α bond, psi (ψ) describes the rotation around the C α -C(O) bond, and omega (ω) describes the rotation around the C(O)-N bond.

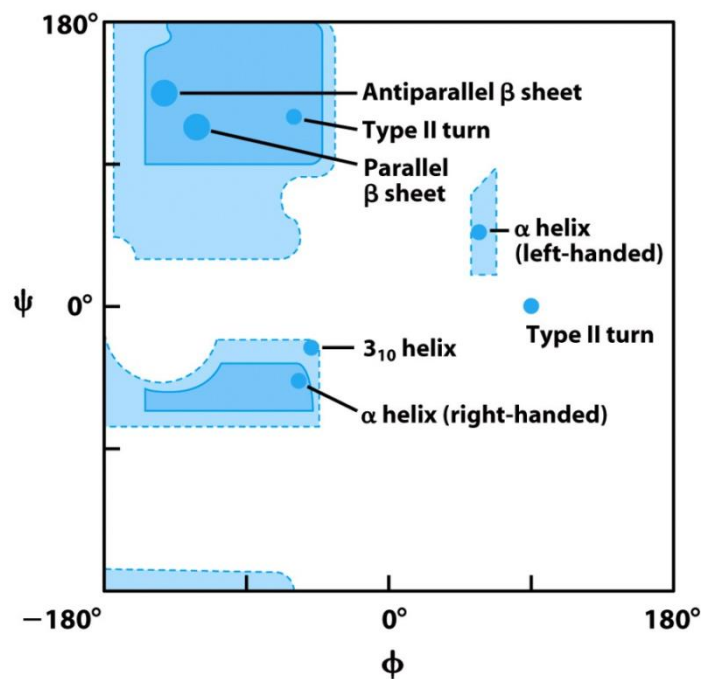


Figure 3. Ramachandran plot used to determine the allowed conformations in the ϕ - ψ plane for all secondary structures. Only angles within the blue shaded areas are accessible to well-defined peptide/protein secondary structures, with the 3_{10} -helix and β -sheet regions clearly shown. (Reproduced from Principles of Biochemistry, 4/e, Figure 4-9a, copyright 2006 Pearson Prentice Hall, Inc.)

1.2.1 3_{10} -helix

The 3_{10} -helix is a less common, but nonetheless important secondary structure in proteins.¹⁶ It is characterized by three amino acid residues per turn, with intramolecular hydrogen bonding occurring between the C=O of the residue in the (i) position and the amide hydrogen situated in the ($i + 3$) position¹⁷ (see Figure 4).

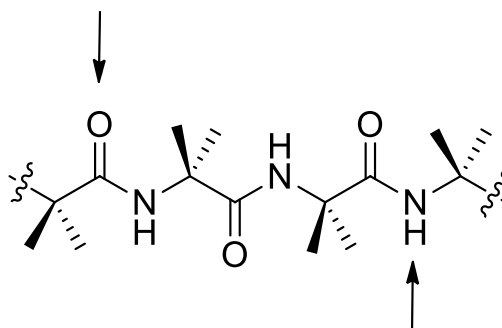


Figure 4. Schematic diagram showing the atoms involved in hydrogen bonding in a 3_{10} -helix (i to $i + 3$).

Chapter 1

Peptides comprising Aib residues, a naturally occurring hydrophobic amino acid found in antibiotics, display a large degree of 3_{10} -helical conformation. Previous studies have shown that stable 3_{10} -helical structures are formed when the peptide exceeds 5 residues in length.^{12, 18} The propensity for generating stable 3_{10} -helical structures has seen Aib residues incorporated into many of the peptides synthesized throughout this thesis. For an ideal right-handed 3_{10} -helix, the dihedral angles should be approximately -57° (Φ) and -30° (Ψ)¹⁹ (see Figures 2 and 3). The backbone torsion angles of a 3_{10} -helix differ from those of an α -helix by approximately 6° (Φ) and 12° (Ψ), with the 3_{10} -helix somewhat more elongated²⁰ (see Figure 5). The shorter, and hence stronger intramolecular hydrogen bonding in a 3_{10} -helix (i to $i + 3$) makes this structure more conductive than an α -helix, which is characterized by (i to $i + 4$) hydrogen bonding.²¹

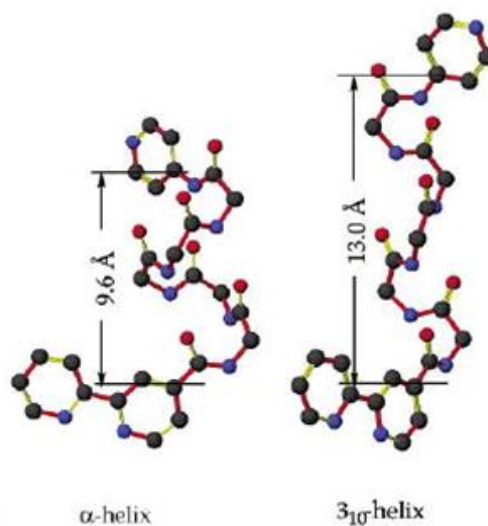


Figure 5. Molecular model schematic of a 3_{10} -helix, with comparison to an α -helix, in cbpy-(gly)₅-ap peptides, with distances between electron donor and acceptor given in angstroms. (The red atoms are oxygen - note the orientation of C=O bonds involved in intramolecular hydrogen bonding with the amide hydrogens).²²

Short 3_{10} -helices have been proposed as possible nucleation sites for the formation of helices during protein folding.²⁰ Recent studies have discovered an abundance of 3_{10} -conformations in trans-membrane helical proteins, including bacterial rhodopsins that are involved in signal transduction, ion channels and G-protein-coupled receptors (GPCRs).²³ Most importantly, the 3_{10} -helix is found in many enzymes responsible for electron transfer,

including cytochrome c oxidase, the final molecule in the mitochondrial electron transfer chain²⁴ (see Figure 6), hence reinforcing its relevance to work described in this thesis.

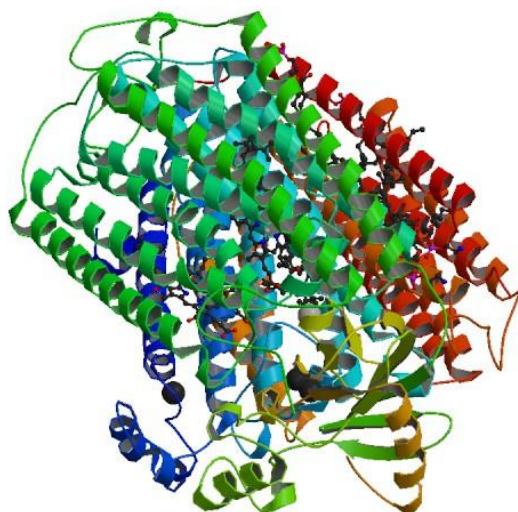


Figure 6. Ribbon image of the helical protein cytochrome c oxidase (taken from X-ray crystal structure).²⁵

1.2.2 β -strand

While considerable research on electron transfer has been performed on helical peptides, the possible role a β -strand plays in these processes has received little attention.²⁶ This structural motif has carbonyl and amide groups positioned orthogonal to the backbone, thus minimizing steric hindrance between the side-chains.²⁷ An ideal, fully extended β -strand is defined by the bond angles -120° (Φ), 120° (Ψ) and 180° (ω),²⁸ however a broader scope extends to between $-160^\circ < \Phi < -100^\circ$ and $90^\circ < \Psi < 160^\circ$.²⁷ Two or more β -strands linked together via intermolecular hydrogen bonding form a β -sheet (either parallel, antiparallel, or mixed), which represents over 30% of all protein structure.²⁸ The allowable range of backbone dihedral angles for a β -sheet is shown in the Ramachandran plot (see Figure 3).

1.2.3 Constrained peptides

Significant research has been conducted on constraining linear peptides, via intramolecular cyclization, into macrocycles with well-defined secondary structure, for example helices and β -strands.^{19, 29} Peptides can be constrained via head to tail interactions, backbone to side-chain, or side-chain to side-chain as depicted in Figures 7 and 8. These structures show important biological properties, for example as potent and selective protease inhibitors³⁰ (see Figure 8 b). A macrocyclic constraint introduced into a linear inhibitor of farnesyltransferase, resulted in a compound with a 20-fold improved potency.³¹ Chen et al introduced a constraint into a linear peptide inhibitor of the cancer target STAT 3, with the cyclic structure found to be three times more potent than the linear analogue.³² However, electron transfer in peptides containing an intramolecular macrocyclic constraint has not been previously investigated, despite the fact that secondary structure is known to play such a key role. Hence such studies are crucial to investigate the link between conformation and function. This thesis aims to address this shortcoming.

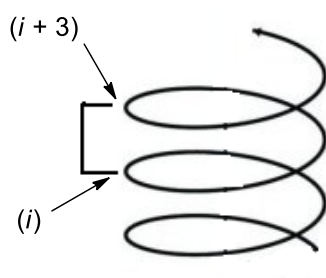


Figure 7. Schematic diagram showing a 3₁₀-helix with constraint between the side chains (i to $i + 3$) representative of one complete turn of the helix.

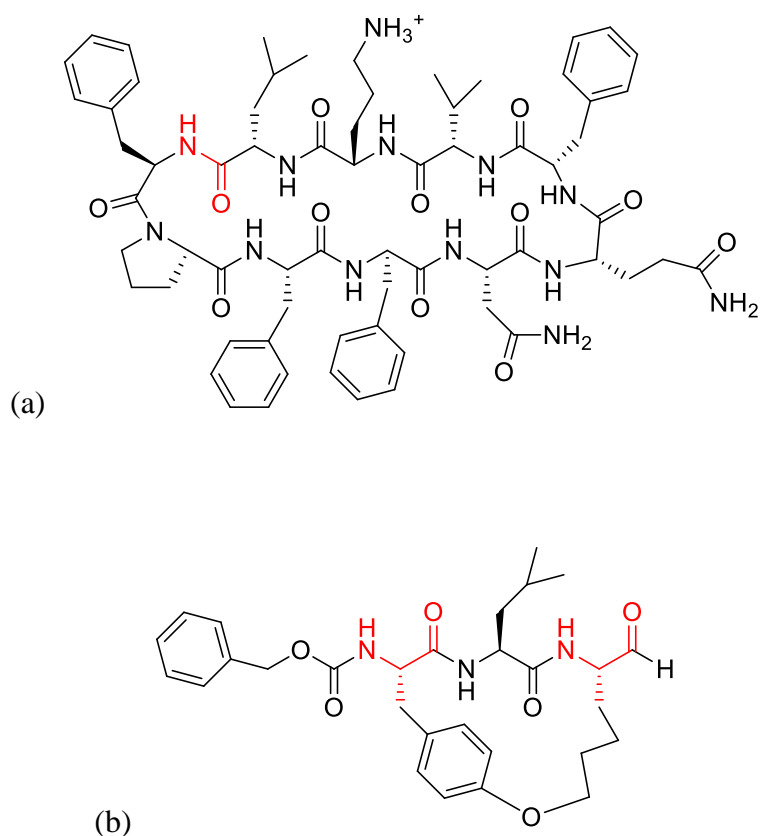


Figure 8. Examples of (a) head to tail cyclization of a peptide (Tyrocidine A),³³ and (b) side-chain to side-chain cyclization of a peptide.³⁰

1.3 Techniques for intramolecular macrocyclization in peptides

There are several different synthetic approaches to constrain a peptide into its preferred conformation via cyclization of a linear precursor. The methods employed in this thesis are click chemistry (Huisgen cycloaddition), ring-closing metathesis (RCM) and lactamization, as discussed below. Cyclization is more readily achieved under conditions of high dilution, which serve to minimize side reactions such as dimer formation. The slow addition of reagents via a syringe pump can further enhance these reactions.³⁴

1.3.1 Click chemistry

In the early 1960s, the forerunner of the ‘click reaction’, the 1,3-dipolar Huisgen cycloaddition reaction was discovered, which couples organic azides with alkynes to form 1,2,3 triazoles.³⁵ This reaction gives mixtures of the 1,4- and 1,5-disubstituted adducts, and was not given much attention until nearly four decades later. In 2002, both the Sharpless and Meldal groups independently discovered that by using catalytic Cu(I) it was possible to enhance the rate by several orders of magnitude, whilst also achieving regioselectivity, resulting in essentially quantitative yields of 1,4-disubstituted 1,2,3-triazole product.³⁶ Also referred to as “copper-catalyzed azide-alkyne cycloaddition” (CuAAC), it has become an important click reaction and a common method to form intramolecular macrocycles.³⁷ CuAAC can be performed either on solid phase³⁸ or in solution,³⁹ with the product being thermodynamically and metabolically stable; resistant to both hydrolysis and oxidation. The 1,4-disubstituted 1,2,3-triazoles are similar to amide bonds insofar as both are planar, while also possessing a strong dipole moment⁴⁰ (see Figure 9). There is a notable difference in the distance between the R₁ and R₂ groups of both structures,^{29a} as depicted in Figure 9, however the 1,4-disubstituted 1,2,3-triazole has previously been used as a surrogate for a *trans*-amide bond.⁴¹

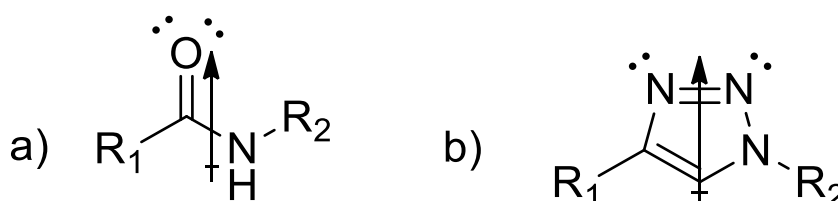


Figure 9. Schematic diagram of (a) amide bond and (b) 1,4-disubstituted 1,2,3-triazole, both sharing similar structural and electronic attributes.⁴⁰

Chapter 1

Linking residues (i to $i + 3$) in a linear 3_{10} -helix, or residues (i to $i + 2$) in a linear β -strand using click chemistry, enhances secondary structure. Recent studies have indicated that while the 3_{10} -helix is a stable peptide structure, constraining the side-chains (i to $i + 3$) results in a more paradigmatic structure than the linear analogue.¹⁹ For example, the X-ray crystal structure of a peptide cyclized side-chain to side-chain using click chemistry, showed that the dihedral angles deviated from an ideal 3_{10} -helix by no more than 2° , whereas the linear analogue was found to possess less helical content (see Figure 10).¹⁹ The triazole constraint rigidifies the macrocycle, in turn reducing entropic loss due to structural pre-organization, as the reactive side-chains are held in close proximity. This also reduces the number of possible conformations available to the peptide.⁴²

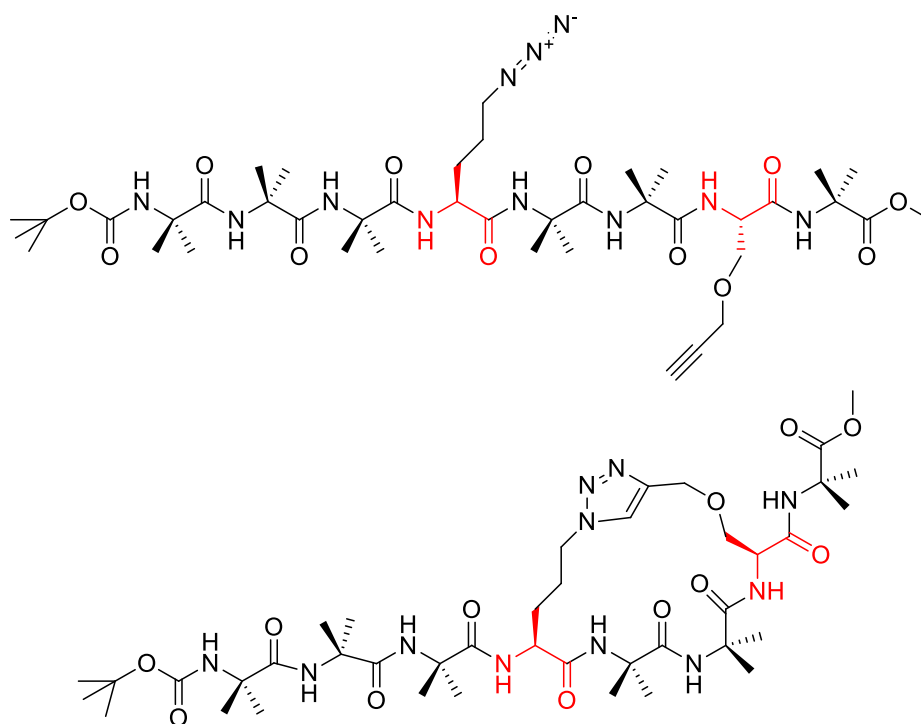


Figure 10. Linear 3_{10} -helical peptide (top) with macrocycle synthesized via click chemistry (below). Crystal structures were generated from both, with the macrocycle (i to $i + 3$) displaying a greater extent of 3_{10} -helicity than the linear analogue.

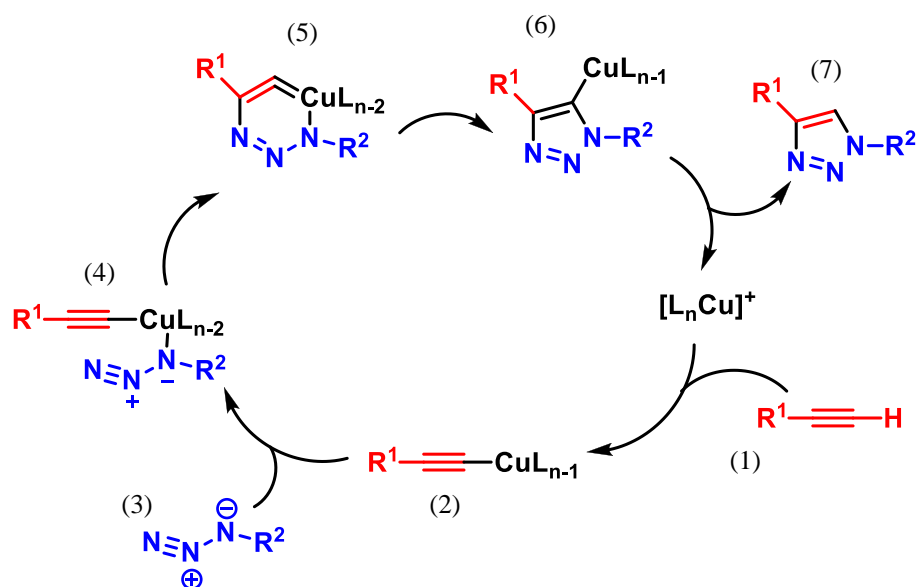


Figure 11. The schematic mechanism of the CuAAC (Huisgen cycloaddition) click reaction.⁴³

The reputed mechanism for the CuAAC reaction is shown in Figure 11. Firstly the alkyne coordinates with the Cu(I) compound, with displacement of a ligand (steps 1 and 2). The azide then coordinates to the Cu atom, displacing another ligand in the process (3 and 4). This results in the formation of a 6-membered intermediate (5), which contracts to form the triazole (6). Finally the Cu catalyst is cleaved, releasing the exclusive product, the 1,4-disubstituted 1,2,3-triazole (7).⁴⁴

1.3.2 Ring closing metathesis (RCM)

RCM is a common and versatile method for intramolecular macrocyclization, and results in the formation of carbon-carbon bonds in the form of cyclic alkenes. Enhancement and rigidification of a 3_{10} -helical conformation in a peptide can be achieved through modification of the amino acid residues at the i and $i + 3$ positions, to carry terminal dienes. These can then be readily linked, as the alkenes are located in a proximal arrangement on the same side of the molecule.^{29c} The Abell group have cyclized dienes

located in the i and $i + 2$ positions to afford a peptide with a stable β -strand backbone, a requirement for binding to many proteins (see Figure 12 b). The conformation of this macrocycle has also been defined by its X-ray crystal structure (see Figure 13).²⁷ This compound was shown to be a key intermediate of a potent inhibitor of the protease calpain 2 (see Figure 8 b), the over activation of which can lead to diseases such as Alzheimer's, stroke, and cataract formation.^{27, 45}

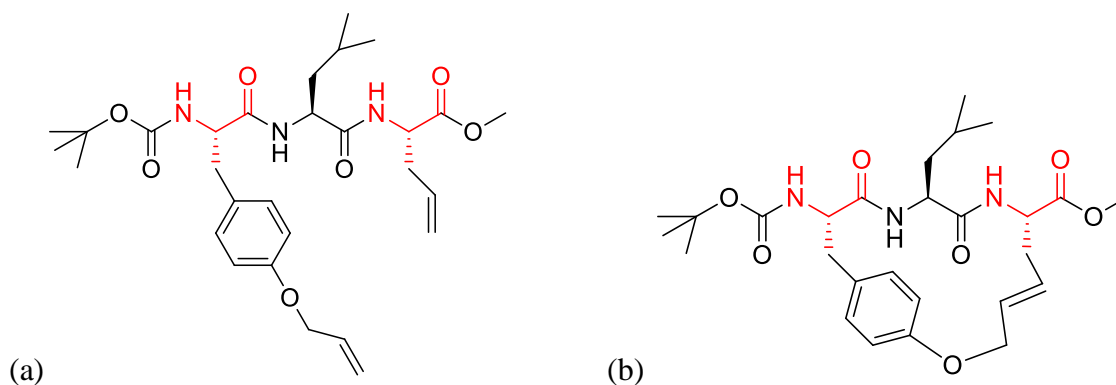


Figure 12. (a) Dienes located in the i and $i + 2$ positions of the linear peptide were linked using RCM to yield (b) a peptide with a stable β -strand backbone that was defined by its X-ray crystal structure (see Figure 13).

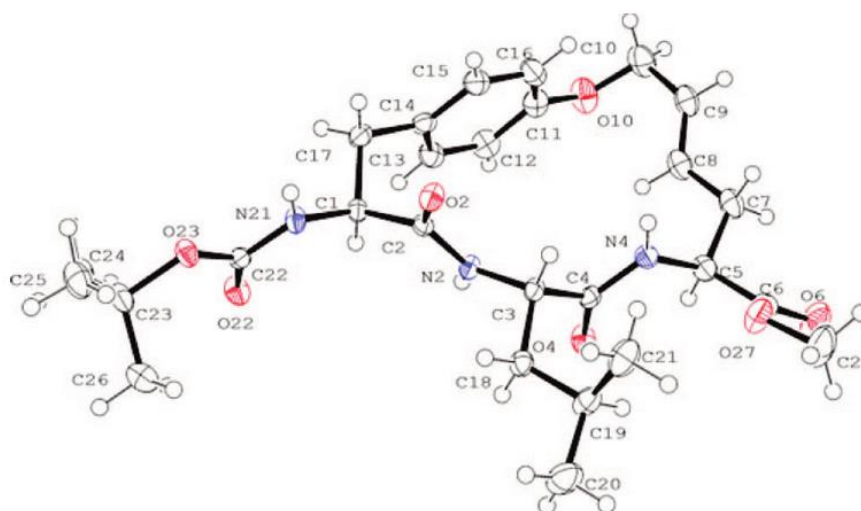


Figure 13. ORTEP diagram of the X-ray crystal structure of a macrocyclic β -strand peptide.²⁷

The advent of ruthenium-based catalysts by Grubbs and co-workers has greatly improved RCM, with these reactions now benefiting from better stereoselectivity. Strategies such as microwave irradiation can also be used to promote ring closure and enhance yields.⁴⁶ Metathesis was initially referred to as “stapling” due to the formation of the double bond in the macrocycle, however Hilinski and co-workers recently synthesized a structurally rigid helical peptide with multiple bridges which exhibited superior cell penetration, which they have termed as “stitched”.⁴⁷

1.3.3 Lactamization

Lactamization is another attractive method for cyclizing a linear precursor into a more stable lactam-bridged macrocycle⁴⁸ (see Figure 14). The range of available amino acid residues with suitable side-chains, and the wide range of protecting groups available for amines and carboxylic acids, means that lactamization can be readily achieved in solution or on solid phase.⁴⁹ Schievano et al demonstrated, through the use of 2D NMR and molecular dynamics (MD) analysis, that by linking amino acid side-chain residues (i to $i + 3$) to form a lactam bridge, enhancement of the 3_{10} -helical conformation can be realized.²⁰ Lactamization of an aspartic acid (i) and lysine ($i + 4$) residue in an extended linear peptide resulted in the stabilization of the α -helical conformation, with the ensuing compound showing improved potency and selectivity for the requisite κ -opioid receptor.⁵⁰ Kirby et al used a lactam bridge to further constrain a peptide into its helical conformation, resulting in greatly improved specific binding affinity ($K_i = 16$ nM and $EC_{50} = 12$ nM) of neuropeptide receptors in human neuroblastoma cells.⁵¹

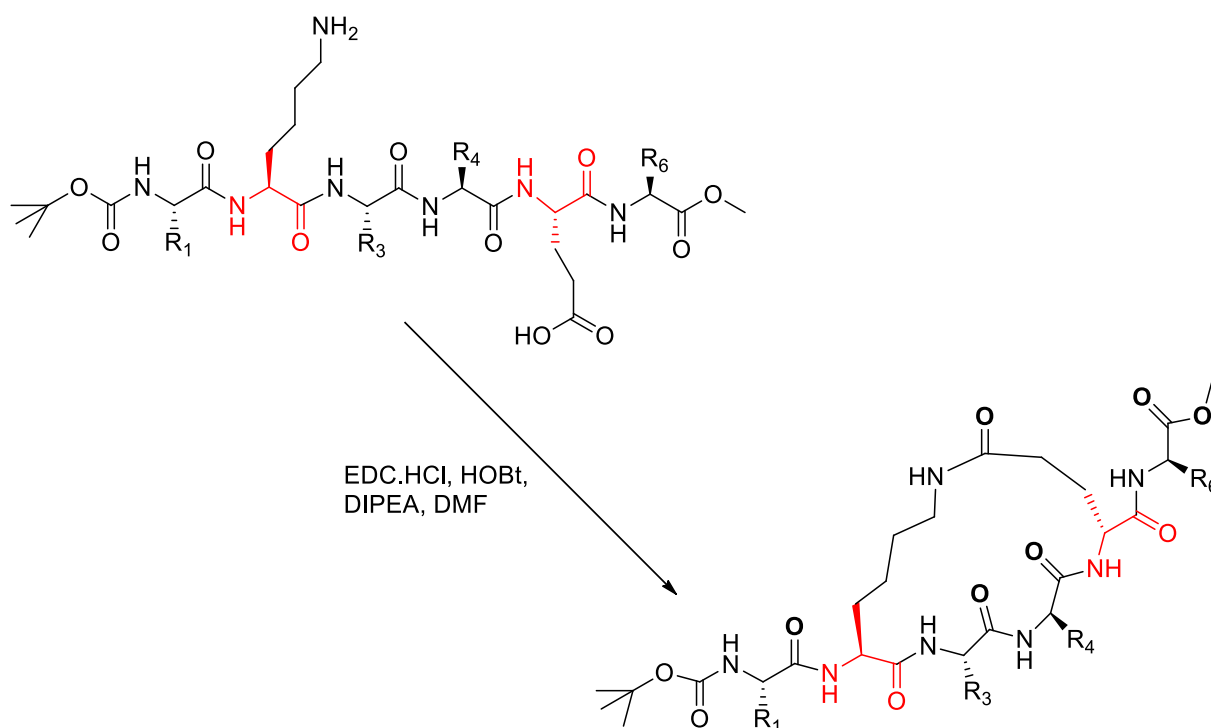


Figure 14. Cyclization of linear 3_{10} -helical precursor (top) via lactamization, to form a lactam-bridged macrocycle (below).

1.4 Characterization of peptide secondary structure

A number of methods can be used to characterize the conformation of peptides, with those utilized in this thesis including Nuclear Magnetic Resonance (NMR), Fourier Transform Infrared Spectroscopy (FTIR), and Circular Dichroism (CD).

1.4.1 Nuclear magnetic resonance (NMR) spectroscopy

^1H NMR is a robust technique used to determine peptide secondary structure in solution. Each hydrogen atom in the peptide generates an individual signal which is distinctive of its chemical environment.⁵² The assignment of individual atoms in the peptide can then be realized. Used in conjunction with two-dimensional (2D) NMR (eg ROESY and COSY), the identity of the compound may be deduced, and most importantly, the geometric

conformation revealed. Correlation Spectroscopy (COSY) is used to identify through-bond connectivities, i.e. nuclei that are coupled to each other. Rotating-frame Overhauser Effect Spectroscopy (ROESY) is used to determine through-space correlations (to approx. 5 Å) (see Figure 15). A combination of 1D, 2D, and carbon (^{13}C NMR), enables a three-dimensional “picture” to be collected, and hence elucidates the particular structural geometry of the peptide. Specifically, a combination of consecutive $\text{NH}(i)$ to $\text{NH}(i+1)$ correlations, $\text{CaH}(i)$ to $\text{NH}(i+1)$ and medium range $\text{CaH}(i)$ to $\text{NH}(i+2)$ ROESY connectivities can be used to determine 3_{10} -helical geometry.⁵² $\text{C}\beta\text{H}_2(i)$ and $\text{NH}(i)$ ROESY interactions are also supportive of a 3_{10} -helical structure.¹⁹ The distance between the peaks of a doublet, representative of the correlation between an amide (i) and alpha (i) hydrogen (^1H NMR $J_{\text{NHC}\alpha\text{H}}$ coupling constant) in a 3_{10} -helix, approximates to between 4.2 Hz⁵³ and 5.6 Hz.⁵⁴ A combination of $\text{NH}(i)$ to $\text{NH}(i+1)$, $\text{CaH}(i)$ to $\text{NH}(i+1)$ and $\text{C}\beta\text{H}(i)$ to $\text{NH}(i+1)$ ROESY correlations are indicative of a β -strand geometry, with ^1H NMR $J_{\text{NHC}\alpha\text{H}}$ coupling constants in the range of 8-10 Hz.⁵⁵

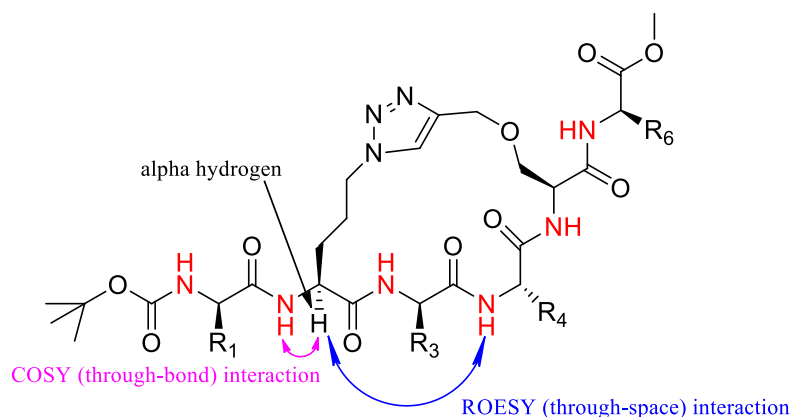


Figure 15. Schematic diagram showing ^1H NMR COSY (through-bond) and ROESY (through-space) interactions between an alpha hydrogen and amide hydrogens in a macrocyclic peptide.

1.4.2 Fourier transform infrared (FTIR) spectroscopy

Molecules absorb specific energetic frequencies characteristic of their molecular structure. When a beam of infrared light is passed through an IR-active sample (i.e. one with a change in the dipole moment), an infrared spectrum is produced. Absorbance occurs when the frequency of the IR radiation matches the transition energy of the vibrating bond or functional group. A transmittance spectrum is then generated, which pinpoints the position and intensity of peaks which are representative of specific chemical environments, thus disclosing details of the associated molecular structure. This is particularly relevant to peptides due to the sensitivity of amide bands to peptide structure.⁵⁶ Hence Amide I and II bands are used extensively in determining peptide/protein secondary structure.⁵⁷ A typical Amide I band for a 3_{10} -helix is in the order of 1654 cm^{-1} .⁵⁸ For antiparallel β -sheets, the Amide I band ranges between 1612 cm^{-1} and 1640 cm^{-1} , with a small shoulder around 1685 cm^{-1} , while the Amide II band ranges between 1510 cm^{-1} and 1530 cm^{-1} .⁵⁷ Furthermore, they should display N-H bond stretching in the region around 3281 cm^{-1} to 3302 cm^{-1} .⁵⁹

1.4.3 Circular dichroism (CD)

CD spectroscopy measures the difference in absorbance of left and right circularly polarized light in an optically active peptide.⁶⁰ The ideal spectral range for determining secondary structure lies between 180 nm and 260 nm, with a 3_{10} -helix displaying a strong negative minimum at approximately 205 nm (amide π to π^* transition) and a far less intense minimum between 220 nm and 230 nm (amide n to π^*).^{29c, 61} Furthermore, a 3_{10} -helix should exhibit a slightly positive band at approximately 195 nm, of far less intensity than that of an α -helix.⁶² CD spectra can be ambiguous, and should only be used as a guide to structural conformation, in conjunction with other methods of characterization.⁶³

1.5 Self-assembled monolayers (SAMs)

The investigation of electron transfer in peptides can be achieved by immobilization of peptides onto a metal electrode to form self-assembled monolayers (SAMs),^{3, 64} or in solution.⁶⁵ For electron transfer studies in solution it is necessary for the peptide to contain both an electron donor and an electron acceptor, with charge transfer between them triggered electrochemically or by UV radiation. An advantage of using SAMs for electrochemical studies is that only one redox active moiety is required, commonly ferrocene.⁶⁶ Marcus theory postulates that the electron transfer rate is reliant on the Gibbs

free energy (ΔG), reorganization energy (λ), temperature (T) and the electronic coupling (H_{AB}) between an electron donor and acceptor.⁶⁷ Hence SAMs have proven to be a great format for studying electron transfer, as each variable, ΔG , λ , T and H_{AB} can be controlled experimentally.⁶⁷ Alkane-thiols can form poorly defined SAMs, however SAMs of helical peptides containing a terminal redox active moiety, covalently attached to a metal surface, have been shown to be highly ordered and an excellent model for investigating electron transfer.⁶⁸ Owing to the ramifications from the density of electronic states in Marcus Theory, accurate measurement of electron transfer rates through a peptide is subject to the correct choice of electrode material. Many metals and semi-conductors have been used as substrates for SAMs, such as silver, palladium, nickel and silicon. However gold has many advantages; it is inert and its strong affinity with sulphur enables the formation of stable thiol bonds between the modified peptide and substrate.⁶⁷ Single walled carbon nanotubes (SWCNTs) have been shown to vertically align with the surface of a gold electrode through self-assembly, acting as molecular wires to enable direct electrical contact between the redox active moiety in a peptide and an electrode (see Figures 16-18). Functionalized SWCNTs have the added advantage of providing a greater surface density for the attachment of the peptide, together with a marked improvement in sensitivity and reproducibility of the electrochemical measurement over bare Au electrodes.⁶⁹ The length of the nanotubes also allows the redox active moieties (gold electrode and ferrocene) to be in close proximity, yet far enough apart to avoid direct collision, making them ideal platforms for electrochemical research (see Figure 18). In the studies conducted throughout this thesis, functionalized SWCNTs have been attached to a gold electrode via thiol bonds, and the structure then immersed into a solution containing the peptide to be electrochemically interrogated, and the coupling reagents. This chemisorption method of forming SAMs also greatly reduces the risk of unspecific adsorption.⁷⁰ Specific details of the 'set-up' are given in Chapter 2 of this thesis (2.5.1: Preparation of Au/SWCNT/ferrocene-derivatised peptide electrode).

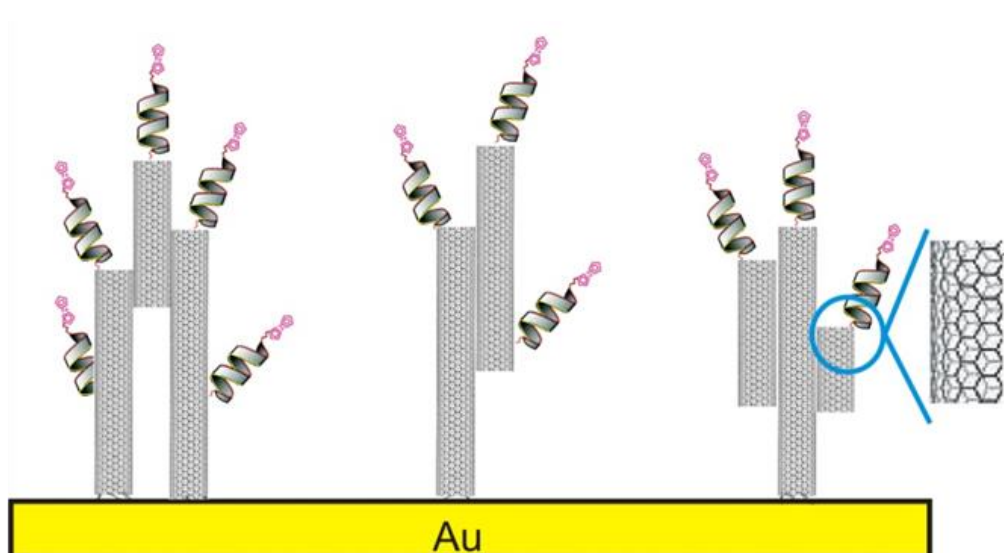


Figure 16. Schematic diagram depicting redox active helical peptides attached to SWCNTs, linked to a gold electrode.

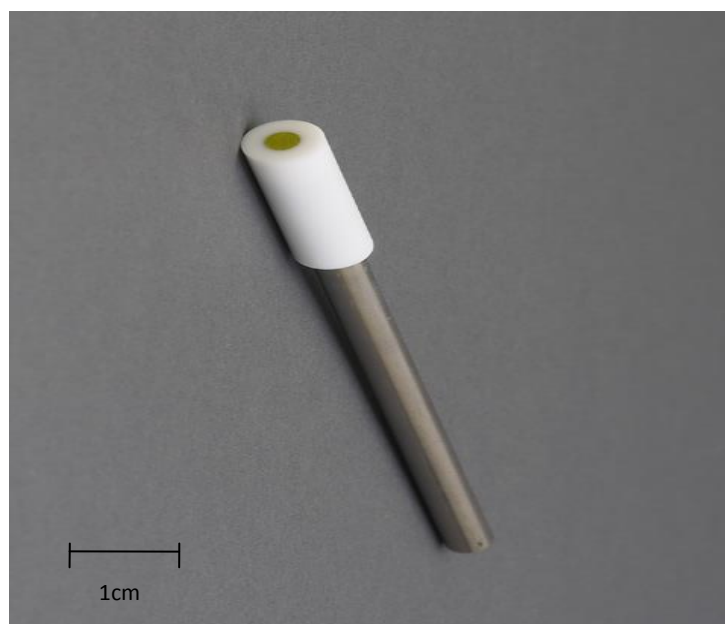


Figure 17. Typical working electrode used for electrochemical analysis of peptides in all electrochemical studies conducted throughout this thesis, showing exposed gold surface (top) ready for addition of functionalized SWCNTs, and ultimately functionalized peptides.

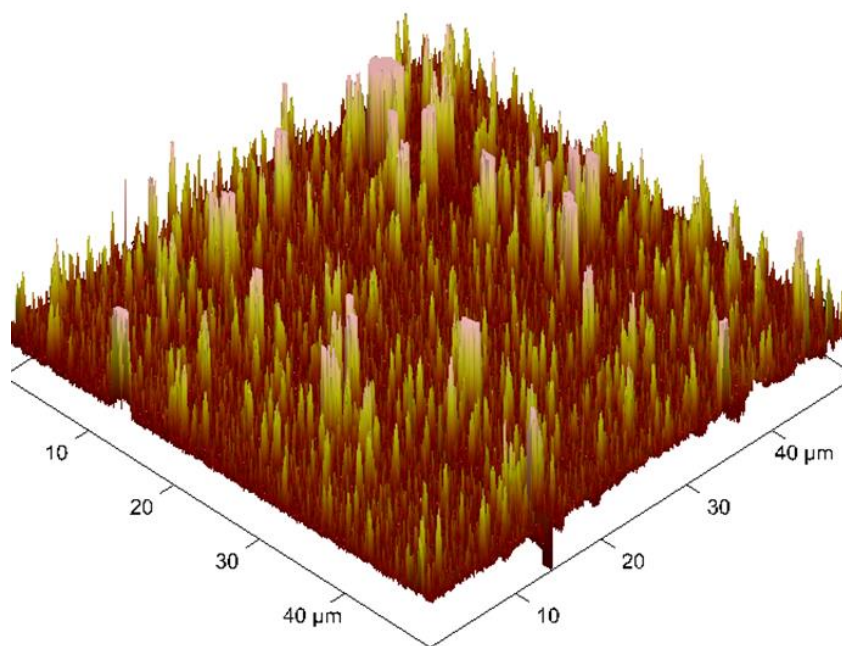


Figure 18. AFM image of a cross section of bundled, vertically aligned SWCNTs covalently bound to a gold electrode.⁷¹

1.6 Cyclic voltammetry

All redox active peptides used in this thesis were analyzed using cyclic voltammetry. This is the most common technique involved in electrochemical measurements, and works by scanning the potential of an electrode and measuring the resulting current. A 3-electrode cell, consisting of a working electrode (Au), counter electrode (Pt) and a reference electrode (Ag/AgCl), was used for all experiments. For each experiment, the immobilized peptide/electrode assembly is immersed into a 0.1 M solution of tetrabutylammonium hexafluorophosphate (TBAPF₆) in acetonitrile, acting as the conductive electrolyte. A potential is applied between the working electrode and the reference electrode, and the current measured between the working electrode and the counter electrode. The current (*i*)/potential (*E*) plot is referred to as a cyclic voltammogram, which is defined by two peak currents and two peak potentials, and provides information relating to electron transfer kinetics⁷² (see Figure 19). The current increases as the peak reaches the oxidation/reduction potential of the peptide being analyzed. The oxidation of ferrocene to the ferrocenium ion (Fc/Fc⁺) is a one-electron transfer process. As this is a reversible reaction, a similar peak is formed when the potential is reversed (see Figure 19).

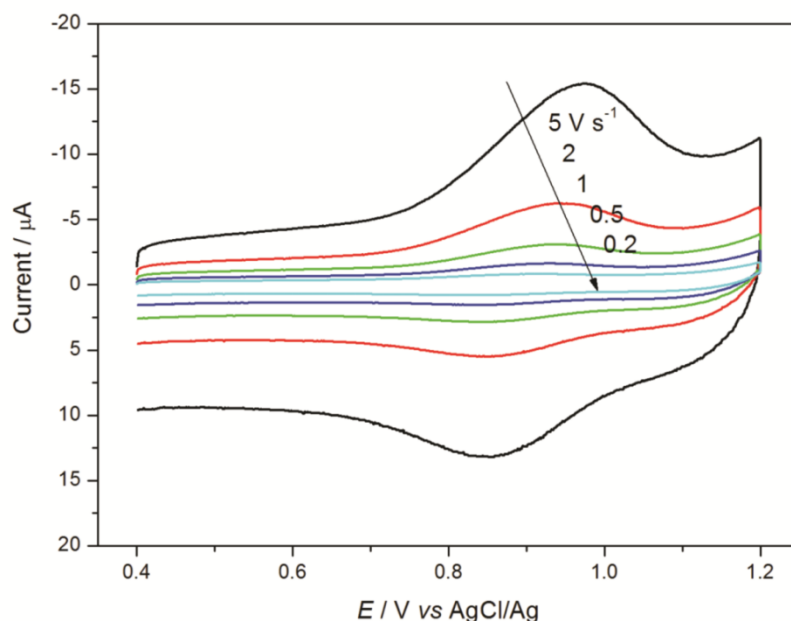


Figure 19. Typical cyclic voltammogram for a redox active peptide immobilized on gold electrode, taken at scan rates of 5, 2, 1, 0.5 and 0.2 V s⁻¹ (from top to centre). Anodic and cathodic current peaks are evident, representative of oxidation/reduction of the ferrocene moiety.

1.7 Determination of electron transfer rate constant (k_{ET}) and significant parameters

The electron transfer rate constants (k_{ET}) for all peptides investigated in this thesis were measured electrochemically using cyclic voltammetry. Following background subtraction, the surface concentration Γ (mol cm⁻²) of the ferrocene-derivatized peptides was calculated from the area under the oxidation/reduction peaks of the cyclic voltammograms, as described by Laviron's formalism.⁷³ The peak current (i_p) is related to the scan rate (ν) as described by the equation:

$$i_p = \frac{n^2 F^2 A \Gamma \nu}{4RT} = \frac{nFQ\nu}{4RT}$$

Chapter 1

where Q is a charge (coulombs) derived from the peak area of the voltammogram, n is the number of electrons involved in the reaction, A is the surface area of the gold electrode (cm^2), R is the gas constant, and F is the Faraday constant.¹⁴ An observed linear relationship between the peak current and the scan rate demonstrates that the electron transfer reaction occurs via a surface bound species (i.e. the observed electrochemical redox peaks arise exclusively from the peptides covalently anchored to the SWCNT/Au electrode).⁷⁴

The relationship between E_p (peak potential) and $\ln(v)$ is described by the following equation:

$$E_p = E^0 + \frac{RT}{\alpha nF} \ln \frac{RTk_{ET}}{\alpha nF} - \frac{RT}{\alpha nF} \ln v$$

where α is the transfer coefficient, E^0 is the formal potential, and k_{ET} is the electron transfer rate constant. Figure 20 shows a plot of E_p vs $\ln(v)$ representative of peptide **8** (see Chapter 2). The electron transfer rate constant (k_{ET}) can be extrapolated from the above equation.

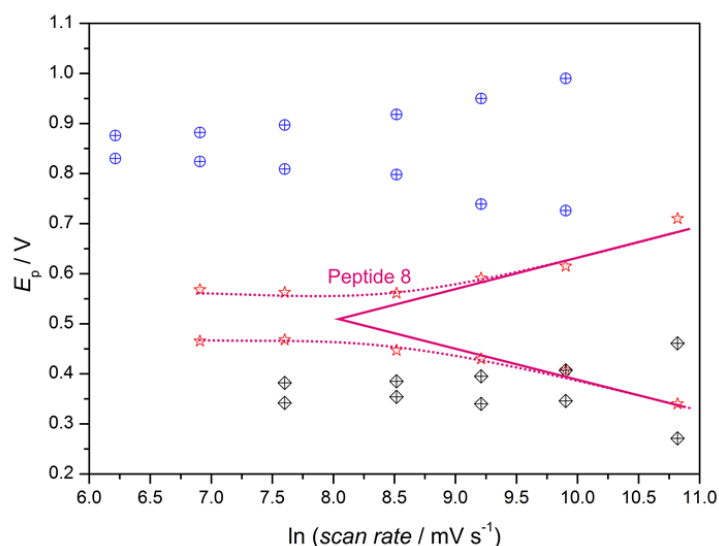


Figure 20. Peak potential as a function of $\ln(\text{scan rate})$ (red lines) representative of Peptide **8** (Chapter 2).⁷¹

Chapter 1

For electron transfer between a donor and acceptor, separated by a bridge (peptide chain), the system effectively has two electronic states. In the initial free energy state (reactant), for a one electron reaction, the electron is located on the donor, whereas the electron is situated on the acceptor in the final state (product) (see Figure 21).

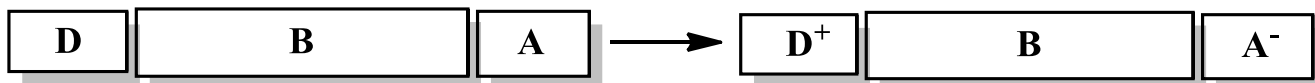


Figure 21. Simplified schematic of electron transfer from a donor (D) to an acceptor (A) through a bridge (B) (peptide chain).

Marcus theory can be used to calculate k_{ET} , and also provide other important parameters such as Gibbs free energy (ΔG), reorganization energy (λ), and the electronic coupling constant (H_{AB}) between an electron donor and acceptor.⁷⁵ The basic equation is as follows:

$$k_{ET} = \frac{2\pi}{h} |H_{AB}|^2 \frac{1}{\sqrt{4\pi\lambda k_b T}} \exp\left(-\frac{(\lambda + \Delta G^0)^2}{4\lambda k_b T}\right)$$

where k_b is the Boltzmann constant, h is Planck's constant, and T is absolute temperature.

Reorganization energy is defined as the energy required for molecular rearrangement from the reactant state to the product state.⁷⁵ The electronic coupling constant defines the strength of the force between the two moieties. Marcus theory assumes that the free energy curves for these two surfaces are the same, with the same curvature, except they are shifted (see Figure 22).

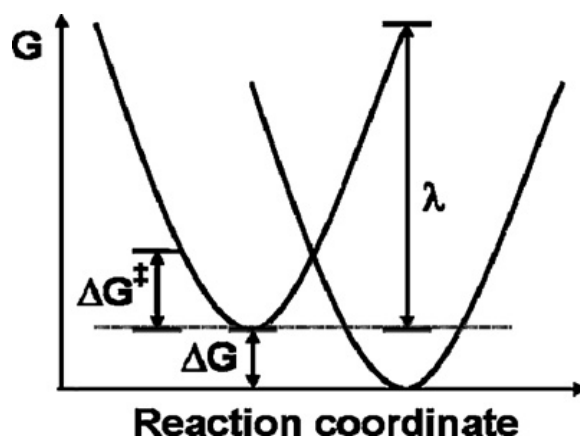


Figure 22. Free energy curves for electron transfer, reactant (left), and product (right).⁷⁵

Electron transfer may occur by the superexchange mechanism when the initial electronic state and final electronic state are degenerate, which occurs at the junction of these two energy surfaces (intersecting parabola) (see Figure 22).⁷⁶ The probability of an electron to transfer from a donor to an acceptor decreases with increasing distance between the donor and acceptor. If the experimentally determined rate constant is much faster than the calculated superexchange rate, another mechanism may be responsible for electron transfer, for example, hopping. For the computational studies conducted in this thesis, the geometry of each diabatic state was optimized using constrained density functional theory (cDFT)⁷⁷ as implemented in NW Chem 6.1⁷⁸ with the B3LYP density functional and 6-31G** basis set, starting from the optimized geometry of an uncharged molecular system. cDFT is used to calculate the potential energy curves of both the donor and acceptor state.⁷⁹ The energy of each of the two diabatic states along the electron transfer reaction coordinate was taken as the energy for geometries linearly annexed between the optimized geometries of the two diabatic states, with the excess electron localized to the part of the molecule corresponding to the diabatic state in question.⁷¹

1.8. Electron transfer in peptides

Many factors have been shown to influence electron transfer in peptides, including the distance separating the electron donor and acceptor,^{9, 21} the dipole moment,⁸⁰ secondary structure,¹⁴ and the nature of the constituent amino acid side chains.^{10, 81} It has been suggested that as the method of charge transfer in proteins is dependent on many factors, it can vary greatly between electron hopping, hole hopping and tunneling.⁸² Many researchers believe that electron transfer within a peptide is dependent on the distance between the electron donor and acceptor. Some are advocates for a tunneling mechanism,⁶⁵ whilst many others believe tunneling to occur over short distances, transferring to a hopping mechanism as the distance increases beyond a critical point.^{3, 83} Sisido and co-workers investigated how the distance between electron donor and acceptor affected electron transfer. Poly-glutamate peptides were prepared with repeat units (n=0-8), with a pyrenyl group incorporated as the electron donor in the centre of the α -helix. The electron transfer rates for each peptide exhibited an exponential dependence to distance between electron donor and acceptor. The distances, 3.9 Å (n=0) and 15.9 Å (n=8), are within the range that the superexchange mechanism is widely believed to operate in. An attenuation factor, which provides information on the conductivity of a species, of 0.66 Å⁻¹ was reported, which is in accordance with tunneling being the operative mechanism. A dependence between the electron transfer rate constant and the number of amino acids spacers in the peptide was found. It was also claimed that intramolecular hydrogen bonding is not only vital for the rigidity of the α -helical peptide, but enables electrons to take shortcuts between these bonds.⁸⁴ Another study using Aib homo-oligomer peptides found that the electron transfer rate increased, despite the distance between the electron donor and acceptor increasing by 3 Å. It was postulated that the intramolecular hydrogen bonds increase electronic coupling between donor and acceptor, and hence increase the rate of electron transfer.^{65a} Malak and co-workers investigated electron transfer using polyproline peptide bridges, ranging from n=0-9. As proline does not contain an amide group, a polyproline peptide does not form intramolecular hydrogen bonds, and is unable to form a well-ordered helical structure. For the peptides with repeat units n=0 to n=4, a clear exponential decay of the electron transfer rate was found as the distance between donor and acceptor increased, indicating that the superexchange mechanism was operational. The distance between donor and acceptor for the peptide n=4 is 18 Å, a figure between the 15-20 Å range that is believed to be transitional from a tunneling to a hopping

mechanism. For the peptides $n=5$ to $n=9$, a weak distance dependence was reported, consistent with a hopping mechanism. The distance between donor and acceptor for these peptides is 21 \AA ($n=5$) and 32 \AA ($n=9$).⁹ Another study was conducted to investigate electron transfer in oligoglycine peptides. For the peptides containing two to five amino acid residues, tunneling was found to be the applicable mechanism, whilst for the hexapeptide, hopping may be the operative mode. The rate of electron transfer for the hexapeptide was determined to be faster than expected, and it was postulated that this may be due to a change in secondary structure from a polyglycine I conformation to a polyglycine II conformation.⁸⁵ A recent electrochemical study was reported by our group on a series of Aib oligomers ($n=0-5$).¹⁴ The peptides ($n=0-2$) gave rise to a random conformation, and the rate of electron transfer decreased exponentially. In comparison, the three structures ($n=3-5$), possess well-defined intramolecular hydrogen bonding which defines their helical secondary structure. The rate of electron transfer for these structures ($n=3-5$) was found to decrease non-exponentially with distance. This suggests that the transition from a superexchange to a hopping mechanism is the result of a change from a random structure to a well-defined helical conformation, and not merely a result of increased chain length¹⁴ (see Figure 23).

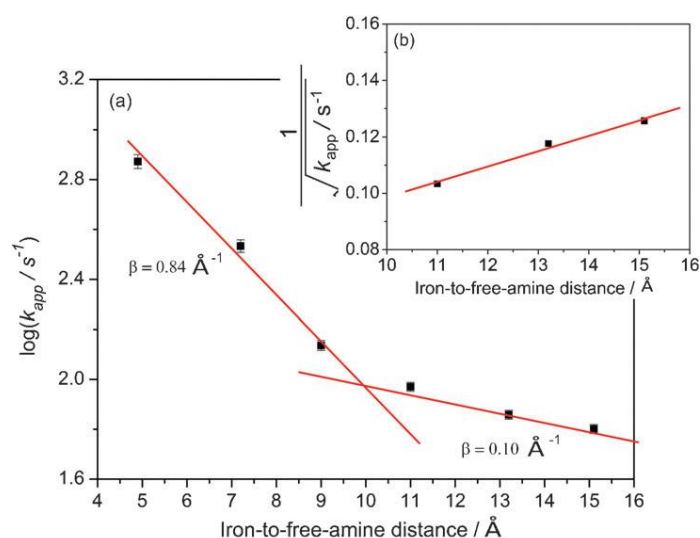


Figure 23. Electrochemical data from a study reported on a series of oligomers of Aib ($n=0-5$), showing the transition between random structure ($n=0-2$), the three data points on left of graph ($5-9 \text{ \AA}$), and helical structure ($n=3-5$), the three data points on right of graph ($11-15 \text{ \AA}$), with the associated transition in electron transfer mechanism from superexchange to hopping.¹⁴

Arikuma and co-workers synthesized a helical peptide with 32 repeat units of (Ala-Aib), over 110 Å in length. Subsequent electrochemical results indicated a non-exponential distance dependence between donor and acceptor. This supported the involvement of the hopping mechanism for charge transfer along this long peptide, using the amide groups coordinated in the intramolecular hydrogen bonding to facilitate electron transport. This is reported to occur when oxidation or reduction of the amide groups is energetically favourable.⁸³ Hopping is a thermally activated mechanism with an energy gap of approximately 0.2 eV, which is similar to that reported for DNA.⁸⁶

The influence of the dipole moment on electron transfer in peptides has also been considered. A helix has a dipole generated by an electrostatic field with a δ^+ charge at the *N*-terminus and a δ^- charge at the carboxyl end (about 3.5 D per amino acid residue).⁸⁷ The rate and direction of electron transfer is affected by the electric field created by the dipole moment of a helical peptide.⁸⁸ Researchers have reported that electron transfer coupled with the dipole moment is faster than electron transfer against the dipole moment in helical peptides.^{87, 89} The Kimura group synthesized two similar helical peptides containing (Leu-Aib) units, one with the redox active moiety (ferrocene) at the *N*-terminal and a disulfide group at the *C*-terminus, and the other at the opposite terminals. Both peptides formed well-ordered SAMs on a gold substrate, with the dipole moments oriented in opposite directions. The rate of electron transfer observed for the peptide containing the disulfide group attached to the gold substrate at the *N*-terminal, was consistently three times faster than that for the other peptide. It was postulated that this was due to the (δ^+) charge at the *N*-terminal lowering the energy barrier between the gold and the nearest amide group. The redox potential was not affected by the dipole moment, suggesting the role of the linker played a large part in accelerating electron transfer.³ Another study used helical peptides on gold surfaces with opposing dipoles, and found that the rates of electron transfer were not substantially affected. However, a six-fold increase in the rate was observed when the methylene chain linker was changed to a more conductive, π -bonded phenylene chain. It was concluded that the rate is determined by electron transfer through the linker.⁶ Nakayama and co-workers synthesized a 3_{10} -helical peptide with alternating (Ala-Aib) units with an attached oligo-phenylene ethynylene moiety, containing a terminal nitro group. Both integral parts are dipolar and hence both have different dipole magnitudes. It was proposed that stabilization of the dipole-dipole interaction between them may be

reached through an antiparallel alignment, forming a planar composition. This would be conducive to self-assembly via stacking (possibly some π - π stacking), as depicted in Figure 24.⁹⁰

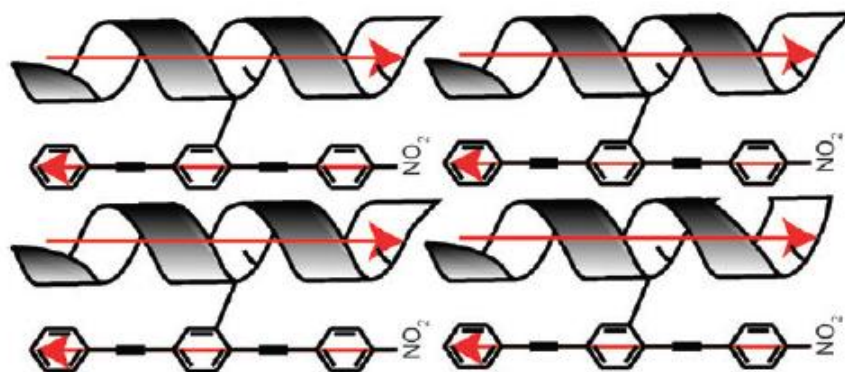


Figure 24. Schematic diagram of a 3₁₀-helical peptide with alternating (Ala-Aib) units with an attached oligo-phenylene ethynylene moiety, containing a terminal nitro group. Red arrows show direction of localized dipoles.⁹⁰

The nature of the constituent amino acid side chains also plays an important role in electron transfer in peptides. The peptide structure and specific amino acid spacers determine the electronic coupling that enables charge transfer to occur between electron donor and acceptor.^{65a} Redox active aromatic amino acids have also been proposed as through-space “stepping stones” for electron transfer.^{13, 91} Studies on model peptides have shown that the rate of electron transfer increases significantly with the introduction of electron-rich side-chains.⁹² Aromatic amino acids such as phenylalanine, tyrosine and tryptophan play vital roles in biology. Not only is tryptophan an essential amino acid used to manufacture serotonin and maintain normal brain and body function, it is believed to play a crucial role in electron transfer.⁹³ Both tryptophan and tyrosine have low oxidation potentials.⁹⁴ Tyrosine acts as an electron donor in many biological signal transduction processes and in photosynthesis, where it readily undergoes deprotonation of its aromatic hydroxyl group, making it the most common radical found in proteins.^{13, 95} X-ray crystallography of a diverse range of proteins has disclosed the presence of oxidizable aromatic amino acids located between metal cofactors, thus advocating their role in the electron transfer process.⁹⁶ Multiple sequence alignment of genomes from the respiratory

Chapter 1

oxidoreductase enzyme NDH1, have revealed the conservation of specific aromatic amino acids from simple prokaryotes through to man, that may serve as candidates for transient charge localization between metal clusters.⁹⁷ Positively charged amino acids are usually located in the neighboring environment, which may lower the energy levels of the aromatic amino acid's vacant orbitals, thus assisting electron transfer to proceed.⁹⁷ A study involving the biological enzyme, class I *Escherichia coli* ribonucleotide reductase, found that a relay shuttle comprising three tyrosine and one tryptophan residue was responsible for the rapid charge transfer spanning 35 Å. The rate of charge transfer, utilizing these redox active sites, was faster than a corresponding single-step tunneling reaction by at least four orders of magnitude⁹⁶ (see Figure 25). Efficient charge transfer through proteins over distances greater than around 20 Å is not achievable via a direct superexchange mechanism, as electron transfer rates decrease exponentially with increasing distance.⁴ Hence it is plausible that charge transfer occurs via a multi-step hopping mechanism, utilizing amino acids with felicitous redox potentials, to overcome this restriction.¹³

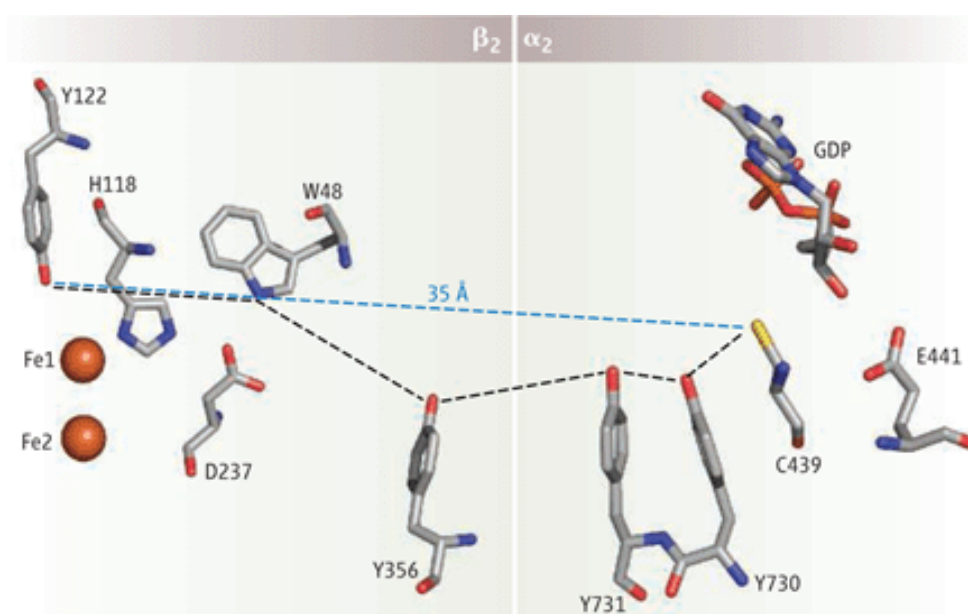


Figure 25. The postulated electron relay chain in *Escherichia coli* ribonucleotide reductase enables long distance electron transfer over 35 Å from Cys⁴³⁹ in the α_2 subunit to Tyr¹²² in the β_2 subunit, utilizing aromatic amino acids in a hopping mechanism.⁹⁵ (adapted from¹¹).

Chapter 1

A tryptophan residue has also been used as a relay station to facilitate electron transfer in a multi-step process in an azurin metallo-protein isolated from *Pseudomonas aeruginosa*. The copper redox centre was oxidized rapidly, with a charge transfer rate in excess of two orders of magnitude greater than that for single-step electron tunneling over the same distance.^{26b} Kimura and co-workers determined that linearly spaced electron-rich naphthyl groups within 3_{10} -helical peptides increase the photocurrent by efficient electron hopping between the moieties, compared to reference peptides containing one or no naphthyl groups. The naphthyl group nearest the gold electrode was photo-excited, and a radical cation was subsequently formed when an electron was transferred from the naphthyl group to the gold. It was postulated that this radical cation then “hops” from the gold to the electron donor at the peptide terminus, using the aromatic naphthyl groups as “stepping stones”.^{64a} A study by Cordes and co-workers investigated how aromatic side chains affect electron transfer by synthesizing peptides with an electron acceptor situated at the C-terminus, and a tyrosine residue functioning as an electron donor at the N-terminus. The peptide bridge consists of two triproline sequences, separated in the centre by one of four possible side chains [2x aromatic (di- and tri-methoxyphenylalanine) and 2x aliphatic]. The rate of electron transfer was determined to be in the order of 20-30 times faster when the central residue was aromatic, compared to the aliphatic amino acid side-chains, indicating intramolecular electron transfer over a distance of 20 Å by way of a two-step hopping mechanism, utilizing the aromatic side chains as “stepping stones”.⁹² Recent work has shown that by incorporating tryptophan into lipid bilayers, the rate of electron transfer is increased by an order of magnitude, compared to that observed through a phospholipid membrane with no tryptophan interaction.⁹⁸ Amdursky used AFM as a probe to measure electrical conductivity in dipeptide networks, containing either two phenylalanine residues or one phenylalanine linked to a tryptophan. The dipeptide containing an FW sequence exhibited a five-fold increase in conductivity over that with the FF array.⁹⁹ Electron hopping has been shown to occur along a pathway exploiting three tryptophan residues in the helical enzyme DNA photolyase on a picosecond timescale.¹⁰⁰ Computational studies by Chen and co-workers indicate that electron transfer between tyrosine and tryptophan not only requires specific conformations within the peptide, but the neighbouring environment is critical to successful electron transfer. When side chains of tyrosine and tryptophan are in close proximity, a hydrogen-bond is formed between them and direct electron transfer can take place, involving proton-coupled electron transfer (PCET). A base

may be used as a proton acceptor when the distance between them is too great, which forms a hydrogen-bond with the tyrosine hydroxyl group. In many biological systems, basic groups such as histidine and lysine are located around these redox active sites and accessible for hydrogen bonding. It was postulated that charge transfer between the tyrosine phenol group and the indole of the tryptophan cation could occur via a hopping mechanism due to the presence of these basic groups.¹⁰¹ It is conceivable that any section of a structure with sufficient electron affinity could act as a through-space “stepping stone” for electron transfer, and this will be discussed further in Chapter 3.

1.9. Molecular electronics

Advancing our fundamental knowledge of electron transfer in peptides is vital to progressing the field in areas such as molecular electronics. Electron transfer pathways in proteins have evolved over millions of years to optimize processes related to energy conversion, so it follows that peptides are ideal candidates for the design and fabrication of molecular electronic components such as switches, diodes, and molecular wires.¹⁰² Molecular electronics was first proposed in 1974, when Aviram and Ratner came up with the idea of a molecular rectifier,¹⁰³ however significant advances in the field have only been realized in recent years. In accordance with Moore’s Law, the traditional “top-down” method of manufacture for semiconductor devices is facing many unavoidable challenges such as photolithography and etching, that can only be addressed by a “bottom up” approach.¹⁰⁴ Single molecules have attracted much interest as molecular components, where they are chemically bound between two metal electrodes to form a molecular junction. A bias voltage is then applied between the electrodes to probe the electronic properties of the single molecule in question.¹⁰² The current/voltage properties of single-molecule junctions have been likened to those of conventional electronic devices.¹⁰⁵ The single-molecule approach to forming molecular junctions started with the discovery of scanning probe microscopy (SPM) in the early 1980’s,¹⁰⁶ and has progressed rapidly with the onset of reliable methods such as conducting probe AFMs (CP-AFM) and STM-break-junctions (STM-BJ).¹⁰⁷ Such nanoscale junctions have led to the use of molecules as prototypes for various electronic components, such as switches,¹⁰⁸ rectifiers,¹⁰⁹ and transistors.¹¹⁰ Peptides have also recently been used in the successful design of single-molecule junctions.¹¹¹ Intramolecular electron transfer in redox active peptides

Chapter 1

immobilized on SAMs is analogous to a bias voltage applied through a single peptide sandwiched between two electrodes.¹⁰² Much recent work has shown that reproducible intermolecular charge transfer utilizing π - π stacking is achievable in aromatic peptides bound between two metallic leads, providing careful design of the structure is realized.¹¹² Hence, systems utilizing both inter- and intra-molecular electron transfer will likely be useful features in future molecular electronic devices. However, all electrochemical studies conducted in this thesis are focused on intramolecular electron transfer within single redox active peptides immobilized on modified SAMs.

1.10 References

1. (a) Bendall, D. S., *Protein Electron Transfer*. BIOS Scientific Publishers: Oxford, UK, 1996; (b) Smestad, G. P.; Gratzel, M., Demonstrating electron transfer and nanotechnology: A natural dye-sensitised nanocrystalline energy converter. *Journal of Chemical Education* **1998**, *75* (6), 752-756.
2. Petrov, E. G.; Shevchenko, Y. V.; May, V., On the length dependence of bridge-mediated electron transfer reactions. *Elsevier* **2003**, *288*, 269-279.
3. Morita, T.; Kimura, S., Long-Range Electron Transfer over 4 nm Governed by an Inelastic Hopping Mechanism in Self-Assembled Monolayers of Helical Peptides. *Journal of the American Chemical Society* **2003**, *125* (29), 8732-8733.
4. Kai, M.; Takeda, K.; Morita, T.; Kimura, S., Distance dependence of long-range electron transfer through helical peptides. *Journal of Peptide Science* **2008**, *14* (2), 192-202.
5. Long, Y. T.; Abu-Rhayem, E.; Kraatz, H. B., Peptide electron transfer: More questions than answers. *Chemistry-A European Journal* **2005**, *11* (18), 5186.
6. Watanabe, J.; Morita, T.; Kimura, S., Effects of dipole moment, linkers, and chromophores at side chains on long-range electron transfer through helical peptides. *Journal of Physical Chemistry B* **2005**, *109* (30), 14416.
7. Schlag, E. W.; Sheu, S. Y.; Yang, D. Y.; Selzle, H. L.; Lin, S. H., Distal charge transport in peptides. *Angewandte Chemie-International Edition* **2007**, *46* (18), 3196-3210.
8. Schlag, E. W.; Sheu, S. Y.; Yang, D. Y.; Selzle, H. L.; Lin, S. H., Charge conductivity in peptides: Dynamic simulations of a bifunctional model supporting experimental data. *Proceedings of the National Academy of Sciences of the United States of America* **2000**, *97* (3), 1068-1072.
9. Malak, R. A.; Gao, Z. N.; Wishart, J. F.; Isied, S. S., Long-range electron transfer across peptide bridges: The transition from electron superexchange to hopping. *Journal of the American Chemical Society* **2004**, *126* (43), 13888.
10. Wang, M.; Gao, J.; Muller, P.; Giese, B., Electron Transfer in Peptides with Cysteine and Methionine as Relay Amino Acids. *Angewandte Chemie-International Edition* **2009**, *48* (23), 4232-4234.
11. Seyedsayamdost, M. R.; Yee, C. S.; Reece, S. Y.; Nocera, D. G.; Stubbe, J., pH Rate Profiles of F_nY356-R₂s (n = 2, 3, 4) in Escherichia coli Ribonucleotide Reductase: Evidence that Y356 Is a Redox-Active Amino Acid along the Radical Propagation Pathway. *Journal of the American Chemical Society* **2006**, *128* (5), 1562-1568.
12. Morita, T.; Yanagisawa, K.; Kimura, S., Enhanced Photocurrent Generation by Electron Hopping through Regularly-Arranged Chromophores in a Helical Peptide Monolayer. *Polym. J* **2008**, *40* (8), 700-709.
13. Cordes, M.; Giese, B., Electron transfer in peptides and proteins. *Chemical Society Reviews* **2009**, *38* (4), 892-901.
14. Yu, J.; Zvarec, O.; Huang, D. M.; Bissett, M. A.; Scanlon, D. B.; Shapter, J. G.; Abell, A. D., Electron Transfer through α -Peptides Attached to Vertically Aligned Carbon Nanotube Arrays: A Mechanistic Transition. *Chemical Communications* **2012**, *48* (8), 1132-1134.
15. Ramachandran, G. N.; Sasisekharan, V., Conformation of Polypeptides and Proteins. *Adv. Protein Chem* **1968**, *23*, 283.
16. Toniolo, C.; Benedetti, E., The polypeptide 310-helix. *Trends in Biochemical Sciences* **1991**, *16* (0), 350-353.

17. Ousaka, N.; Sato, T.; Kuroda, R., Intramolecular Crosslinking of an Optically Inactive 310-Helical Peptide: Stabilization of Structure and Helix Sense. *Journal of the American Chemical Society* **2007**, *130* (2), 463-465.
18. Maekawa, H.; Toniolo, C.; Broxterman, Q. B.; Ge, N.-H., Two-Dimensional Infrared Spectral Signatures of 310- and α -Helical Peptides. *The Journal of Physical Chemistry B* **2007**, *111* (12), 3222-3235.
19. Jacobsen, O.; Maekawa, H.; Ge, N. H.; Gorbitz, C. H.; Rongved, P.; Ottersen, O. P.; Amiry-Moghaddam, M.; Klaveness, J., Stapling of a 3(10)-Helix with Click Chemistry. *Journal of Organic Chemistry* **2011**, *76* (5), 1228.
20. Schievano, E.; Bisello, A.; Chorev, M.; Bisol, A.; Mammi, S.; Peggion, E., Aib-rich peptides containing lactam-bridged side chains as models of the 3(10)-helix. *Journal of the American Chemical Society* **2001**, *123* (12), 2743-2751.
21. Mandal, H. S.; Kraatz, H.-B., Electron Transfer Mechanism in Helical Peptides. *The Journal of Physical Chemistry Letters* **2012**, *3* (6), 709-713.
22. Shin, Y.-g. K.; Newton, M. D.; Isied, S. S., Distance Dependence of Electron Transfer Across Peptides with Different Secondary Structures: The Role of Peptide Energetics and Electronic Coupling. *Journal of the American Chemical Society* **2003**, *125* (13), 3722-3732.
23. (a) Arrondo, J. L. R.; Goñi, F. M., Structure and dynamics of membrane proteins as studied by infrared spectroscopy. *Progress in Biophysics and Molecular Biology* **1999**, *72* (4), 367-405; (b) Riek, R. P.; Rigoutsos, I.; Novotny, J.; Graham, R. M., Non- α -helical elements modulate polytopic membrane protein architecture. *Journal of Molecular Biology* **2001**, *306* (2), 349-362.
24. Beisziinger, M.; Sticht, H.; Sutter, M.; Ejchart, A.; Haehnel, W.; Rosch, P., Solution structure of cytochrome c6 from the thermophilic cyanobacterium *Synechococcus elongatus*. *EMBO J* **1998**, *17* (1), 27-36.
25. Svensson-Ek, M.; Abramson, J.; Larsson, G.; Törnroth, S.; Brzezinski, P.; Iwata, S., The X-ray Crystal Structures of Wild-type and EQ(I-286) Mutant Cytochrome c Oxidases from *Rhodobacter sphaeroides*. *Journal of Molecular Biology* **2002**, *321* (2), 329-339.
26. (a) Langen, R.; Chang, I. J.; Germanas, J. P.; Richards, J. H.; Winkler, J. R.; Gray, H. B., Electron-Tunneling In Proteins - Coupling Through a Beta-Strand. *Science* **1995**, *268* (5218), 1733-1735; (b) Shih, C.; Museth, A. K.; Abrahamsson, M.; Blanco-Rodriguez, A. M.; Di Bilio, A. J.; Sudhamsu, J.; Crane, B. R.; Ronayne, K. L.; Towrie, M.; Vlcek, A.; Richards, J. H.; Winkler, J. R.; Gray, H. B., Tryptophan-accelerated electron flow through proteins. *Science* **2008**, *320* (5884), 1760-1762; (c) Sasaki, H.; Makino, M.; Sisido, M.; Smith, T. A.; Ghiggino, K. P., Photoinduced electron transfer on beta-sheet cyclic peptides. *Journal of Physical Chemistry B* **2001**, *105* (42), 10416-10423.
27. Abell, A. D.; Alexander, N. A.; Aitken, S. G.; Chen, H.; Coxon, J. M.; Jones, M. A.; McNabb, S. B.; Muscroft-Taylor, A., Synthesis of Macrocyclic beta-Strand Templates by Ring Closing Metathesis. *Journal of Organic Chemistry* **2009**, *74* (11), 4354-4356.
28. Loughlin, W. A.; Tyndall, J. D. A.; Glenn, M. P.; Fairlie, D. P., Beta-strand mimetics. *Chemical Reviews* **2004**, *104* (12), 6085-6117.
29. (a) Pedersen, D. S.; Abell, A., 1,2,3-Triazoles in Peptidomimetic Chemistry. *European Journal of Organic Chemistry* **2011**, *2011* (13), 2399-2411; (b) de Araujo, A. D.; Hoang, H. N.; Kok, W. M.; Diness, F.; Gupta, P.; Hill, T. A.; Driver, R. W.; Price, D. A.; Liras, S.; Fairlie, D. P., Comparative α -Helicity of Cyclic Pentapeptides in Water. *Angewandte Chemie* **2014**, *126* (27), 7085-7089; (c) Boal, A. K.; Guryanov, I.; Moretto, A.; Crisma, M.; Lanni, E. L.; Toniolo, C.; Grubbs, R. H.; O'Leary, D. J., Facile and E-

- selective intramolecular ring-closing metathesis reactions in 3(10)-helical peptides: A 3D structural study. *Journal of the American Chemical Society* **2007**, *129* (22), 6986-+.
30. Abell, A. D.; Jones, M. A.; Coxon, J. M.; Morton, J. D.; Aitken, S. G.; McNabb, S. B.; Lee, H. Y. Y.; Mehrtens, J. M.; Alexander, N. A.; Stuart, B. G.; Neffe, A. T.; Bickerstaff, R., Molecular Modeling, Synthesis, and Biological Evaluation of Macrocyclic Calpain Inhibitors. *Angewandte Chemie-International Edition* **2009**, *48* (8), 1455-1458.
31. Driggers, E. M.; Hale, S. P.; Lee, J.; Terrett, N. K., The exploration of macrocycles for drug discovery [mdash] an underexploited structural class. *Nat Rev Drug Discov* **2008**, *7* (7), 608-624.
32. Chen, J.; Nikolovska-Coleska, Z.; Yang, C.-Y.; Gomez, C.; Gao, W.; Krajewski, K.; Jiang, S.; Roller, P.; Wang, S., Design and synthesis of a new, conformationally constrained, macrocyclic small-molecule inhibitor of STAT3 via 'click chemistry'. *Bioorganic & Medicinal Chemistry Letters* **2007**, *17* (14), 3939-3942.
33. White, C. J.; Yudin, A. K., Contemporary strategies for peptide macrocyclization. *Nature Chemistry* **2011**, *3* (7), 509-524.
34. Malesevic, M.; Strijowski, U.; Bächle, D.; Sewald, N., An improved method for the solution cyclization of peptides under pseudo-high dilution conditions. *Journal of Biotechnology* **2004**, *112* (1-2), 73-77.
35. Huisgen, R., 1,3-Dipolar Cycloadditions. Past and Future. *Angewandte Chemie International Edition in English* **1963**, *2* (10), 565-598.
36. (a) Tornøe, C. W.; Christensen, C.; Meldal, M., Peptidotriazoles on Solid Phase: [1,2,3]-Triazoles by Regiospecific Copper(I)-Catalyzed 1,3-Dipolar Cycloadditions of Terminal Alkynes to Azides. *The Journal of Organic Chemistry* **2002**, *67* (9), 3057-3064; (b) Rostovtsev, V. V.; Green, L. G.; Fokin, V. V.; Sharpless, K. B., A Stepwise Huisgen Cycloaddition Process: Copper(I)-Catalyzed Regioselective "Ligation" of Azides and Terminal Alkynes. *Angewandte Chemie International Edition* **2002**, *41* (14), 2596-2599.
37. Lopez, M. S., A. J.; Supuran, C. T.; Poulsen, S.A., Carbonic Anhydrase Inhibitors Developed Through 'Click Tailing'. *Current Pharmaceutical Design* **2010**, *16*, 3277-3287.
38. (a) Ingale, S.; Dawson, P. E., On Resin Side-Chain Cyclization of Complex Peptides Using CuAAC. *Organic Letters* **2011**, *13* (11), 2822-2825; (b) Kapoerchan, V. V.; Wiesner, M.; Overhand, M.; van der Marel, G. A.; Koning, F.; Overkleeft, H. S., Design of azidoproline containing gluten peptides to suppress CD4+ T-cell responses associated with Celiac disease. *Bioorganic & Medicinal Chemistry* **2008**, *16* (4), 2053-2062.
39. (a) Chouhan, G.; James, K., CuAAC Macrocyclization: High Intramolecular Selectivity through the Use of Copper-Tris(triazole) Ligand Complexes. *Organic Letters* **2011**, *13* (10), 2754-2757; (b) Looper, R. E.; Pizzirani, D.; Schreiber, S. L., Macrocycloadditions Leading to Conformationally Restricted Small Molecules. *Organic Letters* **2006**, *8* (10), 2063-2066.
40. Holub, J. M.; Kirshenbaum, K., Tricks with clicks: modification of peptidomimetic oligomers via copper-catalyzed azide-alkyne [3 + 2] cycloaddition. *Chemical Society Reviews* **2010**, *39* (4), 1325-1337.
41. Beierle, J. M.; Horne, W. S.; van Maarseveen, J. H.; Waser, B.; Reubi, J. C.; Ghadiri, M. R., Conformationally Homogeneous Heterocyclic Pseudotetrapeptides as Three-Dimensional Scaffolds for Rational Drug Design: Receptor-Selective Somatostatin Analogues. *Angewandte Chemie International Edition* **2009**, *48* (26), 4725-4729.
42. Holub, J. M.; Jang, H.; Kirshenbaum, K., Fit To Be Tied: Conformation-Directed Macrocyclization of Peptoid Foldamers. *Organic Letters* **2007**, *9* (17), 3275-3278.
43. Himo, F.; Lovell, T.; Hilgraf, R.; Rostovtsev, V. V.; Noodleman, L.; Sharpless, K. B.; Fokin, V. V., Copper(I)-Catalyzed Synthesis of Azoles. DFT Study Predicts

- Unprecedented Reactivity and Intermediates. *Journal of the American Chemical Society* **2004**, *127* (1), 210-216.
44. Angell, Y. L.; Burgess, K., Peptidomimetics via copper-catalyzed azide-alkyne cycloadditions. *Chemical Society Reviews* **2007**, *36* (10), 1674-1689.
45. Pehere, A. D.; Pietsch, M.; Gütschow, M.; Neilsen, P. M.; Pedersen, D. S.; Nguyen, S.; Zvarec, O.; Sykes, M. J.; Callen, D. F.; Abell, A. D., Synthesis and Extended Activity of Triazole-Containing Macrocyclic Protease Inhibitors. *Chemistry – A European Journal* **2013**, *19* (24), 7975-7981.
46. van Lierop, B. J.; Bornschein, C.; Jackson, W. R.; Robinson, A. J., Ring-closing Metathesis in Peptides - the Sting is in the Tail! *Australian Journal of Chemistry* **2011**, *64* (6), 806-811.
47. Hilinski, G. J.; Kim, Y.-W.; Hong, J.; Kutchukian, P. S.; Crenshaw, C. M.; Berkovitch, S. S.; Chang, A.; Ham, S.; Verdine, G. L., Stitched α -Helical Peptides via Bis Ring-Closing Metathesis. *Journal of the American Chemical Society* **2014**.
48. Lundquist, J. T.; Pelletier, J. C., A new tri-orthogonal strategy for peptide cyclization. *Organic Letters* **2002**, *4* (19), 3219-3221.
49. Taylor, J. W., The synthesis and study of side-chain lactam-bridged peptides. *Biopolymers* **2002**, *66* (1), 49-75.
50. Lung, F.-D. T.; Collins, N.; Stropova, D.; Davis, P.; Yamamura, H. I.; Porreca, F.; Hruby, V. J., Design, Synthesis, and Biological Activities of Cyclic Lactam Peptide Analogues of Dynorphin A(1-11)-NH₂. *Journal of Medicinal Chemistry* **1996**, *39* (5), 1136-1141.
51. Kirby, D. A.; Britton, K. T.; Aubert, M. L.; Rivier, J. E., Identification of High-Potency Neuropeptide Y Analogues through Systematic Lactamization†. *Journal of Medicinal Chemistry* **1997**, *40* (2), 210-215.
52. Neuhaus, D. E., P. A., *Methods in Molecular Biology*. Humana Press: NJ, USA, 1993; Vol. 17.
53. Wüthrich, K., *NMR of proteins and nucleic acids*. Wiley: 1986.
54. Smith, L. J.; Bolin, K. A.; Schwalbe, H.; MacArthur, M. W.; Thornton, J. M.; Dobson, C. M., Analysis of Main Chain Torsion Angles in Proteins: Prediction of NMR Coupling Constants for Native and Random Coil Conformations. *Journal of Molecular Biology* **1996**, *255* (3), 494-506.
55. Pehere, A. D.; Abell, A. D., New beta-Strand Templates Constrained by Huisgen Cycloaddition. *Organic Letters* **2012**, *14* (5), 1330-1333.
56. Haris, P. I.; Chapman, D., The conformational analysis of peptides using fourier transform IR spectroscopy. *Biopolymers* **1995**, *37* (4), 251-263.
57. Zhuang, W.; Hayashi, T.; Mukamel, S., Coherent Multidimensional Vibrational Spectroscopy of Biomolecules: Concepts, Simulations, and Challenges. *Angewandte Chemie International Edition* **2009**, *48* (21), 3750-3781.
58. Lakhani, A.; Roy, A.; De Poli, M.; Nakaema, M.; Formaggio, F.; Toniolo, C.; Keiderling, T. A., Experimental and Theoretical Spectroscopic Study of 310-Helical Peptides Using Isotopic Labeling to Evaluate Vibrational Coupling. *The Journal of Physical Chemistry B* **2011**, *115* (19), 6252-6264.
59. Pehere, A. D.; Sumby, C. J.; Abell, A. D., New cylindrical peptide assemblies defined by extended parallel [small beta]-sheets. *Organic & Biomolecular Chemistry* **2013**, *11* (3), 425-429.
60. Peeters, E.; Christiaans, M. P. T.; Janssen, R. A. J.; Schoo, H. F. M.; Dekkers, H. P. J. M.; Meijer, E. W., Circularly Polarized Electroluminescence from a Polymer Light-Emitting Diode. *Journal of the American Chemical Society* **1997**, *119* (41), 9909-9910.

61. Biron, Z.; Khare, S.; Samson, A. O.; Hayek, Y.; Naider, F.; Anglister, J., A monomeric 3(10)-helix is formed in water by a 13-residue peptide representing the neutralizing determinant of HIV-1 on gp41. *Biochemistry* **2002**, *41* (42), 12687-12696.
62. Toniolo, C.; Polese, A.; Formaggio, F.; Crisma, M.; Kamphuis, J., Circular dichroism spectrum of a peptide 3(10)-helix. *Journal of the American Chemical Society* **1996**, *118* (11), 2744-2745.
63. Niggli, D. A.; Ebert, M.-O.; Lin, Z.; Seebach, D.; van Gunsteren, W. F., Helical Content of a β 3-Octapeptide in Methanol: Molecular Dynamics Simulations Explain a Seeming Discrepancy between Conclusions Derived from CD and NMR Data. *Chemistry – A European Journal* **2012**, *18* (2), 586-593.
64. (a) Yanagisawa, K.; Morita, T.; Kimura, S., Efficient photocurrent generation by self-assembled monolayers composed of 3(10)-helical peptides carrying linearly spaced naphthyl groups at the side chains. *Journal of the American Chemical Society* **2004**, *126* (40), 12780-12781; (b) Arikuma, Y.; Takeda, K.; Morita, T.; Ohmae, M.; Kimura, S., Linker Effects on Monolayer Formation and Long-Range Electron Transfer in Helical Peptide Monolayers. *Journal of Physical Chemistry B* **2009**, *113* (18), 6256.
65. (a) Antonello, S.; Formaggio, F.; Moretto, A.; Toniolo, C.; Maran, F., Anomalous distance dependence of electron transfer across peptide bridges. *Journal of the American Chemical Society* **2003**, *125* (10), 2874; (b) Polo, F.; Antonello, S.; Formaggio, F.; Toniolo, C.; Maran, F., Evidence against the hopping mechanism as an important electron transfer pathway for conformationally constrained oligopeptides. *Journal of the American Chemical Society* **2005**, *127* (2), 492.
66. Takeda, K.; Morita, T.; Kimura, S., Effects of Monolayer Structures on Long-Range Electron Transfer in Helical Peptide Monolayer. *The Journal of Physical Chemistry B* **2008**, *112* (40), 12840-12850.
67. Eckermann, A. L., Feld, D.J., Shaw, J.A., Electrochemistry of redox-active self-assembled monolayers. *Elsevier* **2010**, *254*, 1769-1802.
68. Yasutomi, S.; Morita, T.; Imanishi, Y.; Kimura, S., A Molecular Photodiode System That Can Switch Photocurrent Direction. *Science* **2004**, *304* (5679), 1944-1947.
69. Gooding, J. J.; Wibowo, R.; Liu, Y.; Yang, W.; Losic, D.; Orbons, S.; Mearns, F. J.; Shapter, J. G.; Hibbert, D. B., Protein Electrochemistry Using Aligned Carbon Nanotube Arrays. *Journal of the American Chemical Society* **2003**, *125* (30), 9006-9007.
70. Hermanson, G. T., *Bioconjugate Techniques*. 2nd ed.; Academic Press: London U.K., 2008.
71. Yu, J.; Horsley, J. R.; Moore, K. E.; Shapter, J. G.; Abell, A. D., The Effect of a Macrocyclic Constraint on Electron Transfer in Helical Peptides: A Step Towards Tunable Molecular Wires *Chemical Communications* **2014**, *50* (14), 1652.
72. Wang, J., *Analytical Electrochemistry*. 3rd ed.; John Wiley & Sons: Hoboken New Jersey USA, 2006.
73. Laviron, E., The use of linear potential sweep voltammetry and of a.c. voltammetry for the study of the surface electrochemical reaction of strongly adsorbed systems and of redox modified electrodes. *Journal of Electroanalytical Chemistry* **1979**, *100*, 263.
74. Bard, A. J.; Faulkner, L. R., *Electrochemical Methods: Fundamentals and Applications, 2nd Edition*. Wiley, New York: 2000.
75. Eckermann, A. L.; Feld, D. J.; Shaw, J. A.; Meade, T. J., Electrochemistry of redox-active self-assembled monolayers. *Coordination Chemistry Reviews* **2010**, *254* (15-16), 1769-1802.
76. Aubry, S., A nonadiabatic theory for electron transfer and application to ultrafast catalytic reactions. *Journal of Physics: Condensed Matter* **2007**, *19*.

77. Ding, F. Z.; Wang, H. B.; Wu, Q.; Van Voorhis, T.; Chen, S. W.; Konopelski, J. P., Computational Study of Bridge-Assisted Intervalence Electron Transfer. *Journal of Physical Chemistry A* **2010**, *114* (19), 6039-6046.
78. Valiev, M.; Bylaska, E. J.; Govind, N.; Kowalski, K.; Straatsma, T. P.; van Dam, H. J. J.; Wang, D.; Nieplocha, J.; Apra, E.; Windus, T. L.; de Jong, W. A., NWChem: a comprehensive and scalable open-source solution for large scale molecular simulations. *Computer Physics Communications* **2010**, *181*, 1477.
79. Wu, Q.; Van Voorhis, T., Constrained density functional theory and its application in long-range electron transfer. *Journal of Chemical Theory and Computation* **2006**, *2* (3), 765-774.
80. (a) Lauz, M.; Eckhardt, S.; Fromm, K. M.; Giese, B., The influence of dipole moments on the mechanism of electron transfer through helical peptides. *Phys. Chem. Chem. Phys.* **2012**, *14* (40), 13785-13788; (b) Gatto, E.; Porchetta, A.; Scarselli, M.; De Crescenzi, M.; Formaggio, F.; Toniolo, C.; Venanzi, M., Playing with Peptides: How to Build a Supramolecular Peptide Nanostructure by Exploiting Helix center dot center dot center dot Helix Macro-dipole Interactions. *Langmuir* **2012**, *28* (5), 2817-2826.
81. Gao, J.; Mueller, P.; Wang, M.; Eckhardt, S.; Lauz, M.; Fromm, K. M.; Giese, B., Electron Transfer in Peptides: The Influence of Charged Amino Acids. *Angewandte Chemie-International Edition* **2011**, *50* (8), 1926-1930.
82. Han, B.; Chen, X.; Zhao, J.; Bu, Y., A peptide loop and an alpha-helix N-terminal serving as alternative electron hopping relays in proteins. *Phys. Chem. Chem. Phys.* **2012**, *14* (45), 15849-15859.
83. Arikuma, Y.; Nakayama, H.; Morita, T.; Kimura, S., Ultra-Long-Range Electron Transfer through a Self-Assembled Monolayer on Gold Composed of 120-angstrom-Long alpha-Helices. *Langmuir* **2011**, *27* (4), 1530.
84. Sisido, M.; Hoshino, S.; Kusano, H.; Kuragaki, M.; Makino, M.; Sasaki, H.; Smith, T. A.; Ghiggino, K. P., Distance dependence of photoinduced electron transfer along alpha-helical polypeptides. *Journal of Physical Chemistry B* **2001**, *105* (42), 10407-10415.
85. Sek, S.; Sepiol, A.; Tolak, A.; Misicka, A.; Bilewicz, R., Distance Dependence of the Electron Transfer Rate through Oligoglycine Spacers Introduced into Self-Assembled Monolayers. *The Journal of Physical Chemistry B* **2004**, *108* (24), 8102-8105.
86. Petrov, E. G.; Shevchenko, Y. V.; Teslenko, V. I.; May, V., Nonadiabatic donor-acceptor electron transfer mediated by a molecular bridge: A unified theoretical description of the superexchange and hopping mechanism. *Journal of Chemical Physics* **2001**, *115* (15), 7107-7122.
87. Galoppini, E.; Fox, M. A., Effect of the electric field generated by the helix dipole on photoinduced intramolecular electron transfer in dichromophoric alpha-helical peptides. *Journal of the American Chemical Society* **1996**, *118* (9), 2299.
88. Yasutomi, S.; Morita, T.; Kimura, S., pH-Controlled switching of photocurrent direction by self-assembled monolayer of helical peptides. *Journal of the American Chemical Society* **2005**, *127* (42), 14564-14565.
89. (a) Chaudhry, B. R.; Wilton-Ely, J.; Tabor, A. B.; Caruana, D. J., Effect of peptide orientation on electron transfer. *Phys. Chem. Chem. Phys.* **2010**, *12* (34), 9996; (b) Morita, T.; Kimura, S.; Kobayashi, S.; Imanishi, Y., Photocurrent Generation under a Large Dipole Moment Formed by Self-Assembled Monolayers of Helical Peptides Having an N-Ethylcarbazolyl Group. *Journal of the American Chemical Society* **2000**, *122* (12), 2850-2859.
90. Nakayama, H.; Kimura, S., Chirally Twisted Oligo(phenyleneethynylene) by Cyclization with alpha-Helical Peptide. *Journal of Organic Chemistry* **2009**, *74* (9), 3462-3468.

91. Giese, B.; Graber, M.; Cordes, M., Electron transfer in peptides and proteins. *Current Opinion in Chemical Biology* **2008**, *12* (6), 755-759.
92. Cordes, M.; Kottgen, A.; Jasper, C.; Jacques, O.; Boudebous, H.; Giese, B., Influence of amino acid side chains on long-distance electron transfer in peptides: Electron hopping via "Stepping Stones". *Angewandte Chemie-International Edition* **2008**, *47* (18), 3461-3463.
93. Paredes, S. B., C. Reiter, R. Rodriguez, A., Assessment of the Potential Role of Tryptophan as the Precursor of Serotonin and Melatonin for the Aged Sleep-wake Cycle and Immune Function: *Streptopelia Risoris* as a Model. *International Journal of Tryptophan Research* **2009**, *2*, 23-36.
94. Giese, B.; Wang, M.; Gao, J.; Stoltz, M.; Müller, P.; Graber, M., Electron Relay Race in Peptides. *The Journal of Organic Chemistry* **2009**, *74* (10), 3621-3625.
95. Bollinger, J. M., Jr., Biochemistry - Electron relay in proteins. *Science* **2008**, *320* (5884), 1730-1731.
96. Stubbe, J.; Nocera, D. G.; Yee, C. S.; Chang, M. C. Y., Radical Initiation in the Class I Ribonucleotide Reductase: Long-Range Proton-Coupled Electron Transfer? *Chemical Reviews* **2003**, *103* (6), 2167-2202.
97. Wittekindt, C.; Schwarz, M.; Friedrich, T.; Koslowski, T., Aromatic Amino Acids as Stepping Stones in Charge Transfer in Respiratory Complex I: An Unusual Mechanism Deduced from Atomistic Theory and Bioinformatics. *Journal of the American Chemical Society* **2009**, *131* (23), 8134-8140.
98. Sarangi, N. K.; Patnaik, A., L-Tryptophan-Induced Electron Transport across Supported Lipid Bilayers: an Alkyl-Chain Tilt-Angle, and Bilayer-Symmetry Dependence. *Chemphyschem* **2012**, *13* (18), 4258-4270.
99. Amdursky, N., Enhanced solid-state electron transport via tryptophan containing peptide networks. *Phys. Chem. Chem. Phys.* **2013**, *15* (32), 13479-13482.
100. Lukacs, A.; Eker, A. P. M.; Byrdin, M.; Brettel, K.; Vos, M. H., Electron Hopping through the 15 Å Triple Tryptophan Molecular Wire in DNA Photolyase Occurs within 30 ps. *Journal of the American Chemical Society* **2008**, *130* (44), 14394-14395.
101. Chen, X.; Zhang, L.; Zhang, L.; Wang, J.; Liu, H.; Bu, Y., Proton-Regulated Electron Transfers from Tyrosine to Tryptophan in Proteins: Through-Bond Mechanism versus Long-Range Hopping Mechanism. *The Journal of Physical Chemistry B* **2009**, *113* (52), 16681-16688.
102. Sek, S., Review peptides and proteins wired into the electrical circuits: An SPM-based approach. *Biopolymers* **2013**, *100* (1), 71-81.
103. Aviram, A.; Ratner, M. A., Molecular rectifiers. *Chemical Physics Letters* **1974**, *29* (2), 277-283.
104. Maeda, H.; Sakamoto, R.; Nishihara, H., Metal complex oligomer and polymer wires on electrodes: Tactical constructions and versatile functionalities. *Polymer* **2013**, *54* (17), 4383-4403.
105. Benesch, C.; Rode, M. F.; Cizek, M.; Haertle, R.; Rubio-Pons, O.; Thoss, M.; Sobolewski, A. L., Switching the Conductance of a Single Molecule by Photoinduced Hydrogen Transfer. *Journal of Physical Chemistry C* **2009**, *113* (24), 10315.
106. McCreery, R. L.; Bergren, A. J., Progress with Molecular Electronic Junctions: Meeting Experimental Challenges in Design and Fabrication. *Advanced Materials* **2009**, *21* (43), 4303-4322.
107. (a) Marques-Gonzalez, S.; Yufit, D. S.; Howard, J. A. K.; Martin, S.; Osorio, H. M.; Garcia-Suarez, V. M.; Nichols, R. J.; Higgins, S. J.; Cea, P.; Low, P. J., Simplifying the conductance profiles of molecular junctions: the use of the trimethylsilylethynyl moiety as a molecule-gold contact. *Dalton Transactions* **2013**, *42* (2), 338-341; (b) Xu, B.;

Tao, N. J., Measurement of Single-Molecule Resistance by Repeated Formation of Molecular Junctions. *Science* **2003**, *301* (5637), 1221-1223.

108. (a) Darwish, N.; Diez-Perez, I.; Guo, S.; Tao, N.; Gooding, J. J.; Paddon-Row, M. N., Single Molecular Switches: Electrochemical Gating of a Single Anthraquinone-Based Norbornylogous Bridge Molecule. *Journal of Physical Chemistry C* **2012**, *116* (39), 21093-21097; (b) Avellini, T.; Li, H.; Coskun, A.; Barin, G.; Trabolsi, A.; Basuray, A. N.; Dey, S. K.; Credi, A.; Silvi, S.; Stoddart, J. F.; Venturi, M., Photoinduced Memory Effect in a Redox Controllable Bistable Mechanical Molecular Switch. *Angewandte Chemie-International Edition* **2012**, *51* (7), 1611-1615.

109. (a) Staykov, A.; Li, X.; Tsuji, Y.; Yoshizawa, K., Current Rectification in Nitrogen- and Boron-Doped Nanographenes and Cyclophanes. *The Journal of Physical Chemistry C* **2012**, *116* (34), 18451-18459; (b) Ding, W.; Negre, C. F. A.; Palma, J. L.; Durrell, A. C.; Allen, L. J.; Young, K. J.; Milot, R. L.; Schmuttenmaer, C. A.; Brudvig, G. W.; Crabtree, R. H.; Batista, V. S., Linker Rectifiers for Covalent Attachment of Transition Metal Catalysts to Metal- Oxide Surfaces. *Chemphyschem* **2014**, *15* (6), 1138-1147.

110. (a) Chen, Y.-S.; Hong, M.-Y.; Huang, G. S., A protein transistor made of an antibody molecule and two gold nanoparticles. *Nature Nanotechnology* **2012**, *7* (3), 197-203; (b) Xu, Y.; Cui, B.; Ji, G.; Li, D.; Liu, D., Effect of the orientation of nitro group on the electronic transport properties in single molecular field-effect transistors. *Phys. Chem. Chem. Phys.* **2013**, *15* (3), 832-836.

111. Uji, H.; Morita, T.; Kimura, S., Molecular direction dependence of single-molecule conductance of a helical peptide in molecular junction. *Phys. Chem. Chem. Phys.* **2013**, *15* (3), 757-760.

112. (a) Yew, S. Y.; Shekhawat, G.; Wangoo, N.; Mhaisalkar, S.; Suri, C. R.; Dravid, V. P.; Lam, Y. M., Design of single peptides for self-assembled conduction channels. *Nanotechnology* **2011**, *22* (21); (b) Smeu, M.; Wolkow, R. A.; Guo, H., Conduction Pathway of π -Stacked Ethylbenzene Molecular Wires on Si(100). *Journal of the American Chemical Society* **2009**, *131* (31), 11019-11026.

Statement of Authorship

Paper 1

“The effect of a macrocyclic constraint on electron transfer in helical peptides: A step towards tunable molecular wires”, Yu, J.; Horsley, J. R.; Moore, K. E.; Shapter, J. G.; Abell, A. D. *Chemical Communications* **2014**, *50*, 1652.

Mr. John Horsley (candidate)

Performed synthesis and characterization of peptides, attachment to SWCNT/gold electrodes, electrochemistry, analysis of data, provided advanced draft of manuscript and subsequent revisions.

I hereby certify that the statement of contribution is accurate.

Signed

Dated 11/11/2014

Dr. Jingxian Yu

Performed synthesis of some peptides, electrochemistry, theoretical studies, corresponding author, and co-supervisor of candidate.

I hereby certify that the statement of contribution is accurate.

Signed

Dated 11/11/2014

Miss Katherine Moore

Prepared SWCNT/Au electrodes.

I hereby certify that the statement of contribution is accurate.

Signed

Dated 12/11/2014

Prof. Joe Shapter

Supervisor to Miss Katherine Moore. Provided laboratory and instrumentation for electrochemical analysis of peptides.

I hereby certify that the statement of contribution is accurate.

Signed

Dated

12/11/14

Prof. Andrew Abell

Supervised development of work, revised manuscript, and is corresponding author.

I hereby certify that the statement of contribution is accurate.

Signed

Dated

16/2/2015

Paper 2

“Unraveling the Interplay of Backbone Rigidity and Electron Rich Side-Chains on Electron Transfer in Peptides: The Realization of Tunable Molecular Wires”, Horsley, J. R.; Yu, J.; Moore, K. E.; Shapter, J. G.; Abell, A. D. *Journal of the American Chemical Society* **2014**, *136*, 12479.

Mr. John Horsley (candidate)

Performed synthesis and characterization of peptides, attachment to SWCNT/gold electrodes, electrochemistry, analysis of data, provided advanced draft of manuscript and subsequent revisions.

I hereby certify that the statement of contribution is accurate.

Signed

Dated

11/11/2014

Dr. Jingxian Yu

Performed synthesis of some peptides, electrochemistry, theoretical studies, corresponding author, and co-supervisor of candidate.

I hereby certify that the statement of contribution is accurate.

Signed

Dated

11/11/2014

Miss Katherine Moore

Prepared SWCNT/Au electrodes.

I hereby certify that the statement of contribution is accurate.

Signed

Dated

12/11/2014

Prof. Joe Shapter

Supervisor to Miss Katherine Moore. Provided laboratory and instrumentation for electrochemical analysis of peptides.

I hereby certify that the statement of contribution is accurate.

Signed

Dated

12/11/14

Prof. Andrew Abell

Supervised development of work, revised manuscript, and is corresponding author.

I hereby certify that the statement of contribution is accurate.

Signed

Dated

16/2/2015

I hereby give permission for John Horsley to use the following papers in his PhD Thesis:
“The effect of a macrocyclic constraint on electron transfer in helical peptides: A step towards tunable molecular wires”, Yu, J.; Horsley, J. R.; Moore, K. E.; Shapter, J. G.; Abell, A. D. *Chemical Communications* **2014**, *50*, 1652 and “Unraveling the Interplay of Backbone Rigidity and Electron Rich Side-Chains on Electron Transfer in Peptides: The Realization of Tunable Molecular Wires”, Horsley, J. R.; Yu, J.; Moore, K. E.; Shapter, J. G.; Abell, A. D. *Journal of the American Chemical Society* **2014**, *136*, 12479.

Signed

Date

11/2/2015

I hereby give permission for John Horsley to use the following papers in his PhD Thesis:

Yu, J.; Horsley, J. R.; Moore, K. E.; Shapter, J. G.; Abell, A. D. *Chemical Communications*, **2014**, *50*, 1652.

Horsley, J. R.; Yu, J.; Moore, K. E.; Shapter, J. G.; Abell, A. D. *Journal of the American Chemical Society*, **2014**, *136*, 12479.

Horsley, J. R., Yu, J., Abell, A. D. "The Correlation of Electrochemical Measurements and Molecular Junction Conductance Simulations in β -Strand Peptides" *Chemistry A European Journal*, **2015**, *21*, 5926-5933.

Horsley, J. R., Yu, J., Abell, A. D. "Understanding the Role of the Amide Bond and Electron Transfer Mechanisms in Macrocyclic Peptides" (Prepared in publication format "text in manuscript").

Signed

Date

19/6/2015

Signed

Date

19/06/2015

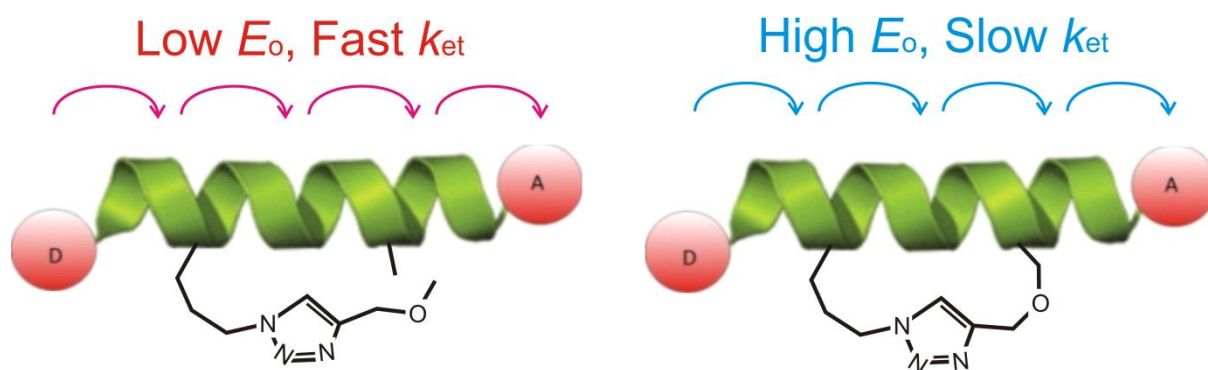
CHAPTER 2

The Effect of a Macrocyclic Constraint on Electron Transfer in Helical Peptides: A Step Towards Tunable Molecular Wires

Jingxian Yu,^{*,†} John R. Horsley,[†] Katherine E. Moore,[‡] Joe G. Shapter,[‡] and Andrew D. Abell^{*,†}

[†] ARC Centre of Excellence for Nanoscale BioPhotonics (CNBP), School of Chemistry and Physics, The University of Adelaide, Adelaide, SA 5005, Australia

[‡] Centre for Nanoscale Science and Technology, School of Chemical & Physical Science, Flinders University, Bedford Park, SA 5042, Australia



Jingxian Yu, John R. Horsley, Katherine E. Moore, Joe G. Shapter, and Andrew D. Abell, *Chem. Comm.*, **2014**, 50, 1652-1654.

2.1 Abstract

Two helical peptides, one constrained by a covalent side-chain staple, exhibit vastly different electronic properties despite adopting essentially the same backbone conformation. High level calculations, using the latest constrained density functional theory (cDFT), confirm that these differences are due to the additional backbone rigidity imparted by the macrocyclic constraint.

2.2 Introduction

Helical domains in peptides and proteins provide a good medium for electron transfer¹ over surprisingly long molecular distances (>100 Å).² Such structures present as ideal candidates for use as molecular wires, particularly when combined with an ability to be precisely functionalized.³ However, more detailed understanding on exactly what defines and controls the mechanisms and efficiency of electron transfer in peptides is required before this promise can be fully realized. Toward this goal, we recently demonstrated that intramolecular hydrogen bonding within helical Aib (α -aminoisobutyric acid) containing oligomers plays a critical role in defining the mechanism of electron transfer.⁴ Recent theoretical studies suggest that low-frequency rotation between neighbouring amino acids brings adjacent carbonyl groups into alignment to allow efficient charge transfer through the peptide.⁵ As such any feature that enhances backbone rigidity should restrict molecular motion and consequently retard electron transfer in peptides. However, the exact influence of backbone rigidity on electron transfer requires significant further investigation.⁶ Here we present electrochemical and theoretical studies on a helical peptide constrained by a side-chain tether to begin to unravel these effects in isolation from other factors such as chain length, dipole orientation and the associated hydrogen bonding that are known to influence electron transfer.

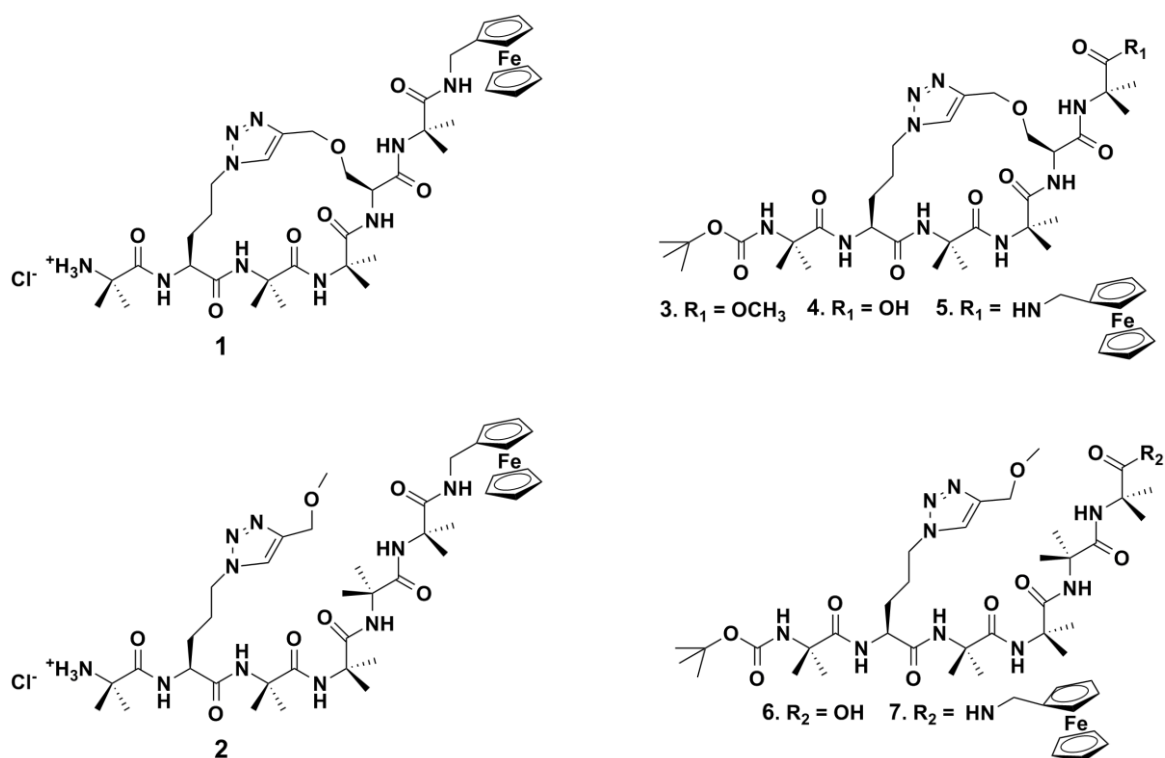
2.3 Results and discussion

2.3.1 Conformational analysis of peptides

The required Aib-rich hexapeptide stapled with an i to $i+3$ macrocyclic constraint by Husigen cycloaddition (peptide **1**) and a linear analogue (peptide **2**) were synthesized as described in section 2.5.8 Peptide Synthesis. The peptides were designed to share a common 3_{10} -helical backbone conformation, with peptide **1** possessing a rigid backbone conformation as defined by the side-chain constraint (see Scheme 1).

Chapter 2

Scheme 1. Structures of target peptides **1** and **2** and key synthetic intermediates.



The geometries of peptides **1** and **2** were confirmed as 3_{10} -helical by ^1H NMR spectroscopy. In particular, NH (i) to NH ($i+1$) ROESY correlations were observed for both peptides and also their synthetic precursors, **3-5** and **6-7**. Furthermore, C α H (i) to NH ($i+1$) and medium range C α H (i) to NH ($i+2$) were found for **1** and **2**, as shown in Figure 1, with long range C α H (i) to NH ($i+3$) correlations evident in peptides **3**, **5** and **7**. A lack of C α H (i) to NH ($i+4$) correlations for all peptides precludes the possibility of an α -helical structure, which is characterized by (i to $i+4$) hydrogen bonds.⁷ A strong negative minimum near 202 nm, with a significantly weaker minimum at approximately 232 nm was observed in a representative CD spectrum of the constrained peptide **3** (see Figure 2), which further supports a 3_{10} -helical conformation.⁸ Collectively, this information confirms the presence of a 3_{10} -helical backbone structure and that the C-terminal ferrocene and the constraint do not impinge on the backbone helicity.

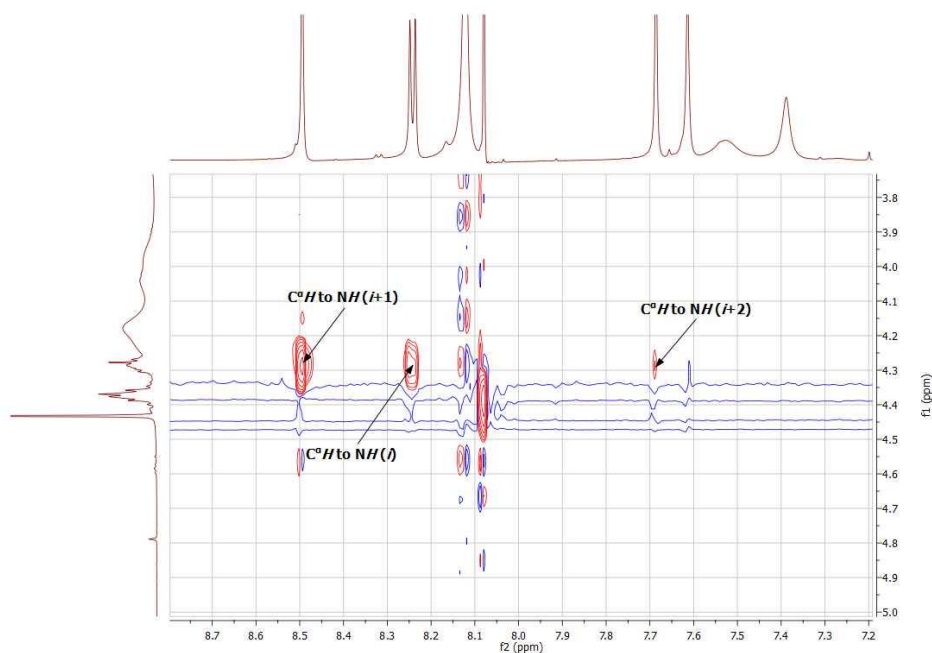


Figure 1. ¹H NMR ROESY spectrum representative of peptide **2**, showing C^αH (*i*) to NH (*i*+1) and medium range C^αH (*i*) to NH (*i*+2) interactions, indicative of a 3₁₀-helical structure.

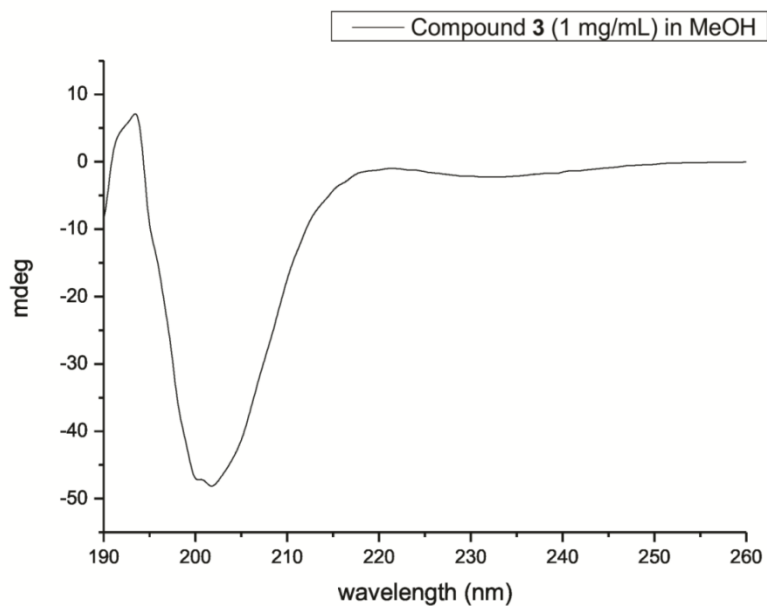


Figure 2. CD spectrum of macrocyclic peptide **3**, showing an intense negative minimum around 202 nm and a significantly less intense minimum around 230 nm, with a small positive maximum around 193 nm, indicative of a right-handed 3₁₀-helical structure.

The lowest energy conformers for the *N*-protected peptides **5** and **7** were determined by molecular modelling (using a hybrid B3LYP method with 6-31G** basis set) in order to further define the backbone conformations of the constrained and unconstrained peptides (see Figure 3). The *N*-protected peptides were used in these studies as free amines are known to give rise to unrealistic electrostatic interactions, resulting in unstable lowest energy conformers.⁹ The resulting structures reveal that the distances from the first to last carbonyl carbons (backbone lengths) of the two peptides are similar, 11.94 Å and 12.02 Å for peptides **5** and **7** respectively. In addition, the greatest variation between hydrogen bond lengths is 0.14 Å. The mean dihedral angles for residues 1-4 of peptide **5** were calculated to be (-56.86° for Φ) and (-31.29° for Ψ), deviating from an ideal 3_{10} -helix by 0.14° and 1.29° respectively,¹⁰ whilst the mean dihedral angles for residues 1-4 deviated from an ideal 3_{10} -helix by 1.33° and 3.75° in peptide **7**. These studies demonstrate that the two structures have essentially the same conformations, such that they differ only in the presence (or absence) of the constraint and the associated effect that this has on backbone rigidity.

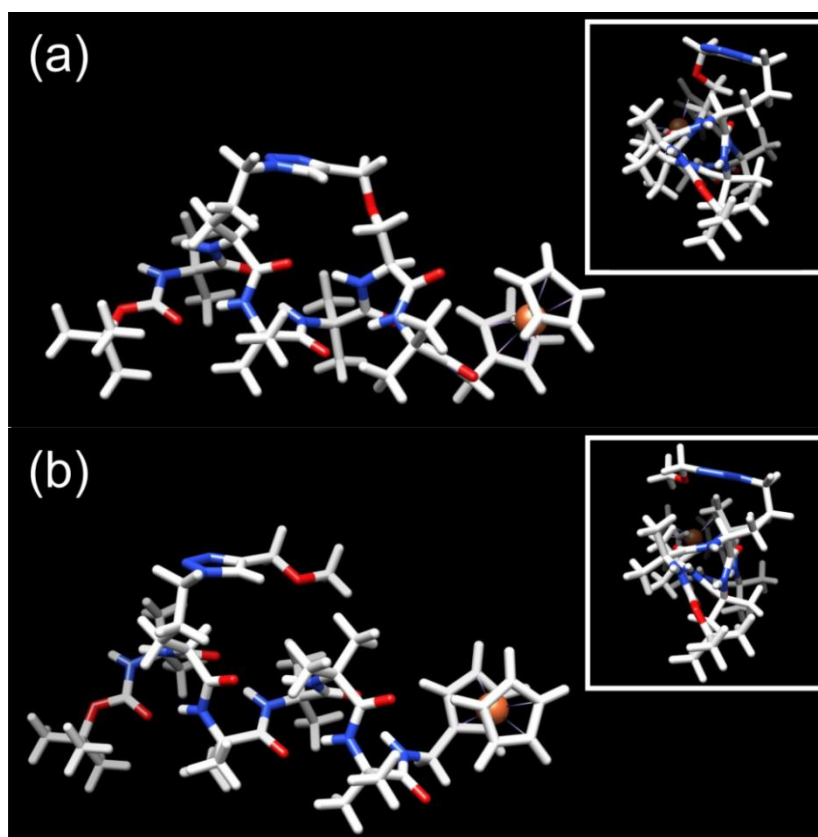


Figure 3. The lowest energy conformers for peptides (a) **5** and (b) **7**, optimized by the hybridB3LYP method with 6-31G** basis set. (Inset: top view looking down helix.)

2.3.2 Electrochemical analysis of intramolecular electron transfer

The constrained peptide **1** and linear analogue **2**, were next separately attached to vertically aligned single-walled carbon nanotube array/gold (SWCNTs/Au) electrodes¹¹ (see Figure 4) in order to study their electron transfer kinetics. SWCNTs/Au electrodes provide a high surface concentration of attached redox probes and hence high sensitivity and reproducibility of electrochemical measurement.¹²

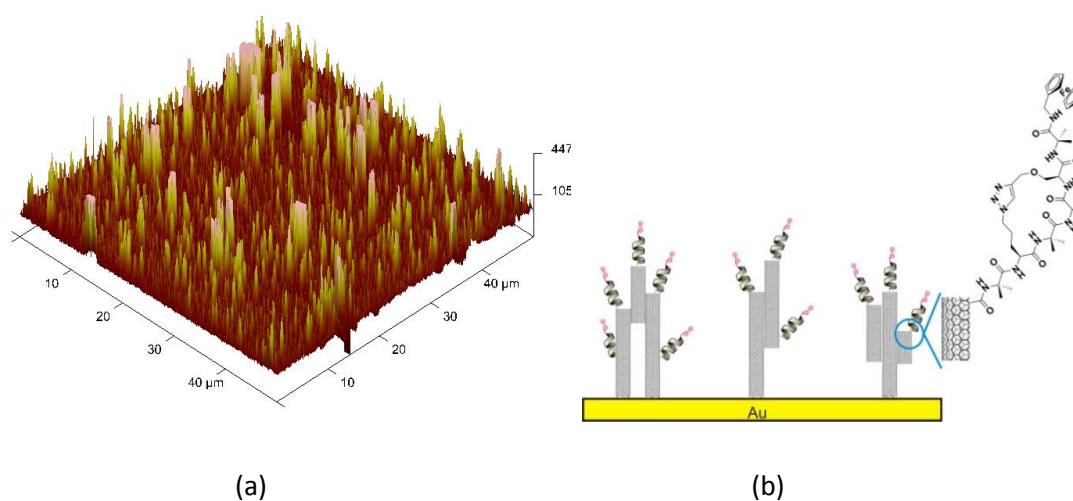


Figure 4. (a) AFM image of vertically aligned single-walled carbon nanotube array/gold (SWCNTs/Au) electrode ($50 \times 50 \mu\text{m}^2$). The average height of single-walled nanotubes is 206 nm. (b) Schematic of ferrocene-derivatized peptides immobilized onto SWCNTs/Au electrode.

Figure 5 shows the cyclic voltammograms obtained for the two target peptides immersed in 0.1 mol L^{-1} TBAPF₆/CH₃CN solutions. These show a pair of redox peaks, characteristic of a one-electron oxidation / reduction reaction (Fc^+/Fc). The surface concentrations of the peptides were determined by integrating background current subtracted peak areas to be $3.76 \times 10^{-10} \text{ mol cm}^{-2}$ for **1** and $2.52 \times 10^{-10} \text{ mol cm}^{-2}$ for **2** (see Table 1). These surface concentrations are comparable to other carbon nanotube electrode studies.^{4a, 11a} The formal potentials (E_o) and apparent electron transfer rate constants (k_{app}) were estimated to be 0.853 V and 28.1 s^{-1} for **1** and 0.371 V and 117.3 s^{-1} for **2** respectively (as detailed in Table 1), using Laviron's formalism.¹³

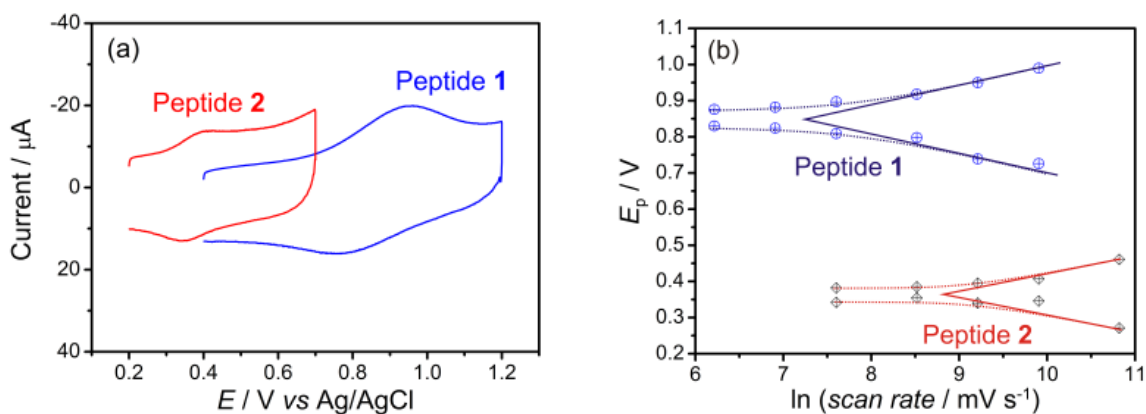


Figure 5. (a) Cyclic voltammograms for peptide **1** (blue) and peptide **2** (red) immobilized on SWCNTs/Au electrodes taken at 5 V s^{-1} . (b) Peak potential versus $\ln(\text{scan rate})$ for peptides **1** and **2** after background current subtraction.

Table 1 Electron transfer rate constants (k_{app}), surface concentrations and formal potentials (E_o) of the constrained (peptide **1**) and linear analogue (peptide **2**).

Peptide	Surface concentration ($\times 10^{-10} \text{ mole.cm}^{-2}$)	E_o (V vs AgCl/Ag)	k_{app} / s^{-1}
1	3.76 ± 0.35	0.853	28.1 ± 3.6
2	2.52 ± 0.18	0.371	117.3 ± 9.9

Despite having very similar backbone geometries, the two target peptides exhibit considerably different formal potentials and electron transfer rate constants. Side-bridge stapling as in peptide **1** results in a significant formal potential shift to the positive of approximately 480 mV in comparison to peptide **2**. Thus oxidation/reduction of the redox-active ferrocene moiety in the constrained peptide is energetically much less favourable

than in the linear analogue. Such a dramatic formal potential shift has not, to the best of our knowledge, previously been reported in ferrocene-derivatized peptides. As both peptides essentially differ only in the presence (or absence) of the side-bridge constraint, the significant formal potential shift found in **1**, is clearly a result of additional backbone rigidity imparted by this constraint. Our experimental data also reveals a significant decrease in the electron transfer rate constant (approx 25%) on introducing the constraint of **1**. Previous studies have shown that electron transfer rate constants in peptides can vary greatly,^{2, 4a, 6d} but without such a significant difference in formal potential as reported here. Our results suggest that side-bridge stapling creates an additional reorganization energy barrier that impedes electron transfer within the peptide, in turn decreasing the charge transfer rate. Hence reducing the backbone flexibility within a helical peptide through the introduction of a constraint, lowers the rate of electron transfer by restricting the precise torsional motions that lead to facile intramolecular electron transfer along the backbone. Thus side-bridge stapling provides a unique approach to manipulate energy barriers and conductance in peptides.

Interestingly, the all Aib containing linear peptide **8** (see Figure 6), gave a formal potential shift to the positive of 137 mV and approximate two-fold decrease in the electron transfer rate constant compared to **2**. This peptide adopts essentially the same backbone conformation as the earlier peptides based on NMR and modelling studies. The mean dihedral angles for residues 1-4 of peptide **12** (*N*-protected analogue of **8**) were calculated to be (-56.54° for ϕ) and (-28.52° for ψ), deviating from an ideal 3_{10} -helix by 0.46° and 1.48° respectively (see Figure 7). However, it would be expected to have somewhat reduced backbone flexibility relative to **2** with the inclusion of an additional geminally disubstituted residue. The electrochemical data is consistent with this notion, where the electron transfer rate constant is intermediary between that of the constrained peptide **1** and its linear analogue **2**. This observation further supports the link between backbone flexibility and the rate of electron transfer, as has also been noted for DNA and PNA.¹⁴

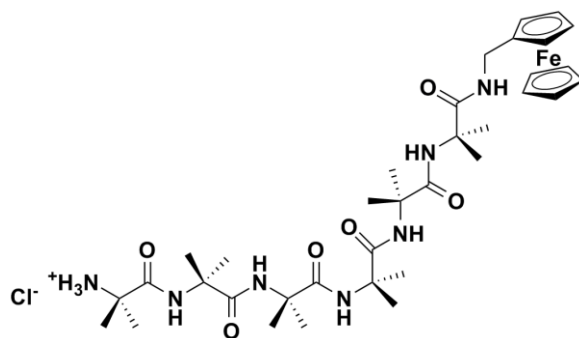


Figure 6. The all Aib containing 3_{10} -helical control peptide **8**.

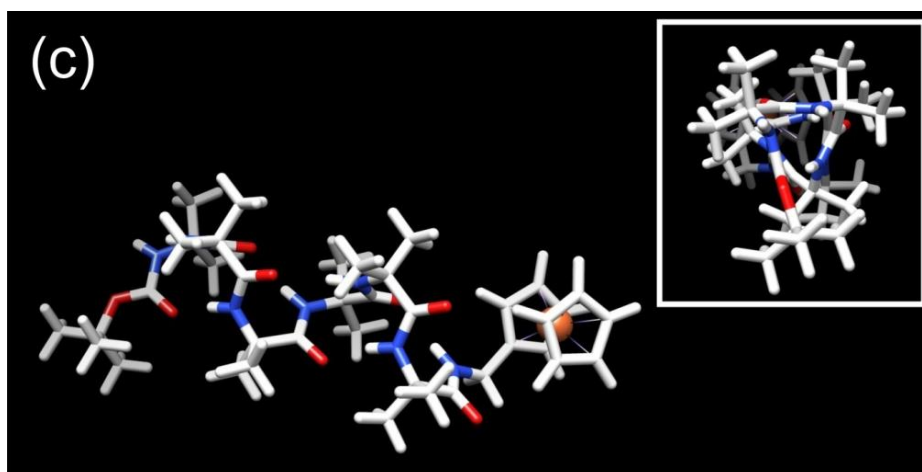


Figure 7. The lowest energy conformer for peptide **12** (*N*-protected analogue of **8**) optimized by the hybrid B3LYP method with 6-31G** basis set. (Inset: top view looking down helix).

2.3.3 Computational study of intramolecular electron transfer

Theoretical calculations, using the latest constrained density functional theory (cDFT),¹⁵ were performed on the model peptides **9** and **10** (see Figure 8) in order to corroborate the experimental observations. These peptides were chosen for this study since they contain the same sequence as **1** and **2**, but with ferrocene units at both termini to act as both a donor and acceptor. Calculation of reorganization energies for electron transfer along the

Chapter 2

backbone then provides an insight into the intramolecular electron transfer dynamics. Diabatic states were constructed by individually localizing an overall charge of 1 on each of the ferrocene units and amino acids, as shown in Figure 8. Diabatic potential profiles were determined by assuming that during an electron hopping step, the nuclear configuration changes smoothly between the optimized geometries of the diabatic states in which the excess charge is localized before and after electron transfer¹⁶ (see Figure 9) Peptides **9** and **10** showed comparable reorganization energies for all electron hopping steps, except those involving diabatic state S3. The reorganization energies for the forward and backward electron hopping steps from diabatic state S3 in **9** are much higher than the corresponding steps in **10** (see Table 2). The introduction of the side-bridge gives rise to a significant increase in reorganization energy, in the range of 3.14 – 6.97 kcal.mol⁻¹ (0.136 eV – 0.302 eV). Thus the higher reorganization energy barrier in peptide **9** is a direct result of the side-bridge constraint, thus further supporting the experimental results.

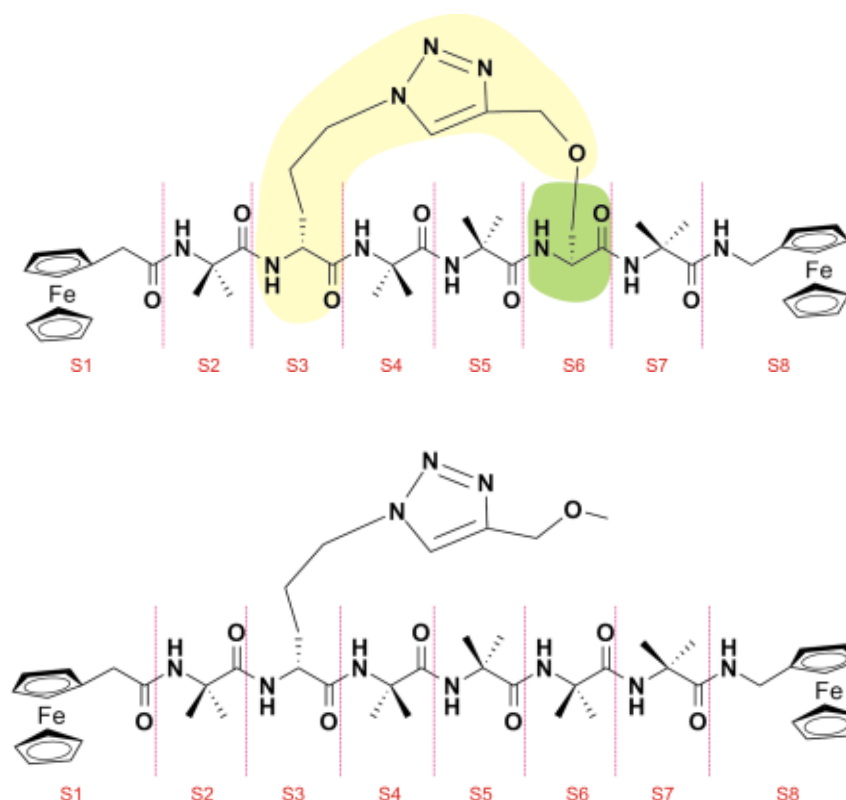


Figure 8. Constructed diabatic states in constrained peptide **9** (top) and unconstrained linear peptide **10** (bottom). Charge localization fragments of the molecule involving the side bridge are indicated using two different colours in peptide **9**.

Chapter 2

Table 2 Comparison of computed reorganization energies for electron hopping steps involving diabatic state S3 in the two model peptides (**9** and **10**).

Hopping step	Peptide 9 (kcal.mol ⁻¹)	Peptide 10 (kcal.mol ⁻¹)	Difference (kcal.mol ⁻¹)
S2 → S3	28.99	24.09	4.90
S3 → S2	30.62	24.57	6.05
S3 → S4	25.41	22.27	3.14
S4 → S3	30.68	23.71	6.97

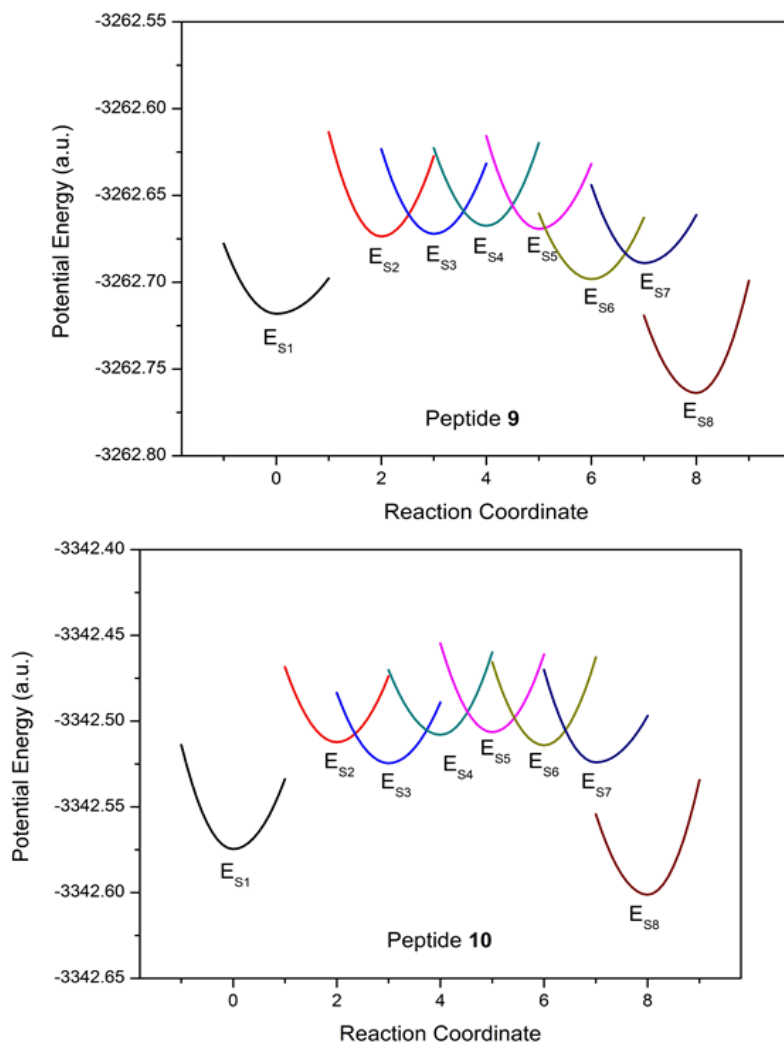


Figure 9. Diabatic potential profiles in the two model peptides **9** (top) and **10** (bottom).

Chapter 2

In summary, electrochemical studies are reported on two peptides containing Aib residues that constrain the backbones into a well-defined 3_{10} -helix, a secondary structure known to favour electron transfer. The first of these peptides (**1**) has its helical geometry stabilized with a covalent constraint that links the i and $i+3$ side chains, resulting in additional conformational rigidity in the backbone. Electrochemical studies revealed that peptide **1** exhibited a significant formal potential shift to the positive (480 mV), and a substantial decrease in the electron transfer rate constant (25%), compared to the unconstrained peptide **2**. These differences reflect the extent of backbone rigidity imparted by the side-bridge constraint. In support, the all Aib containing linear peptide **8** displayed formal potential and electron transfer rate constant values between those of peptides **1** and **2**. This reflects an intermediary backbone rigidity for this peptide. High level calculations confirm that the additional reorganization energy barrier is a direct result of the backbone rigidity imparted by the side-bridge constraint. Thus the tether significantly impedes intramolecular electron transfer by enhancing the rigidity of the peptide backbone. This then generates an additional reorganization energy barrier which restricts the necessary torsional motions that lead to facile intramolecular electron transfer along the backbone. The results provide definitive evidence of a direct link between backbone rigidity and electron transfer in peptides. These findings provide a new means to fine tune the rates of electron transfer in peptides, which represent an important step towards their implementation into molecular electronic assemblies.

2.4 Acknowledgements

We would like to acknowledge the financial support from the Australian Research Council (ARC). The computational aspects of this work were supported for Dr. Jingxian Yu by an award under the National Computational Merit Allocation Scheme.

2.5 Experimental methods

2.5.1 Preparation of Au/SWCNT/ferrocene-derivatised peptide electrode

The SWCNTs (0.2 mg mL^{-1}) functionalized with carboxyl groups, were suspended in a solution of DMSO containing DCC (0.25 mg mL^{-1}) and DMAP (0.14 mg mL^{-1}). Polished flat gold disk electrodes (2 mm diameter) were cleaned in 25 % v/v $\text{H}_2\text{O}_2/\text{KOH}$ (50 mM) for 20 min and then electrochemically cleaned by cycling between 0 and 1.5 V vs. Ag/AgCl in 50 mM KOH. This cleaning process yielded clean gold surfaces with peak separations of 59 mV in 1 mM $\text{Ru}(\text{NH}_3)_6^{+3/2}$ solution. The clean surfaces were then incubated in cysteamine for 24 h resulting in exposed amine groups. These substrates were then exposed to the functionalized SWCNTs/DMSO suspensions for 24 h, after which they were rinsed with propan-2-ol and dried under nitrogen flow. The surfaces were then exposed to 0.01 M ferrocene-derivatised peptide in DMF solution containing 0.5 M HATU and 0.5 M DIPEA for 48 h before being further rinsed and dried, prior to electrochemical analysis.

2.5.2 Chemicals

Fmoc-Aib-OH, Fmoc-OSu, Boc-Aib-OH, Boc-Ser-OH, Boc-Orn-OH, 2-chlorotriyl chloride polystyrene resin, 1-hydroxy-7-azabenzotriazole (HOAt), 2-(1H-7-azabenzotriazol-1-yl)-1,1,3,3-tetramethyl uronium hexafluorophosphate methanaminium (HATU) and 1-ethyl-3-(3-dimethylaminopropyl)carbodiimide HCl (EDC HCl) were purchased from GL Biochem (Shanghai) Ltd., China. Dichloromethane (DCM), diethyl ether, ethyl acetate, methanol and ethanol were purchased from Ajax Finechem Pty Ltd (Australia). Piperidine, acetonitrile, propan-2-ol, LiOH and *N,N*-dimethylformamide (DMF) were purchased from Merck, Australia. Anhydrous *N,N*-Dimethylformamide, dimethyl sulfoxide (DMSO),

2,2,2-trifluoroethanol (TFE), trifluoroacetic acid (TFA), 4M HCl/dioxane solution, *N,N'*-dicyclohexylcarbodiimide (DCC), dimethylaminopyridine (DMAP), cysteamine, $\text{CuSO}_4 \cdot 5\text{H}_2\text{O}$, sodium ascorbate, methyl propargyl ether, trifluoromethane sulfonic anhydride, iodo(triethyl phosphate)copper (I) and diisopropylethyl amine (DIPEA) were purchased from Sigma-Aldrich, Australia. NaHCO_3 was purchased from Chem Supply, Australia. Sodium azide was purchased from BDH Chemicals, UK. Triethylamine was purchased from Scharlau Chemie SA., Spain. Single-walled carbon nanotubes (P2-SWCNTs) were purchased from Carbon Solutions Inc., USA. Ferrocenylmethylamine¹⁷ was prepared as published. All solvents and reagents were used without purification unless noted.

2.5.3 NMR spectroscopy

¹H NMR spectra were recorded in DMSO-*d*₆ or CDCl_3 solutions using a Varian Gemini-300 NMR. ¹³C NMR and two-dimensional NMR experiments utilized COSY, ROESY, HSQC and HMBC were obtained on a Varian Inova 600 MHz spectrometer. Chemical shifts are reported in ppm (δ) using TMS (0.00 ppm) as the internal standard. Signals are reported as s (singlet), d (doublet), t (triplet) or m (multiplet).

2.5.4 Mass spectroscopy

Low resolution mass spectral data were analyzed using a Finnigan MAT LCQ spectrometer with MS/MS and ESI probe, utilizing XCalibur software. High resolution mass spectral data were analyzed using an Ultimate 3000 RSL HPLC (Thermo Fisher Scientific Inc., MA) and an LTQ Orbitrap XL ETD using a flow injection method, with a flow rate of 5 $\mu\text{L}/\text{min}$. The HPLC flow is interfaced with the mass spectrometer using the Electrospray source (Thermo Fisher Scientific Inc., MA). Mass spectra were obtained over a range of $100 < m/z < 1000$. Data was analyzed using XCalibur software (Version 2.0.7, Thermo Fisher Scientific).

2.5.5 Circular dichroism (CD)

CD spectra were acquired with a JASCO J-815 CD spectrometer (JASCO, UK) using an optical cell of 0.1 cm optical path length at the residue concentration of 2.7 mM in methanol at 22°C. Ten scans were taken with the following control parameters: scan speed, 10 nm min^{-1} ; slit width, 0.2 nm; bandwidth, 1 nm; response time, 0.5 s and N_2

purging flow rate, 10 L/min. These scans were averaged, and a blank solvent spectrum was subtracted to generate the corrected spectrum.

2.5.6 FTIR spectroscopy

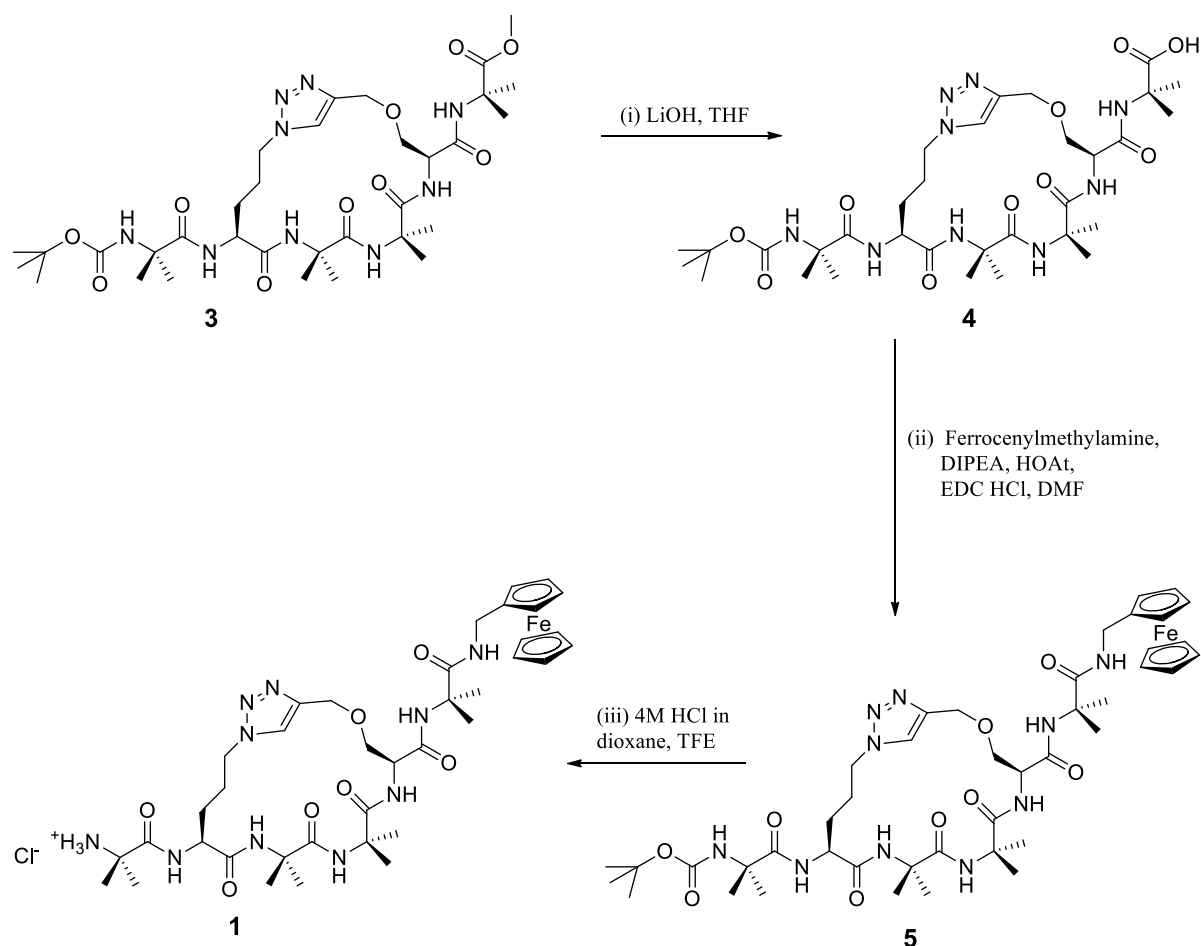
Infrared spectra were collected on a Perkin Elmer Spectrum 100 FT-IR spectrometer, with attenuated total reflectance (ATR) imaging capabilities, fitted with a ZnSe crystal, with an average reading taken from 4 scans at 4 cm⁻¹ resolution.

2.5.7 High-performance liquid chromatography (HPLC)

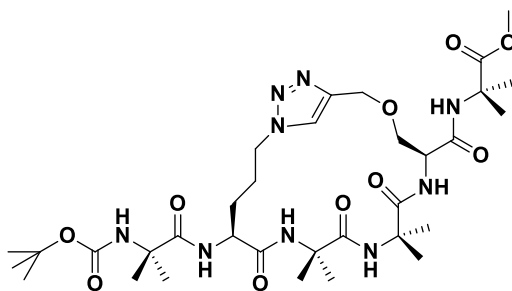
The synthetic peptides were analyzed and purified by reverse phase HPLC, using an HP 1100 LC system equipped with a Phenomenex C18 column (250 x 4.6 mm) for analytical traces and a Phenomenex C18 column (250 x 21.2 mm) for purification, a photodiode array detector, and a Sedex evaporative light scattering detector. ACN/TFA (100/0.0008 by v/v) and water/TFA (100/0.001 by v/v) solutions were used as organic and aqueous buffers.

2.5.8 Peptide synthesis

Scheme 2. The final synthetic steps for Peptide 1.



Peptide 3



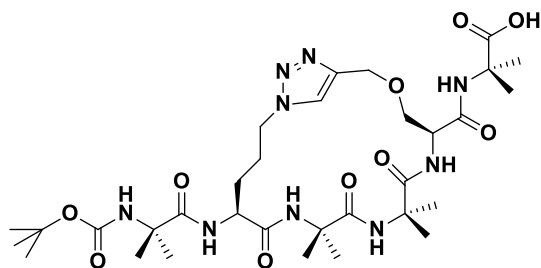
(5*S*,14*S*)-14-((1-methoxy-2-methyl-1-oxopropan-2-yl)carbamoyl)-8,8,11,11-tetramethyl-6,9,12-trioxo-16-oxa-1,7,10,13,19,20-hexaazabicyclo[16.2.1]henicoso-18(21),19-dien-5-aminium 2,2,2-trifluoroacetate¹⁰ (100 mg, 0.15 mmol) was added to Boc-Aib-OH (36 mg, 0.18 mmol) and the mixture dissolved in anhydrous DMF (2.4 mL). Anhydrous DIPEA (68 mg, 0.525 mmol), HOAt hydrate (20 mg, 0.15 mmol) and EDC HCl (31 mg, 0.165 mmol) were added, and the reaction mixture was stirred at rt for 41 hours, under an N₂ atmosphere. The reaction mixture was diluted with DCM (40 mL) and washed with 5% (w/w) citric acid (1 x 25 mL), K₂CO₃ (7.5% w/w) (1 x 25 mL) and brine (25 mL), and dried with MgSO₄. The crude product was purified using column chromatography (eluent DCM/MeOH (95/5%)) and the solvent removed *in vacuo*, yielding a white precipitate (50 mg, 38%).

¹H NMR (600 MHz, CDCl₃) δ 7.91 (s, 1H), 7.78 (s, 1H), 7.51 (s, 1H), 7.24 (d, 1H, *J*=9.1 Hz), 7.07 (s, 1H), 6.72 (br s, 1H), 5.22 (s, 1H), 4.78 (ddd, 1H, *J*=8.9, 5.3, 3.4 Hz), 4.72 (d, 1H, *J*=12.1 Hz), 4.58 (d, 1H, *J*=12.1 Hz), 4.48 (m, 1H), 4.38 (ddd, 1H, *J*=14.0, 6.9, 3.7 Hz), 4.12 (dd, 1H, *J*=8.9, 5.3 Hz), 3.69 (s, 3H), 3.66 (dd, 1H, *J*=9.0, 3.4 Hz), 2.87 (m, 1H), 2.16 (m, 1H), 1.95 (m, 1H), 1.79 (m, 1H), 1.74 (m, 1H), 1.55 (s, 3H), 1.52 (s, 6H), 1.46 (s, 3H), 1.44 (s, 3H), 1.41 (s, 3H), 1.39 (s, 15H).

¹³C NMR (150 MHz, CDCl₃) δ 175.2, 175.1, 174.8, 174.8, 171.4, 169.5, 155.6, 145.7, 124.6, 81.4, 77.2, 77.0, 76.7, 69.4, 65.0, 56.9, 56.8, 56.0, 53.9, 53.6, 52.2, 50.1, 29.3, 28.2, 27.7, 27.2, 27.0, 25.1, 24.7, 24.1, 23.4, 23.2, 22.9.

HRMS (*m/z*): [MH]⁺ calculated for C₃₃H₅₆N₉O₁₀ 738.4144, found 738.4141.

Peptide 4



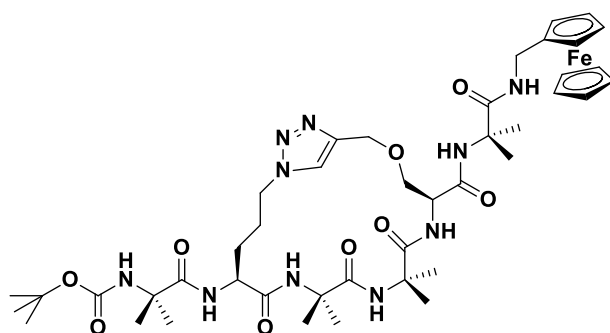
Peptide **3** (64 mg, 0.09 mmol) was dissolved in 1:1 THF/H₂O (20 mL / 1 g ester). 2M LiOH (8 equivs.) was added and the reaction mixture stirred at rt for 42 hours. THF was removed *in vacuo* and the resultant solution neutralized with 2M HCl and lyophilized to yield the desired acid (white precipitate) in quantitative yield.

¹H NMR (600 MHz, DMSO-d₆) δ 8.23 (s, 1H), 8.00 (s, 1H), 7.90 (s, 1H), 7.52 (s, 1H), 7.41 (s, 1H), 7.33 (s, 1H), 7.27 (d, 1H, *J*=9.0 Hz), 4.73 (d, 1H, *J*=13.0 Hz), 4.45 – 4.25 (m, 4H), 3.74 (m, 1H), 3.63 (m, 1H), 3.59 (m, 1H), 1.96 (m, 1H), 1.77 (m, 1H), 1.74 (m, 1H), 1.53 (m, 1H), 1.38 – 1.22 (m, 33H).

¹³C NMR (150 MHz, DMSO-d₆) δ 175.5, 174.6, 174.0, 172.7, 168.2, 155.2, 143.1, 124.8, 79.1, 78.9, 78.7, 68.4, 63.3, 56.1, 56.0, 55.7, 54.1, 52.7, 50.2, 47.9, 31.2, 28.9, 28.6, 28.1, 27.3, 26.0, 25.7, 24.6, 24.4, 23.3, 22.8, 22.0.

HRMS (*m/z*): [MH]⁺ calculated for C₃₂H₅₄N₉O₁₀ 724.3988, found 724.3997.

Peptide 5



Chapter 2

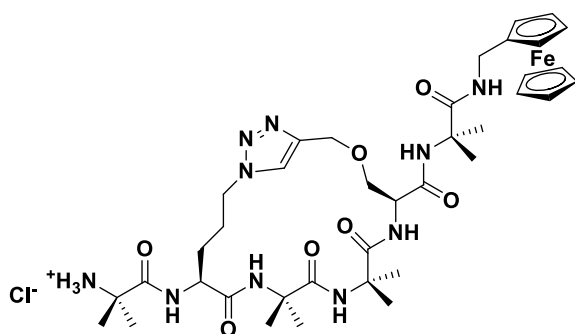
Peptide **4** was dissolved in anhydrous DMF (1.4 mL / 100 mg propanoic acid) and ferrocenylmethylamine (1.1 equiv.) was added. Anhydrous DIPEA (3.5 equiv.) was added, followed by HOAt (1 equiv.) and EDC HCl (1.1 equiv.) and the reaction mixture was stirred under an N₂ atmosphere at rt for 42 hr. Solvent removed to reveal a brown solid. The product was purified by reverse phase HPLC.

¹H NMR (600 MHz, DMSO-d₆) δ 8.33 (br s, 1H), 8.02 (s, 1H), 7.88 (s, 1H), 7.57 (s, 1H), 7.45 (s, 1H), 7.37 (s, 1H), 7.33 (d, 1H, *J*=7.6 Hz), 7.09 (s, 1H), 4.74 (d, 1H, *J*=13.3 Hz), 4.45 – 4.34 (m, 3H), 4.30 (s, 1H), 4.25 – 3.50 (m, 14H), 1.91 (d, 1H, *J*=4.2 Hz), 1.78 (m, 1H), 1.60 – 1.51 (m, 2H), 1.42 (s, 9H), 1.41 – 1.39 (m, 6H), 1.35 (s, 6H), 1.34 (s, 6H), 1.32 (s, 6H).

¹³C NMR (150 MHz, DMSO-d₆) δ 175.4, 174.9, 174.7, 173.17, 173.13, 168.8, 155.3, 143.0, 124.9, 78.8, 68.3 (Cp), 67.9 (Cp), 67.0, 64.8, 63.4, 56.4, 56.04, 56.02, 55.7, 54.8, 52.7, 47.9, 40.0, 37.8, 28.1, 26.9, 25.9, 25.57, 25.54, 25.0, 24.7, 24.6, 23.4, 22.9.

HRMS (*m/z*): [M]⁺ calculated for C₄₃H₆₄FeN₁₀O₉ 920.4201, found 920.4208.

Peptide 1



Compound **5** (9.5 mg, 0.01 mmol) was dissolved in trifluoroethanol (2.5 mL) and 4M HCl in dioxane (2.5 mL) was added. The reaction mixture was stirred at rt for 30 min. and the solvent was removed *in vacuo*. A subsequent HPLC trace confirmed the presence of starting material only, indicating that the reaction had not proceeded. The sample was

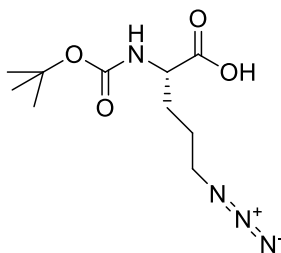
Chapter 2

again dissolved in trifluoroethanol (2.5 mL) and another 4M HCl in dioxane (2.5 mL) was added. The reaction mixture was stirred at rt for a further 30 min., and the solvent removed *in vacuo*. The product was purified by reverse phase HPLC to yield a sandy precipitate (3 mg, 35%).

^1H NMR (600 MHz, DMSO- d_6) δ 8.23 (d, 1H, $J=7.1$ Hz), 8.12 (s, 4H), 7.95 (s, 1H), 7.74 (s, 1H), 7.59 (br s, 1H), 7.24 (br s, 1H), 7.19 (s, 1H), 4.73 (d, 1H, $J=13.3$ Hz), 4.49 – 4.39 (m, 4H), 4.25 – 3.63 (m, 11H), 3.48 (t, 1H, $J=5.3$ Hz), 3.41 (m, 1H), 1.90 – 1.81 (d, 1H, $J=6.3$ Hz), 1.76 – 1.70 (dt, 1H, $J=14.1, 5.6$ Hz), 1.50 – 1.32 (m, 26H).

^{13}C NMR (150 MHz, DMSO- d_6) δ 174.7, 174.0, 171.8, 171.3, 168.7, 157.7, 157.5, 143.6, 124.3, 72.2, 68.3, 67.0, 63.3, 60.2, 56.4, 56.0, 55.9, 54.0, 52.8, 48.8, 40.0, 37.8, 35.0, 27.1, 26.2, 25.7, 25.6, 25.5, 24.4, 23.4, 23.3, 23.2.

HRMS (m/z): $[\text{M}]^+$ calculated for $\text{C}_{38}\text{H}_{56}\text{FeN}_{10}\text{O}_7$ 820.3677, found 820.3684.

5-azido-2-((*tert*-butoxycarbonyl)amino)pentanoic acid

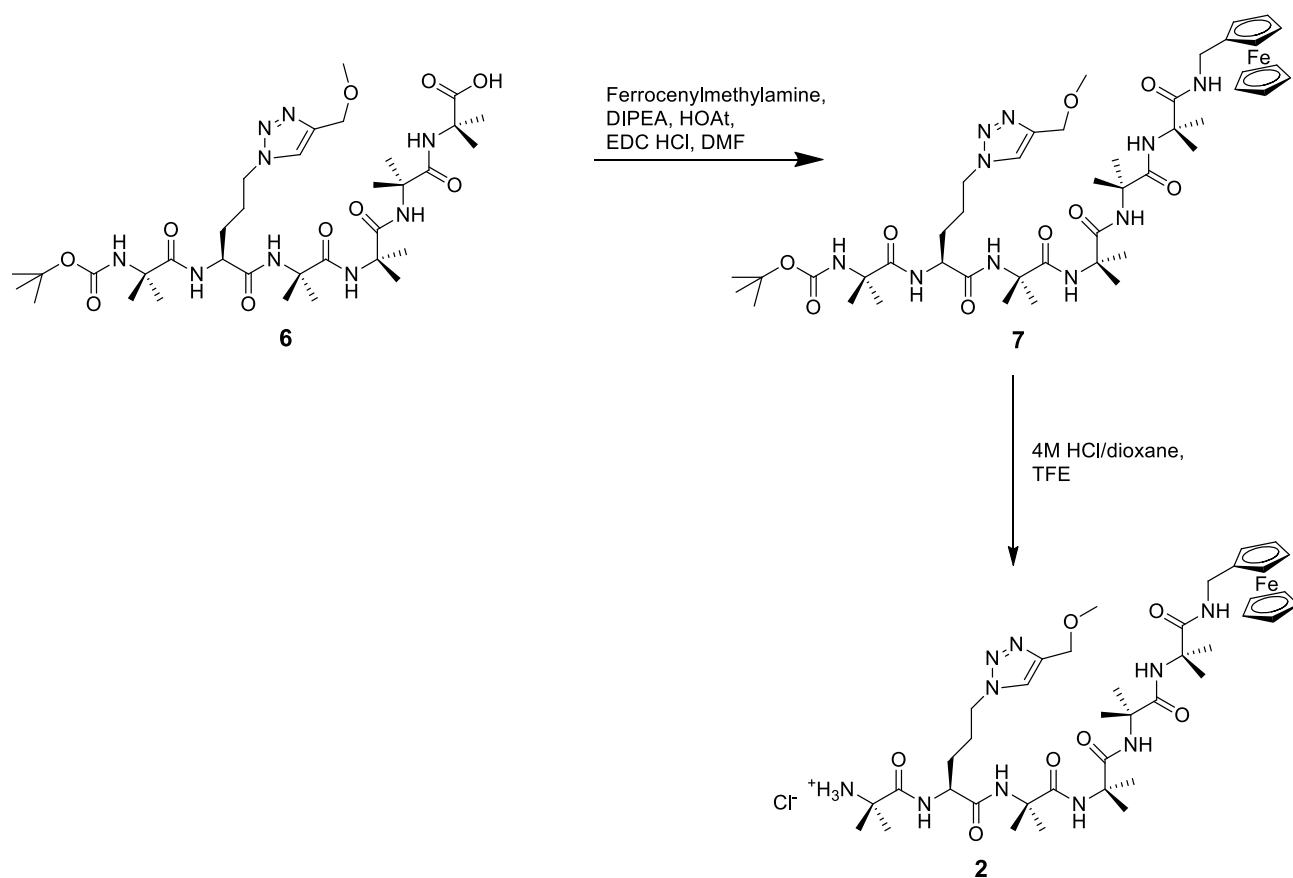
Sodium azide (3.8 g, 0.06 mol) was suspended in anhydrous acetonitrile (60 mL) and cooled to 0°C in an ice bath, with stirring, under a nitrogen atmosphere. Trifluoromethanesulfonic anhydride (13.7 g, 0.05 mol, 8.2 mL) was added dropwise and the solution stirred for 3 h. The mixture was filtered, giving a solution of crude triflic azide. 5-amino-2-((*tert*-butoxycarbonyl)amino)pentanoic acid (8.3 g, 0.04 mol) was suspended in acetonitrile (100 mL) and de-ionised H₂O (40 mL) and the mixture vigorously stirred. Triethylamine (12.3 g, 0.12 mol, 17 mL) and CuSO₄ pentahydrate (0.10 g, 0.4 mmol) were added and the mixture cooled in an ice bath to 0°C. The triflic azide solution was added dropwise and the reaction stirred for 24 h at rt. The acetonitrile was evaporated and the remaining aqueous solution washed with ethyl acetate (2 x 100 mL). The aqueous phase was acidified with 2 M HCl (40 mL) and extracted with ethyl acetate (100 mL). The organic phase was dried over MgSO₄, filtered, and the solvent evaporated. The organic phase was subjected to column chromatography (eluent: DCM/MeOH (99:1)), to provide crude compound as a pale yellow, oily residue (1.82 g). The triflyl amide by-product formed a precipitate following the addition of cold chloroform, and filtration yielded a pure compound as pale yellow oil (4.79 g, 50%).

¹H NMR (300 MHz, d₆-DMSO) δ 12.40 (s, 1H), 7.13–7.10 (d, 1H, *J*=8.0 Hz), 3.87–3.76 (m, 1H), 3.32–3.28 (t, 2H, *J*=6.4 Hz), 1.80–1.50 (m, 4H), 1.37 (s, 9H).

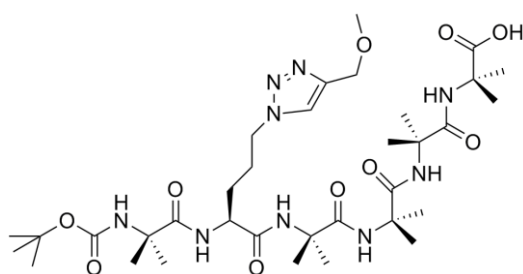
FTIR: 2098.07 cm⁻¹ (Azide peak).

Chapter 2

Scheme 3. The final synthetic steps for Peptide 2.



Peptide 6



Chapter 2

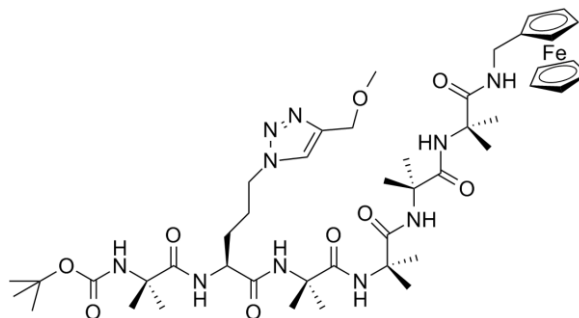
Peptide **6** was synthesized using standard Fmoc solid phase synthesis. Stepwise coupling of *N*αF-moc protected Aib amino acids using reagents HATU and DIPEA was conducted on 2-chlorotrityl resin with a 0.4 mmol/g loading capacity. Fmoc protected Aib amino acid (1.5 g, 4.4 mmol) was weighed out and DMF (6 mL) was added, followed by DIPEA (3 molar equiv.) and 0.5M HATU/DMF (6 mL). The solution was placed in a sintered glass funnel with Teflon stopcock, and left to react for 2 hr. Fmoc deprotection was performed using piperidine (25% v/v) in DMF, which was added to the resin/peptide and left to stand for 30 mins. The solution was drained and the resin washed with DCM (3 x 20 mL), DMF (3 x 20 mL) and DCM (3 x 20 mL), before a TNBS test confirmed the presence of a terminal primary amine. This process was repeated until the peptide reached four residues in length. (2*S*)-2-(9H-fluoren-9-ylmethoxycarbonylamino)-5-[4-(methoxymethyl)triazol-1-yl]pentanoic acid (0.6 g, 1.3 mmol) was then added to the growing peptide using the above-mentioned procedure. The final residue, Boc-Aib-OH was added, before the peptide was cleaved from the resin using TFA/DCM (1% v/v) for 15 min. The solvent was removed *in vacuo*.

¹H NMR (600 MHz, DMSO-*d*₆): δ 8.21 (m, 1H), 8.19 (m, 1H), 8.03 (s, 1H), 7.56 (s, 1H), 7.29 (s, 1H), 7.27 (s, 1H), 7.25 (s, 1H), 4.42 (s, 2H), 4.35 (t, 2H, *J*=7.0 Hz), 3.91 (s, 1H), 3.25 (s, 3H), 1.88 – 1.78 (m, 2H), 1.71 – 1.65 (m, 2H), 1.37 – 1.28 (m, 39H).

¹³C NMR (150 MHz, DMSO-*d*₆) δ 175.8, 175.7, 174.5, 173.4, 173.1, 172.2, 143.6, 123.6, 116.1, 114.2, 78.6, 64.9, 57.1, 56.0, 55.9, 55.6, 54.8, 54.5, 53.7, 48.8, 28.0, 26.6, 26.3, 25.2, 25.0, 24.8, 24.6, 24.5.

LRMS (*m/z*): [M+H]⁺ calculated for C₃₄H₅₉N₉O₁₀ 754.4, found 754.4.

Peptide 7



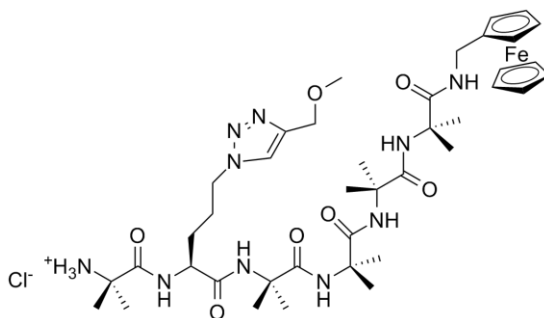
Peptide **6** (190 mg, 0.25 mmol) was dissolved in anhydrous DMF (4.2 mL) and ferrocenylmethylamine (59 mg, 0.27 mmol) added. The solution was stirred briefly, followed by the addition of 174 μ L of anhydrous DIPEA (129 mg, 1.00 mmol), HOAt (34 mg, 0.25 mmol) and HATU (105 mg, 0.27 mmol). The reaction was stirred at rt for 19 hours, and the solvent removed *in vacuo*. The residue was taken up in EtOAc (40 mL) and H₂O (40 mL). The pH was adjusted to pH 2-3 and the organic layer separated and washed with NaHCO₃ (40 mL) and brine (40 mL), before drying over MgSO₄. The solvent was removed *in vacuo* to yield a brown solid (150 mg). Purification on HPLC yielded a light brown solid (16%).

¹H NMR (600 MHz, DMSO-d₆): δ 8.24 (bs, 1H), 8.18 (bs, 1H), 8.03 (s, 1H), 7.67 (s, 1H), 7.57 (s, 1H), 7.52 (bs, 1H), 7.32 (s, 1H), 7.30 (bs, 1H), 4.42 (s, 2H), 4.36 (t, 2H, $J=7.0$ Hz), 4.22 – 3.94 (m, 12H), 3.24 (s, 3H), 1.88 – 1.78 (m, 2H), 1.71 – 1.66 (m, 2H), 1.41 – 1.30 (m, 39H).

¹³C NMR (150 MHz, DMSO-d₆) δ 175.6, 174.9, 174.7, 173.7, 173.4, 172.3, 155.0, 143.6, 123.6, 78.6, 68.3, 66.8, 64.9, 57.1, 56.2, 56.1, 56.0, 55.8, 55.6, 53.6, 48.8, 40.0, 37.7, 28.0, 26.8, 26.2, 25.7, 25.1, 24.7, 24.2.

LRMS (m/z): [M]⁺ calculated for C₄₅H₇₀FeN₁₀O₉ 950.4, found 950.4.

Peptide 2

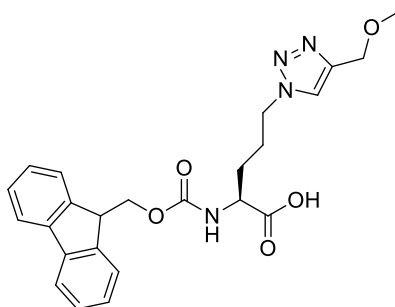


Peptide **7** (25 mg, 0.03 mmol) was dissolved in TFE (2 mL) and stirred at rt for 5 mins. 4M HCl in dioxane (2 mL) was added dropwise and the reaction mixture stirred at rt for 25 mins. The solvent was removed *in vacuo* and purified on reverse phase HPLC to reveal a pale yellow solid (58%).

^1H NMR (600 MHz, DMSO- d_6): δ 8.49 (s, 1H), 8.25 (d, 1H, $J=7.2$ Hz), 8.12 (bs, 3H), 8.08 (s, 1H), 7.69 (s, 1H), 7.61 (s, 1H), 7.53 (bs, 1H), 7.39 (bs, 1H), 4.43 (s, 2H), 4.37 (m, 2H), 4.29 (m, 1H), 4.25 – 3.88 (m, 11H), 3.26 (s, 3H), 1.93 – 1.81 (m, 3H), 1.68 – 1.61 (m, 1H), 1.50 – 1.28 (m, 30H).

^{13}C NMR (150 MHz, DMSO- d_6) δ 174.8, 174.2, 173.3, 171.8, 171.6, 158.0, 157.8, 143.7, 123.7, 68.4, 64.9, 57.3, 56.3, 56.0, 55.9, 55.8, 52.9, 48.9, 28.9, 28.6, 27.9, 26.5, 25.7, 25.1, 24.8, 24.6, 24.4, 24.3, 23.4, 23.3.

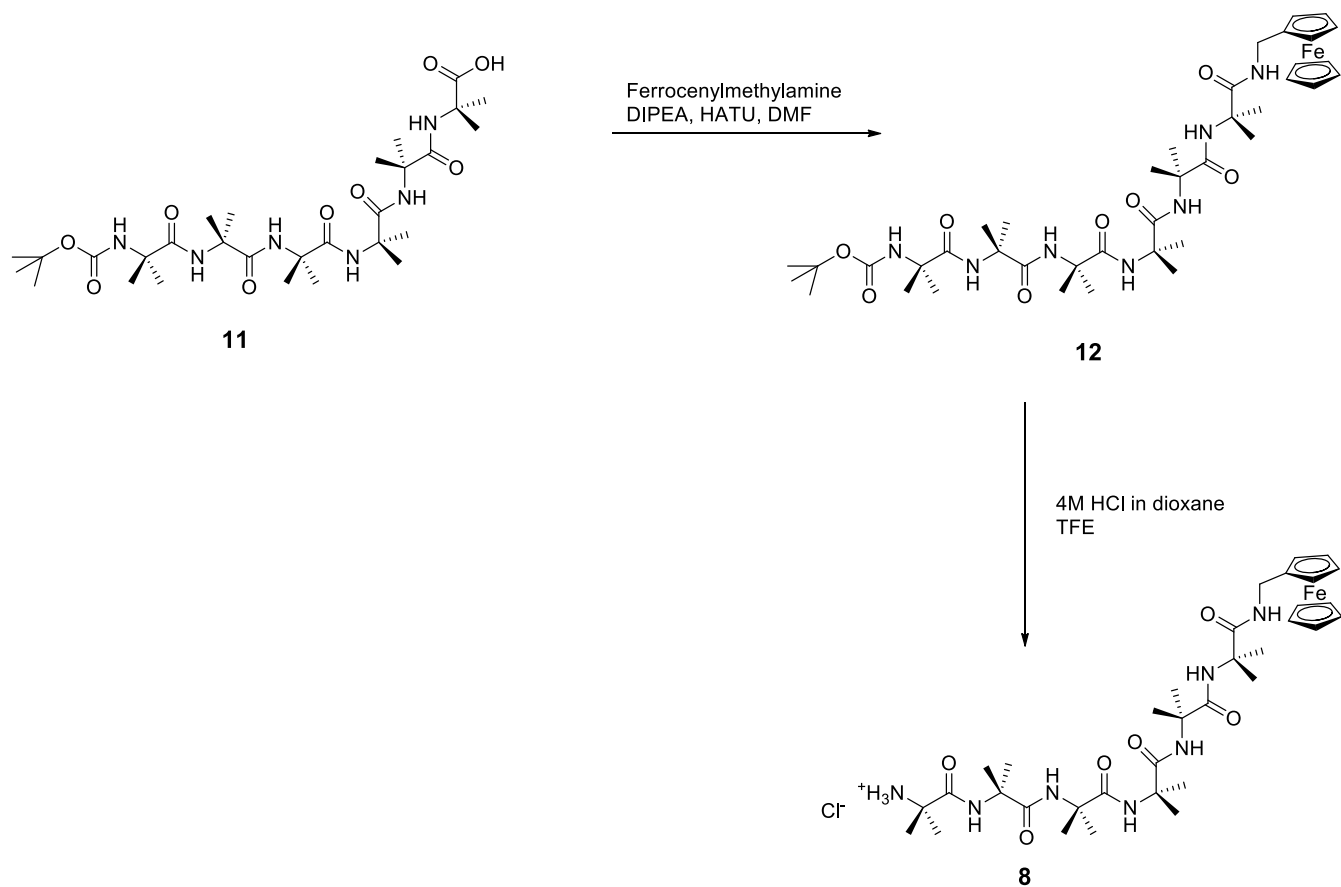
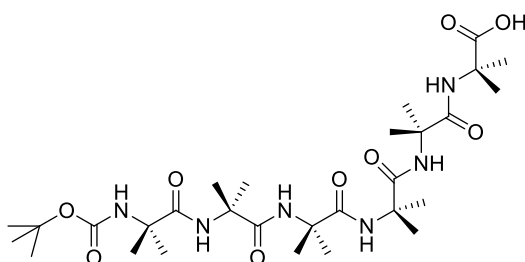
LRMS (m/z): $[\text{M} + \text{Na}]^+$ calculated for $\text{C}_{40}\text{H}_{63}\text{FeN}_{10}\text{O}_7$ 873.4, found 873.4.

(2S)-2-(9H-fluoren-9-ylmethoxycarbonylamino)-5-[4-(methoxymethyl)triazol-1-yl]pentanoic acid

5-azido-2-((*tert*-butoxycarbonyl)amino)pentanoic acid (2.0 g, 7.8 mmol) was dissolved in DCM (110 mL) and H₂O (110 mL). Methyl propargyl ether (550 mg, 7.8 mmol) was added, followed by CuSO₄·5H₂O (971 mg, 3.9 mmol) and sodium ascorbate (386 mg, 1.95 mmol), and the solution stirred at rt for 23 hr. The organic phase was separated and dried with MgSO₄ to yield a pale green solid (1.5 g, 59%). The Boc protecting group was then removed using DCM/TFA (50% v/v) over 30 min. to obtain a pale green oil (quant.). This compound was then dissolved in 1,4-dioxane, and NaHCO₃ (2 equiv.) and Fmoc-OSu (1 equiv.) added. The pH was adjusted to pH 9 by the addition of NaOH and the mixture stirred at rt for 30 hr. The organic solvent was removed *in vacuo* and 2.5% (w/w) NaCO₃ (50 mL) added and washed with diethyl ether (3 x 30 mL), before being acidified to pH 1. The product was extracted with EtOAc (3 x 50 mL), washed with brine (150 mL) and dried with MgSO₄. The solvent was removed *in vacuo* to yield a pale yellow solid (71%).

¹H NMR (600 MHz, DMSO-d₆): δ 8.08 (s, 1H), 7.89 (d, 2H, *J*=7.5 Hz), 7.72 (dd, 2H, *J*=7.4, 2.4 Hz), 7.68 (d, 1H, *J*=8.1 Hz), 7.41 (t, 2H, *J*=7.5 Hz), 7.32 (td, 2H, *J*=7.4, 2.6 Hz), 4.44 (s, 2H), 4.36 (t, 2H, *J*=7.0 Hz), 4.32 – 4.27 (m, 2 H), 4.22 (t, 1H, *J*=7.0 Hz), 3.98 (td, 1H, *J*=8.9, 5.0 Hz), 3.26 (s, 3H), 1.90 – 1.83 (m, 2H), 1.70 – 1.64 (m, 1H), 1.61 – 1.55 (m, 1H).

¹³C NMR (150 MHz, DMSO-d₆) δ 173.4, 156.1, 143.8, 143.7, 140.6, 127.5, 127.0, 125.3, 125.2, 123.7, 120.1, 120.0, 66.3, 65.5, 64.9, 59.7, 57.2, 53.2, 48.8, 46.6, 27.7, 26.5.

Scheme 4. The final synthetic steps for Peptide **8**.**Peptide 11**

Peptide **11** was synthesized using standard Fmoc solid phase synthesis. Stepwise coupling of *N*^F-moc protected Aib amino acids using reagents HATU and DIPEA was conducted on 2-chlorotrityl resin with a 0.6 mmol/g loading capacity. Fmoc protected Aib amino acid

Chapter 2

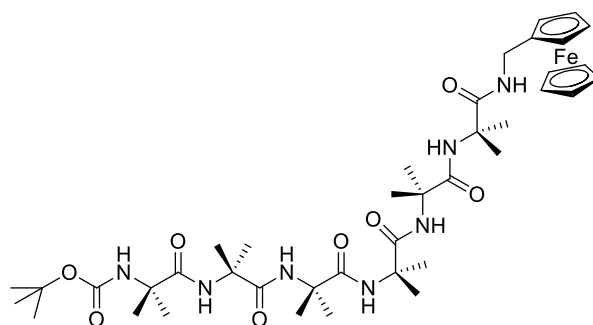
(1.3 g, 4.0 mmol) was weighed out and DMF (10 mL) was added, followed by DIPEA (2 molar equiv.) and 0.5M HATU/DMF (7 mL). The solution was placed in a sintered glass funnel with Teflon stopcock, and left to react for 2 hr. Fmoc deprotection was performed using piperidine (25% v/v) in DMF, which was added to the resin/peptide and left to stand for 30 mins. The solution was drained and the resin washed with DCM (3 x 20 mL), DMF (3 x 20 mL) and DCM (3 x 20 mL) before a TNBS test confirmed the presence of terminal primary amine. This process was repeated until the peptide reached five residues in length, with the final residue replaced with Boc-Aib-OH. The peptide was cleaved from the resin using TFA/DCM (1% v/v) for 15 min. The solvent was removed *in vacuo* and the peptide purified using reverse phase HPLC.

^1H NMR (600 MHz, DMSO- d_6): δ 11.82 (br s, 1H), 8.33 (s, 1H), 7.95 (s, 1H), 7.81 (s, 1H), 7.42 (s, 1H), 7.31 (s, 1H), 7.27 (s, 1H), 1.44 (s, 9H), 1.36 – 1.30 (m, 36H).

^{13}C NMR (150 MHz, DMSO- d_6): δ 175.3, 175.1, 175.0, 173.4, 155.4, 79.0, 56.0, 55.9, 55.8, 55.7, 55.6, 54.5, 40.0, 28.9, 28.0, 24.6.

LRMS (m/z): $[\text{M} + \text{Na}]^+$ calculated for $\text{C}_{29}\text{H}_{52}\text{N}_6\text{O}_9$ 651.7, found 651.2.

Peptide 12



Peptide **11** (150 mg, 0.24 mmol) and ferrocenylmethylamine (51 mg, 0.24 mmol) were dissolved in anhydrous DMF (2 mL). DIPEA (4 equiv.) and HATU (4 equiv.) were added

Chapter 2

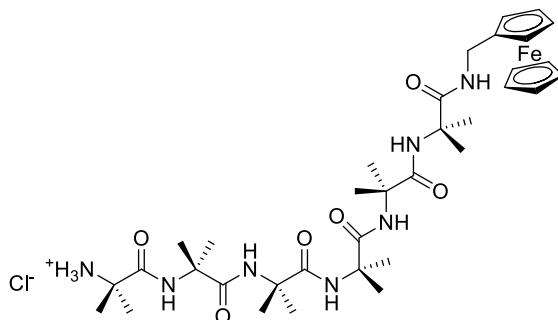
and the reaction mixture stirred under an N₂ atmosphere at rt for 24 hr. The solvent was removed *in vacuo* and the peptide purified using reverse phase HPLC.

¹H NMR (300 MHz, DMSO-d₆) δ 8.36 (s, 1H), 7.98 (s, 1H), 7.89 (s, 1H), 7.64 (s, 1H), 7.53 (t, 1H, *J*=6.1 Hz), 7.43 (s, 1H), 7.31 (s, 1H), 4.22 (s, 2H), 4.16, (s, 5H), 4.04 (m, 2H), 4.01 (d, 2H, *J*=6.1 Hz), 1.44 – 1.31 (m, 45H).

¹³C NMR (150 MHz, DMSO-d₆) δ 175.7, 175.4, 159.0, 119.1, 109.5, 86.6, 68.3, 66.9, 66.8, 56.0, 55.8, 41.0, 40.0, 28.9, 28.0, 24.4, 22.0.

LRMS (*m/z*): [M + Na]⁺ calculated for C₄₀H₆₃FeN₇O₈Na 848.4, found 848.2.

Peptide 8



Peptide **12** (10 mg, 0.012 mmol) was dissolved in trifluoroethanol (1 mL) and 4M HCl in dioxane (200 μL) was added. The reaction mixture was stirred at rt for 20 min. The solvent was removed *in vacuo* and the peptide purified using reverse phase HPLC.

¹H NMR (600 MHz, DMSO-d₆) δ 8.43 (s, 1H), 8.04 (s, br 3H), 7.92 (s, 1H), 7.72 (s, 1H), 7.50 (t, 1H, *J*=6.0 Hz), 7.36 (s, 1H), 7.34 (s, 1H), 4.19 (s, 2H), 4.13 (s, 5H), 4.00 (s, 2H), 3.98 (d, 2H, *J*=6.0 Hz), 1.51 (s, 6H), 1.39 – 1.29 (m, 30H).

¹³C NMR (150 MHz, DMSO-d₆) δ 175.3, 174.5, 174.2, 173.8, 173.5, 171.7, 86.7, 68.7, 68.3, 66.9, 66.8, 56.4, 56.3, 56.1, 56.0, 55.9, 55.8, 40.0, 37.7, 25.5, 24.9, 24.5, 24.1, 23.3.

HRMS (*m/z*): [MH]⁺ calculated for C₃₅H₅₆FeN₇O₆ 726.3636, found 726.3631.

2.6 References

1. (a) Mandal, H. S.; Kraatz, H.-B., Electron Transfer Mechanism in Helical Peptides. *J. Phys. Chem. Lett.* **2012**, *3* (6), 709; (b) Malak, R. A.; Gao, Z. N.; Wishart, J. F.; Isied, S. S., Long-range electron transfer across peptide bridges: The transition from electron superexchange to hopping. *J. Am. Chem. Soc.* **2004**, *126* (43), 13888; (c) Brooksby, P. A.; Anderson, K. H.; Downard, A. J.; Abell, A. D., Voltammetric and Electrochemical Impedance Study of Ferrocenyl Containing beta-Peptide Monolayers on Gold. *J. Phys. Chem. C* **2011**, *115* (15), 7516; (d) Yu, J.; Huang, D. M.; Shapter, J. G.; Abell, A. D., Electrochemical and Computational Studies on Intramolecular Dissociative Electron Transfer in beta-Peptides. *J. Phys. Chem. C* **2012**, *116* (50), 26608.
2. Arikuma, Y.; Nakayama, H.; Morita, T.; Kimura, S., Electron Hopping over 100 angstrom Along an alpha Helix. *Angew. Chem. Int. Ed.* **2010**, *49* (10), 1800.
3. (a) Gao, J. A.; Muller, P.; Wang, M.; Eckhardt, S.; Lauz, M.; Fromm, K. M.; Giese, B., Electron Transfer in Peptides: The Influence of Charged Amino Acids. *Angew. Chem. Int. Ed.* **2011**, *50* (8), 1926; (b) Watanabe, J.; Morita, T.; Kimura, S., Effects of dipole moment, linkers, and chromophores at side chains on long-range electron transfer through helical peptides. *J. Phys. Chem. B* **2005**, *109* (30), 14416.
4. (a) Yu, J.; Zvarec, O.; Huang, D. M.; Bissett, M. A.; Scanlon, D. B.; Shapter, J. G.; Abell, A. D., Electron Transfer through α -Peptides Attached to Vertically Aligned Carbon Nanotube Arrays: A Mechanistic Transition. *Chem. Commun.* **2012**, *48* (8), 1132; (b) Yu, J.; Horsley, J. R.; Abell, A. D., The Influence of Secondary Structure on Electron Transfer in Peptides. *Aust. J. Chem.* **2013**, *66*, 848.
5. (a) Schlag, E. W.; Sheu, S. Y.; Yang, D. Y.; Selzle, H. L.; Lin, S. H., Charge conductivity in peptides: Dynamic simulations of a bifunctional model supporting experimental data. *Proc. Natl. Acad. Sci. U. S. A.* **2000**, *97* (3), 1068; (b) Schlag, E. W.; Sheu, S. Y.; Yang, D. Y.; Selzle, H. L.; Lin, S. H., Distal charge transport in peptides. *Angew. Chem. Int. Ed.* **2007**, *46* (18), 3196.
6. (a) Okamoto, S.; Morita, T.; Kimura, S., Electron Transfer through a Self-Assembled Monolayer of a Double-Helix Peptide with Linking the Terminals by Ferrocene. *Langmuir* **2009**, *25* (5), 3297; (b) Orłowski, G. A.; Chowdhury, S.; Kraatz, H. B., The effect of alkali metal ions on the electrochemical behavior of ferrocene-peptide conjugates immobilized on gold surfaces. *Electrochim. Acta* **2007**, *53* (4), 2034; (c) Takeda, K.; Morita, T.; Kimura, S., Effects of monolayer structures on long-range electron transfer in helical peptide monolayer. *J. Phys. Chem. B* **2008**, *112* (40), 12840; (d) Galka, M. M.; Kraatz, H. B., Electron transfer studies on self-assembled monolayers of helical ferrocenoyl-oligoproline-cystamine bound to gold. *Chemphyschem* **2002**, *3* (4), 356-+.
7. Biron, Z.; Khare, S.; Samson, A. O.; Hayek, Y.; Naider, F.; Anglister, J., A monomeric 3(10)-helix is formed in water by a 13-residue peptide representing the neutralizing determinant of HIV-1 on gp41. *Biochemistry* **2002**, *41* (42), 12687-12696.
8. (a) Toniolo, C.; Polese, A.; Formaggio, F.; Crisma, M.; Kamphuis, J., Circular dichroism spectrum of a peptide 3(10)-helix. *J. Am. Chem. Soc.* **1996**, *118* (11), 2744; (b) Boal, A. K.; Guryanov, I.; Moretto, A.; Crisma, M.; Lanni, E. L.; Toniolo, C.; Grubbs, R. H.; O'Leary, D. J., Facile and E-selective intramolecular ring-closing metathesis reactions in 3(10)-helical peptides: A 3D structural study. *J. Am. Chem. Soc.* **2007**, *129* (22), 6986.
9. Burton, N. A.; Harrison, M. J.; Hart, J. C.; Hillier, I. H.; Sheppard, D. W., Prediction of the mechanisms of enzyme-catalysed reactions using hybrid quantum mechanical molecular mechanical methods. *Faraday Disc. Chem. Soc.* **1998**, *110*, 463.

10. Jacobsen, O.; Maekawa, H.; Ge, N. H.; Gorbitz, C. H.; Rongved, P.; Ottersen, O. P.; Amiry-Moghaddam, M.; Klaveness, J., Stapling of a 3(10)-Helix with Click Chemistry. *Journal of Organic Chemistry* **2011**, *76* (5), 1228.
11. (a) Gooding, J. J.; Wibowo, R.; Liu, J. Q.; Yang, W. R.; Losic, D.; Orbons, S.; Mearns, F. J.; Shapter, J. G.; Hibbert, D. B., Protein electrochemistry using aligned carbon nanotube arrays. *J. Am. Chem. Soc.* **2003**, *125* (30), 9006; (b) Moore, K. E.; Flavel, B. S.; Ellis, A. V.; Shapter, J. G., Comparison of double-walled with single-walled carbon nanotube electrodes by electrochemistry. *Carbon* **2011**, *49* (8), 2639-2647.
12. (a) Moore, K. E.; Flavel, B. S.; Yu, J.; Abell, A. D.; Shapter, J. G., Increased redox-active peptide loading on carbon nanotube electrodes. *Electrochim. Acta* **2013**, *89*, 206; (b) Constantopoulos, K. T.; Shearer, C. J.; Ellis, A. V.; Voelcker, N. H.; Shapter, J. C., Carbon Nanotubes Anchored to Silicon for Device Fabrication. *Adv. Mater.* **2010**, *22* (5), 557; (c) Diao, P.; Liu, Z. F., Vertically Aligned Single-Walled Carbon Nanotubes by Chemical Assembly - Methodology, Properties, and Applications. *Adv. Mater.* **2010**, *22* (13), 1430.
13. Laviron, E., The use of linear potential sweep voltammetry and of a.c. voltammetry for the study of the surface electrochemical reaction of strongly adsorbed systems and of redox modified electrodes. *J. Electroanal. Chem.* **1979**, *100*, 263.
14. (a) Wierzbinski, E.; de Leon, A.; Yin, X.; Balaeff, A.; Davis, K. L.; Reppireddy, S.; Venkatramani, R.; Keinan, S.; Ly, D. H.; Madrid, M.; Beratan, D. N.; Achim, C.; Waldeck, D. H., Effect of Backbone Flexibility on Charge Transfer Rates in Peptide Nucleic Acid Duplexes. *J. Am. Chem. Soc.* **2012**, *134* (22), 9335; (b) Hatcher, E.; Balaeff, A.; Keinan, S.; Venkatramani, R.; Beratan, D. N., PNA versus DNA: Effects of structural fluctuations on electronic structure and hole-transport mechanisms. *J. Am. Chem. Soc.* **2008**, *130* (35), 11752.
15. Van Voorhis, T.; Kowalczyk, T.; Kaduk, B.; Wang, L. P.; Cheng, C. L.; Wu, Q., The Diabatic Picture of Electron Transfer, Reaction Barriers, and Molecular Dynamics. *Annual Review of Physical Chemistry, Vol 61* **2010**, *61*, 149-170.
16. Farazdel, A.; Dupuis, M.; Clementi, E.; Aviram, A., Electric-Field Induced Intramolecular Electron Transfer In Spiro PI-Electron Systems And Their Suitability As Molecular Electronic Devices - A Theoretical Study. *Journal of the American Chemical Society* **1990**, *112* (11), 4206-4214.
17. (a) Beer, P. D.; Smith, D. K., Tunable bis(ferrocenyl) receptors for the solution-phase electrochemical sensing of transition-metal cations. *Journal of the Chemical Society-Dalton Transactions* **1998**, (3), 417; (b) Ossola, F.; Tomasin, P.; Benetollo, F.; Foresti, E.; Vigato, P. A., Synthesis, structure and properties of new ferrocene-containing compounds. *Inorganica Chimica Acta* **2003**, *353*, 292-300.

Statement of Authorship

Paper 1

“The effect of a macrocyclic constraint on electron transfer in helical peptides: A step towards tunable molecular wires”, Yu, J.; Horsley, J. R.; Moore, K. E.; Shapter, J. G.; Abell, A. D. *Chemical Communications* **2014**, *50*, 1652.

Mr. John Horsley (candidate)

Performed synthesis and characterization of peptides, attachment to SWCNT/gold electrodes, electrochemistry, analysis of data, provided advanced draft of manuscript and subsequent revisions.

I hereby certify that the statement of contribution is accurate.

Signed

Dated 11/11/2014

Dr. Jingxian Yu

Performed synthesis of some peptides, electrochemistry, theoretical studies, corresponding author, and co-supervisor of candidate.

I hereby certify that the statement of contribution is accurate.

Signed

Dated 11/11/2014

Miss Katherine Moore

Prepared SWCNT/Au electrodes.

I hereby certify that the statement of contribution is accurate.

Signed

Dated 12/11/2014

Prof. Joe Shapter

Supervisor to Miss Katherine Moore. Provided laboratory and instrumentation for electrochemical analysis of peptides.

I hereby certify that the statement of contribution is accurate.

Signed

Dated

12/11/14

Prof. Andrew Abell

Supervised development of work, revised manuscript, and is corresponding author.

I hereby certify that the statement of contribution is accurate.

Signed

Dated

16/2/2015

Paper 2

“Unraveling the Interplay of Backbone Rigidity and Electron Rich Side-Chains on Electron Transfer in Peptides: The Realization of Tunable Molecular Wires”, Horsley, J. R.; Yu, J.; Moore, K. E.; Shapter, J. G.; Abell, A. D. *Journal of the American Chemical Society* **2014**, *136*, 12479.

Mr. John Horsley (candidate)

Performed synthesis and characterization of peptides, attachment to SWCNT/gold electrodes, electrochemistry, analysis of data, provided advanced draft of manuscript and subsequent revisions.

I hereby certify that the statement of contribution is accurate.

Signed

Dated 11/11/2014

Dr. Jingxian Yu

Performed synthesis of some peptides, electrochemistry, theoretical studies, corresponding author, and co-supervisor of candidate.

I hereby certify that the statement of contribution is accurate.

Signed

Dated 11/11/2014

Miss Katherine Moore

Prepared SWCNT/Au electrodes.

I hereby certify that the statement of contribution is accurate.

Signed

Dated 12/11/2014

Prof. Joe Shapter

Supervisor to Miss Katherine Moore. Provided laboratory and instrumentation for electrochemical analysis of peptides.

I hereby certify that the statement of contribution is accurate.

Signed

Dated 12/11/14

Prof. Andrew Abell

Supervised development of work, revised manuscript, and is corresponding author.

I hereby certify that the statement of contribution is accurate.

Signed

Dated 16/2/2015

I hereby give permission for John Horsley to use the following papers in his PhD Thesis:
“The effect of a macrocyclic constraint on electron transfer in helical peptides: A step towards tunable molecular wires”, Yu, J.; Horsley, J. R.; Moore, K. E.; Shapter, J. G.; Abell, A. D. *Chemical Communications* **2014**, *50*, 1652 and “Unraveling the Interplay of Backbone Rigidity and Electron Rich Side-Chains on Electron Transfer in Peptides: The Realization of Tunable Molecular Wires”, Horsley, J. R.; Yu, J.; Moore, K. E.; Shapter, J. G.; Abell, A. D. *Journal of the American Chemical Society* **2014**, *136*, 12479.

Signed

Date

11/2/2015

I hereby give permission for John Horsley to use the following papers in his PhD Thesis:

Yu, J.; Horsley, J. R.; Moore, K. E.; Shapter, J. G.; Abell, A. D. *Chemical Communications*, **2014**, *50*, 1652.

Horsley, J. R.; Yu, J.; Moore, K. E.; Shapter, J. G.; Abell, A. D. *Journal of the American Chemical Society*, **2014**, *136*, 12479.

Horsley, J. R., Yu, J., Abell, A. D. "The Correlation of Electrochemical Measurements and Molecular Junction Conductance Simulations in β -Strand Peptides" *Chemistry A European Journal*, **2015**, *21*, 5926-5933.

Horsley, J. R., Yu, J., Abell, A. D. "Understanding the Role of the Amide Bond and Electron Transfer Mechanisms in Macrocyclic Peptides" (Prepared in publication format "text in manuscript").

Signed

Date

19/6/2015

Signed

Date

19/06/2015

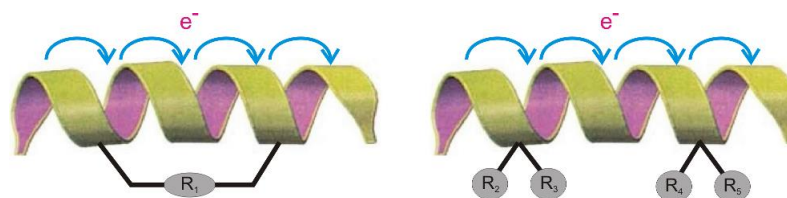
CHAPTER 3

Unraveling the Interplay of Backbone Rigidity and Electron Rich Side-Chains on Electron Transfer in Peptides: The Realization of Tunable Molecular Wires

John R. Horsley,[†] Jingxian Yu,^{*,†} Katherine E. Moore,[‡] Joe G. Shapter,[‡] and Andrew D. Abell^{*,†}

[†] ARC Centre of Excellence for Nanoscale BioPhotonics (CNBP), School of Chemistry and Physics, The University of Adelaide, Adelaide, SA 5005, Australia

[‡] Centre for Nanoscale Science and Technology, School of Chemical & Physical Science, Flinders University, Bedford Park, SA 5042, Australia



R ₁	R ₂	R ₃	R ₄	R ₅	k_{ET} (s ⁻¹)
Alkene					17
Alkane					31
	CH ₃	CH ₃	CH ₃	CH ₃	62
	Alkene	H	CH ₃	CH ₃	260
	Alkene	H	CH ₃	H	307
	Alkene	H	Alkene	H	388

John R. Horsley, Jingxian Yu, Katherine E. Moore, Joe G. Shapter, and Andrew D. Abell, *J. Am. Chem. Soc.* **2014**, 136, 12479–12488

3.1 Abstract

Electrochemical studies are reported on a series of peptides constrained into either a 3_{10} -helix (**1-6**) or β -strand (**7-9**) conformation, with variable numbers of electron rich alkene containing side chains. Peptides (**1** and **2**) and (**7** and **8**) are further constrained into these geometries with a suitable side chain tether introduced by ring closing metathesis (RCM). Peptides **1**, **4** and **5**, each containing a single alkene side chain reveal a direct link between backbone rigidity and electron transfer, in isolation from any effects due to the electronic properties of the electron rich side-chains. Further studies on the linear peptides **3-6**, confirm the ability of the alkene to facilitate electron transfer through the peptide. A comparison of the electrochemical data for the unsaturated tethered peptides (**1** and **7**) and saturated tethered peptides (**2** and **8**) reveals an interplay between backbone rigidity and effects arising from the electron rich alkene side-chains on electron transfer. Theoretical calculations on β -strand models analogous to **7**, **8** and **9** provide further insights into the relative roles of backbone rigidity and electron rich side-chains on intramolecular electron transfer. Furthermore, electron population analysis confirms the role of the alkene as a 'stepping stone' for electron transfer. These findings provide a new approach for fine tuning the electronic properties of peptides by controlling backbone rigidity, and through the inclusion of electron rich side-chains. This allows for manipulation of energy barriers and hence conductance in peptides, a crucial step in the design and fabrication of molecular-based electronic devices.

3.2 Introduction

Electron transfer in proteins plays an important role in a wide range of metabolic processes at the cellular level.¹ Many factors have been shown to influence this electron transfer, including the distance separating the electron donor and acceptor,² the extent of secondary structure,³ dipole moment,⁴ and the nature of the constituent amino acid side chains.⁵ Of particular significance is the suggestion that peptides can undergo electron transfer via either a bridge-assisted superexchange or an electron hopping mechanism.⁶ While electron superexchange is a one step process that is exponentially dependent on distance, the hopping model involves a multi-step process for electron translocations across long distances, whereby the charge temporarily resides on the bridge between redox centres.⁷ Consequently, electron hopping through a peptide can be facilitated by redox-active amino acid side chains in the sequence that act as ‘stepping stones’ for electron transfer.⁸ Studies on model peptides have confirmed this, where the rate of electron transfer increases significantly with the introduction of electron-rich side-chains into the peptide.^{5a} For example, Kimura and co-workers demonstrated that linearly spaced electron-rich naphthyl groups within synthetic peptides increase the photocurrent by efficient electron hopping between the moieties, compared to reference peptides containing one or no naphthyl groups.⁹ An electron rich tryptophan side chain has also been shown to act as a ‘relay station’ to facilitate multi-step electron transfer in an azurin metallo-protein isolated from *Pseudomonas aeruginosa*.¹⁰ Multiple sequence alignment of genomes from the respiratory oxidoreductase enzyme NDH1, have revealed the conservation of specific aromatic amino acids from simple prokaryotes through to man, that may serve as candidates for transient charge localization between metal clusters.¹¹ The majority of research conducted thus far has focused on aromatic amino acids as the source of electron-rich ‘stepping stones’.

Recent work with an Aib (α -aminoisobutyric acid) rich hexapeptide, constrained into a 3_{10} -helix by a triazole-containing covalent tether linking its i to $i+3$ residues,¹² has shown that backbone rigidity also plays a significant role in defining the rate of electron transfer in peptides. Increased rigidity restricts backbone torsional motion, resulting in an additional reorganization energy barrier to electron transfer. In the study reported here, a series of alkene containing peptides, both linear (see **4**, **5**, **6**, and **9**, Figures 1 and 2) and also a series of alkene tethered peptides (see **1** and **7**, Figures 1 and 2), is used to begin to unravel the interplay of peptide backbone rigidity and the nature of the amino acid side chains in defining the rate of electron transfer, where until now these effects have been considered

Chapter 3

without factoring in the other variable. Electrochemical and theoretical studies are presented on peptides constrained into both a 3_{10} -helix (see **1** and **2**, Figure 1) and a β -strand (see **7** and **8**, Figure 2). The alkene group in the peptides is shown to promote electron transfer, with its influence on backbone rigidity and its role as an electron rich ‘stepping stone’ discussed to explore the generality and connectivity of these effects.

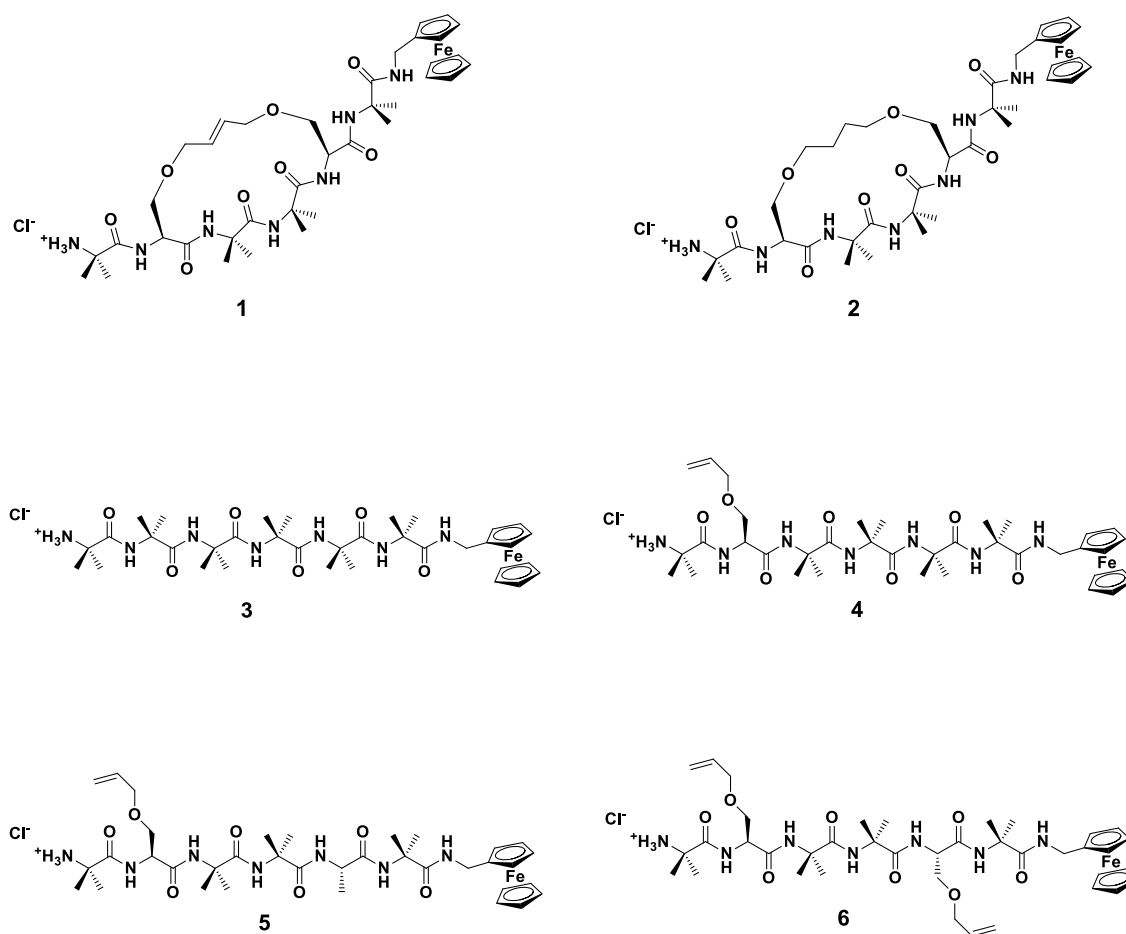


Figure 1. Structures of helical peptides **1-6**.

Note: Compound **3** (above) is Compound **8** in Chapter 2.

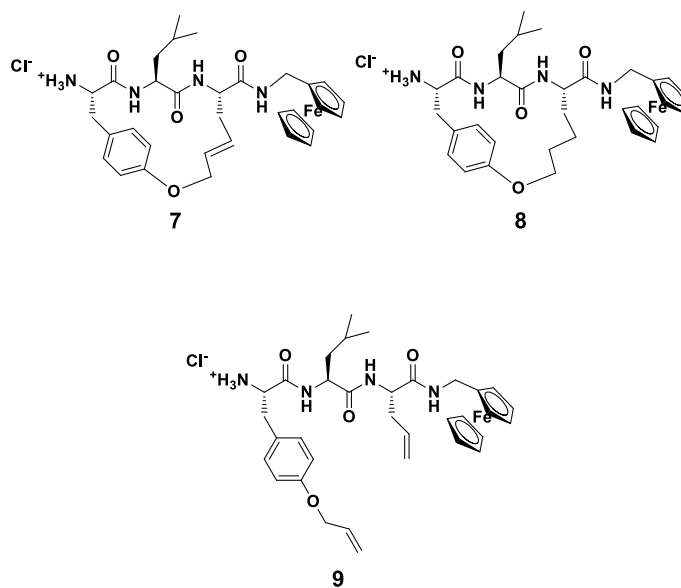


Figure 2. Structures of β -strand peptides **7-9**.

3.3 Results and discussion

3.3.1 Peptide design

Aib residues were incorporated into peptides **1-6** in order to promote the formation of a unifying 3_{10} -helical secondary structure.¹² The peptides **1**, **4**, **5**, and **6** also contain alkenes as potential hopping sites for electron transfer, where this group is part of the macrocycle of **1**. The peptides **2** and **3** lack an alkene and hence provide suitable controls. The diene of **6** is positioned in the i and $i+3$ residues, to locate the alkenes on the same side of the molecule in the helix in a proximal arrangement to promote electron transfer. This diene also allows cyclization by ring closing metathesis (RCM) to introduce a covalent tether to further constrain the peptide backbone into a 3_{10} -helix and to rigidify the backbone into this geometry. The β -strand constrained peptides (**7** and **8**) have the covalent tether linking the i and $i+2$ residues. Such a 17-membered ring, with an aryl group at the N -terminus is known to stabilize a β -strand geometry with the associated rigidification of the backbone.¹³ The linear diene **9** was also prepared as a control for the electrochemical studies.

3.3.2 Conformational analysis of peptides

The geometry of peptides **1-6** was confirmed as 3_{10} -helical by ^1H NMR spectroscopy. In particular, strong $\text{NH}(i)$ to $\text{NH}(i+1)$ ROESY correlations were found for peptides **1-6**, together with $\text{CaH}(i)$ to $\text{NH}(i+1)$ and medium range $\text{CaH}(i)$ to $\text{NH}(i+2)$ correlations, as shown in Figure 3. A $\text{CaH}(i)$ to $\text{NH}(i+2)$ cross peak is only possible for a 3_{10} -helix,¹⁴ as the distance between these two hydrogen atoms is in the order of 3.5 Å, whereas in an α -helix the distance between $\text{CaH}(i)$ to $\text{NH}(i+2)$ atoms is approximately 4.5 Å, and near the limit of detection.¹⁵ An absence of $\text{CaH}(i)$ to $\text{NH}(i+4)$ correlations was noted for all peptides, thus excluding the possibility of an α -helical structure, which is characterized by $(i$ to $i+4)$ hydrogen bonds.¹⁶ Strong correlations were also evident for $\text{C}\beta\text{H}_2(i)$ and $\text{NH}(i)$ in peptides **1** and **2**.¹⁷ Hence the cumulative ^1H NMR data confirms the presence of 3_{10} -helical structures for each of peptides **1-6**.

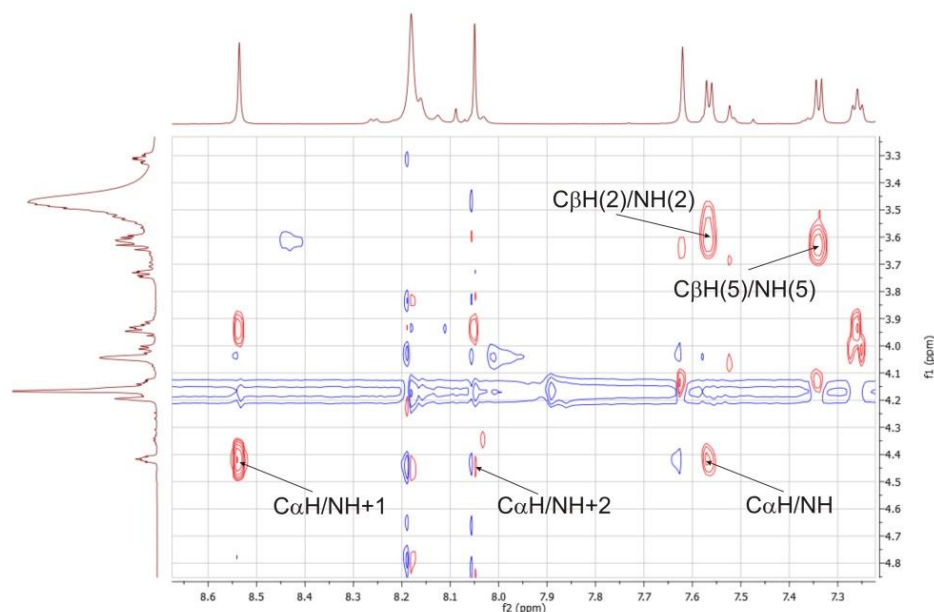


Figure 3. ^1H NMR ROESY spectrum representative of peptide **2**, showing $\text{CaH}(i)$ to $\text{NH}(i+1)$, $\text{CaH}(i)$ to $\text{NH}(i+2)$ and $\text{C}\beta\text{H}_2(i)$ and $\text{NH}(i)$ crosspeaks, indicative of a 3_{10} -helical conformation.

Chapter 3

The conformations of peptides **7-9** were confirmed as β -strand by a combination of ^1H NMR and FTIR spectroscopy. $\text{C}\alpha\text{H}$ (i) to NH ($i+1$) and $\text{C}\beta\text{H}$ (i) to NH ($i+1$) ROESY correlations were found for all three peptides, indicative of a β -strand geometry¹⁸ (see Figure 4). Furthermore, ^1H NMR $J_{\text{NH}\text{C}\alpha\text{H}}$ coupling constants¹⁸ of 8-10 Hz were observed for these peptides. Amide I and II bands, used extensively in peptide/protein structural determination, were found to be in the range assigned to a β -strand conformation¹⁹ for all three tripeptides. Amide A (N-H stretching) frequencies between 3277 cm^{-1} and 3293 cm^{-1} were also observed in the IR spectra of peptides **7-9**, indicative of the presence of hydrogen bonding within ordered β -sheets²⁰ (see Figure 5).

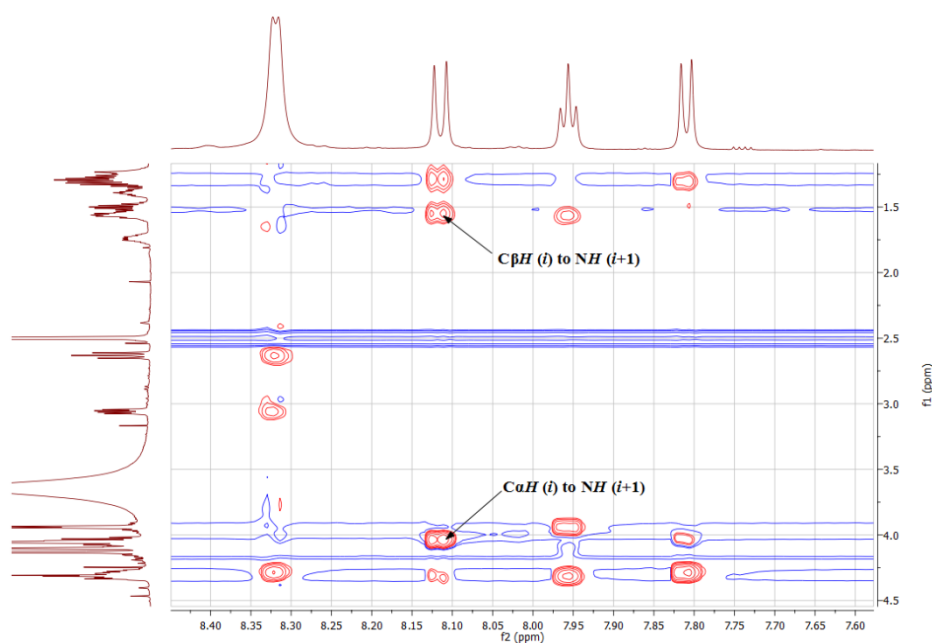


Figure 4. ^1H NMR ROESY spectrum representative of peptide **8**, showing $\text{C}\alpha\text{H}$ (i) to NH ($i+1$) and $\text{C}\beta\text{H}$ (i) to NH ($i+1$).

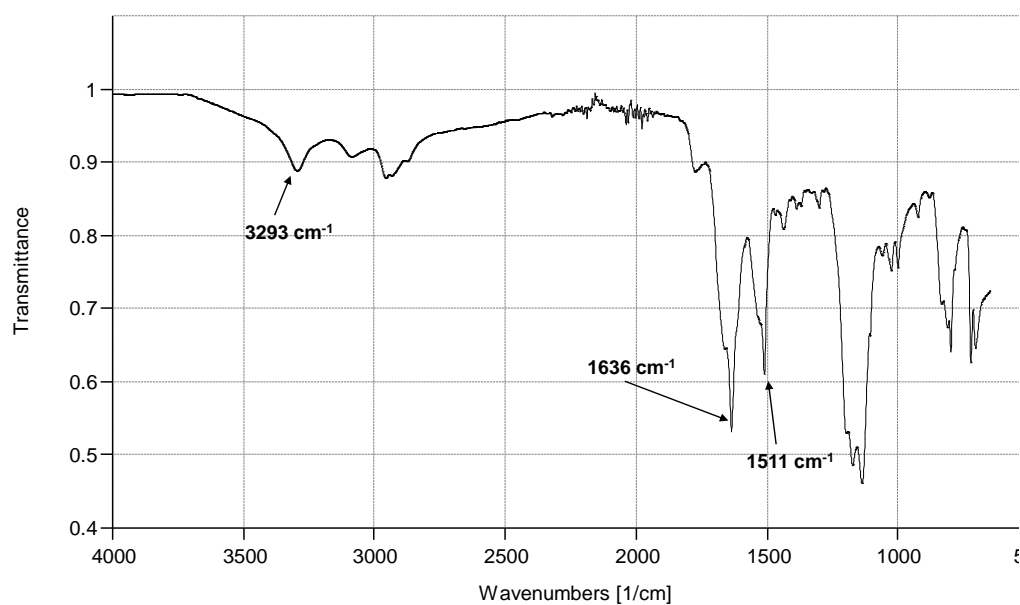


Figure 5. FTIR spectrum representative of peptide **8**.

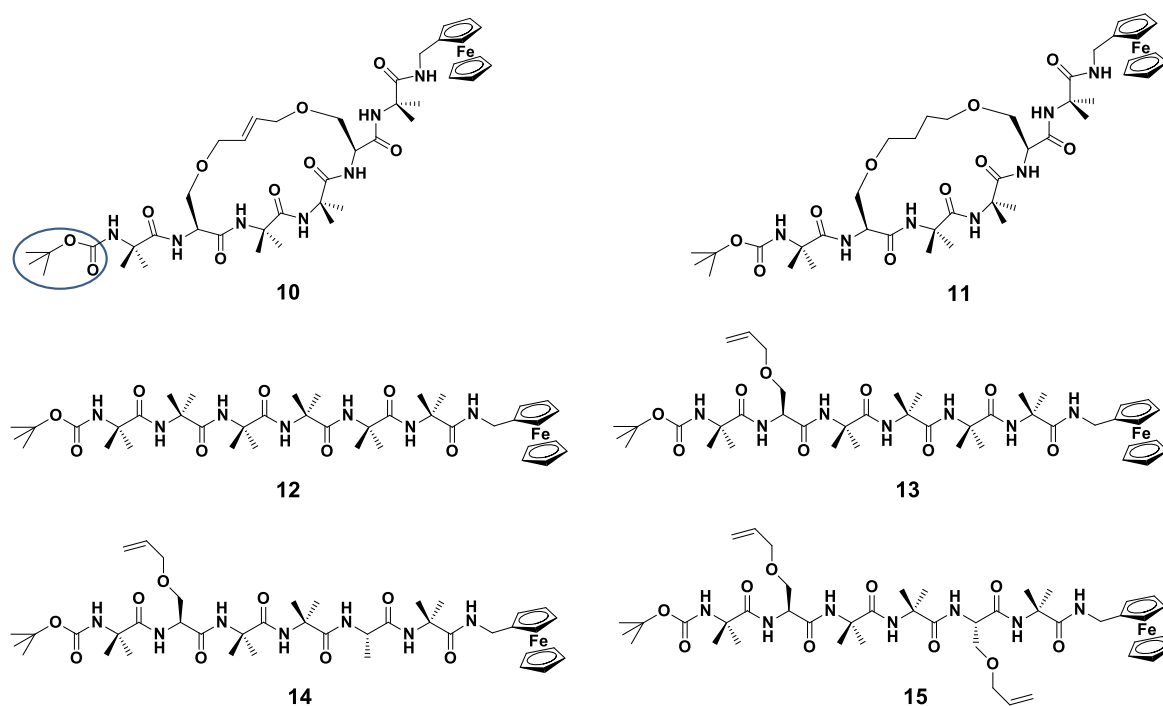


Figure 6. The lowest energy conformers for the *N*-protected analogues of **1-6** (peptides **10-15**). The *N*-Boc protection group is circled in Peptide **10**.

Chapter 3

The lowest energy conformers for the *N*-protected analogues of **1-9** (see peptides **10-18**, Figures 6 and 8) were determined by molecular modeling in order to further define the backbone geometries. The *N*-protected peptides were used in these studies as free amines are known to give rise to unrealistic electrostatic interactions, resulting in unstable lowest energy conformers.²¹ The lowest energy conformers for the *N*-protected helical hexapeptides **10-15** (see Figure 6) were calculated. The resulting models indicate that the backbone lengths (from first to last carbonyl carbons) are almost identical, differing by no more than 0.04 Å. The mean hydrogen bond lengths in the constrained helical peptides **10** and **11** is 2.10 Å, which is in accordance with similar 3_{10} -helical structures,^{12, 17, 22} and 2.12 Å in the unconstrained helical peptides **12-15**, also similar to those reported elsewhere.^{12, 17, 22} The most significant difference in the intramolecular hydrogen bond lengths for each of the helical peptides is only 0.15 Å, between residues 2 and 5 in peptides **10** and **15**, which correspond to the *i* and *i*+3 positions of the constraint. The average dihedral angles for residues 1-6 in each of the *N*-Boc protected analogues, deviate from an ideal 3_{10} -helix by no more than 3.6° and 5.9° for Φ and ψ respectively. Figure 7 shows the lowest energy conformer for **15**, revealing that the side-chains are positioned on the same side of the molecule, with the terminal alkenes separated by 6 Å.

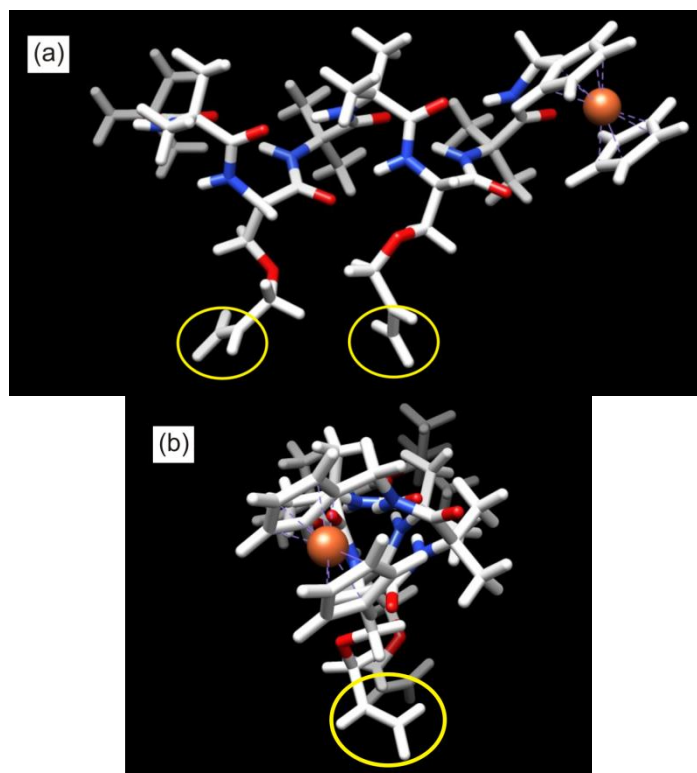


Figure 7. (a) The lowest energy conformer for peptide **15** (analogue of **6**) showing the two side-chains facing each other in a proximal arrangement (circled) and (b) the view looking down the helix, which indicates that the two side-chains are in the same plane (circled). (Optimized by the hybrid B3LYP method with 6-31G** basis set for all C, H, O, N atoms and Lan12dz for Fe atom).

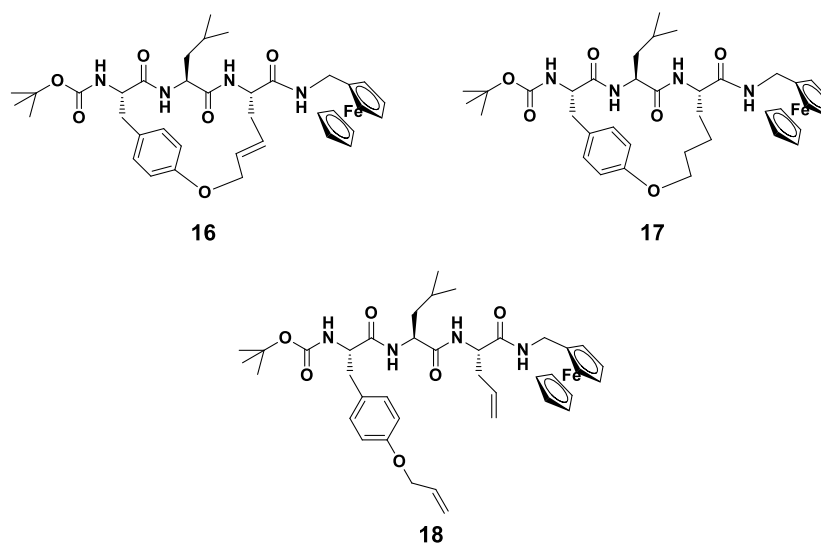


Figure 8. The lowest energy conformers for the *N*-protected analogues of **7-9** (peptides **16-18**)

Chapter 3

The calculated lowest energy conformers for the *N*-protected β -strand peptides **16**, **17** and **18**, (see Figure 8) indicate that the backbone length (from first to last carbonyl carbons) are once again almost identical, with the backbone length of the constrained peptides differing by only 0.05 Å. The largest variation in backbone length is 0.30 Å, between the linear analogue (**18**) and the unsaturated peptide (**16**). All other dimensions critical to the characterization of a β -strand conformation, such as $NH(i)$ to $NH(i+1)$, $CaH(i)$ to $NH(i+1)$ and $C\beta H_2(i)$ to $NH(i+1)$ distances are in accordance with literature values.²³ Figure 9 shows the lowest energy conformers for peptides **16** and **17**, highlighting the structural difference between the side-chains of the saturated and unsaturated molecules.

A combination of the molecular modeling studies and the 1H NMR and FTIR data demonstrates that peptides **10-15** share remarkably similar 3_{10} -helical conformations, while peptides **16-18** exhibit a common β -strand geometry. Thus the prominent structural differences between each of these peptides and hence the analogues (**1-6** and **7-9**) are simply the variation in the number of electron rich alkenes, the presence (or absence) of the side-bridge constraint, and the associated effect that this has on backbone rigidity as discussed in the following section.

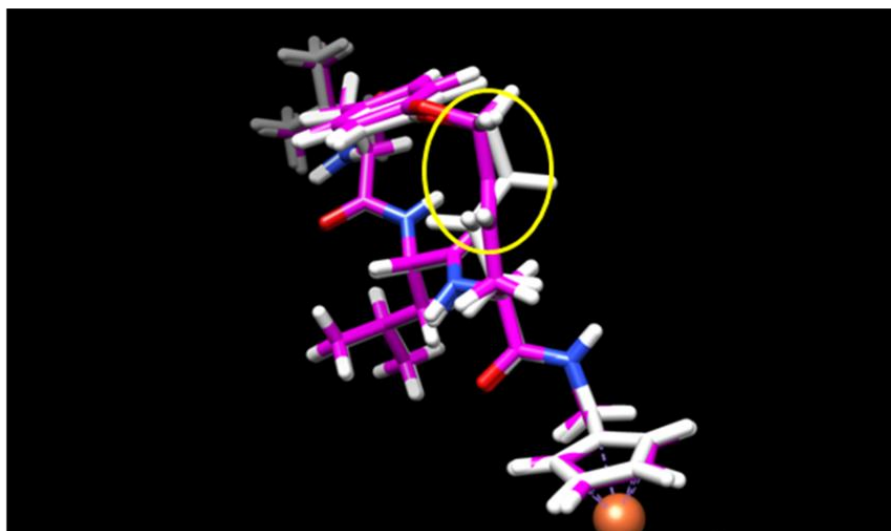


Figure 9. The lowest energy conformers for peptides **16** and **17**, analogues of **7** and **8** (overlapped), optimized by the hybrid B3LYP method with 6-31G** basis set for all C, H, O, N atoms and Lan12dz for Fe atom. The side-chain of the unsaturated **16** is depicted in white, with that of peptide **17** in pink. The saturated/unsaturated models overlap fittingly, with the exception of the highlighted region about the double bond.

3.3.3 Electrochemical analysis of intramolecular electron transfer

Each of the peptides **1-9** was separately attached to vertically aligned single-walled carbon nanotube array/gold (SWCNTs/Au) electrodes²⁴ in order to study their electron transfer kinetics. SWCNTs/Au electrodes were used in this study to provide a high surface concentration of redox probes, with an associated significant increase in sensitivity and reproducibility of the electrochemical measurement over bare Au electrodes.²⁴ Analysis of the electrochemical results for the helical peptides **1-6** reveal a pair of redox peaks in each cyclic voltammogram, characteristic of a one-electron oxidation / reduction reaction (Fc^+/Fc) (see Figure 10). The formal potentials (E_o) and apparent electron transfer rate constants (k_{app}) were estimated using Laviron's formalism,²⁵ and given in Table 1.

Chapter 3

Table 1. Electron transfer rate constants (k_{app}), surface concentrations and formal potentials (E_o) for the helical peptides (**1-6**)

Peptide	Surface concentration ($\times 10^{-10}$ mole.cm $^{-2}$)	E_o (V vs AgCl/Ag)	k_{app} / s^{-1}
1	4.37 \pm 0.43	0.844	17.49 \pm 1.46
2	4.19 \pm 0.35	0.881	31.88 \pm 2.82
3	9.79 \pm 0.21	0.508	62.90 \pm 5.35
4	4.02 \pm 0.41	0.380	260.38 \pm 25.32
5	4.12 \pm 0.48	0.379	307.11 \pm 30.61
6	3.58 \pm 0.37	0.375	388.44 \pm 37.94

A comparison of the data for the peptides **1**, **4** and **5** provides some insight into the influence of backbone rigidity, where these peptides share a common 3_{10} -helical geometry and the presence of a single alkene. Peptide **1** is constrained and hence rigidified by its tether. Peptide **4** contains five Aib residues, while peptide **5** would be the most flexible of the three with an Ala residue in place of one Aib at the site of cyclization in **1**. The data on these compounds reveals an electron transfer rate constant for the macrocyclic peptide **1** of 17 s^{-1} , a clear 15-20 fold lower than that of peptides **4** and **5**. Peptide **4** gave the next lowest electron transfer rate constant (260 s^{-1}), with the most flexible peptide **5** displaying a value of 307 s^{-1} . Thus there is a clear correlation between the electron transfer rate constant and the flexibility of the peptide backbone. Increased rigidity impedes electron transfer, presumably by restricting the precise torsional motions required by a hopping mechanism, that lead to facile intramolecular electron transfer along the peptide.^{12, 26}

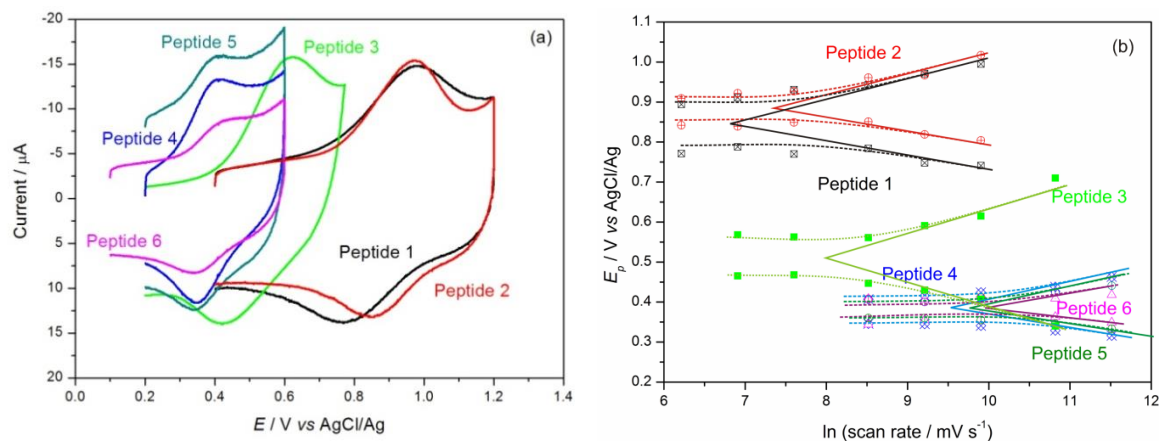


Figure 10. (a) Cyclic voltammograms for peptides **1-6** immobilized on SWCNTs/Au electrodes taken at 5 V s^{-1} . (b) Peak potential versus \ln (scan rate) for peptides **1-6** after background current subtraction.

A dramatic shift to the positive in the formal potential of the constrained peptide **1**, compared to those of the linear analogues **4** and **5**, was also observed. The difference between the formal potentials of the constrained (**1**) and unconstrained (**4** and **5**) peptides was a significant 465 mV. This is similar to results from our previous study involving a hexapeptide that was also stapled i to $i + 3$, but by a triazole containing linker introduced by an alternative Huisgen cycloaddition strategy (480 mV).¹² Such a marked disparity between the formal potentials of these linear and macrocyclic peptides is further evidence of the additional backbone rigidity imparted by the side-bridge constraint. The observed effect on electron transfer is the result of cyclization and the associated rigidification, rather than by the makeup of the component macrocycle.

A comparison of the data for the three linear hexapeptides (**3**, **4**, and **6**) provides a measure of the influence of the electron rich alkene side-chains on the rate of electron transfer somewhat in isolation from the effects of backbone rigidity. Peptide **6**, with alkenes at both the i and $i+3$ positions, exhibited the largest electron transfer rate constant of 388 s^{-1} . The peptide containing one alkene side chain (**4**) gave an electron transfer rate constant of 260 s^{-1} . Peptide **3**, which lacks an alkene side chain in its sequence, gave a much reduced electron transfer rate constant of 62 s^{-1} . The electron transfer rate constant clearly increases with the increasing number of electron rich alkenes in the peptides, which presumably facilitate electron transfer, by way of a hopping mechanism utilizing the alkenes as ‘stepping stones’.

Chapter 3

It is important to note that the relative rigidity of the backbones of peptides **3**, **4**, and **6** may also contribute to the rate of electron transfer, which would be expected to decrease with increasing numbers of Aib units through the series as discussed above and elsewhere.¹² A comparison of the data for peptides **5** and **6** sheds further light on this suggestion. These two peptides contain the same number of Aib units and differ only in the number of alkenyl groups to act as potential ‘stepping stones’. The observed electron transfer rate constant for **6** was 388 s^{-1} , 20% higher compared to that for **5** (307 s^{-1}). This clearly demonstrates the ability of the alkene groups to facilitate electron transfer through the peptide by acting as a ‘stepping stone’. It is thus clear that a combination of both the electronic properties and the extent of backbone rigidity determines the rate of electron transfer in peptides.

Table 2. Electron transfer rate constants (k_{app}), surface concentrations and formal potentials (E_o) for the β -strand peptides (**7-9**).

Peptide	Surface concentration ($\times 10^{-10} \text{ mole.cm}^{-2}$)	E_o (V vs AgCl/Ag)	k_{app} / s^{-1}
7	9.21 \pm 0.89	0.676	11.72 \pm 1.16
8	7.13 \pm 0.68	0.827	23.62 \pm 2.13
9	5.56 \pm 0.31	0.408	421.36 \pm 41.51

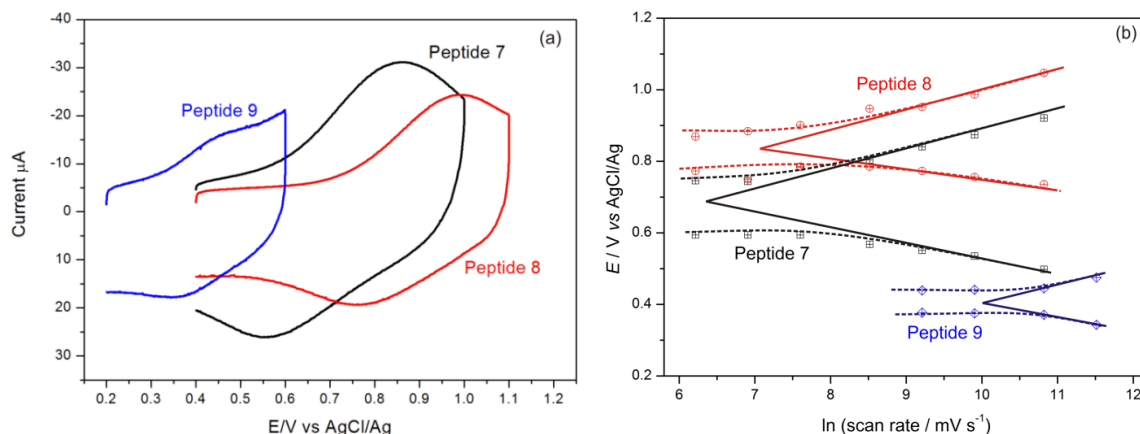


Figure 11. (a) Cyclic voltammograms for β -strand peptides **7-9** immobilized on SWCNTs/Au electrodes taken at 5 V s^{-1} . (b) Peak potential versus $\ln(\text{scan rate})$ for peptides **7-9** after background current subtraction.

A comparison of the unsaturated and saturated macrocyclic peptides **1** and **2** provides further insights into the role of these two effects on the efficiency of electron transfer. Unlike the linear peptides **4**, **5** and **6**, the planar alkene of **1** is able to influence both the backbone rigidity and potentially the electronic properties with its inclusion in a ring. One might expect this alkene to enhance backbone rigidity, while at the same time providing a potential ‘stepping stone’ for electron transfer. These effects are opposing, with the first expected to decrease the electron transfer rate and the second to increase it. Interestingly, the unsaturated macrocycle **1** gave an approximate two-fold decrease in the electron transfer rate relative to **2**, with values of 17 s^{-1} and 31 s^{-1} respectively. This observation is reinforced for the two β -strand constrained peptides, the unsaturated macrocycle **7** and the saturated analogue **8** which displayed electron transfer rates of 11 s^{-1} and 23 s^{-1} respectively (see Tables 1 and 2). Clearly, increasing backbone rigidity in both secondary structures (3_{10} -helix and β -strand) decreases the efficiency of electron transfer. Curiously, the saturated helical peptide **2** exhibited a formal potential shift to the positive of 37 mV compared to the unsaturated analogue **1**. The saturated β -strand peptide **8** recorded an even greater formal potential shift to the positive of 151 mV relative to its unsaturated analogue **7** (see Figure 11). Thus oxidation/reduction of the ferrocene moiety in both of the saturated peptides is energetically less favorable than in the corresponding unsaturated peptides. However, the observed electron transfer rate constants for both saturated peptides are almost double that of their unsaturated counterparts. As noted here for **1**, **2**, **7**, **8**, and

Chapter 3

elsewhere¹², peptides constrained by a side-chain tether give rise to a significant increase in the formal potentials relative to their linear analogues, reflecting the associated increase in backbone rigidity. Thus any formal potential shift to the positive is usually combined with a reduction in the electron transfer rate constant. Therefore, while the effect of backbone rigidity appears to be the dominant factor in this case, it would also be expected that the electron rich alkene in the tether of peptides **1** and **7** should enhance electronic coupling. However, further investigation is required to substantiate this notion, and this is developed further in the following Computational study section.

3.3.4 Computational study of intramolecular electron transfer

High level theoretical calculations, using the latest constrained density functional theory (cDFT), were conducted on β -strand models **19**, **20** and **21** in order to provide further insights into the relative roles of backbone rigidity and electron rich side-chains on intramolecular electron transfer (see Figure 12). These peptides are analogous to **7**, **8** and **9**, but with ferrocene units included at both termini to act as both donor and acceptor. Diabatic states were constructed by individually localizing an overall charge of +1 on each of the amino acids and ferrocene units,²⁷ as shown in Figure 12. Reorganization energies (λ) for electron transfer along the backbone were calculated, together with electronic coupling constants (H_{ab}) in order to provide an insight into the overall intramolecular electron transfer dynamics.

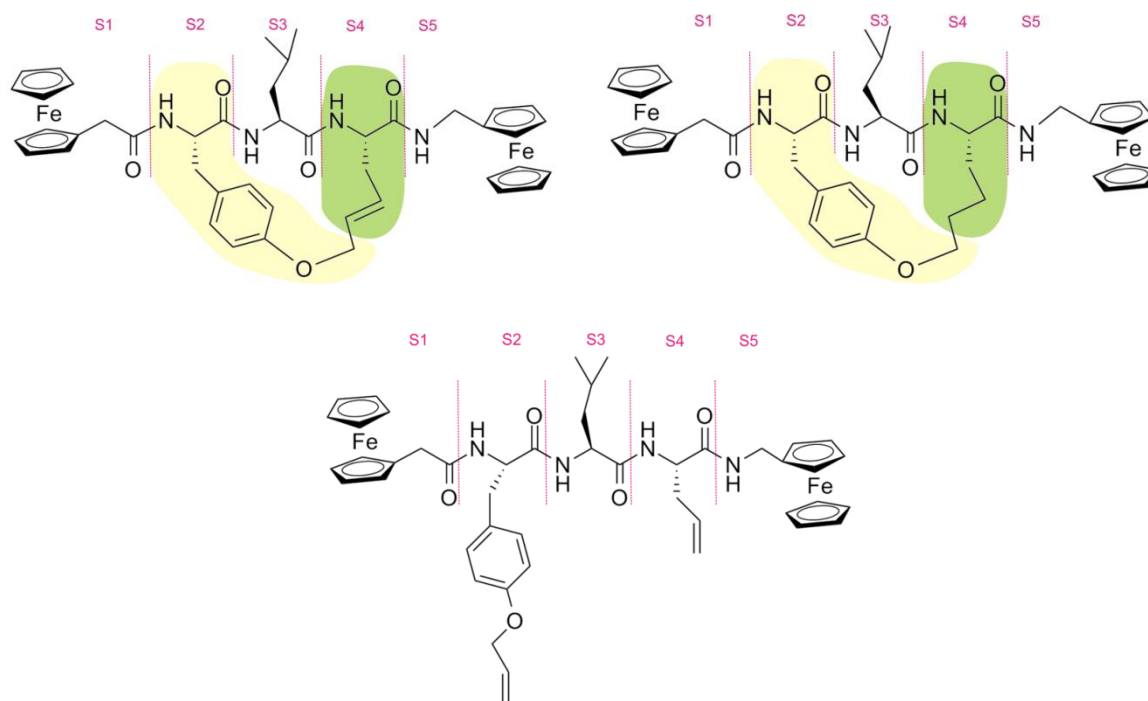


Figure 12. Constructed diabatic states in model peptides **19** (top left), **20** (top right) and **21** (bottom).

Chapter 3

A trend between the electronic coupling constants (H_{ab}) and the number of double bonds in each side-chain is evident. The structure with the greatest number of electron rich side-chains (unconstrained peptide **21**) has the largest coupling constant (0.106 eV). This is sequentially followed by the unsaturated peptide **19** (0.087 eV), and the saturated peptide **20** (0.049 eV) (see Table 3). Significantly, the electronic coupling constant for unsaturated **19** (0.087 eV) is almost double that of the saturated analogue **20** (0.049 eV). This clearly indicates that the electron rich alkene in the tether of the unsaturated peptide does indeed enhance electronic coupling.

Table 3. The electronic coupling constants (H_{ab}), the number of double bonds in each side-chain and average reorganization energies (λ) for peptides **19-21**, and the formal potentials (E_o) and electron transfer rate constants (k_{app}) for their analogues, peptides **7-9**.

Peptide	Formal Potential (E_o) (V vs AgCl/Ag)	H_{ab} (eV)	Number of C=C in side chains	Average reorganization energy (λ) (eV)	k_{app} s ⁻¹
20 (8)	0.827	0.049	0	0.65	23
19 (7)	0.676	0.087	1	0.74	11
21 (9)	0.408	0.106	2	0.35	421

Furthermore, the formal potential observed experimentally for the unsaturated peptide **7** is significantly lower than that observed for the saturated **8** (see Table 3). This lower potential is clearly attributable to the effect of the electron rich alkene since the only structural difference between these constrained peptides is the presence or otherwise of the electron-rich π -bond in the side-chain of **7**. In contrast, the higher reorganization energy calculated for the derivative of **7** (unsaturated analogue **19** (0.74 eV)), relative to the derivative of **8** (saturated analogue **20** (0.65 eV)), is likely the direct consequence of the lack of rotational freedom available in the side-chain of the unsaturated peptide. This leads

Chapter 3

to an increase in the rigidity of the backbone and consequently to the lower rate of electron transfer observed for unsaturated **7**, compared to saturated **8**.

Additionally, a large difference of up to 0.49 eV is apparent between the reorganization energies of the constrained peptides (**19** and **20**), and those of the unconstrained **21** (see Table 4). The unconstrained peptide **21** gave rise to the highest calculated (H_{ab}) and the lowest calculated (λ) based on Marcus theory,²⁸ which suggests that oxidation/reduction of the ferrocene moiety is energetically more favorable in the linear peptide, than in either of the constrained compounds. This supports the earlier experimental observation where the linear peptide **9** exhibited the lowest formal potential relative to the two constrained peptides **7** and **8** (by between 268-419 mV), and the highest electron transfer rate constant (an 18-38 fold increase) relative to **7** and **8** (see Table 3). This is indicative of the additional backbone rigidity imparted by the constraint. Thus the influence of the electron rich alkenes and any effects arising from a change in backbone rigidity can be studied in isolation using a combination of experimental and theoretical studies. Both factors clearly contribute to the rate of electron transfer in peptides.

Chapter 3

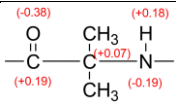
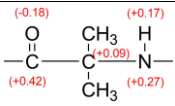
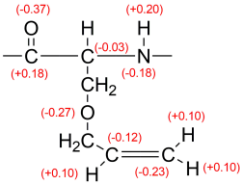
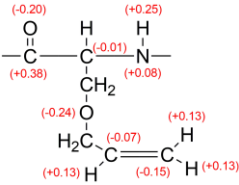
Table 4. Comparison of computed reorganization energies (λ) for electron hopping steps involving diabatic states S1 to S5 in the model peptides **19-21**.

Hopping Step	Peptide 19 (eV)	Peptide 20 (eV)	Peptide 21 (eV)
S1 \rightarrow S2	0.71	0.62	0.25
S2 \rightarrow S1	0.76	0.64	0.37
S2 \rightarrow S3	0.74	0.60	0.33
S3 \rightarrow S2	0.78	0.67	0.29
S3 \rightarrow S4	0.77	0.70	0.36
S4 \rightarrow S3	0.72	0.66	0.44
S4 \rightarrow S5	0.72	0.68	0.37
S5 \rightarrow S4	0.76	0.72	0.43

Electron population analysis (EPA) was conducted to further elucidate the role of electron rich side-chains as ‘stepping stones’ for electron transfer. The amino acid residues used in the synthesis of the linear helical peptides (**4**, **5** and **6**), namely an Aib and a modified serine with electron rich alkene side-chain were considered. A Löwdin analysis of the charge distribution from the cDFT calculations on the charged and uncharged amino acid residues is shown in Table 5. Approximately 88% of the extra charge is distributed on the amide region when the positive charge (+1) was injected into the Aib residue. This emphasizes the significant contribution made by the amide region to intramolecular electron transfer through the peptide backbone, clearly demonstrating the participation of a through-bond hopping mechanism.^{3b} However, when the positive charge (+1) was injected into the modified serine residue, only 68% of the extra charge was distributed on the amide region, with the electron rich alkene side-chain holding approximately 20% of the extra charge localized on the residue (see Table 5). Thus these results confirm the role of the electron rich alkene side-chain as a ‘stepping stone’ for electron transfer.

Chapter 3

Table 5. Löwdin analysis of the charge distribution on uncharged and charged amino acid residues (1) Aib, and (2) Modified serine with electron rich alkene side-chain.

	Uncharged peptide unit	With overall charge of +1 localized on single peptide unit	The extra charge localized in amide bonding region	The extra charge localized in CH=CH ₂ region
(1) Aib			0.88	
(2) Modified serine with electron rich alkene side-chain			0.68	0.22

3.4 Conclusion

Electrochemical studies are reported on a series of peptides (**1-9**) in order to elucidate the effect of backbone rigidity and the nature of the amino acid side chains in defining the rate of electron transfer. Aib residues were incorporated into peptides **1-6** to promote the formation of a unifying 3_{10} -helical secondary structure, with the number of alkenes in their side-chains varying from 0-2. The backbones of peptides **1** and **2** were further constrained into a 3_{10} -helix with a side chain tether introduced by RCM. The side-chain of **1** contains a single C=C double bond, while peptide **2** is fully saturated. Peptides **7-9** share a common β -strand conformation, with **7** (unsaturated) and **8** (saturated) further rigidified into this geometry via cyclization by RCM. Electrochemical studies conducted on peptides **1**, **4** and **5**, each containing a single alkene in their structure, revealed a direct link between backbone rigidity and the efficiency of electron transfer. The significant difference in the formal potentials of the constrained **1** and unconstrained **4** and **5**, (465 mV) is in accordance with our previous study (480 mV).¹² This demonstrates a general observation, where a tether hinders electron transfer in peptides by restricting backbone flexibility. Further studies on the linear peptides **3-6**, containing between 0 and 2 electron rich side-chains in their structure, confirmed the ability of the alkene to facilitate electron transfer through the peptide, while nullifying the effects of backbone rigidity.

The macrocyclic helical peptides reveal a formal potential shift to the positive and subsequent reduction of the electron transfer rate constant for unsaturated **1**, relative to saturated **2**. Comparable results were also evident for the unsaturated (**7**) and saturated (**8**) β -strand peptides. The only structural difference between the unsaturated and saturated peptides is the presence or otherwise of the electron-rich π -bond in the side-chain, so the lower the electron transfer rate constants observed for both unsaturated peptides (**1** and **7**) are likely a direct consequence of the lack of rotational freedom about this double bond, which results in further rigidification of the peptide backbone. High level calculations performed on peptides **19** and **20** (analogues of **7** and **8**) confirmed that the reorganization energy is greater in the unsaturated peptide (**19**), thus supporting the observed lower electron transfer rate constant of **7**, relative to saturated **8**. However, the lower formal potential observed experimentally for the unsaturated **7**, suggests that oxidation/reduction of the ferrocene moiety is energetically more favorable in **7**. Theoretical calculations show that the derivative of the unsaturated peptide **7** (**19**), exhibited a higher electronic coupling

constant than its saturated counterpart **20**, which helps to explain this paradox, while further demonstrating the ability of the alkene to facilitate electron transfer. Thus the theoretical electronic coupling constants and reorganization energies, together with the formal potentials and electron transfer rate constants observed experimentally for the macrocyclic peptides, reveal for the first time an interplay between electron rich alkene side-chains and backbone rigidity, with both factors clearly shown to contribute to the efficiency of electron transfer in peptides. Additional high level calculations were also performed on the amino acid residues used in the synthesis of the linear helical peptides (**4**, **5** and **6**), namely an Aib and a modified serine with electron rich alkene side-chain. Injection of a positive charge into the modified serine residue shows that approximately 20% of the extra charge is localized on the electron rich side-chain, so confirming the role of the alkene as a ‘stepping stone’ for electron transfer.

These findings provide a new approach to fine tune the electronic properties of peptides through chemical modification of the backbone to increase/decrease rigidity, and through the inclusion of electron rich side-chains. Such structurally diverse peptides with controllable electronic functions open new avenues in the design and fabrication of efficient components for molecular-based electronic devices.

3.5 Acknowledgements

We would like to thank Miss Kyra Middlemiss for her assistance with the synthesis of helical peptide precursors. The financial support of this work by the Australian Research Council is gratefully acknowledged. The computational aspects of this work were supported by an award under the National Computational Merit Allocation Scheme for Dr. Jingxian Yu on the National Computing Infrastructure (NCI) National Facility at the Australian National University (ANU).

3.6 Experimental methods

3.6.1 Chemicals

Fmoc-Aib-OH, Boc-Aib-OH, Boc-Ser-OH, Fmoc-OSu, 2-chlorotriyl chloride polystyrene resin, 1-hydroxy-7-azabenzotriazole (HOAt) and 2-(1H-7-azabenzotriazol-1-yl)-1,1,3,3-tetramethyl uronium hexafluorophosphate methanaminium (HATU) were purchased from GL Biochem (Shanghai) Ltd., China. Dichloromethane (DCM), diethyl ether (Et₂O), ethyl acetate (EtOAc), methanol and ethanol were purchased from Ajax Finechem Pty Ltd (Australia). Piperidine, acetonitrile, propan-2-ol and *N,N*-dimethylformamide (DMF) were purchased from Merck, Australia. Anhydrous *N,N*-Dimethylformamide (DMF), dimethyl sulfoxide (DMSO), tetrahydrofuran (THF), Second-generation Grubbs' catalyst, Pd/C catalyst, ethyl vinyl ether, 2,2,2-trifluoroethanol (TFE), trifluoroacetic acid (TFA), 4 M HCl/dioxane solution, *N,N'*-dicyclohexylcarbodiimide (DCC), dimethylaminopyridine (DMAP), cysteamine and diisopropylethylamine (DIPEA) were purchased from Sigma-Aldrich, Australia. NaOH was purchased from Chem Supply, Australia. Single-walled carbon nanotubes (P2-SWCNTs) were purchased from Carbon Solutions Inc., USA. Boc-Ser(Al)-OH²² and ferrocenylmethylamine²⁹ were prepared as published. All solvents and reagents were used without purification unless noted.

3.6.2 High-performance liquid chromatography (HPLC)

The synthetic peptides were analyzed and purified by reverse phase HPLC, using an HP 1100 LC system equipped with a Phenomenex C18 column (250 x 4.6 mm) for analytical traces and a Phenomenex C18 column (250 x 21.2 mm) for purification, a photodiode array detector, and a Sedex evaporative light scattering detector. Water/TFA (100/0.1 by v/v) and ACN/TFA (100/0.08 by v/v) solutions were used as aqueous and organic buffers.

3.6.3 NMR spectroscopy

¹H NMR spectra were recorded in DMSO-d₆ or CDCl₃-d solutions using a Varian Gemini-300 NMR. ¹³C NMR and two-dimensional NMR experiments utilizing COSY, ROESY, HSQC and HMBC, were obtained on a Varian Inova 600 MHz spectrometer. Chemical shifts are reported in ppm (δ) using TMS (0.00 ppm) as the internal standard. Signals are reported as s (singlet), d (doublet), t (triplet) or m (multiplet).

3.6.4 Mass spectroscopy

Low resolution mass spectral data were analyzed using a Finnigan MAT LCQ spectrometer with MS/MS and ESI probe, utilizing XCalibur software. High resolution mass spectral data were analyzed using an Ultimate 3000 RSL HPLC (Thermo Fisher Scientific Inc., MA) and an LTQ Orbitrap XL ETD using a flow injection method, with a flow rate of 5 $\mu\text{L}/\text{min}$. The HPLC flow is interfaced with the mass spectrometer using the Electrospray source (Thermo Fisher Scientific Inc., MA). Mass spectra were obtained over a range of $100 < m/z < 1000$. Data was analyzed using XCalibur software (Version 2.0.7, Thermo Fisher Scientific).

3.6.5 FTIR spectroscopy

Infrared spectra were collected on a Perkin Elmer Spectrum 100 FT-IR spectrometer, with attenuated total reflectance (ATR) imaging capabilities, fitted with a ZnSe crystal, with an average reading taken from 4 scans at 4 cm^{-1} resolution.

3.6.6 Electrochemistry

All electrochemical measurements were taken with a CHI 650D Electrochemical Analyzer (CH Instruments Inc) with ohmic-drop correction at room temperature. A peptide modified gold surface formed the working electrode¹² (geometric area of 0.33 cm^2), with a platinum mesh and Ag/AgCl wire used as the counter and reference electrodes, respectively. The Ag/AgCl reference electrode was calibrated after each experiment against the ferrocene/ferricenium couple. Ferrocene-derivatized peptide electrodes were electrochemically characterized in 0.1 mol L^{-1} tetra-*n*-butylammonium hexafluorophosphate (TBAPF₆) / CH₃CN solutions. The digitized, background-subtracted curves were analyzed using a Data Master 2003 program.

3.6.7 Computational methods

The lowest energy conformers for all of the *N*-protected peptides were determined in Gaussian 09, with tight convergence criteria using a hybrid B3LYP method with 6-31G** basis set for all C, H, N, O atoms, and Lanl2dz basis set for the Fe atom in order to define the backbone conformations of all peptides. The geometry of each diabatic state was optimized using the latest constrained Density Functional Theory (cDFT)²⁷ as implemented in NWChem 6.1.1³⁰ using the B3LYP density functional method with 6-

31G** basis set for all C, H, N, O atoms, and Lanl2dz basis set for the Fe atom. Diabatic potential profiles were determined by assuming that during an electron transfer step the nuclear configuration changes smoothly between the optimized geometries of the diabatic states in which the excess electron is localized before and after electron transfer.³¹ Thus, the energy of each of the two diabatic states along the electron transfer reaction coordinate was taken as the energy for geometries linearly interpolated between the optimized geometries of the two diabatic states, with the excess electron localized to the part of the molecule corresponding to the diabatic state in question. In these calculations, the solvent effects were taken into account approximately by the COSMO approach. The Löwdin electron population analysis for uncharged and charged amino acids was conducted by respectively placing the charge of 0 and +1 on the individual residue within the linear helical peptide, namely an Aib or a modified serine with electron rich alkene side-chain, using the B3LYP density functional method with 6-31G** basis set for all C, H, N, O atoms, and Lanl2dz basis set for the Fe atom.^{3b}

3.6.8 General procedure for *N*-Boc cleavage

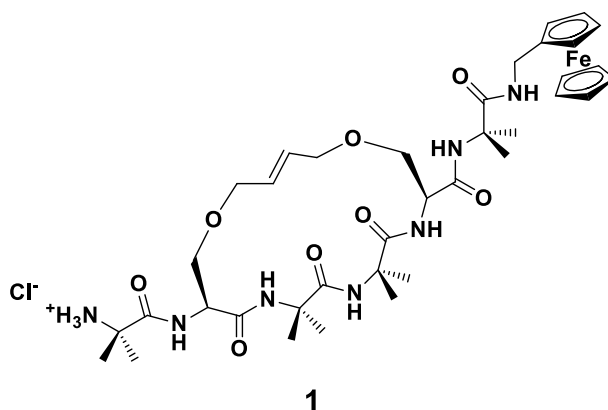
The *N*-Boc protected peptides **1–9** were dissolved in trifluoroethanol (TFE) and 4 M HCl in 1,4-dioxane was added. The reaction solution was stirred at rt for 20–30 min., and the solvent removed *in vacuo*.

3.6.9 Peptide synthesis

The linear hexapeptides (**3**,¹² **4**, **5** and **6**) were synthesized using solid phase peptide synthesis on 2-chlorotrityl chloride resin using Fmoc-Aib-OH, Fmoc-protected allyl serine, and HATU/DIPEA coupling conditions as detailed in this section. Cleavage from the resin was followed by C-terminal coupling with ferrocenylmethylamine, and the *N*-terminal Boc group was removed to give the free amine for coupling to a single-walled carbon nanotube (SWCNTs)/Au electrode assembly. The 3_{10} -helical (**1**) and β -strand (**7**) macrocycles were prepared by ring closing metathesis of the appropriate dienes as detailed in this section. Peptide **1** involves linking the *i* to *i*+3 residues using a strategy previously reported by O'Leary and co-workers.²² In this study the geometry of a related sequence was confirmed by X-ray crystallography.²² For both of these peptides a single alkene isomer was obtained which was assigned the (*E*)-configuration based on the alkene coupling constant¹³ (15.8 Hz for **7**). The C-terminal ferrocenyl group and *N*-terminal free amine were introduced as

above. The saturated analogues (**2** and **8**) were prepared by hydrogenation of the macrocyclic alkenes and the linear peptide **9** was prepared by simple peptide coupling in solution. All peptides (**1-9**) were purified using reverse phase HPLC prior to attachment to the SWCNTs/Au electrode by HATU/DIPEA.

Peptide 1



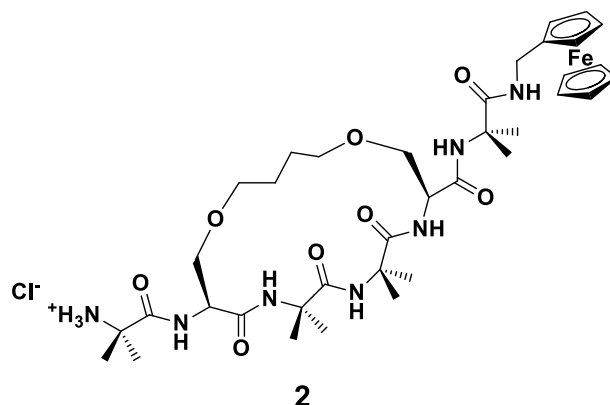
Peptide **10** (34 mg, 0.04 mmol) was deprotected according to General procedure for *N*-Boc cleavage, and the crude product purified on reverse phase HPLC to yield **1** (34%).

^1H NMR (600 MHz, DMSO-d_6): δ 8.49 (s, 1H, NH, Aib4), 8.38 (d, 1H, NH, $J=7.9$ Hz, residue2), 8.12 (bs, 3H, NH_3 , Aib1), 7.87 (s, 1H, NH, Aib3), 7.72 (s, 1H, NH, Aib6), 7.45 (d, 1H, NH, $J=8.2$ Hz, residue 5), 7.20 (br s, 1H, NH, Fc), 5.73-5.61 (m, 2H, $\text{CH}=\text{CH}$), 4.55 (td, 1H, $\text{C}\alpha\text{H}$, $J=8.2, 5.1$ Hz), 4.41 (s, 1H, $\text{C}\alpha\text{H}$), 4.20-3.20 (m, 19H, Cp, $5\times\text{CH}_2$), 1.53-1.32 (m, 24H, $8\times\text{CH}_3$).

^{13}C NMR (150 MHz, DMSO-d_6): δ 174.74, 174.27, 173.16, 171.62, 169.67, 168.72, 157.97, 157.75, 131.00, 126.08, 86.45, 69.45, 69.31, 68.31, 68.00, 66.98, 65.88, 56.46, 56.41, 56.37, 56.19, 56.13, 54.78, 52.58, 37.85, 26.11, 26.00, 25.61, 25.34, 24.92, 24.41, 24.30, 23.36, 23.28, 23.22, 23.11.

HRMS: $[\text{M}]^+_{\text{calcd}}=782.34561$, $[\text{M}]^+_{\text{found}}=782.34567$.

Peptide 2



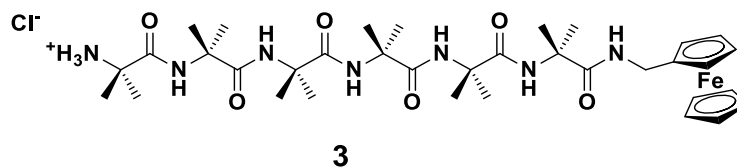
Peptide **11** (45 mg, 0.05 mmol) was deprotected according to General procedure for *N*-Boc cleavage, and the crude product purified on reverse phase HPLC to yield **2** (37%).

¹H NMR (600 MHz, DMSO-*d*₆): δ 8.54 (s, 1H, *NH*, Aib3), 8.18 (bs, 3H, *NH*₃, Aib1), 8.05 (s, 1H, *NH*, Aib4), 7.62 (s, 1H, *NH*, Aib6), 7.57 (d, 1H, *NH*, *J*=6.4 Hz, residue2), 7.34 (d, 1H, *NH*, *J*=6.7 Hz, residue5), 7.26 (t, 1H, *NH* (Fc), *J*=5.8 Hz), 4.42 (m, 1H, Cα*H*), 4.14 (m, 1H, Cα*H*), 4.20-3.30 (m, 19H, Cp, 2xCα*HCH*₂, 3x*CH*₂), 1.73-1.33 (m, 28H, 2x*CH*₂, 8x*CH*₃).

¹³C NMR (150 MHz, DMSO-*d*₆): δ 175.14, 174.58, 173.33, 171.20, 169.38, 168.87, 86.45, 71.42, 69.40, 69.33, 68.74, 68.55, 68.32, 67.02, 66.96, 66.91, 56.46, 56.34, 56.20, 56.18, 55.90, 55.66, 53.31, 48.56, 37.87, 26.76, 26.46, 26.10, 25.50, 24.35, 24.32, 23.53, 23.50, 23.45, 23.33, 23.21, 23.01.

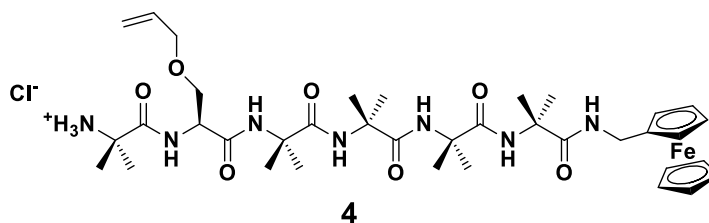
HRMS: [M]⁺_{calcd}=783.36126, [M]⁺_{found}=783.3611.

Peptide 3



^1H NMR (600 MHz, DMSO- d_6), ^{13}C NMR (150 MHz, DMSO- d_6) as previously reported.¹²

Peptide 4



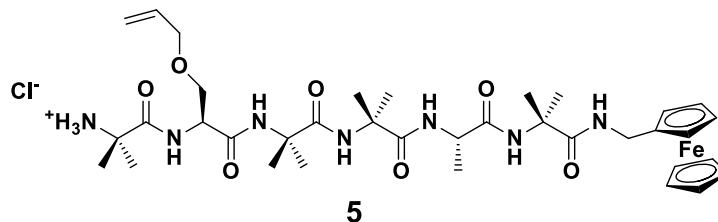
Peptide **13** (60 mg, 0.07 mmol) was deprotected according to General procedure for *N*-Boc cleavage, and the crude product purified on reverse phase HPLC to yield **4** (38%).

^1H NMR (600 MHz, DMSO- d_6): δ 8.65 (s, 1H, NH), 8.29 (d, 1H, NH, $J=7.4$ Hz), 8.12 (br s, 3H, NH_3), 7.63 (s, 1H, NH), 7.59 (s, 1H, NH), 7.54 (t, 1H, NH, $J=6.0$ Hz), 7.38 (s, 1H, NH), 5.90 (ddt, 1H, $\text{CH}=\text{CH}_2$, $J=17.3, 10.5, 5.3$ Hz), 5.29 (ddd, 1H, $\text{CH}=\text{CHH}$, $J=17.3, 3.4, 1.6$ Hz), 5.19 (dd, 1H, $\text{CH}=\text{CHH}$, $J=10.5, 1.6$ Hz), 4.56 (dd, 1H, $\text{C}\alpha\text{H}$, $J=13.0, 7.4$ Hz), 4.22 - 3.92 (m, 13H, Cp, CH_2 , OCH_2), 3.79 (dd, 1H, CHCHHCO , $J=10.1, 5.4$ Hz), 3.64 (dd, 1H, CHCHHCO , $J=10.1, 8.0$ Hz), 1.50-1.29 (m, 30H, $10\times\text{CH}_3$).

^{13}C NMR (150 MHz, DMSO- d_6) δ 174.76, 174.24, 173.80, 173.46, 171.81, 169.70, 134.80, 116.73, 86.73, 71.07, 68.98, 68.79, 68.72, 68.62, 68.35, 66.97, 66.84, 56.34, 56.16, 56.04, 55.99, 55.95, 53.25, 37.78, 28.98, 26.00, 25.36, 25.04, 24.97, 24.79, 24.47, 24.08, 23.46, 23.34.

HRMS: $[\text{M}]^+_{\text{calcd}}=768.3747$, $[\text{M}]^+_{\text{found}}=768.3764$.

Peptide 5



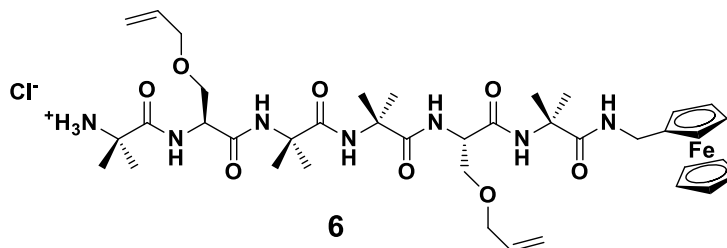
Peptide **14** (40 mg, 0.05 mmol) was deprotected according to General procedure for *N*-Boc cleavage, and the crude product purified on reverse phase HPLC to yield **5** (43%).

^1H NMR (600 MHz, DMSO-d_6): δ 8.71 (s, 1H, NH), δ 8.28 (d, 1H, NH, $J=6.9$ Hz), δ 8.14 (br s, 3H, NH), δ 7.63 – 7.58 (m, 3H, NH), δ 7.31 (br s, 1H, NH), δ 5.90 (ddd, 1H, OCH_2CH , $J=22.3, 10.5, 5.2$), δ 5.28 (d, 1H, $\text{OCH}_2\text{CH,CHH}$, $J=17.2$ Hz), δ 5.18 (d, 1H, OCH_2CHCHH , $J=10.5$ Hz), δ 4.54 (dd, 1H, $\text{C}\alpha\text{H}$, $J=13.0, 6.9$ Hz), δ 4.27 – 4.08 (m, 9H, Cp), 4.06 – 3.99 (m, 2H, OCH_2CH), δ 3.95 – 3.87 (m, 2H, CH_2Fc), δ 3.90 (m, 1H, $\text{C}\alpha\text{H}$), δ 3.78 (dd, 1H, $\text{C}\alpha\text{HCHH}$, $J=10.0, 5.5$ Hz), δ 3.63 (m, 1H, $\text{C}\alpha\text{HCHH}$), δ 1.48 – 1.31 (m, 24H, $8\times\text{CH}_3$), δ 1.30 – 1.27 (m, 3H, CH_3 alanine).

^{13}C NMR (150 MHz, $\text{d}_6\text{-DMSO}$) δ 175.5, 174.5, 172.5, 172.3, 170.3, 135.3, 117.2, 83.4, 71.4, 69.2, 56.8, 56.6, 56.5, 56.3, 53.8, 50.8, 50.3, 26.6, 26.2, 25.5, 25.1, 24.39, 24.30, 23.9, 23.7.

HRMS: $[\text{M}]^+_{\text{calcd}}=754.3585$, $[\text{M}]^+_{\text{found}}=754.3588$.

Peptide 6



Chapter 3

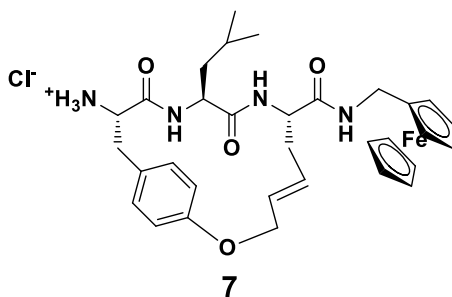
Peptide **15** (60 mg, 0.07 mmol) was deprotected according to General procedure for *N*-Boc cleavage, and the crude product purified on reverse phase HPLC to yield **6** (43%).

^1H NMR (600 MHz, DMSO- d_6): δ 8.60 (s, 1H, NH), 8.24 (d, 1H, NH, $J=6.9$ Hz), 8.12 (s, 3H, NH_3), 7.73 (s, 1H, NH), 7.60 (d, 1H, NH, $J=6.3$ Hz), 7.50 (s, 1H, NH), 7.32 (t, 1H, NH, 5.7 Hz), 5.84 (m, 2H, $2\times\text{CH}=\text{CH}_2$), 5.30-5.10 (m, 4H, $2\times\text{CH}=\text{CH}_2$), 4.56 (dd, 1H, $\text{C}\alpha\text{H}$, $J=13.2, 6.9$ Hz), 4.25-3.60 (m, 20H, Cp, $\text{C}\alpha\text{H}$, $5\times\text{CH}_2$), 1.55-1.25 (m, 24H, $8\times\text{CH}_3$).

^{13}C NMR (150 MHz, DMSO- d_6) δ 175.00, 173.94, 173.30, 171.74, 169.57, 169.14, 134.87, 134.74, 116.80, 116.29, 109.51, 86.41, 73.00, 71.07, 70.83, 69.35, 68.83, 68.70, 68.53, 68.30, 68.14, 67.06, 67.02, 66.98, 66.94, 56.36, 56.10, 55.95, 54.54, 53.32, 37.80, 25.66, 25.33, 25.13, 25.01, 24.13, 24.06, 23.46, 23.31.

HRMS: $[\text{M}]^+_{\text{calcd}}=810.3852$, $[\text{M}]^+_{\text{found}}=810.3834$.

Peptide 7



Peptide **16** (24 mg, 0.03 mmol) was deprotected according to General procedure for *N*-Boc cleavage, and the crude product purified on reverse phase HPLC to yield **7** (25%).

^1H NMR (600 MHz, d_6 -DMSO) δ 8.30 (d, 3H, NH Tyr, $J=3.4$ Hz), δ 8.20 (d, 1H, NH Gly, $J=8.7$ Hz), δ 7.99 (t, 1H, NH Fc, $J=5.8$ Hz), δ 7.93 (d, 1H, NH Leu, $J=8.0$ Hz), δ 6.96 (d, 2H, ArH, $J=7.9$ Hz), δ 6.72 (d, 2H, ArH, $J=8.7$ Hz), δ 5.64 – 5.60 (dt, 1H, OCH_2CH , $J=15.8, 4.3$ Hz), δ 5.54 – 5.50 (m, 1H, OCH_2CHCH), δ 4.67 – 4.60 (m, 2H, OCH_2CH), δ 4.41 – 4.37 (ddd, 1H, $\text{C}\alpha\text{H}$ Gly, $J=11.8, 8.7, 2.7$ Hz), δ 4.23 -4.18 (m, 1H, $\text{C}\alpha\text{H}$ Tyr), δ

Chapter 3

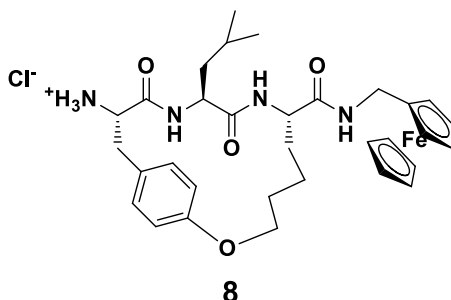
4.16 – 4.10 (m, 1H, C α H Leu), δ 4.16 – 4.04 (m, 9H, Cp), δ 4.00 – 3.91 (dd, 2H, CH₂Fc, J = 14.8, 5.8 Hz), δ 3.05 – 3.02 (dd, 1H, C α HCHHPH, J =13.1, 5.7 Hz), δ 2.71 – 2.67 (dd, 1H, C α HCHHPH, J =12.9, 10.6 Hz), δ 2.35 (d, 1H, OCH₂CHCHCH, J =15.5 Hz), δ 2.27 – 2.21 (m, 1H, OCH₂CHCHCH), δ 1.54 – 1.48 (m, 1H, C α HCH₂CH(CH₃)₂), δ 1.36 – 1.27 (m, 2H, C α HCH₂CH(CH₃)₂), δ 0.84 – 0.82 (m, 6H, C α HCH₂CH(CH₃)₂).

¹³C NMR (150 MHz, d₆-DMSO) δ 170.5, 166.4, 156.0, 129.8, 129.2, 127.3, 114.9, 86.0, 72.9, 69.4, 69.3, 68.2, 67.3, 67.2, 67.1, 65.8, 52.6, 52.5, 50.8, 43.5, 37.3, 36.0, 33.6, 23.6, 22.8, 22.7.

HRMS: [M+H]⁺ _{calcd}=600.23916, [M+H]⁺ _{found}= 600.23935.

IR: 1635 cm⁻¹, 1686 cm⁻¹ (shoulder) (Amide I Band); 1513 cm⁻¹, 1529 cm⁻¹ (Amide II Band); 3292 cm⁻¹ (Amide A Band).

Peptide 8



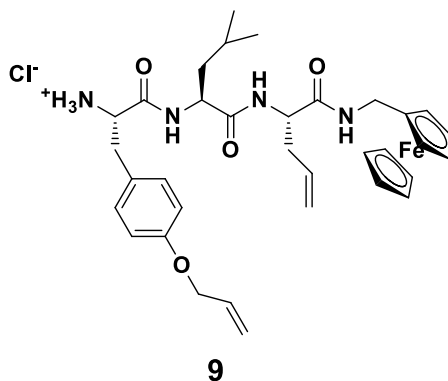
Peptide **17** (37 mg, 0.05 mmol) was deprotected according to General procedure for *N*-Boc cleavage, and the crude product purified on reverse phase HPLC to yield **8** (44%).

^1H NMR (600 MHz, d_6 -DMSO) δ 8.32 (d, 3H, *NH* Tyr, $J=4.1$ Hz), δ 8.11 (d, 1H, *NH* Gly, $J=9.1$ Hz), δ 7.96 (t, 1H, *NH* Fc, $J=5.9$ Hz), δ 7.80 (d, 1H, *NH* Leu, $J=7.8$ Hz), δ 7.00 (d, 2H, *ArH*, $J=7.7$ Hz), δ 6.79 (d, 2H, *ArH*, $J=8.6$ Hz), δ 4.35 – 4.25 (m, 3H, *OCHHCH*₂*CH*₂, *CaH* Gly, *CaH* Tyr), δ 4.19 – 4.01 (m, 11H, Cp, *CH*₂, *OCHHCH*₂*CH*₂, *CaH* Leu), δ 3.97 – 3.92 (dd, 2H, *CH*₂Fc, $J=15.8, 5.9$ Hz), δ 3.08 – 3.05 (dd, 1H, *CaHCHHPh*, $J=12.8, 5.8$ Hz), δ 2.65 – 2.61 (m, 1H, *CaHCHHPh*), δ 1.78 – 1.70 (m, 1H, *OCH*₂*CHHCH*₂), δ 1.61 – 1.47 (m, 3H, *OCH*₂*CH*₂*CHHCHH*, *CaHCH*₂*CH(CH*₃_{)₂), δ 1.43 – 1.21 (m, 5H, *OCH*₂*CHHCHHCHH*, *CaHCH*₂*CH(CH*₃_{)₂), δ 0.83 – 0.81 (m, 6H, *CaHCH*₂*CH(CH*₃_{)₂).}}}

^{13}C NMR (150 MHz, d_6 -DMSO) δ 171.1, 170.2, 166.4, 156.3, 130.1, 126.2, 115.5, 86.1, 73.0, 69.4, 69.3, 68.7, 67.3, 67.2, 67.1, 66.2, 52.6, 50.8, 50.7, 43.6, 40.0, 37.3, 36.2, 31.2, 26.8, 23.6, 22.8, 22.7, 21.7.

HRMS: $[\text{M}+\text{H}]^+$ $_{\text{calcd}}=602.25500$, $[\text{M}+\text{H}]^+$ $_{\text{found}}=602.25488$.

IR: 1636 cm^{-1} (Amide I Band); 1511 cm^{-1} (Amide II Band); 3293 cm^{-1} (Amide A Band).

Peptide **9**

Peptide **18** (37 mg, 0.05 mmol) was deprotected according to General procedure for *N*-Boc cleavage, and the crude product purified on reverse phase HPLC to yield **9** (45%).

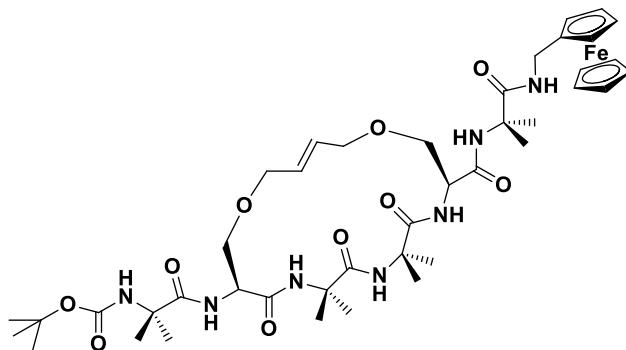
^1H NMR (600 MHz, d_6 -DMSO) δ 8.60 (d, 1H, *NH* Leu, $J=8.2$ Hz), δ 8.21 (d, 1H, *NH* Gly, $J=8.2$ Hz), δ 8.11 (t, 1H, *NH* Fc, $J=5.9$ Hz), δ 8.02 (d, 3H, *NH* Tyr, $J=4.1$ Hz), δ 7.16 (d, 2H, *ArH*, $J=8.5$ Hz), δ 6.88 (d, 2H, *ArH*, $J=8.6$ Hz), δ 6.06 – 6.00 (dtt, 1H, $\text{OCH}_2\text{CHCH}_2$, $J=15.8, 10.4, 5.2$ Hz), δ 5.77 – 5.69 (m, 1H, $\text{C}\alpha\text{HCH}_2\text{CHCH}_2$), δ 5.37 (ddd, 1H, OCH_2CHCHH , $J=17.3, 10.4, 1.5$ Hz), δ 5.25 (dd, 1H, OCH_2CHCHH , $J=10.4, 1.5$ Hz), δ 5.08 (dd, 1H, $\text{C}\alpha\text{HCH}_2\text{CHCHH}$, $J=17.1, 1.4$ Hz), δ 5.00 (d, 1H, $\text{C}\alpha\text{HCH}_2\text{CHCHH}$, $J=10.2$ Hz), δ 4.53 (d, 2H, $\text{OCH}_2\text{CHCH}_2$, $J=5.2$ Hz), δ 4.46 – 4.37 (m, 2H, $\text{C}\alpha\text{H}$ Leu, $\text{C}\alpha\text{H}$ Gly), δ 4.19 – 3.94 (m, 12H, Cp, $\text{C}\alpha\text{H}$ Tyr, CH_2Fc), δ 3.06 – 3.03 (dd, 1H, $\text{C}\alpha\text{HCHHPh}$, $J=14.4, 4.7$ Hz), δ 2.86 – 2.83 (dd, 1H, $\text{C}\alpha\text{HCHHPh}$, $J=14.4, 8.1$ Hz), δ 2.45 – 2.30 (m, 2H, $\text{C}\alpha\text{HCH}_2\text{CHCH}_2$), δ 1.66 – 1.59 (td, 1H, $\text{CH}_2\text{CH}(\text{CH}_3)_2$, $J=13.5, 6.7$ Hz), δ 1.50 – 1.45 (m, 2H, $\text{CH}_2\text{CH}(\text{CH}_3)_2$), δ 0.90 – 0.86 (m, 6H, $\text{C}\alpha\text{HCH}_2\text{CH}(\text{CH}_3)_2$).

^{13}C NMR (150 MHz, d_6 -DMSO) δ 171.1, 170.1, 167.6, 157.3, 134.0, 133.7, 130.6, 126.6, 117.3, 114.6, 85.9, 71.5, 70.9, 70.3, 68.3, 68.1, 67.5, 67.4, 67.3, 67.2, 67.1, 53.2, 52.0, 51.0, 48.5, 41.1, 40.0, 37.4, 36.3, 36.0, 23.9, 22.9, 21.6.

HRMS: $[\text{M}+\text{H}]^+$ $_{\text{calcd}}=628.27065$, $[\text{M}+\text{H}]^+$ $_{\text{found}}=628.26923$.

IR: 1641 cm^{-1} (Amide I Band); 1512 cm^{-1} (Amide II Band); 3277 cm^{-1} (Amide A Band).

Peptide 10



(*E* isomer)

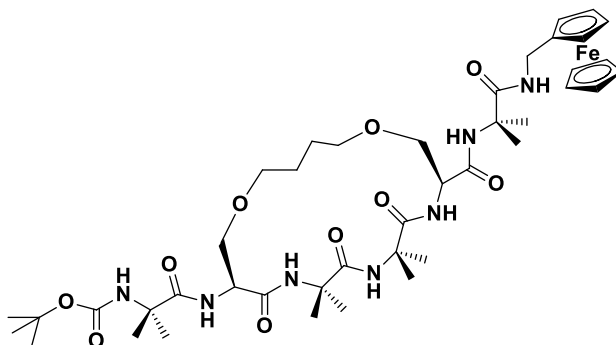
Peptide **22** (78 mg, 0.11 mmol) and ferrocenylmethylamine (35 mg, 0.16 mmol) were dissolved in anhydrous DMF (3 mL). DIPEA (80 μ L, 4 equiv.), HOAt (50 mg, 2 equiv.) and HATU (4 equiv.) were added. Reaction mixture was stirred overnight under an N_2 atmosphere at rt. The solvent was removed *in vacuo* and the peptide purified using reverse phase HPLC.

1H NMR (300 MHz, DMSO- d_6): δ 8.34 (s, 1H, NH), δ 7.99 (br s, 1H, NH), δ 7.77 (s, 1H, NH), δ 7.53 (s, 1H, NH), δ 7.49 (d, 1H, NH, $J=8.1$ Hz), δ 7.27 (s, 1H, NH), δ 7.07 (br s, 1H, NH), δ 5.68 (m, 2H, CH=CH), δ 4.44 (d, 1H, C α H, $J=6.4$ Hz), 4.31 – 3.68 (m, 18H, Cp, C α H, 4xCH $_2$), δ 3.58 – 3.49 (m, 2H, C α HCH $_2$), δ 1.42-1.28 (m, 33H, Boc, 8xCH $_3$).

^{13}C NMR (150 MHz, DMSO- d_6): δ 175.18, 174.89, 174.81, 174.68, 174.28, 173.13, 171.23, 168.76, 158.26, 158.02, 155.04, 131.20, 128.30, 109.53, 78.87, 78.63, 68.57, 67.00, 66.04, 56.46, 56.26, 56.13, 55.76, 54.82, 52.64, 37.82, 28.17, 26.72, 25.47, 25.00, 24.68, 23.46, 22.88.

LRMS: $[M+Na]^+$ $_{calcd}=904.4$, $[M+Na]^+$ $_{found}=904.4$.

Peptide 11



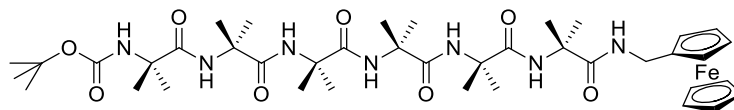
Peptide **23** (101 mg, 0.15 mmol) and ferrocenylmethylamine (35 mg, 0.16 mmol) were dissolved in anhydrous DMF (3 mL). DIPEA (100 μ L, 4 equiv.), HOAt (40mg, 2 equiv.) and HATU (110 mg, 4 equiv.) were added. Reaction mixture was stirred overnight under an N₂ atmosphere at room temperature. The solvent was removed *in vacuo* and the peptide purified using reverse phase HPLC.

¹H NMR (300 MHz, DMSO-d₆): δ 8.63 (s, 1H, NH), δ 8.06 (s, 1H, NH), δ 7.55 (s, 1H, NH), δ 7.35 (br s, 1H, NH), δ 7.33 (s, 1H, NH), δ 7.24 (br s, 1H, NH), δ 7.15 (br s, 1H, NH), δ 4.45 (br s, 1H, CaH), δ 4.24 – 3.90 (m, 12H, Cp, CaH, CH₂ (Fc)), δ 3.81 (d, 1H, CH, $J=6.9$ Hz), δ 3.68 – 3.58 (m, 4H, 2xCH₂), δ 3.41 (dd, 1H, CH, $J=9.6, 3.7$ Hz), δ 3.21 (td, 1H, CH, $J=9.2, 2.2$ Hz), δ 1.75 (m, 1H, CH), δ 1.64 (m, 1H, CH), δ 1.53 (m, 1H, CH), δ 1.44-1.25 (m, 35H, Boc, CH₂, 8xCH₃).

¹³C NMR (150 MHz, DMSO-d₆): δ 175.38, 174.76, 173.70, 173.40, 170.31, 168.84, 86.40, 78.24, 72.14, 70.83, 69.55, 68.91, 68.33, 67.01, 56.53, 56.44, 55.79, 55.75, 52.00, 37.88, 28.15, 27.43, 26.86, 26.46, 25.55, 24.03, 23.92, 23.18, 22.64.

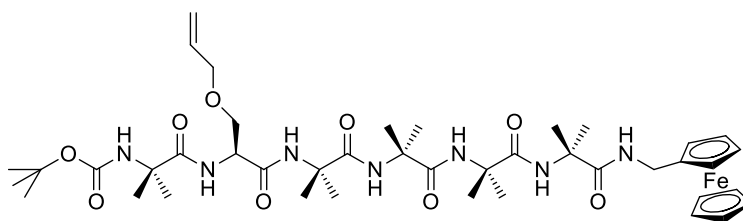
LRMS: [M+Na]⁺_{calcd}=906.4, [M+Na]⁺_{found}=906.4.

Peptide 12



^1H NMR (300 MHz, DMSO- d_6), ^{13}C NMR (150 MHz, DMSO- d_6), LRMS: Previously reported.¹²

Peptide 13

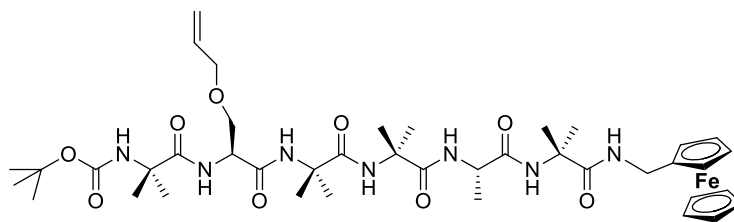


Peptide **24** (460 mg, 0.69 mmol) and ferrocenylmethylamine (163 mg, 0.76 mmol) were dissolved in anhydrous DMF (10 mL). DIPEA (480 μL , 4 equiv.), HOAt (190 mg, 2 equiv.) and HATU (4 equiv.) were added. Reaction mixture was stirred overnight under an N_2 atmosphere at room temperature. The solvent was removed *in vacuo* and the peptide purified using reverse phase HPLC.

^1H NMR (300 MHz, DMSO- d_6): δ 8.31 (br s, 1H, NH), δ 7.98 (br s, 1H, NH), δ 7.61 (s, 1H, NH), δ 7.56 (s, 1H, NH), δ 7.52 (br s, 1H, NH), δ 7.37 (s, 1H, NH), δ 7.31 (s, 1H, NH), δ 5.92-5.77 (ddd, 1H, $\text{CH}=\text{CH}_2$, $J=22.5, 10.4, 5.2$ Hz), δ 5.20 (m, 2H, $\text{CH}=\text{CH}_2$), δ 4.35-3.45 (m, 16H, Cp, NHCHCO , $2\times\text{CH}_2$), δ 1.65-1.05 (m, 39H, $10\times\text{CH}_3$, Boc).

LRMS: $[\text{M}+\text{Na}]^+_{\text{calcd}}=890.5$, $[\text{M}+\text{Na}]^+_{\text{found}}=890.5$.

Peptide 14

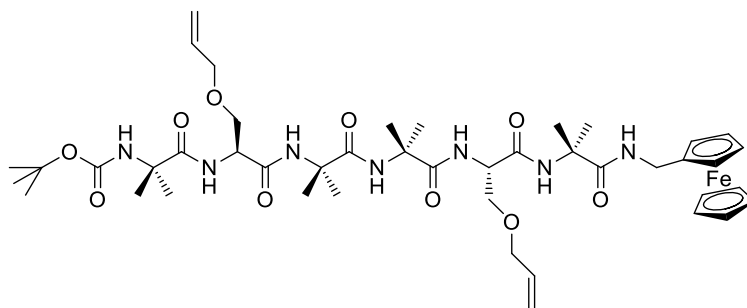


Peptide **25** (200 mg, 0.30 mmol) and ferrocenylmethylamine (72 mg, 0.33 mmol) were dissolved in anhydrous DMF (5 mL). DIPEA (212 μ L, 4 equiv.), HOBt (37 mg, 0.9 equiv.) and HATU (1.1 equiv.) were added. Reaction mixture was stirred for 39 h under an N_2 atmosphere at room temperature. The solvent was removed *in vacuo* and the peptide purified using reverse phase HPLC.

1H NMR (300 MHz, DMSO- d_6): δ 8.29 (br s, 1H, NH), δ 7.96 (br s, 1H, NH), δ 7.56 (d, 1H, NH, $J=6.0$ Hz), δ 7.50 (s, 1H, NH), δ 7.43 (s, 1H, NH), δ 7.39 (s, 1H, NH), δ 7.26 (t, 1H, NH, $J=6.1$ Hz), δ 5.87-5.80 (ddd, 1H, $CH=CH_2$, $J=22.4, 10.4, 5.2$ Hz), δ 5.23 (dd, 1H, $CH=CHCH$, $J=17.3, 1.5$ Hz), δ 5.14 (d, 1H, $CH=CHCH$, $J=10.4$ Hz), δ 4.20-4.02 (m, 10H, Cp, $C\alpha H$), δ 3.97-3.90 (m, 5H, $C\alpha H$, $2 \times CH_2$), δ 3.74-3.65 (m, 2H, CH_2), δ 1.41-1.32 (m, 33H, $8 \times CH_3$, Boc), δ 1.31-1.29 (m, 3H, CH_3 Alanine).

LRMS: $[M+Na]^+$ $_{calcd}=876.4$, $[M+Na]^+$ $_{found}=876.4$.

Peptide 15



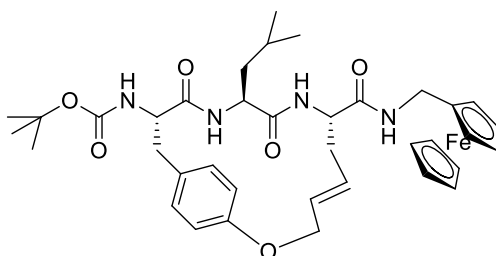
Chapter 3

Peptide **26** (240 mg, 0.32 mmol) and ferrocenylmethylamine (88 mg, 0.41 mmol) were dissolved in anhydrous DMF (5 mL). DIPEA (240 μ L, 4 equiv.), HOAt (80 mg, 2 equiv.) and HATU (4 equiv.) were added. The reaction mixture was stirred overnight under an N₂ atmosphere at room temperature. The solvent was removed *in vacuo* and the peptide purified using reverse phase HPLC.

¹H NMR (300 MHz, DMSO-d₆): δ 8.27 (br s, 1H, NH), δ 8.05 (br s, 1H, NH), δ 7.62 (d, 1H, NH, $J=6.4$ Hz), δ 7.54 (s, 1H, NH), δ 7.49 (s, 1H, NH), δ 7.43 (br s, 1H, NH), δ 7.27 (t, 1H, NH, $J=6.3$ Hz), δ 5.90 – 5.78 (m, 2H, 2xCH=CH₂), δ 5.25 – 5.08 (m, 4H, 2xCH=CH₂), δ 4.25-3.65 (m, 21H, Cp, 2xCaH, 5xCH₂), δ 1.65-1.05 (m, 33H, 8xCH₃, Boc).

LRMS: [M+Na]⁺_{calcd}=932.5, [M+Na]⁺_{found}=932.5.

Peptide 16



Peptide **27** (116 mg, 0.23 mmol) was dissolved in anhydrous DMF (3.85 mL) and the solution stirred at r.t. for 10 min. Ferrocenylmethylamine (54 mg, 0.25 mmol) was added, followed by DIPEA (119 mg, 0.92 mmol, 160 μ L), HATU (95 mg, 0.25 mmol) and HOAt (34 mg, 0.25 mmol). The reaction mixture was stirred under an N₂ atmosphere at rt for 20 h, and subsequently diluted with water (20 mL) and ethyl acetate (20 mL), and the pH adjusted to pH 3. The organic phase was separated and washed with brine (2 x 20 mL) and dried with MgSO₄. The solvent was removed *in vacuo* to yield a pale brown solid (63 mg), that was used in the next step without further purification.

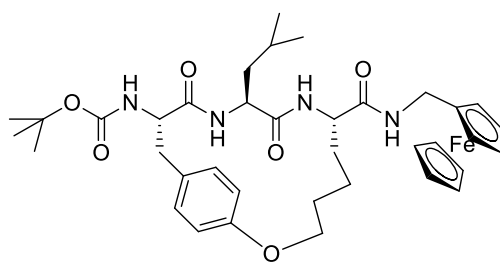
Chapter 3

^1H NMR (600 MHz, d_6 -DMSO) δ 7.97 (d, 1H, *NH* Gly, $J=8.6$ Hz), δ 7.90 (t, 1H, *NH* Fc, $J=5.8$ Hz), δ 7.07 (d, 1H, *NH* Leu, $J=7.8$ Hz), δ 6.97 (d, 2H, ArH, $J=7.7$ Hz), δ 6.87 (d, 1H, *NH* Tyr, $J=7.2$ Hz), δ 6.68 (d, 2H, ArH, $J=8.6$ Hz), δ 5.57- 5.54 (d, 1H, $\text{OCH}_2\text{CHCHCH}_2$, $J=14.9$ Hz), δ 5.49 – 5.44 (dd, 1H, $\text{OCH}_2\text{CHCHCH}_2$, $J=14.9$, 6.7 Hz), δ 4.63- 4.57 (m, 2H, $\text{OCH}_2\text{CHCHCH}_2$), δ 4.35 – 4.33 (m, 1H, *CaH* Gly), δ 4.25 – 3.92 (m, 9H, Cp), δ 4.21 – 4.17 (m, 1H, *CaH* Tyr), δ 4.07 – 4.05 (m, 1H, *CaH* Leu), δ 3.96 (m, 2H, CH_2Fc), δ 2.81 – 2.77 (dd, 1H, *CaHCHHPh*, $J=13.0$, 5.2 Hz), δ 2.69 – 2.61 (m, 1H, *CaHCHHPh*), δ 2.38 – 2.22 (m, 2H, $\text{OCH}_2\text{CHCHCH}_2$), δ 1.52 – 1.46 (tt, 1H, *CaHCH}_2\text{CH}(\text{CH}_3)_2, $J=13.3$, 6.6 Hz), δ 1.38 (s, 9H, $(\text{CH}_3)_3$), δ 1.31 – 1.23 (m, 2H, *CaHCH}_2\text{CH}(\text{CH}_3)_2), δ 0.79 – 0.77 (m, 6H, *CaHCH}_2\text{CH}(\text{CH}_3)_2).***

^{13}C NMR (150 MHz, d_6 -DMSO) δ 170.9, 170.5, 162.2, 155.5, 129.7, 129.1, 127.3, 114.9, 85.9, 77.9, 72.2, 71.5, 70.3, 69.2, 68.9, 68.8, 68.7, 68.3, 68.2, 67.9, 67.3, 60.2, 52.6, 50.4, 43.1, 40.0, 38.2, 37.4, 35.7, 30.7, 28.1, 23.5, 23.1, 22.4.

LRMS: $[\text{M} + \text{Na}]^+$ $_{\text{calcd}}=723.2$, $[\text{M} + \text{Na}]^+$ $_{\text{found}}=723.2$.

Peptide 17



Peptide **28** (200 mg, 0.40 mmol) was dissolved in anhydrous DMF (6.7 mL) and stirred at rt for 10 min. Ferrocenylmethylamine (95 mg, 0.44 mmol) was added, followed by DIPEA (206 mg, 1.60 mmol, 280 μL), HATU (167 mg, 0.44 mmol) and HOAt (60 mg, 0.44 mmol). The reaction mixture was stirred at r.t. under N_2 conditions for 24 h, and subsequently diluted with water (32 mL) and ethyl acetate (32 mL), and the pH adjusted to pH 3-4. The organic phase was separated and washed with NaHCO_3 (30 mL) and brine (2

Chapter 3

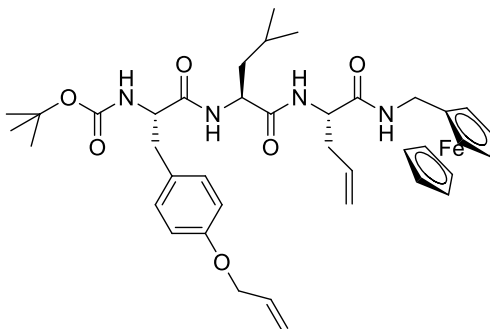
x 30 mL), and dried with MgSO₄. The solvent was removed *in vacuo* to yield a pale brown solid (300 mg), that was used in the next step without further purification.

¹H NMR (600 MHz, d₆-DMSO) δ 7.96 (d, 1H, NH Gly, *J*=9.8 Hz), δ 7.89 (m, 1H, NH Fc), δ 7.20 – 6.96 (m, 3H, ArH and NH Tyr), δ 6.88 – 6.62 (m, 3H, ArH and NH Leu), δ 4.34 – 4.02 (m, 2H, OCH₂CH₂CH₂), δ 4.29 – 4.25 (m, 1H, CαH Gly), δ 4.23 – 3.96 (m, 9H, Cp), δ 4.20 – 3.96 (m, 2H, 2x CαH), δ 3.96 (d, 2H, CH₂Fc, *J*=5.7 Hz), δ 2.82 – 2.79 (dd, 1H, CαHCHHPh, *J*=12.6, 5.5 Hz), δ 2.64 – 2.59 (m, 1H, CαHCHHPh), δ 1.77 – 1.68 (br s, 2H, OCH₂CH₂CH₂), δ 1.59 -1.42 (td, 3H, CαHCH₂CH(CH₃)₂, *J*=13.1, 6.4 Hz), δ 1.38 (s, 9H, (CH₃)₃), δ 1.34 – 1.19 (m, 4H, OCH₂CH₂CH₂CH₂), δ 0.88 – 0.74 (m, 6H, CαHCH₂CH(CH₃)₂).

¹³C NMR (150 MHz, d₆-DMSO) δ 171.2, 170.8, 169.7, 162.2, 155.8, 128.5, 115.4, 86.0, 77.8, 73.0, 70.3, 69.4, 68.8, 68.7, 67.2, 67.1, 66.8, 59.7, 56.0, 50.8, 50.3, 43.2, 40.0, 38.2, 37.3, 36.6, 35.7, 31.2, 30.7, 28.0, 27.0, 23.5, 23.1, 22.6, 21.8, 20.7.

LRMS: [M + Na]⁺ _{calcd}=725.3, [M + Na]⁺ _{found}=725.1.

Peptide 18



Peptide **29** (200 mg, 0.38 mmol) was dissolved in anhydrous DMF (6.4 mL). Ferrocenylmethylamine (90 mg, 0.42 mmol) was added, followed by DIPEA (196 mg, 1.52 mmol, 265 μL), HATU (160 mg, 0.42 mmol) and HOAt (57 mg, 0.42 mmol). The reaction mixture was stirred under an N₂ atmosphere at rt for 24 h, and subsequently diluted with water (30 mL) and ethyl acetate (30 mL), and the pH adjusted to pH 3-4. The

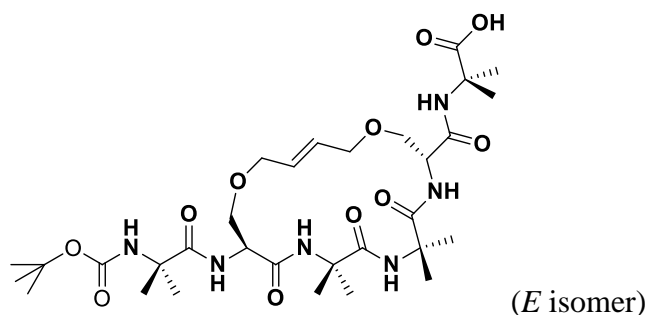
Chapter 3

organic phase was separated and washed with NaHCO_3 (30 mL) and brine (30 mL), and dried with MgSO_4 . The solvent was removed *in vacuo* to yield a brown solid (280 mg), that was used in the next step without further purification.

^1H NMR (300 MHz, d_6 -DMSO) δ 8.11 – 7.91 (m, 3H, NH), δ 7.14 (d, 2H, ArH, $J=8.1$ Hz), δ 6.88 (d, 1H, NH, $J=8.9$ Hz), δ 6.82 (d, 2H, ArH, $J=8.2$ Hz), δ 6.08 – 5.96 (m, 1H, $\text{OCH}_2\text{CHCH}_2$), δ 5.76 – 5.66 (m, 1H, $\text{C}\alpha\text{HCH}_2\text{CHCH}_2$), δ 5.34 (d, 1H, CH_2CHCHH , $J=17.3$ Hz), δ 5.22 (d, 1H, CH_2CHCHH , $J=10.3$ Hz), δ 5.09 – 4.98 (m, 2H, CH_2CHCHH), δ 4.50 (d, 1H, $\text{OCH}_2\text{CHCH}_2$, $J=4.0$ Hz), δ 4.38 – 4.30 (m, 1H, $\text{C}\alpha\text{H}$), δ 4.21 – 4.02 (m, 11H, Cp and 2x $\text{C}\alpha\text{H}$), δ 3.96 (d, 2H, CH_2Fc , $J=6.1$ Hz), δ 2.93 – 2.60 (m, 2H, $\text{C}\alpha\text{HCH}_2\text{Ph}$), δ 2.47 – 2.27 (m, 2H, $\text{C}\alpha\text{HCH}_2\text{CHCH}_2$), δ 1.68 – 1.23 (m, 3H, $\text{CH}_2\text{CH}(\text{CH}_3)_2$), δ 1.30 (s, 9H, $(\text{CH}_3)_3$), δ 0.91 – 0.82 (m, 6H, $\text{C}\alpha\text{HCH}_2\text{CH}(\text{CH}_3)_2$).

LRMS: $[\text{M} + \text{Na}]^+$ $\text{calcd}=751.3$, $[\text{M} + \text{Na}]^+$ $\text{found}=751.2$.

Peptide 22



Peptide **26** (0.839 g, 1.2 mmol) was dissolved in anhydrous DCM (60 mL) in a nitrogen-flushed flask equipped with a water-cooled condenser. Second-generation Grubbs' catalyst (0.071 g, 7 mol%) was added in a single portion and the flask was then immersed in an oil bath maintained at 50 °C. After refluxing for 30 min., the reaction was quenched by adding ethyl vinyl ether (400 μL) directly to the flask after removing it from the oil bath. Stirring continued for 20 min., after which the solvent was removed under reduced pressure. The

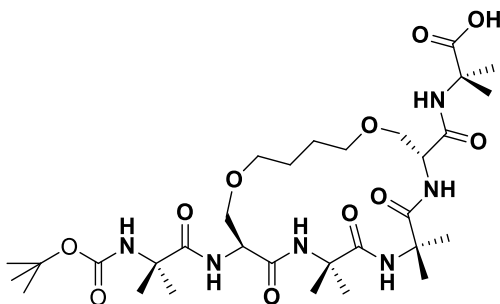
Chapter 3

residue was purified by column chromatography (DCM with 2% →10% methanol) to afford the *E*-selective isomer (475 mg, 57%).

^1H NMR (300 MHz, CDCl_3): δ 8.17 (s, 1H, NH), δ 7.53 (d, 1H, NH, $J=8.8$ Hz), δ 7.42 (s, 1H, NH), δ 7.08 (d, 1H, NH, $J=6.0$ Hz), δ 6.98 (s, 1H, NH), δ 5.77-5.67 (m, 2H, CH=CH), δ 5.31 (s, 1H, NH), δ 4.75-4.47 (m, 2H, 2xNHCHCO), δ 4.28-3.60 (m, 8H, 2x CH₂-CH=CH, 2xCHCH₂O), δ 1.65-1.37 (m, 33H, 8xCH₃, Boc).

LRMS: $[\text{M}+\text{Na}]^+_{\text{calcd}}=707.4$, $[\text{M}+\text{Na}]^+_{\text{found}}=707.4$.

Peptide 23

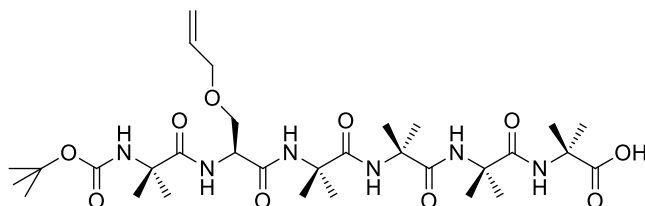


To a solution of **22** (100 mg, 0.146 mmol) in anhydrous ethyl acetate (30 mL), was added 20 mg Pd/C (20% w/w). The reaction was purged with nitrogen and then placed under a hydrogen atmosphere. After stirring for 2 h, the reaction was filtered and concentrated *in vacuo* to reveal a white solid (100 mg, quant).

^1H NMR (300 MHz, CDCl_3): δ 8.12 (s, 1H, NH), δ 7.58 (d, 1H, NH, $J=8.8$ Hz), δ 7.44 (s, 1H, NH), δ 7.18 (d, 1H, NH, $J=4.0$ Hz), δ 7.10 (s, 1H, NH), δ 5.45 (s, 1H, NH), δ 4.62 (m, 1H, NHCHCO), δ 4.51 (m, 1H, NHCHCO), δ 4.11 (m, 2H, CH₂CH₂O), δ 3.84 (m, 2H, CHCH₂O), δ 3.70 (m, 2H, OCH₂CH₂), δ 3.50 (m, 2H, CHCH₂O), δ 1.70-1.35 (m, 37H, 2xCH₂, 8xCH₃, Boc).

LRMS: $[\text{M}+\text{Na}]^+_{\text{calcd}}=709.4$, $[\text{M}+\text{Na}]^+_{\text{found}}=709.4$.

Peptide 24



Fmoc-Aib-OH loaded 2-chlorotriyl chloride resin (2.0 g, typically 0.5 mmol/ gram of resin) was transferred into a sintered funnel fitted with a Teflon stopcock, and then rinsed with DCM (2x20 mL). After air drying, the Fmoc group was removed by reaction with a solution of 25% piperidine in DMF (20 mL) for 30 min followed by washing successively with DCM (3x20 mL), DMF (3x20 mL), and DCM (3x20 mL). To a solution of Fmoc-Aib-OH (1.0 g, 2 equiv) in DMF (4 mL) was added a 0.5 M solution of HATU in DMF (2 mL) followed by DIPEA (1.2 mL, 4-fold excess) and the resultant solution was added to the deprotected resin. The mixture was left for 2 h, with occasional stirring. The resin was isolated by filtration and rinsed successively with DCM (3x50 mL), DMF (3x50 mL), and DCM (3x50 mL). The sequence was repeated twice to ensure complete coupling. Successive additions of Fmoc Aib-OH were carried out to give the appropriate oligotetrapeptide. Following additions of Fmoc-Ser(AI)-OH were carried out, using this protocol, to give the appropriate pentapeptide. The pentapeptide was then capped with Boc-Aib-OH in the last cycle using the same protocol and the resulting hexapeptide was cleaved from the resin with 2% TFA/DCM (v/v). The crude products were purified using reverse phase HPLC.

^1H NMR (300 MHz, CDCl_3): δ 7.99 (s, 1H, NH), δ 7.67 (s, 1H, NH), δ 7.65 (s, 1H, NH), δ 7.24 (s, 1H, NH), δ 7.19 (d, 1H, NH, $J=4.7$ Hz), δ 5.80 (ddd, 1H, $\text{CH}=\text{CH}_2$, $J=15.9, 10.4, 5.6$ Hz), δ 5.22 (m, 2H, $\text{CH}=\text{CH}_2$), δ 5.20 (s, 1H, NH), δ 4.13 (m, 1H, NHCHCO), δ 3.99 (m, 2H, CHCH_2O), δ 3.87 (dd, 1H, $\text{CHHCH}=\text{CH}_2$, $J=10.4, 3.2$ Hz), δ 3.72 (dd, 1H, $\text{CHHCH}=\text{CH}_2$, $J=10.0, 3.5$ Hz), δ 1.60-1.11 (m, 39H, 10x CH_3 , Boc).

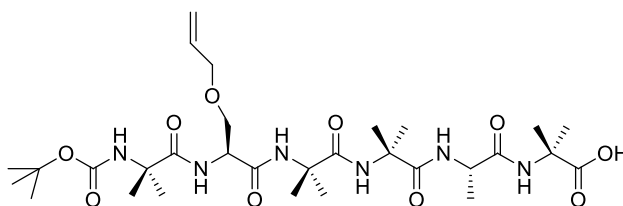
^{13}C NMR (150 MHz, CDCl_3) δ 176.24, 175.89, 175.48, 174.74, 170.72, 155.47, 133.56, 117.90, 81.46, 77.21, 77.00, 76.79, 72.22, 67.97, 59.53, 57.09, 56.90, 56.74, 56.18, 50.81,

Chapter 3

31.91, 31.23, 29.68, 29.64, 29.35, 28.29, 28.25, 27.23, 26.61, 26.45, 25.55, 24.65, 23.52, 23.43, 23.33, 23.64, 22.68, 14.10.

LRMS: $[M+Na]^+$ $_{\text{calcd}}=693.4$, $[M+Na]^+$ $_{\text{found}}=693.4$.

Peptide 25

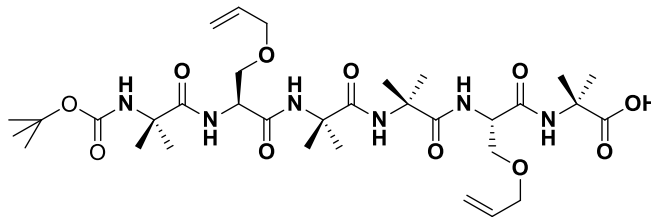


Peptide **25** was synthesized on SPPS using the protocol for peptide **24**, with an Fmoc-Ala-OH residue at position 2, in lieu of Fmoc-Aib-OH.

^1H NMR (300 MHz, DMSO- d_6): δ 8.22 (br s, 1H, NH), δ 7.94 (br s, 1H, NH), δ 7.42 (d, 1H, NH, $J=3.5$ Hz), δ 7.42 – 7.37 (m, 3H, NH), δ 5.83 (m, 1H, OCH_2CH), δ 5.23 (dd, 1H, CHCHH, $J=13.9, 1.6$ Hz), δ 5.13 (dd, 1H, CHCHH, $J=13.9, 1.6$ Hz), δ 4.10 (br s, 1H, $\text{C}\alpha\text{H}$), δ 3.96 (dd, 2H, OCH_2CH , $J=3.5, 1.6$ Hz), δ 3.68 (ddd, 2H, $\text{C}\alpha\text{HCH}_2$, $J=13.9, 9.9, 4.6$ Hz), δ 1.39 – 1.29 (m, 33H, Boc, 4xAibs), δ 1.27 – 1.25 (d, 3H, CH_3 Alanine, $J=7.3$ Hz).

HRMS: $[M]^+$ $_{\text{calcd}}=657.3823$, $[M]^+$ $_{\text{found}}=657.3891$.

Peptide 26

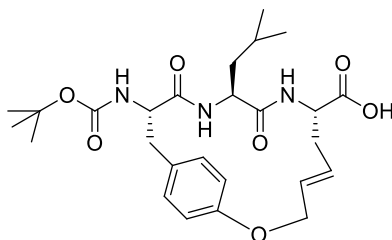


Fmoc-Aib-OH loaded 2-chlorotrityl chloride resin (2.0 g, typically 0.5 mmol/ gram of resin) was transferred into a sintered funnel fitted with a Teflon stopcock, and then rinsed with DCM (2x20 mL). After air drying, the Fmoc group was removed by reaction with a solution of 25% piperidine in DMF (20 mL) for 30 min followed by washing successively with DCM (3x20 mL), DMF (3x20 mL) and DCM (3x20 mL). To a solution of Fmoc-Ser(AI)-OH (1.0 g, 2 equiv) in DMF (4 mL) was added a 0.5 M solution of HATU in DMF (2 mL) followed by DIPEA (1.2 mL, 4-fold excess) and the resulting solution was added to the deprotected resin. The mixture was left for 2 h, with occasional stirring. The resin was isolated by filtration and rinsed successively with DCM (3x50 mL), DMF (3x50 mL), and DCM (3x50 mL). The sequence was repeated 2 more times to ensure complete coupling. Following additions of Fmoc-Aib-OH and Fmoc-Ser(AI)-OH were carried out, using this protocol, to give the appropriate pentapeptide. The pentapeptide was capped with Boc-Aib-OH in the last cycle using the same protocol and the resulting hexapeptide was cleaved from the resin with 2% TFA/DCM (v/v). The crude products were purified by HPLC.

^1H NMR (300 MHz, CDCl_3): δ 8.13 (s, 1H, NH), δ 7.72 (s, 1H, NH), δ 7.71 (d, 1H, NH, $J=9.0$ Hz), δ 7.20 (s, 1H, NH), δ 7.17 (d, 1H, NH, $J=5.3$ Hz), δ 5.82 (m, 2H, $2\times\text{CH}=\text{CH}_2$), δ 5.30 (s, 1H, NH), δ 5.20 (m, 4H, $2\times\text{CH}=\text{CH}_2$), δ 4.53 (m, 2H, $2\times\text{NHCHCO}$), δ 3.99 (m, 4H, $2\times\text{CHCH}_2\text{O}$), δ 3.90-3.64 (m, 4H, $2\times\text{CH}_2\text{CH}=\text{CH}_2$), δ 1.65-1.35 (m, 33H, $8\times\text{CH}_3$, Boc).

LRMS: $[\text{M}+\text{Na}]^+$ _{calcd}=735.4, $[\text{M}+\text{Na}]^+$ _{found}=735.4.

Peptide 27



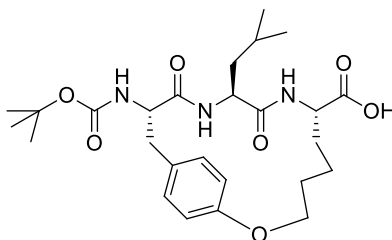
Methyl (4*E*,7*S*,10*S*,13*S*)-13-([(tert-butoxy)carbonyl]amino)-10-(2-methylpropyl)-9,12-dioxo-2-oxa-8,11-diazabicyclo[13.2.2]nonadeca-1(17),4,15,18-tetraene-7-carboxylate (584 mg, 1.13 mmol) was dissolved in THF (4 mL). To this stirring reaction 1.6M NaOH (1.2 mL) was added, followed by MeOH (2 mL). The solution was stirred at rt for 22 h, diluted with H₂O (20 mL) and ethyl acetate (20 mL), and the pH adjusted to pH 3. The organic phase was separated, washed with brine (20 mL), and dried with MgSO₄. The solvent was removed *in vacuo* to yield a white crystalline solid (495 mg, 87%).

¹H NMR (600 MHz, d₆-DMSO) δ 7.97 (d, 1H, *NH* Gly, *J*=8.4 Hz), δ 7.19 (d, 1H, *NH* Leu, *J*=8.2 Hz), δ 6.97 (d, 2H, *ArH*, *J*=7.3 Hz), δ 6.87 (d, 1H, *NH* Tyr, *J*=7.3 Hz), δ 6.68 (d, 2H, *ArH*, *J*=8.7 Hz), δ 5.56 (d, 1H, OCH₂CHCHCH₂, *J*=15.7 Hz), δ 5.47 – 5.43 (m, 1H, OCH₂CHCHCH₂), δ 4.65 – 4.57 (m, 2H, OCH₂CHCHCH₂), δ 4.27 – 4.23 (m, 1H, *CaH* Gly), δ 4.22 – 4.17 (m, 1H, *CaH* Tyr), δ 4.09 – 4.06 (m, 1H, *CaH* Leu), δ 2.80 – 2.77 (dd, 1H, *CaH* CHHPh, *J*=13.0, 5.2 Hz), δ 2.69 – 2.65 (m, 1H, *CaH* CHHPh), δ 2.49 – 2.46 (m, 1H, OCH₂CHCHCHH), δ 2.25 – 2.20 (m, 1H, OCH₂CHCHCHH), δ 1.58 – 1.51 (m, 1H, *CaH*CH₂CH(CH₃)₂), δ 1.38 (s, 9H, (CH₃)₃), δ 1.34 – 1.23 (m, 2H, *CaH*CH₂CH(CH₃)₂), δ 0.84 – 0.79 (m, 6H, *CaH*CH₂CH(CH₃)₂).

¹³C NMR (150 MHz, d₆-DMSO) δ 172.7, 171.9, 171.0, 170.2, 169.8, 155.4, 154.6, 129.7, 128.9, 77.9, 72.2, 65.9, 60.2, 59.7, 55.3, 51.8, 50.4, 42.9, 32.6, 28.1, 23.4, 23.0, 22.4, 21.0, 20.7.

LRMS: [M]⁻ _{calcd}=502.2, [M]⁻ _{found}=502.2.

Peptide 28

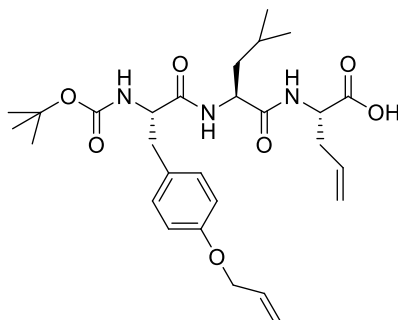


Methyl (7S,10S,13S)-13-[[tert-butoxy]carbonyl]amino}-10-(2-methylpropyl)-9,12-dioxo-2-oxa-8,11-diazabicyclo[13.2.2]nonadeca-1(17),15,18-triene-7-carboxylate (558 mg, 1.08 mmol) was dissolved in THF (3.2 mL). To this stirring reaction, 1.6M NaOH (1.1 mL) was added, followed by MeOH (1.84 mL). The solution was stirred at rt for 22 h, diluted with H₂O (20 mL) and ethyl acetate (20 mL), and the pH adjusted to pH 3-4. The organic phase was separated, washed with brine (20 mL), and dried with MgSO₄. The solvent was removed *in vacuo* to yield a white solid (400 mg, 73%).

¹H NMR (300 MHz, d₆-DMSO) δ 8.03 (d, 1H, NH, *J*=8.9 Hz), δ 7.01 (d, 3H, NH and ArH, *J*=7.6 Hz), δ 6.81 (d, 1H, NH, *J*=8.0 Hz), δ 6.75 (d, 2H, ArH, *J*=8.6 Hz), δ 4.39 – 4.30 (d, 1H, C α H, *J*=11.9 Hz), δ 4.25 – 4.12 (m, 2H, OCH₂CH₂CH₂), δ 4.07 – 3.91 (dd, 2H, (2x C α H), *J*=14.4, 7.3 Hz), δ 2.85 – 2.77 (dd, 1H, C α HCHHPh, *J*=12.2, 5.1 Hz), δ 2.67 – 2.54 (t, 1H, C α HCHHPh, *J*=12.2 Hz), δ 1.78 – 1.62 (br s, 2H, OCH₂CH₂CH₂), δ 1.61 – 1.45 (m, 3H, C α HCH₂CH(CH₃)₂), δ 1.38 (s, 9H, (CH₃)₃), δ 1.35 – 1.20 (m, 4H, OCH₂CH₂CH₂CH₂), δ 0.81 – 0.76 (m, 6H, C α HCH₂CH(CH₃)₂).

LRMS: [M + H]⁺ _{calcd}=506.2, [M + H]⁺ _{found}=505.9.

Peptide 29



Methyl(2S)-2-[(2S)-2-[(2S)-2-[(tert-butoxy)carbonyl]amino]-3-[4-(prop-2-en-1-yloxy)phenyl] propanamido]-4-methylpentanamido]pent-4-enoate¹³ (485 mg, 0.89 mmol) was dissolved in THF (3 mL). To this stirring reaction 1.6M NaOH (890 μ L) was added, followed by MeOH (1.5 mL). The solution was stirred at rt for 23 h, diluted with H₂O (20 mL) and ethyl acetate (20 mL), and the pH adjusted to pH 3-4. The organic phase was separated, washed with brine (20 mL), and dried over MgSO₄. The solvent was removed *in vacuo* to yield a white solid (405 mg, 86%).

¹H NMR (300 MHz, d₆-DMSO) δ 8.11 (d, 1H, NH, $J=7.7$ Hz), δ 7.87 (d, 1H, NH, $J=8.4$ Hz), δ 7.14 (d, 2H, ArH, $J=8.2$ Hz), δ 6.88 (d, 1H, NH, $J=8.9$ Hz), δ 6.82 (d, 2H, ArH, $J=7.9$ Hz), δ 6.09 – 5.96 (ddd, 1H, OCH₂CHCH₂, $J=22.4, 10.4, 5.2$ Hz), δ 5.82 – 5.68 (td, 1H, C α HCH₂CHCH₂, $J=16.9, 6.9$ Hz), δ 5.34 (d, 1H, CH₂CHCHH, $J=17.3$ Hz), δ 5.22 (d, 1H, CH₂CHCHH, $J=10.3$ Hz), δ 5.07 (d, 1H, CH₂CHCHH, $J=17.3$ Hz), δ 5.02 (d, 1H, CH₂CHCHH, $J=10.3$ Hz), δ 4.51 (m, 1H, OCH₂CHCH₂), δ 4.42 – 4.35 (m, 1H, C α H), δ 4.26 – 4.19 (dd, 1H, C α H, $J=13.0, 7.7$ Hz) δ 4.13 – 3.97 (m, 1H, C α H), δ 2.91 – 2.84 (d, 1H, C α HCHHPh, $J=10.3$ Hz), δ 2.64 – 2.60 (m, 1H, C α HCHHPh), δ 2.47 – 2.32 (m, 2H, C α HCH₂CHCH₂), δ 1.70 – 1.24 (m, 3H, CH₂CH(CH₃)₂), δ 1.30 (s, 9H, (CH₃)₃), δ 0.90 – 0.84 (m, 6H, C α HCH₂CH(CH₃)₂).

3.7 References

1. (a) Isied, S. S.; Ogawa, M. Y.; Wishart, J. F., Peptide-Mediated Intramolecular Electron Transfer - Long-Range Distance Dependence. *Chemical Reviews* **1992**, 92 (3), 381; (b) Ron, I.; Sepunaru, L.; Itzhakov, S.; Belenkova, T.; Friedman, N.; Pecht, I.; Sheves, M.; Cahen, D., Proteins as Electronic Materials: Electron Transport through Solid-State Protein Monolayer Junctions. *Journal of the American Chemical Society* **2010**, 132 (12), 4131-4140.
2. (a) Yu, J.; Zvarec, O.; Huang, D. M.; Bissett, M. A.; Scanlon, D. B.; Shapter, J. G.; Abell, A. D., Electron Transfer through α -Peptides Attached to Vertically Aligned Carbon Nanotube Arrays: A Mechanistic Transition. *Chemical Communications* **2012**, 48 (8), 1132-1134; (b) Mandal, H. S.; Kraatz, H.-B., Electron Transfer Mechanism in Helical Peptides. *The Journal of Physical Chemistry Letters* **2012**, 3 (6), 709-713; (c) Malak, R. A.; Gao, Z. N.; Wishart, J. F.; Isied, S. S., Long-range electron transfer across peptide bridges: The transition from electron superexchange to hopping. *Journal of the American Chemical Society* **2004**, 126 (43), 13888.
3. (a) Yu, J.; Horsley, J. R.; Abell, A. D., The Influence of Secondary Structure on Electron Transfer in Peptides. *Australian Journal of Chemistry* **2013**, 66, 848-851; (b) Yu, J.; Huang, D. M.; Shapter, J. G.; Abell, A. D., Electrochemical and Computational Studies on Intramolecular Dissociative Electron Transfer in beta-Peptides. *Journal of Physical Chemistry C* **2012**, 116 (50), 26608-26617.
4. (a) Chaudhry, B. R.; Wilton-Ely, J.; Tabor, A. B.; Caruana, D. J., Effect of peptide orientation on electron transfer. *Phys. Chem. Chem. Phys.* **2010**, 12 (34), 9996; (b) Lauz, M.; Eckhardt, S.; Fromm, K. M.; Giese, B., The influence of dipole moments on the mechanism of electron transfer through helical peptides. *Phys. Chem. Chem. Phys.* **2012**, 14 (40), 13785-13788; (c) Yasutomi, S.; Morita, T.; Imanishi, Y.; Kimura, S., A molecular photodiode system that can switch photocurrent direction. *Science* **2004**, 304 (5679), 1944-1947.
5. (a) Cordes, M.; Kottgen, A.; Jasper, C.; Jacques, O.; Boudebous, H.; Giese, B., Influence of amino acid side chains on long-distance electron transfer in peptides: Electron hopping via "Stepping Stones". *Angewandte Chemie-International Edition* **2008**, 47 (18), 3461-3463; (b) Gao, J.; Mueller, P.; Wang, M.; Eckhardt, S.; Lauz, M.; Fromm, K. M.; Giese, B., Electron Transfer in Peptides: The Influence of Charged Amino Acids. *Angewandte Chemie-International Edition* **2011**, 50 (8), 1926-1930; (c) Wang, M.; Gao, J.; Muller, P.; Giese, B., Electron Transfer in Peptides with Cysteine and Methionine as Relay Amino Acids. *Angewandte Chemie-International Edition* **2009**, 48 (23), 4232-4234; (d) Watanabe, J.; Morita, T.; Kimura, S., Effects of dipole moment, linkers, and chromophores at side chains on long-range electron transfer through helical peptides. *Journal of Physical Chemistry B* **2005**, 109 (30), 14416.
6. Long, Y. T.; Abu-Rhayem, E.; Kraatz, H. B., Peptide electron transfer: More questions than answers. *Chemistry-A European Journal* **2005**, 11 (18), 5186.
7. (a) Wenger, O. S., How Donor-Bridge-Acceptor Energetics Influence Electron Tunneling Dynamics and Their Distance Dependences. *Accounts of Chemical Research* **2011**, 44 (1), 25; (b) Polo, F.; Antonello, S.; Formaggio, F.; Toniolo, C.; Maran, F., Evidence against the hopping mechanism as an important electron transfer pathway for conformationally constrained oligopeptides. *Journal of the American Chemical Society* **2005**, 127 (2), 492.
8. (a) Giese, B.; Graber, M.; Cordes, M., Electron transfer in peptides and proteins. *Current Opinion in Chemical Biology* **2008**, 12 (6), 755-759; (b) Cordes, M.; Giese, B.,

Electron transfer in peptides and proteins. *Chemical Society Reviews* **2009**, 38 (4), 892-901.

9. Yanagisawa, K.; Morita, T.; Kimura, S., Efficient photocurrent generation by self-assembled monolayers composed of 3(10)-helical peptides carrying linearly spaced naphthyl groups at the side chains. *Journal of the American Chemical Society* **2004**, 126 (40), 12780-12781.

10. Shih, C.; Museth, A. K.; Abrahamsson, M.; Blanco-Rodriguez, A. M.; Di Bilio, A. J.; Sudhamsu, J.; Crane, B. R.; Ronayne, K. L.; Towrie, M.; Vlcek, A.; Richards, J. H.; Winkler, J. R.; Gray, H. B., Tryptophan-accelerated electron flow through proteins. *Science* **2008**, 320 (5884), 1760-1762.

11. Wittekindt, C.; Schwarz, M.; Friedrich, T.; Koslowski, T., Aromatic Amino Acids as Stepping Stones in Charge Transfer in Respiratory Complex I: An Unusual Mechanism Deduced from Atomistic Theory and Bioinformatics. *Journal of the American Chemical Society* **2009**, 131 (23), 8134-8140.

12. Yu, J.; Horsley, J. R.; Moore, K. E.; Shapter, J. G.; Abell, A. D., The Effect of a Macrocyclic Constraint on Electron Transfer in Helical Peptides: A Step Towards Tunable Molecular Wires *Chemical Communications* **2014**, 50 (14), 1652.

13. Abell, A. D.; Alexander, N. A.; Aitken, S. G.; Chen, H.; Coxon, J. M.; Jones, M. A.; McNabb, S. B.; Muscroft-Taylor, A., Synthesis of Macrocyclic beta-Strand Templates by Ring Closing Metathesis. *Journal of Organic Chemistry* **2009**, 74 (11), 4354-4356.

14. Blackwell, H. E.; Sadowsky, J. D.; Howard, R. J.; Sampson, J. N.; Chao, J. A.; Steinmetz, W. E.; O'Leary, D. J.; Grubbs, R. H., Ring-closing metathesis of olefinic peptides: Design, synthesis, and structural characterization of macrocyclic helical peptides. *Journal of Organic Chemistry* **2001**, 66 (16), 5291-5302.

15. Wüthrich, K., *NMR of proteins and nucleic acids*. Wiley: 1986.

16. Biron, Z.; Khare, S.; Samson, A. O.; Hayek, Y.; Naider, F.; Anglister, J., A monomeric 3(10)-helix is formed in water by a 13-residue peptide representing the neutralizing determinant of HIV-1 on gp41. *Biochemistry* **2002**, 41 (42), 12687-12696.

17. Jacobsen, O.; Maekawa, H.; Ge, N. H.; Gorbitz, C. H.; Rongved, P.; Ottersen, O. P.; Amiry-Moghaddam, M.; Klaveness, J., Stapling of a 3(10)-Helix with Click Chemistry. *Journal of Organic Chemistry* **2011**, 76 (5), 1228.

18. Pehere, A. D.; Abell, A. D., New beta-Strand Templates Constrained by Huisgen Cycloaddition. *Organic Letters* **2012**, 14 (5), 1330-1333.

19. Zhuang, W.; Hayashi, T.; Mukamel, S., Coherent Multidimensional Vibrational Spectroscopy of Biomolecules: Concepts, Simulations, and Challenges. *Angewandte Chemie International Edition* **2009**, 48 (21), 3750-3781.

20. Pehere, A. D.; Sumbly, C. J.; Abell, A. D., New cylindrical peptide assemblies defined by extended parallel beta-sheets. *Organic & Biomolecular Chemistry* **2013**, 11 (3), 425-429.

21. Burton, N. A.; Harrison, M. J.; Hart, J. C.; Hillier, I. H.; Sheppard, D. W., Prediction of the mechanisms of enzyme-catalysed reactions using hybrid quantum mechanical molecular mechanical methods. *Faraday Discussions* **1998**, 110, 463-475.

22. Boal, A. K.; Guryanov, I.; Moretto, A.; Crisma, M.; Lanni, E. L.; Toniolo, C.; Grubbs, R. H.; O'Leary, D. J., Facile and E-selective intramolecular ring-closing metathesis reactions in 3(10)-helical peptides: A 3D structural study. *Journal of the American Chemical Society* **2007**, 129 (22), 6986-+.

23. Gillespie, P.; Cicariello, J.; Olson, G. L., Conformational analysis of dipeptide mimetics. *Peptide Science* **1997**, 43 (3), 191-217.

Chapter 3

24. Gooding, J. J.; Wibowo, R.; Liu, J. Q.; Yang, W. R.; Losic, D.; Orbons, S.; Mearns, F. J.; Shapter, J. G.; Hibbert, D. B., Protein electrochemistry using aligned carbon nanotube arrays. *Journal of the American Chemical Society* **2003**, *125* (30), 9006-9007.
25. Laviron, E., The use of linear potential sweep voltammetry and of a.c. voltammetry for the study of the surface electrochemical reaction of strongly adsorbed systems and of redox modified electrodes. *Journal of Electroanalytical Chemistry* **1979**, *100*, 263.
26. Schlag, E. W.; Sheu, S. Y.; Yang, D. Y.; Selzle, H. L.; Lin, S. H., Distal charge transport in peptides. *Angewandte Chemie-International Edition* **2007**, *46* (18), 3196-3210.
27. Ding, F. Z.; Wang, H. B.; Wu, Q.; Van Voorhis, T.; Chen, S. W.; Konopelski, J. P., Computational Study of Bridge-Assisted Intervalence Electron Transfer. *Journal of Physical Chemistry A* **2010**, *114* (19), 6039-6046.
28. Marcus, R. A.; Sutin, N., Electron Transfers In Chemistry And Biology. *Biochimica Et Biophysica Acta* **1985**, *811* (3), 265-322.
29. (a) Beer, P. D.; Smith, D. K., Tunable bis(ferrocenyl) receptors for the solution-phase electrochemical sensing of transition-metal cations. *Journal of the Chemical Society-Dalton Transactions* **1998**, (3), 417; (b) Ossola, F.; Tomasin, P.; Benetollo, F.; Foresti, E.; Vigato, P. A., Synthesis, structure and properties of new ferrocene-containing compounds. *Inorganica Chimica Acta* **2003**, *353*, 292-300.
30. Valiev, M.; Bylaska, E. J.; Govind, N.; Kowalski, K.; Straatsma, T. P.; van Dam, H. J. J.; Wang, D.; Nieplocha, J.; Apra, E.; Windus, T. L.; de Jong, W. A., NWChem: a comprehensive and scalable open-source solution for large scale molecular simulations. *Computer Physics Communications* **2010**, *181*, 1477.
31. Farazdel, A.; Dupuis, M.; Clementi, E.; Aviram, A., Electric-Field Induced Intramolecular Electron Transfer In Spiro PI-Electron Systems And Their Suitability As Molecular Electronic Devices - A Theoretical Study. *Journal of the American Chemical Society* **1990**, *112* (11), 4206-4214.

Paper 3

“The Correlation of Electrochemical Measurements and Molecular Junction Conductance Simulations in β -Strand Peptides”, Horsley, J.R., Yu, J., Abell, A.D. *Chemistry A European Journal*, Accepted 26 January 2015.

Mr. John Horsley (candidate)

Performed synthesis and characterization of peptides, attachment to SWCNT/gold electrodes, electrochemistry, analysis of data, provided advanced draft of manuscript and subsequent revisions.

I hereby certify that the statement of contribution is accurate.

Signed

Dated 26/2/2015

Dr. Jingxian Yu

Performed theoretical studies, corresponding author, and co-supervisor of candidate.

I hereby certify that the statement of contribution is accurate.

Signed

Dated 16/2/2015

Prof. Andrew Abell

Supervised development of work, revised manuscript, and is corresponding author.

I hereby certify that the statement of contribution is accurate.

Signed

Dated 16/2/2015

I hereby give permission for John Horsley to use the following papers in his PhD Thesis:

Yu, J.; Horsley, J. R.; Moore, K. E.; Shapter, J. G.; Abell, A. D. *Chemical Communications*, **2014**, *50*, 1652.

Horsley, J. R.; Yu, J.; Moore, K. E.; Shapter, J. G.; Abell, A. D. *Journal of the American Chemical Society*, **2014**, *136*, 12479.

Horsley, J. R., Yu, J., Abell, A. D. "The Correlation of Electrochemical Measurements and Molecular Junction Conductance Simulations in β -Strand Peptides" *Chemistry A European Journal*, **2015**, *21*, 5926-5933.

Horsley, J. R., Yu, J., Abell, A. D. "Understanding the Role of the Amide Bond and Electron Transfer Mechanisms in Macrocyclic Peptides" (Prepared in publication format "text in manuscript").

Signed

Date

19/6/2015

Signed

Date

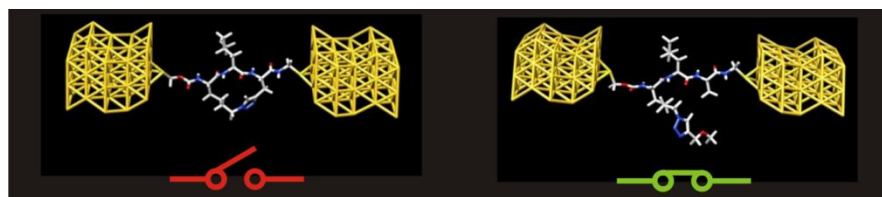
19/06/2015

CHAPTER 4

The Correlation of Electrochemical Measurements and Molecular Junction Conductance Simulations in β - Strand Peptides

John R. Horsley,[†] Jingxian Yu,^{*,†} and Andrew D. Abell^{*,†}

[†] ARC Centre of Excellence for Nanoscale BioPhotonics (CNBP), School of Chemistry
and Physics, The University of Adelaide, Adelaide, SA 5005, Australia



John R. Horsley, Jingxian Yu, and Andrew D. Abell,
Chemistry A European Journal, **2015**, 21, 5926-5933

4.1 Abstract

Understanding the electronic properties of single peptides is not only of fundamental importance, but it is also paramount to the realization of peptide-based molecular electronic components. Electrochemical and theoretical studies are reported on two β -strand-based peptides, one with its backbone constrained with a triazole-containing tether introduced by Huisgen cycloaddition (**1**) and the other a direct linear analogue (**2**). Density functional theory (DFT) and non-equilibrium Green's function were used to investigate conductance in molecular junctions containing peptides **3** and **4** (analogues of **1** and **2**). While the peptides share a common β -strand conformation, they display vastly different electronic transport properties due to the presence (or absence) of the side-bridge constraint and the associated effect on backbone rigidity. These studies reveal that the electron transfer rate constants of **1** and **2**, and the conductance calculated for **3** and **4**, differ by approximately one order of magnitude, thus providing two distinctly different conductance states and what is essentially a molecular switch. A definitive correlation of electrochemical measurements and molecular junction conductance simulations is demonstrated using two different charge transfer techniques. This study furthers our understanding of the electronic properties of peptides at the molecular level, which provides an opportunity to fine-tune their molecular orbital energies through suitable structural manipulation.

4.2 Introduction

A ‘bottom-up’ approach for the fabrication of electronic components (wires, diodes, and transistors) for the electronics industry is required if we are to overcome the physical limits associated with traditional ‘top-down’ methods such as photolithography and etching.¹ Peptides present as ideal candidates for such a purpose. In particular, peptides can self assemble on a conducting surface such as gold² or silicon,³ while also having an ability to be specifically functionalized along their backbone to enable precision-branching, a critical factor in the design of well-defined three-dimensional molecular circuitry.⁴ Peptides are readily synthesized to a predisposed size and geometry, particularly secondary structure,⁵ where this is known to influence the efficiency of electron transfer.⁶ Lastly, the properties of peptides complement those of other potential building blocks used to construct molecular electronics to allow an expansion of the options available. For example, the conformations of peptides are less rigid and more easily controlled than those of carbon nanotubes and oligo-phenylenes, which all display good conductivity for use as molecular wires. However, the exploitation of peptides as electronic components requires us to first make fundamental advances in our understanding of the associated electron transfer kinetics. Charge transfer within a peptide can be defined electrochemically as attached to an electrode at one end and a redox-active moiety at the other, or measured across two electrodes at a molecular junction. The latter technique provides current-voltage (I-V) characteristics of a molecule of interest bridged between the electrodes, through the application of an external potential.^{2, 7} Recent studies have shown that peptides can be used in the design of a molecular junction⁸ using scanning probe techniques such as AFM,⁹ and STM,¹⁰ to measure the associated conductance. Significant work has also been reported on studying molecular junctions by theoretical methods, using density functional theory (DFT) and Green’s function techniques.¹¹ The replacement of the metallic electrodes of a molecular junction with an electron donor and acceptor, also allows for electron transfer kinetics to be investigated electrochemically. This is one of the most common methods used to study electron transfer in peptides.¹²

To date molecular junction conductance simulations and electrochemical measurements have been considered in isolation and studies are needed to establish a link between the two, in order to further our fundamental understanding of electronic transport properties in peptides. Peptides that possess distinctly different electronic properties are required for

Chapter 4

such studies. Any definitive disparity between the rates of charge transfer in these systems can then be compared in separate molecular junction conductance and electrochemical studies. Here we consider such a link by investigating two novel peptides, one with its backbone constrained into a β -strand by coupling the i and $i+2$ residues by Huisgen cycloaddition (peptide **1**), and the other a direct linear analogue that is conformationally more mobile (peptide **2**, see Figure 1). We have previously shown that charge transfer in peptides is sensitive to conformation, and can be significantly restricted by the introduction of a covalent tether that links amino acid side-chains, resulting in additional backbone rigidity.¹³ These new peptides (**1** and **2**) are used in the first comparative study on electrochemical measurements and molecular junction conductance simulations (peptides **3** and **4**, analogues of **1** and **2**, see Figure 2). In addition, the charge transfer pathway is defined by measuring the electron transfer rate at various concentrations of peptide **1** bound to the electrode.

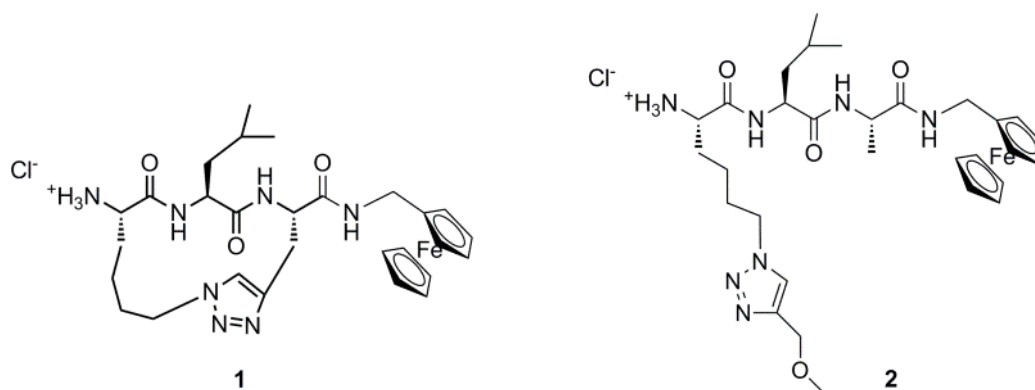


Figure 1. Synthetic peptides.

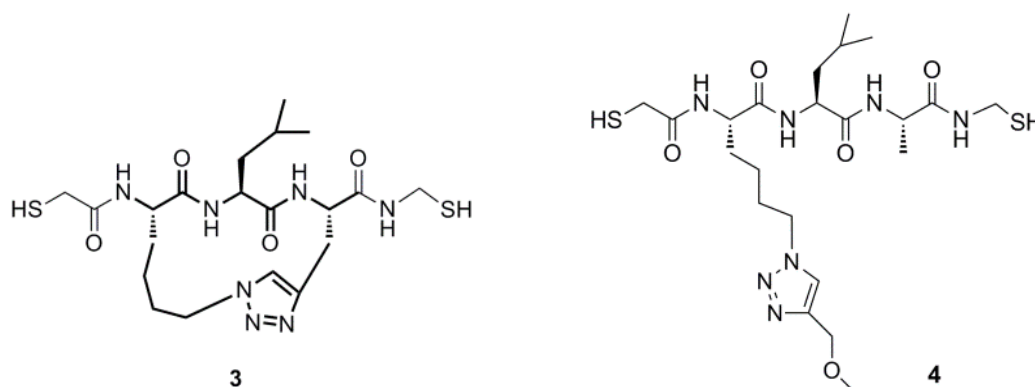


Figure 2. Peptides for use in simulation studies.

4.3 Results and discussion

4.3.1 Peptide design

Macrocyclic peptide **1** was designed to adopt a β -strand conformation, with a triazole-based tether linking the i and $i+2$ residues. A direct linear analogue (**2**) of the β -strand macrocycle was also prepared as a control for the electrochemical studies. Both peptides were synthesized using solution phase chemistry, with the macrocycle of **1** being introduced by Huisgen cycloaddition,¹⁴ all as detailed in the Experimental section. Both peptides were purified by reverse phase HPLC prior to attachment to single-walled carbon nanotubes/gold (SWCNTs/Au) electrodes by HATU/DIPEA.

4.3.2 Conformational analysis of peptides

The conformations of peptides **1** and **2** were confirmed as β -strand by ^1H NMR spectroscopy. In particular, NH (i) to NH ($i+1$), C α H (i) to NH ($i+1$) and C β H (i) to NH ($i+1$) ROESY correlations were found for both peptides, indicative of a β -strand geometry¹⁵ (see Figures 3 and 4). ^1H NMR $J_{\text{NHC}\alpha\text{H}}$ coupling constants between 8-10 Hz¹⁵ were also observed for peptide **1**, supporting a β -strand conformation. Due to spectral overlap, only one doublet characteristic of an amide hydrogen was evident in peptide **2**, with a $J_{\text{NHC}\alpha\text{H}}$ coupling constant of 8.1 Hz.

Chapter 4

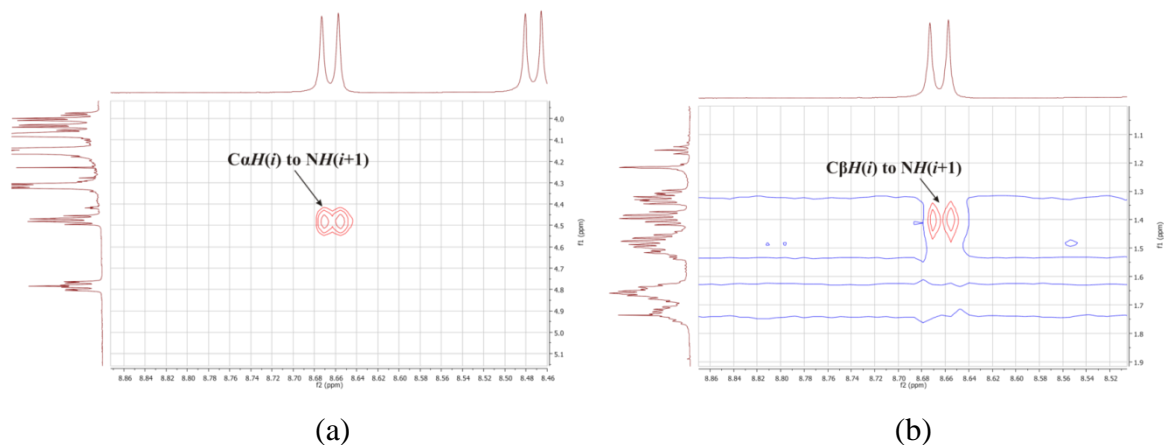


Figure 3. ROESY spectra of **1** showing (a) $\text{CaH}(i)$ to $\text{NH}(i+1)$ and (b) $\text{C}\beta\text{H}(i)$ to $\text{NH}(i+1)$ correlations, both indicative of a β -strand conformation.

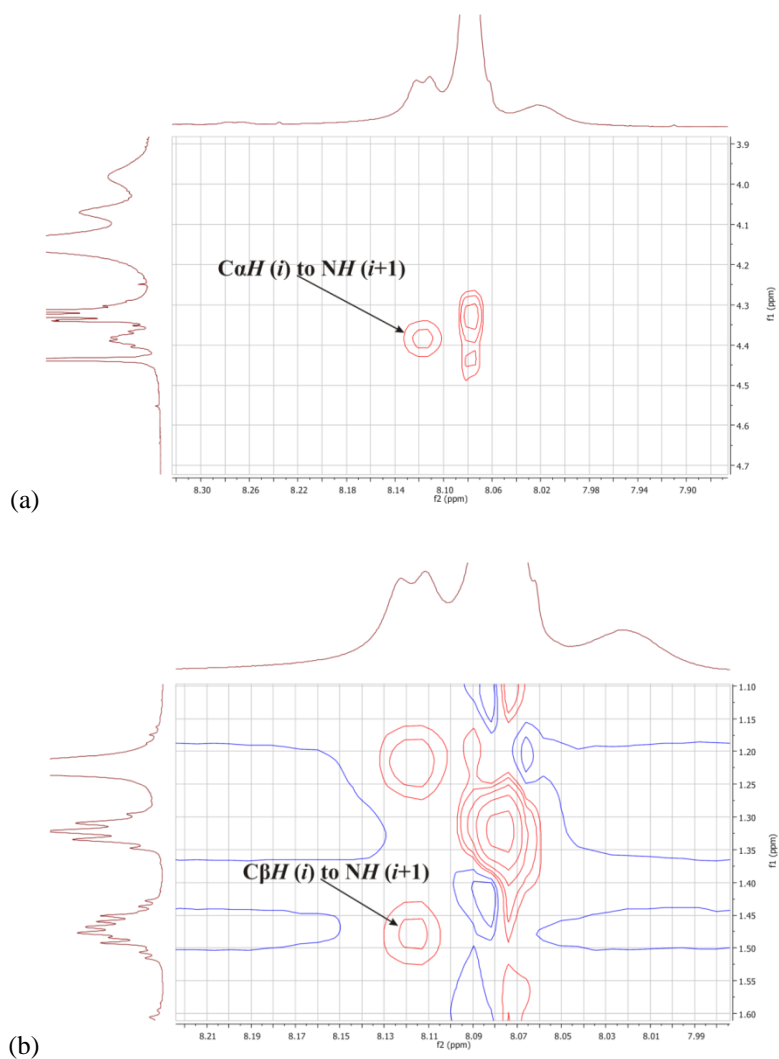


Figure 4. ROESY spectra of **2** showing (a) $\text{CaH}(i)$ to $\text{NH}(i+1)$ and (b) $\text{C}\beta\text{H}(i)$ to $\text{NH}(i+1)$ correlations, both indicative of a β -strand conformation.

Chapter 4

The backbone geometries of the constrained (**1**) and linear (**2**) peptides were further defined by determining the lowest energy conformers of the *N*-Boc protected analogues **5** and **6** by molecular modeling (see Figure 5). *N*-Protected peptides were used here as free amines are known to give rise to unrealistic electrostatic interactions, resulting in unstable lowest energy conformers.¹⁶ A combination of ¹H NMR and IR spectroscopy was used to resolve the secondary structure of peptides **5** and **6**. Observed NH (*i*) to NH (*i*+1), CαH (*i*) to NH (*i*+1) and CβH (*i*) to NH (*i*+1) ROESY interactions were in accordance with values assigned to a β-strand geometry.¹⁷ ¹H NMR $J_{NH\alpha H}$ coupling constants between 8-10 Hz¹⁵ were also observed for peptides **5** and **6**. Amide I, Amide II and Amide A signals found for the Boc-protected peptides were all within the frequencies characteristic of a β-strand,¹⁴ with the Amide I signal for **6** borderline (1643 cm⁻¹, see Figures 6 and 7).

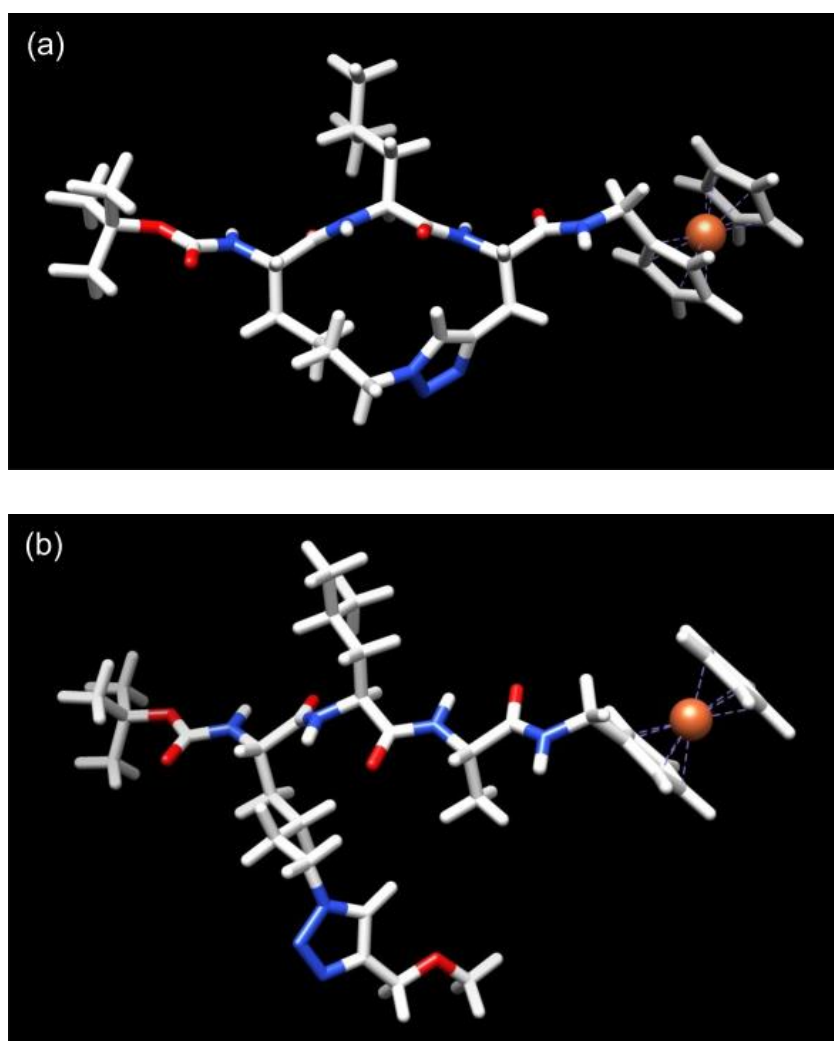
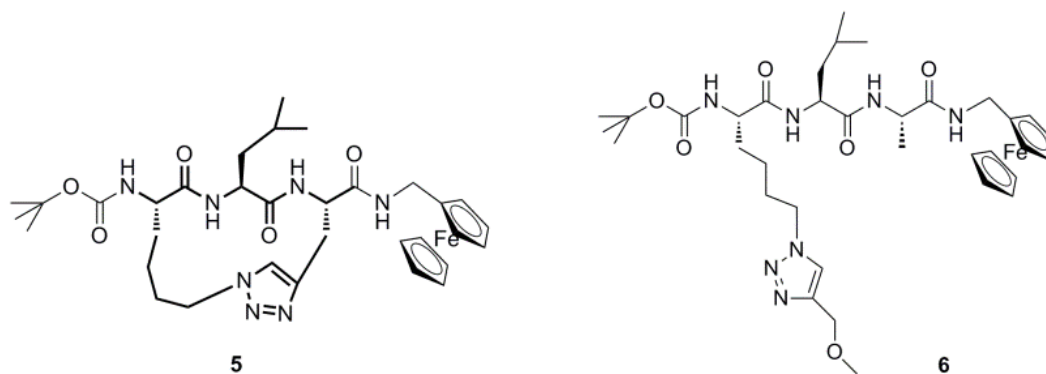


Figure 5. (a) Lowest energy conformer for **5** and (b) lowest energy conformer for **6**, both optimized by the hybrid B3LYP method with 6-31G** basis set for all C, H, N, O atoms, and Lan12dz basis set for the Fe atom.

Chapter 4

Theoretical studies show that the structures of the two peptides are remarkably similar, with the length of their backbones differing by only 0.23 Å. The theoretical studies support the ^1H NMR and IR spectroscopic data, confirming that both peptides, constrained and linear, share a common β -strand conformation. As such they essentially only differ in the presence (or absence) of the side-bridge constraint and the associated effect on backbone rigidity.

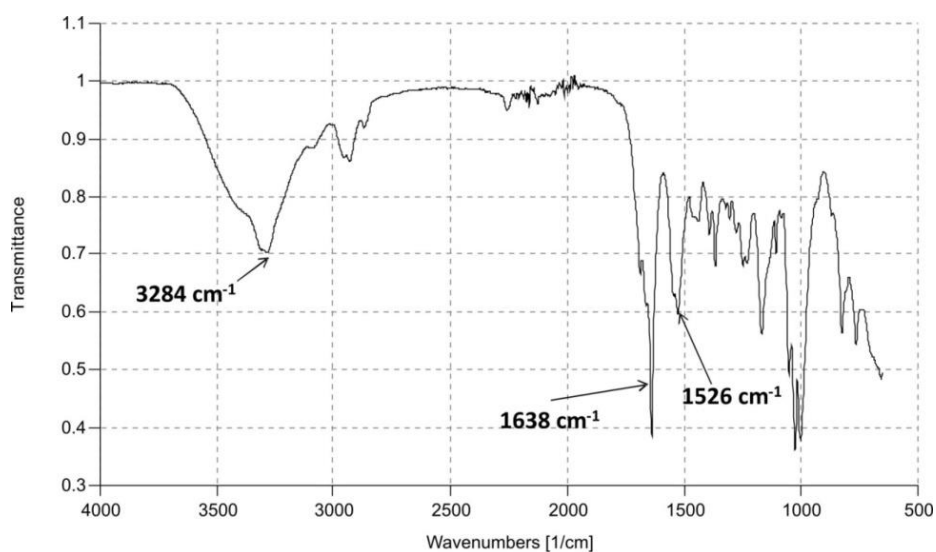


Figure 6. IR spectrum of peptide 5.

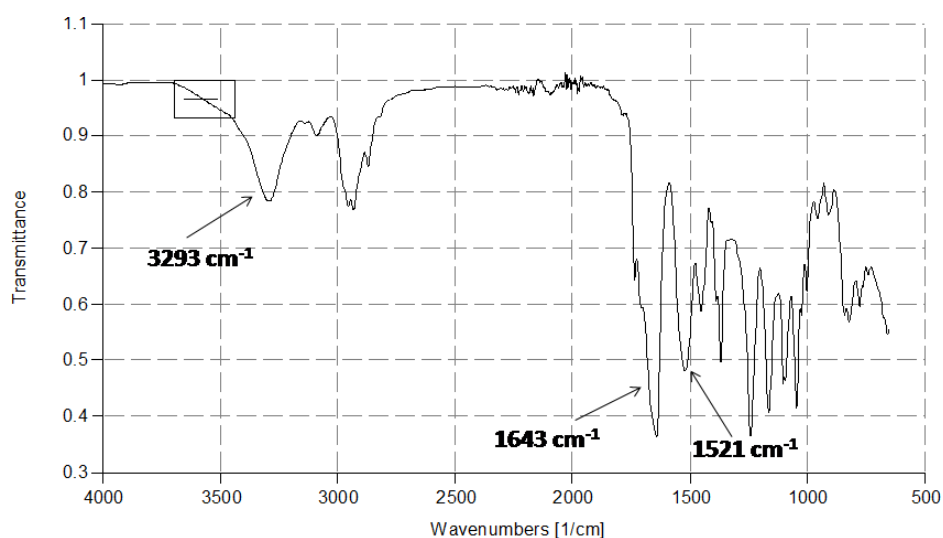


Figure 7. IR spectrum of peptide 6.

4.3.3 Electrochemical analysis of intramolecular electron transfer

The redox active peptides **1** and **2** were separately attached to vertically aligned single-walled carbon nanotube array/gold (SWCNTs/Au) electrodes on treatment with HATU/DIPEA^{13b}. Electrochemical analysis gave rise to a pair of redox peaks in each cyclic voltammogram, characteristic of a one-electron oxidation/reduction reaction (Fc^+/Fc) for both peptides (see Figure 8). The formal potentials (E_o) and apparent electron transfer rate constants (k_{app}) were estimated to be 0.825 V and 22.5 s^{-1} for **1**, and 0.349 V and 223.2 s^{-1} for **2**, respectively, as detailed in Table 1 using Laviron's formalism.¹⁸ The observed formal potential for the linear peptide **2** is similar to the formal potentials reported for other ferrocene-derivatized linear peptides attached to a gold surface, without carbon nanotubes.^{12b, 19} This further supports previous observations that carbon nanotubes have no significant effect on the electron transfer rate-limiting step.^{6, 20} As both peptides share a similar electrochemical environment around the ferrocene unit, any difference in their formal potentials and hence k_{app} , reflects the structural difference between the peptides - i.e. the presence (or absence) of the side-bridge constraint.

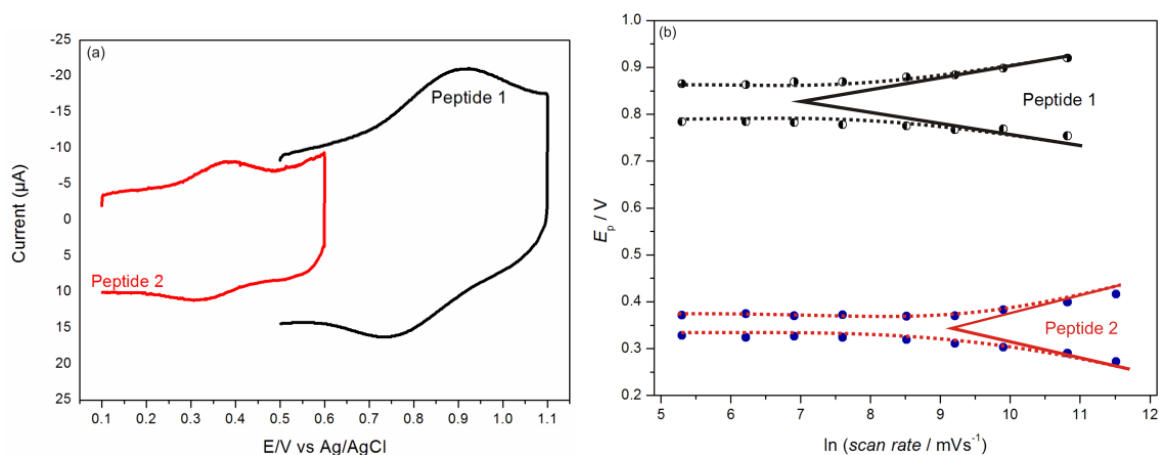


Figure 8. (a) Cyclic voltammograms for peptides **1** and **2** immobilized on SWCNTs/Au electrodes taken at 5 V s^{-1} . (b) Peak potential versus $\ln(\text{scan rate})$ for peptides **1** and **2** after background current subtraction.

Table 1. Formal potentials (E_o), electron transfer rate constants (k_{app}) and surface concentrations for the constrained peptide (**1**) and linear analogue (**2**).

Peptide	E_o (V vs Ag/AgCl)	Surface concentration ($\times 10^{-10}$ mole. cm^{-2})	k_{app} (s^{-1})
1	0.825	5.86 ± 0.54	22.5 ± 2.1
2	0.349	2.73 ± 0.26	223.2 ± 23.2

The two peptides share comparable backbone geometries as discussed above, yet exhibit significantly different electronic properties. A considerable formal potential shift to the positive of approximately 480 mV was observed for the constrained peptide **1**, relative to the linear **2**, and a 10-fold disparity in the electron transfer rate constant for **1** (22.5 s^{-1}) and **2** (223.2 s^{-1}) was also observed. This clearly demonstrates that an increase in backbone rigidity, imparted by the side-chain constraint as in **1**, significantly hinders oxidation/reduction of the redox-active ferrocene moiety. Similar observations were evident from our earlier work involving a β -strand tripeptide constrained by an alternative alkane-based tether introduced by ring closing metathesis (0.82 V and 23 s^{-1}).^{13b} Our previous theoretical evidence¹³ has shown that the side-chain tether introduces an additional reorganization energy that impedes intramolecular electron transfer by restricting the backbone torsional motions necessary for such transference. This current study adds to an increasing body of data that demonstrates an important link between backbone rigidity and the efficiency of electron transfer in peptides.¹³ It also extends the generality of the effect, with a triazole-based tether introduced by Huisgen cycloaddition. The shift in the formal potential of 480 mV is significantly higher compared to other conformation-dependent structures such as cis-trans cyclohexasilanes (110 mV).²¹ This vast formal potential drop in our peptides provides two distinct states (i.e. on/off) with a sizeable differential, which is ideal for the design of molecular switches. Defining the electron transfer pathway in peptides attached to a monolayer (electrode) is crucial to the design of single molecule junction devices. Currently there is an ongoing dispute

Chapter 4

concerning the electron transfer pathway in tightly-packed and loosely-packed peptide monolayers, particularly as to whether electron transfer proceeds via an inter-molecular²² or intra-molecular manner.²³ In order to address this in our system, a range of concentrations of peptide **1** attached to SWCNTs/Au electrodes was prepared by regulating the coupling times between 0.5 seconds and 48 hours (see Table 2). This gave rise to surface concentrations of **1**, ranging from a relatively sparse coverage of 1.02×10^{-10} mole.cm⁻² to a significantly more tightly packed 5.89×10^{-10} mole.cm⁻², as summarized in Table 2.

Table 2. Electron transfer rate constants (k_{app}) and surface concentrations for the constrained peptide **1**, with different exposure times for coupling reactions to SWCNTs/Au electrodes.

Exposure time	Surface concentration ($\times 10^{-10}$ mole.cm ⁻²)	k_{app} (s ⁻¹)
48 hours	5.86 ± 0.54	22.5 ± 2.1
30 min	5.89 ± 0.58	23.2 ± 2.4
5 min	4.68 ± 0.45	22.7 ± 2.5
30 sec	2.72 ± 0.28	23.2 ± 2.0
0.5 sec	1.02 ± 0.11	23.9 ± 2.7

Subsequent electrochemical analysis on these samples showed that the observed electron transfer rate constant remained essentially unchanged (ranging from 22.5 ± 2.1 s⁻¹ to 23.9 ± 2.7 s⁻¹) over the range of surface concentrations that varied up to 6-fold. This is consistent with intramolecular transfer, whereas a significant dependence on surface concentration of the peptide would be expected for intermolecular charge transfer. An intramolecular pathway is analogous to charge transfer through a molecular junction involving a single peptide.

4.3.4 Molecular junction conductance simulations

Density functional theory (DFT) and the non-equilibrium Green's function were used to investigate the electronic transport properties in molecular junctions^{11d} containing peptides **3** and **4**, analogues of **1** and **2** (see Figure 2). These methods enable explicit calculation of the current–voltage (I–V) characteristics of single molecules, and ultimately conductance. Each peptide was separately bound between two gold electrodes separated by 17 Å, via thiol groups that contribute efficient electronic coupling at the peptide/electrode interface²⁴ (see Figure 9 and Table 3).

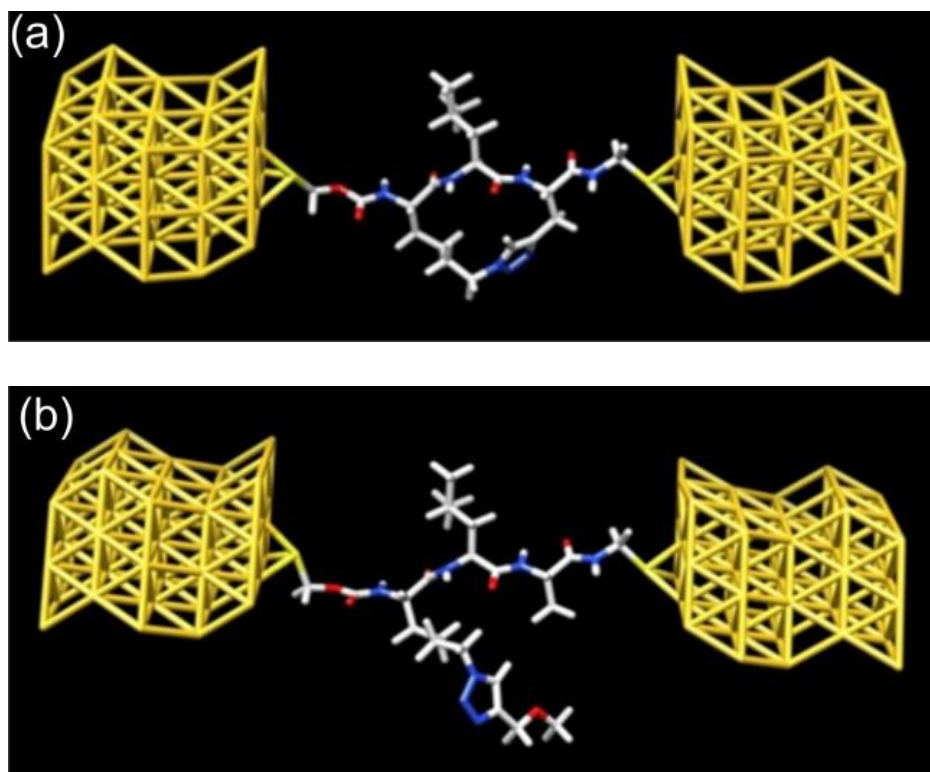


Figure 9. (a) Constrained peptide **3** and (b) linear **4** wired between two gold electrodes, each forming a peptide molecular junction.

Chapter 4

Table 3. Critical distances for peptides **3** and **4**.

	Peptide 3 (constrained)	Peptide 4 (linear)	Difference
Distance between backbone CH ₂ s	14.919 Å	15.248 Å	0.329 Å
Distance between Au electrodes	17.102 Å	16.944 Å	0.158 Å

Transmission spectra for molecular junctions containing peptides **3** and **4** were computed with bias voltages ranging between -1.5 V and 1.5 V (see Figures 10 and 11). The current for a given voltage was next determined through integration of the transmission using the Landauer formula,²⁵ which then enabled calculation of conductance. The molecular orbital energy levels in the peptides were shifted with the externally applied bias, but only electrons with energies similar to the Au Fermi level entered the ‘bias window’ and contributed to the current.²⁶ The transmission spectra show that the electronic transport properties of the molecular junctions containing peptides **3** and **4** are predominantly defined by the frontier molecular orbitals, i.e. highest occupied molecular orbital (HOMO) and lowest unoccupied molecular orbital (LUMO),^{11c, 26} (see Figures 10 and 11).

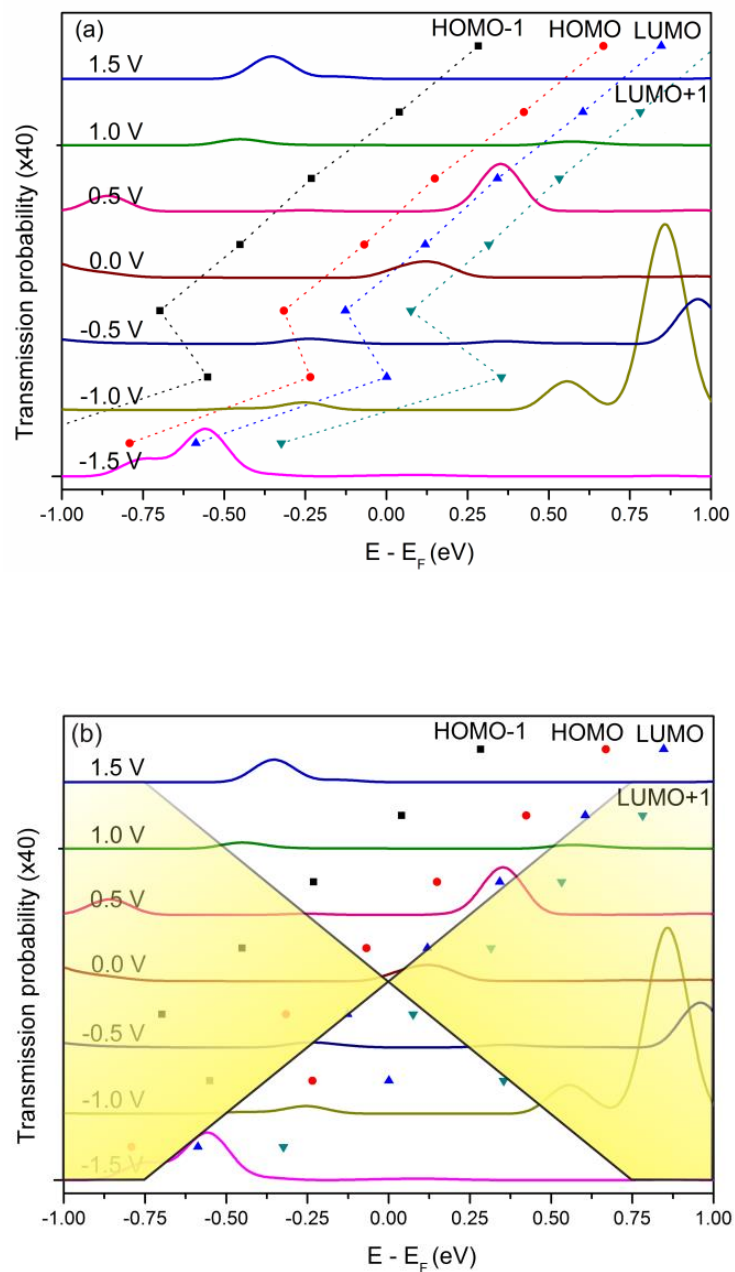


Figure 10. Transmission spectrum of the linear peptide **4** at bias voltages between -1.5 V and 1.5 V (a) indicating the molecular orbital energy levels in proximity to the Au Fermi level (E_f) as a function of bias, and (b) indicating the area within the bias window (white area). The Au Fermi level is set to zero.

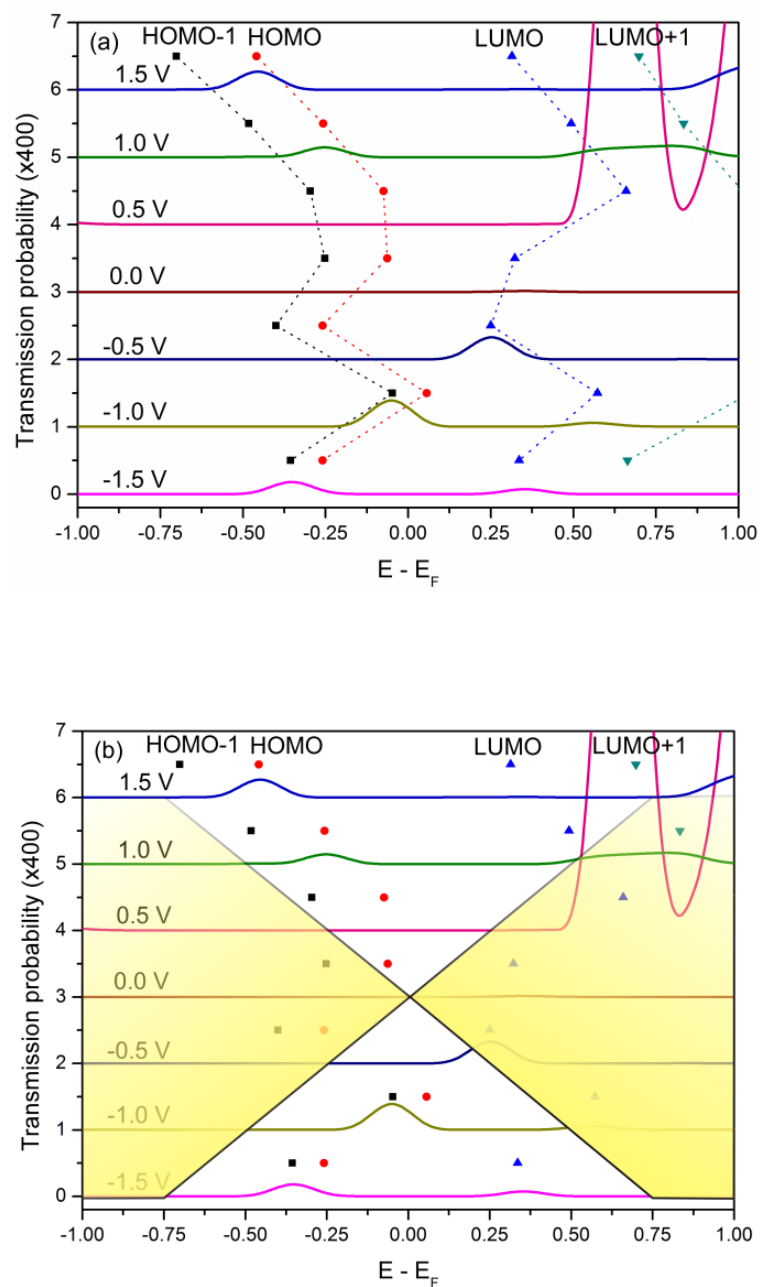


Figure 11. Transmission spectrum of the constrained peptide **3** at bias voltages between -1.5 V and 1.5 V (a) indicating the molecular orbital energy levels in proximity to the Au Fermi level (E_f) as a function of bias, and (b) indicating the area within the bias window (white area). The Au Fermi level is set to zero. Note the transmission probability (Y-axis) is ten times the magnitude of that for the linear peptide to enable visualization of the relevant transmission peaks.

In particular, for the linear peptide, the appearance of a large transmission peak located at -0.58 eV in Figure 10, shows the LUMO as the major contributor to the current under a bias of -1.5 V. When a bias of -1.0 V was applied, a smaller transmission peak at -0.23 eV is noticeable, with the HOMO being the major contributor to the current. Another small transmission peak at 0.3 eV is evident under a positive bias of 0.5 V as shown in Figure 10, with the LUMO making the major contribution to the electronic transport. The presence of transmission peaks between -0.3 eV and -0.5 eV in Figure 10, indicate that the HOMO and LUMO are not the main contributors to the current for positive voltages of 1.0 V and 1.5 V.

The appearance of transmission peaks for voltages of ± 1.0 V and ± 1.5 V for the constrained peptide **3** as shown in Figure 11, clearly indicates that the HOMO and HOMO-1 are the major contributors to the current. Under a bias of -1.0 V and -1.5 V the HOMO-1 is dominant, with peaks within the bias window situated at -0.05 eV and -0.35 eV respectively. Under a positive bias of 1.0 V and 1.5 V the HOMO is dominant, with peaks within the bias window at -0.25 eV and -0.45 eV respectively. The exception is for a voltage of -0.5 V where the LUMO is clearly the major contributor, as can be seen from the transmission peak at 0.25 eV in Figure 11 (barely within the bias window). Purposely, the transmission probability (Y-axis) in Figure 11 (x 400) is ten-fold that of the linear peptide in Figure 10 (x 40), to enable visualization of the relevant transmission peaks. This clearly indicates that the HOMO and LUMO resonances are significantly weaker in the constrained peptide, hence currents in constrained **3** are markedly lower than those in the linear peptide **4**. A relatively narrow HOMO-LUMO energy gap (~ 0.2 eV) was found for the linear peptide **4**, whereas a significantly greater energy gap ($\sim 0.5 - 0.75$ eV) exists for the constrained **3**, which is evident in Figures 10 and 11. This greater HOMO-LUMO energy gap is conducive to poor conductivity²⁶ in the constrained peptide. We note that a much higher HOMO-LUMO gap (~ 5 eV)²⁷ has been previously reported in peptides. However, these orbital energies were calculated under infinite boundary conditions, without considering the presence of the external electric field. Such a method gives a higher HOMO-LUMO energy gap²⁸ when compared to the method used in this study. We believe our calculations more closely resemble the gold-peptide-gold system.

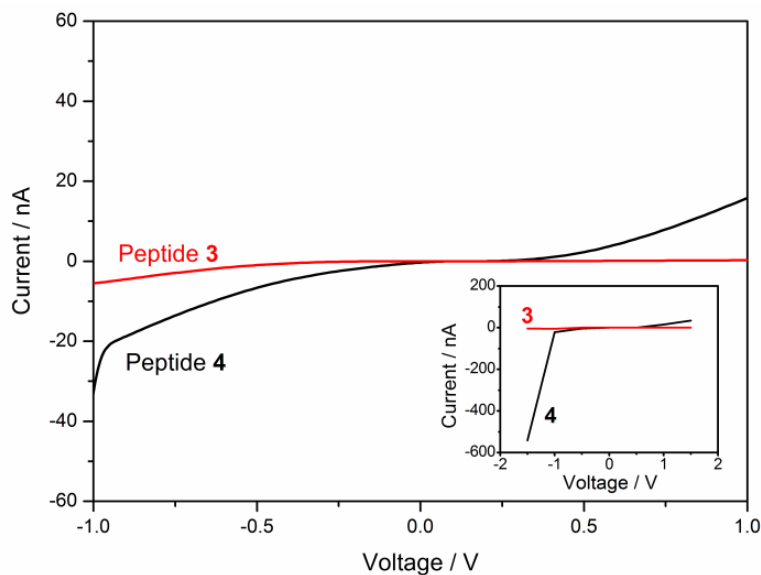


Figure 12. I-V plot for the constrained peptide **3** (red) and linear **4** (black) for bias voltages between -1.0 V and 1.0 V. **Inset:** I-V plot for both peptides within a broader voltage range of -1.5 V and 1.5 V.

The current–voltage (I–V) characteristics of peptides **3** and **4** were next calculated through integration of the area under the transmission peaks within a given bias window, as this is representative of the current of electrons passing through the molecular junction (see Figure 12). For bias voltages between -1.0 V and 1.0 V, the current for both peptides is relatively symmetric, but is significantly greater in the linear **4** relative to that of the constrained peptide **3** (see Figure 12). However, a spike in the current was observed under negative bias between -1.0 V and -1.5 V for the linear peptide **4** (see Figure 12, inset), which is only evident in the simulation study. Electrochemical measurements were unable to reveal this additional information, as electrochemistry was conducted in the range required for oxidation/reduction of the redox active ferrocene moiety, i.e. between 0.1 V and 1.1 V vs Ag/AgCl, for the linear and constrained peptide. The current for the linear peptide **4** was found to increase rapidly as the voltage increased from -1.0 V to -1.5 V, reaching a current in excess of 500 nA at -1.5 V (see Figure 12, inset). In contrast, for a positive bias of 1.5 V, the current calculated for **4** was less than 50 nA. Thus a larger current in one bias (reverse) was favored over the other (forward). This phenomenon epitomizes a molecular rectifier, a diode-like electronic component where asymmetry of the forward and reverse current occurs upon altering the bias voltage across a molecular

junction.²⁹ Peptide **4** exhibits significant rectification behavior with a strong negative bias, culminating in a rectification ratio (RR) of 16 (at $V = -1.5$ and 1.5). This is within the range of commercially available doped Si, Ge, or GaAs p-n junction rectifiers.

Based on the I-V data, the conductance was calculated to be 1.7×10^{-9} S for the constrained peptide **3**, and 14.9×10^{-9} S for the linear **4** within the bias range of -1.0 V to 1.0 V. This corresponds remarkably well to the results from the electrochemical study, where the electron transfer rate constant for the linear peptide **2** (223.2 s^{-1}) was also approximately one order of magnitude greater than that of the constrained peptide **1** (22.5 s^{-1}). These results provide a definitive correlation between our solution phase electrochemical measurements and the molecular junction conductance calculations. Thus, the ten-fold difference in charge transfer observed between peptides **1** and **2**, and molecular junctions containing peptides **3** and **4**, occurs despite both sharing a common β -strand conformation, ostensibly differing only in the presence (or absence) of the side-bridge constraint and the associated backbone rigidity. Such vast differences in electronic transport properties provide two distinctly different conductance states, in what is essentially a molecular switch. This demonstrates that conductance can be either enhanced or suppressed through felicitous structural manipulation of the peptide backbone.

4.4 Conclusion

In summary, electrochemical and theoretical studies are reported on a series of novel peptides in order to establish a link between molecular junction conductance simulations and electrochemical measurements. Peptide **1** was constrained into a β -strand conformation using Huisgen cycloaddition, with peptide **2** providing a direct linear analogue. A combination of ^1H NMR and IR spectroscopy confirmed that the backbones of the two peptides share remarkably similar β -strand conformations, essentially differing only in the presence (or absence) of the side-bridge constraint. A dramatic shift to the positive of approximately 480 mV was observed in the formal potential of peptide **1**, relative to **2**, together with a ten-fold difference in the electron transfer rate constants (22.5 s^{-1} for **1**) and (223.2 s^{-1} for **2**). These results clearly reflect the additional backbone rigidity

derived from the side-bridge constraint of **1**, and add to the large body of work highlighting the generality of this effect. The electron transfer pathway in our system was further defined using SWCNTs/Au electrodes bound to a series of different concentrations of peptide **1**, prepared using coupling times ranging from 0.5 seconds to 48 hours. The electron transfer rate constant ostensibly remained unchanged in every case, despite up to a 6-fold variation in the surface concentration of peptide **1**, demonstrating that the charge proceeded via an intramolecular pathway.

High-level theoretical studies using density functional theory (DFT) and the non-equilibrium Green's function to simulate the electronic properties of peptides **3** and **4** (analogues of **1** and **2**) were conducted, with each wired between two gold electrodes to form a single peptide molecular junction. Transmission spectra were computed to define the specific molecular orbitals that contribute to the current in each of the peptides at various applied biases between -1.5 V and 1.5 V. The HOMO was found to be the major contributor to the current in the constrained **3**, whereas the LUMO was the major contributor to the linear **4**. A narrow HOMO-LUMO energy gap was evident for the linear **4**, with a significantly greater energy gap in the constrained **3**, which is conducive to poor conductivity. Additionally, the I-V curve calculated for peptide **4**, displayed markedly asymmetric current under negative bias between -1.0 V and -1.5 V, characteristic of a molecular rectifier.

The conductance of each peptide was calculated as 1.7×10^{-9} S for **3**, and 14.9×10^{-9} S for **4**, within the bias range of -1.0 V to 1.0 V. Peptides **3** and **4**, (analogues of **1** and **2**), display vastly different electronic transport properties (approximately one order of magnitude) due to the presence (or absence) of the side-bridge constraint and the associated effect this has on backbone rigidity. Thus, two distinctly different charge transfer states (i.e. on/off), were evidenced between the linear (**2** and **4**) and constrained peptides (**1** and **3**), by two different charge transfer techniques. Hence these studies demonstrate a definitive correlation between electrochemical measurements and molecular junction conductance simulations in β -strand peptides. Furthermore, appropriate structural manipulation of the peptide backbone enables orbital energies to be finely tuned and thus exploited in the design of functional molecular electronic components.

4.5 Experimental section

4.5.1 Chemicals

H-Leu-OMe.HCl, 1-hydroxy-7-azabenzotriazole (HOAt), 1-hydroxybenzotriazole.hydrate (HOBt), EDC.HCl and 2-(1H-7-azabenzotriazol-1-yl)-1,1,3,3-tetramethyl uronium hexafluorophosphate methanaminium (HATU) were purchased from GL Biochem (Shanghai) Ltd., China. Dichloromethane (DCM), ethyl acetate (EtOAc), and methanol (MeOH) were purchased from Merck, Australia. Boc-Lys-OH, Boc-propargyl-Gly-OH, CuBr, DBU, *N,N*-dimethylformamide (DMF), dimethyl sulfoxide (DMSO), tetrahydrofuran (THF), 2,2,2-trifluoroethanol (TFE), 4 M HCl/dioxane solution, methyl propargyl ether, sodium azide and diisopropylethylamine (DIPEA) were purchased from Sigma-Aldrich, Australia. NaOH was purchased from Chem Supply, Australia. Single-walled carbon nanotubes (P2-SWCNTs) were purchased from Carbon Solutions Inc., USA. (S)-2-((tert-butoxycarbonyl)amino)-6-(4-(methoxymethyl)-1H-1,2,3-triazol-1-yl) hexanoic acid^{13a} and ferrocenylmethylamine³⁰ were prepared as published. All solvents and reagents were used without purification unless noted.

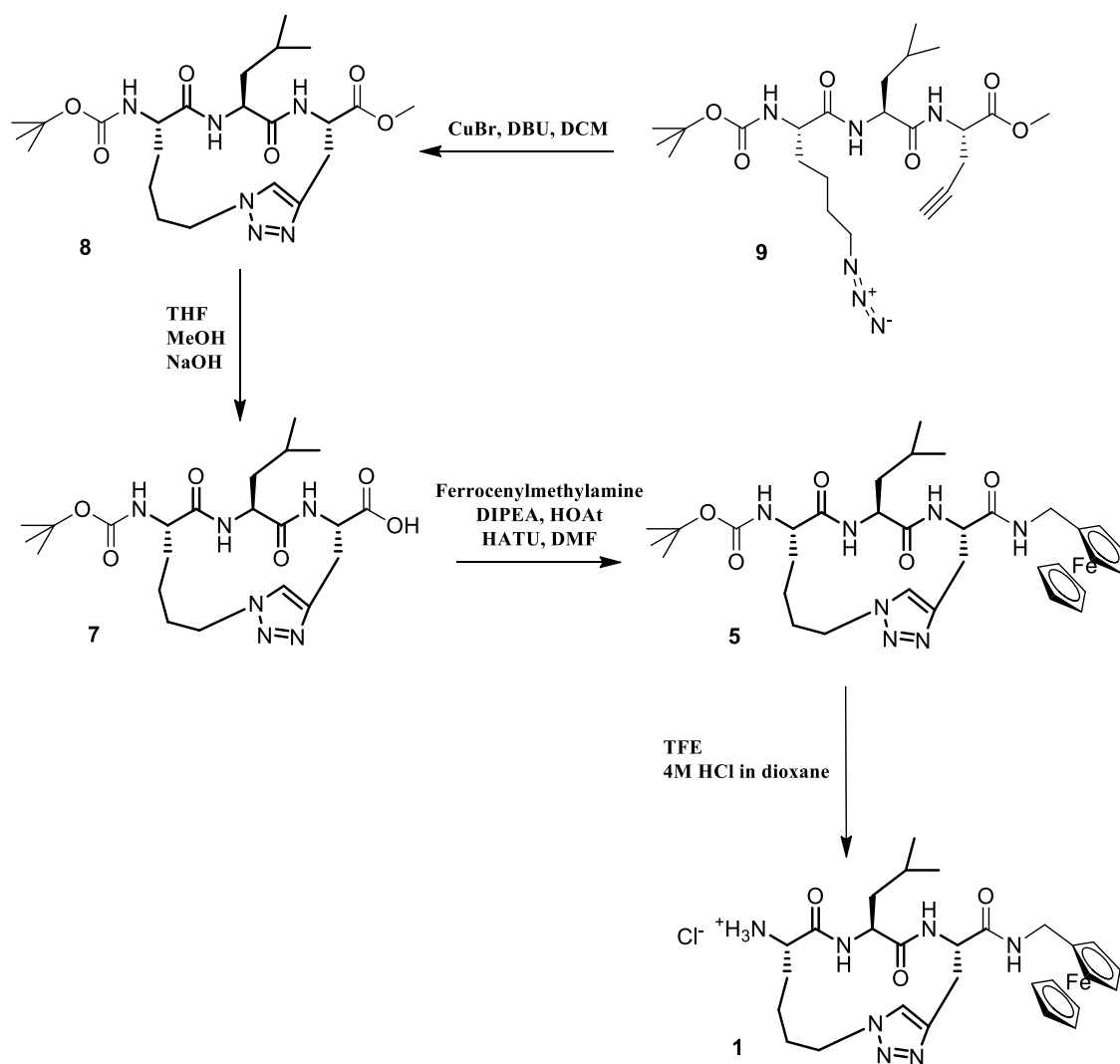
4.5.2 Instrumentation and methods

¹H NMR spectra were recorded in DMSO-d₆ or CDCl₃-d solutions using a Varian Gemini-300 NMR. ¹³C NMR and two-dimensional NMR experiments utilized COSY, ROESY, HSQC and HMBC, and were obtained on a Varian Inova 600 MHz spectrometer. Chemical shifts are reported in ppm (δ) using TMS (0.00 ppm) as the internal standard. Signals are reported as s (singlet), d (doublet), t (triplet) or m (multiplet). Low resolution mass spectral data were analyzed using a Finnigan MAT LCQ spectrometer with MS/MS and ESI probe, utilizing XCalibur software. High resolution mass spectral data were analyzed using an Agilent Technologies 6200 series TOF LC/MS 6500 with an Agilent Technologies 1260 Infinity LC system, with a flow rate of 0.5 mL/min. Mass spectra were obtained over a range of 100 <*m/z*< 1000. Data was analyzed using Agilent MassHunter Qualitative Analysis B.06.00. Infrared spectra were collected on a Perkin Elmer Spectrum 100 FT-IR spectrometer, with attenuated total reflectance (ATR) imaging capabilities, fitted with a ZnSe crystal, with an average reading taken from 4 scans at 4 cm⁻¹ resolution. The synthetic peptides were analyzed and purified by reverse phase HPLC, using a Gilson

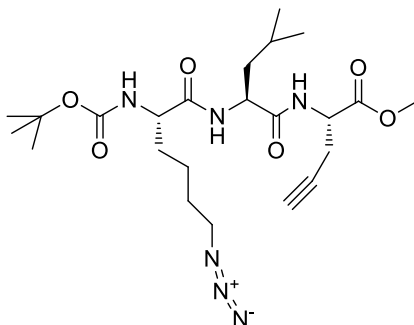
GX-271 preparative system with Trilution LC 2.1 software, equipped with a Supelco C18 column (250x 10 mm) at a flow rate of 4 mL/min. Water/TFA (100/0.1 by v/v) and ACN/TFA (100/0.08 by v/v) solutions were used as aqueous and organic buffers.

4.5.3 Peptide synthesis

Scheme 1. The final synthetic steps for macrocyclized β -strand peptide (**1**) via Huisgen cycloaddition.



Peptide 9

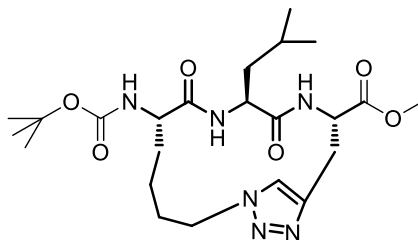


(S)-2-((S)-6-azido-2-((tert-butoxycarbonyl)amino)hexanamido)-4-methylpentanoic acid (943 mg, 2.45 mmol) and (S)-1-methoxy-1-oxopent-4-yn-2-aminium chloride (373 mg, 2.94 mmol) were dissolved in anhydrous DCM (25 mL). HATU (1.02 g, 2.70 mmol), HOAt (367 mg, 2.70 mmol) and DIPEA (1.70 mL, 9.80 mmol) were added and the solution stirred under an N₂ atmosphere for 19 h. The solvent was removed *in vacuo* and EtOAc (125 mL) and H₂O (125 mL) were added to the residue. The pH was adjusted to pH 3-4 and the organic layer separated and washed with NaHCO₃ (2 x 50 mL), brine (50 mL) and dried over MgSO₄. The solvent was removed *in vacuo* to reveal a crude yellow oil (1.13 g). The crude was purified using column chromatography (DCM/MeOH 99:1) to yield a white solid (654 mg, 54%).

¹H NMR (300 MHz, d-DMSO) δ 8.43 (d, 1H, NH, *J*=7.3 Hz), δ 7.79 (d, 1H, NH, *J*=8.4 Hz), δ 6.90 (d, 1H, NH, *J*=8.3 Hz), δ 4.43 – 4.36 (m, 2H, (2 x CαH)), δ 3.91 (d, 1H, CαH), δ 3.62 (s, 3H, OCH₃), δ 3.28 (m, 2H, CH₂), δ 2.90 (t, 1H, CCH, *J*=2.6 Hz), δ 2.60 (dd, 2H, CH₂, *J*=6.6, 2.6 Hz), δ 1.66 – 1.40 (m, 9H, CαHazineCH₂CH₂CH₂, CαH LeuCH₂CH), δ 1.37 (s, 9H, Boc), δ 0.89 – 0.83 (m, 6H, (CH₃)₂).

LRMS (*m/z*) : [M + Na]⁺ calculated for C₂₃H₃₈N₆O₆Na, 517.2; found 517.1.

Peptide 8

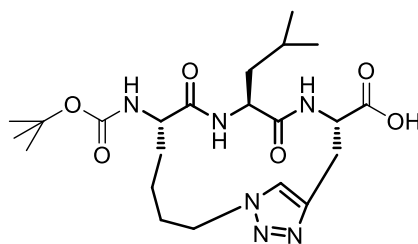


Peptide **9** (440 mg, 0.891 mmol) was dissolved in anhydrous DCM (40 mL) and stirred for 5 min. under an N₂ atmosphere. The solution was then transferred to a 1L rb flask and further anhydrous DCM (440 mL) was added. After 5 min. of stirring, DBU (400 μL, 3 equiv) was added and the mixture stirred for 15 min. CuBr (127 mg, 0.891 mmol) was then added and the reaction stirred under N₂ for 7 h. H₂O (450 mL) was added and the solution stirred vigorously for 30 min. and the pH adjusted to pH 3-4 using conc. HCl. The organic layer was separated and washed with brine (450 mL) and dried over MgSO₄. The solvent was removed *in vacuo* to reveal an off-white solid (333 mg, 76%).

¹H NMR (300 MHz, d-DMSO) δ 8.58 (d, 1H, NH, *J*=8.8 Hz), δ 8.14 (d, 1H, NH, *J*=9.0 Hz), δ 7.53 (s, 1H, triazoleH), δ 6.56 (d, 1H, NH, *J*=9.3 Hz), δ 4.75 (m, 1H, CαH), δ 4.40 (m, 1H, CαH), δ 4.30 (m, 2H, CH₂), δ 3.94 (m, 1H, CαH), δ 3.68 (s, 3H, OCH₃), δ 3.22 (m, 1H, CHH), δ 2.94 (m, 1H, CHH), δ 1.79 – 1.20 (m, 9H, CαHCH₂CH₂CH₂, CαH LeuCH₂CH), δ 1.35 (s, 9H, Boc), δ 0.86 (m, 6H, (CH₃)₂).

LRMS (*m/z*) : [M + Na]⁺ calculated for C₂₃H₃₈N₆O₆Na, 517.2; found 517.2.

Peptide 7



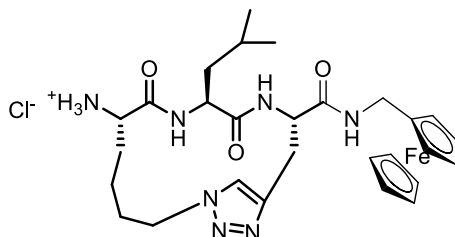
Chapter 4

Peptide **8** (308 mg, 0.623 mmol) was dissolved in THF (5 mL) and MeOH (2.4 mL). 1.6M NaOH (623 μ L) was added and the solution stirred at rt for 17 h. The solvent was removed *in vacuo* and the residue taken up in EtOAc (25 mL) and H₂O (25 mL). The pH was adjusted to pH 3 and the organic layer collected and washed with brine (25 mL) and dried over MgSO₄ to yield a white solid (212 mg, 71%).

¹H NMR (300 MHz, d-DMSO) δ 8.46 (d, 1H, NH, $J=9.1$ Hz), δ 8.09 (d, 1H, NH, $J=8.4$ Hz), δ 7.51 (s, 1H, triazoleH), δ 6.53 (d, 1H, NH, $J=7.4$ Hz), δ 4.64 (m, 1H, C α H), δ 4.40 (d, 1H, C α H, $J=8.4$ Hz), δ 4.29 (m, 2H, CH₂), δ 3.96 (m, 1H, C α H), δ 3.20 (d, 1H, CHH, $J=15.4$ Hz), δ 2.91 (m, 1H, CHH), δ 1.81 – 1.30 (m, 9H, C α HCH₂CH₂CH₂, C α H LeuCH₂CH), δ 1.35 (s, 9H, Boc), δ 0.85 (m, 6H, (CH₃)₂).

LRMS (m/z) : [M + Na]⁺ calculated for C₂₂H₃₆N₆O₆Na, 503.2; found 503.2.

Peptide 1



Peptide **7** (121 mg, 0.25mmol) and ferrocenylmethylamine (60 mg, 0.27mmol) were dissolved in anhydrous DMF (4.2 mL) and stirred under an N₂ atmosphere. DIPEA (175 μ L) was added, followed by HATU (105 mg, 0.27 mmol) and HOAt (34 mg, 0.25 mmol) and the mixture stirred at rt for 24 h. The solvent was removed *in vacuo* and the residue taken up in EtOAc (25 mL) and H₂O (25 mL). The pH was adjusted to pH 3 with the addition of dilute aqueous HCl, and the organic layer collected and washed with aqueous NaHCO₃ (25 mL), brine (25 mL) and dried over MgSO₄ to yield peptide **5** as a brown solid (95 mg), that was used in the next step without further purification.

¹H NMR (600 MHz, d₆-DMSO) δ 8.48 (d, 1H, NH, $J=8.9$ Hz), δ 8.08 (d, 1H, NH, $J=8.6$ Hz), δ 7.98 (t, 1H, NH, $J=5.6$ Hz), δ 7.50 (s, 1H, triazoleH), δ 6.51 (d, 1H, NH, $J=7.0$ Hz),

Chapter 4

δ 4.69 (t, 1H, C α H, $J=8.9$ Hz), δ 4.45 (m, 1H, C α H), δ 4.31 (t, 2H, CH₂, $J=10.6$ Hz), δ 4.21 – 4.09 (m, 9H, Cp), δ 4.03 (t, 2H, CH₂, $J=5.6$ Hz), δ 3.95 (m, 1H, C α H), δ 3.05 (dd, 1H, CHH, $J=20.0, 7.3$ Hz), δ 2.94 (d, 1H, CHH, $J=12.5$ Hz), δ 1.80 – 1.36 (m, 9H, C α H azideCH₂CH₂CH₂, C α H LeuCH₂CH), δ 1.35 (s, 9H, Boc), δ 0.82 (m, 6H, (CH₃)₂).

¹³C NMR (150 MHz, DMSO-d₆) δ 171.5, 170.0, 162.2, 154.5, 142.9, 122.4, 85.9, 77.8, 68.7, 68.5, 68.3, 67.3, 67.2, 66.8, 53.1, 51.5, 50.2, 48.5, 41.3, 40.0, 38.2, 37.5, 35.7, 31.1, 30.7, 28.9, 28.7, 28.0, 23.8, 22.8, 22.0, 20.6.

LRMS (m/z): [M]⁺ calculated for C₃₃H₄₇FeN₇O₅, 677.2; found 677.1.

IR: 1638 cm⁻¹ (Amide I), 1526 cm⁻¹ (Amide II), 3284 cm⁻¹ (Amide A).

Peptide **5** (40 mg, 0.05 mmol) was dissolved in TFE (3 mL) and 4M HCl in dioxane (3 mL) added. The reaction was stirred at rt for 25 min., and the solvent removed *in vacuo* to reveal a brown solid. The crude product was purified using reverse phase HPLC to give **1** as a pale yellow solid, (12 mg, 36%).

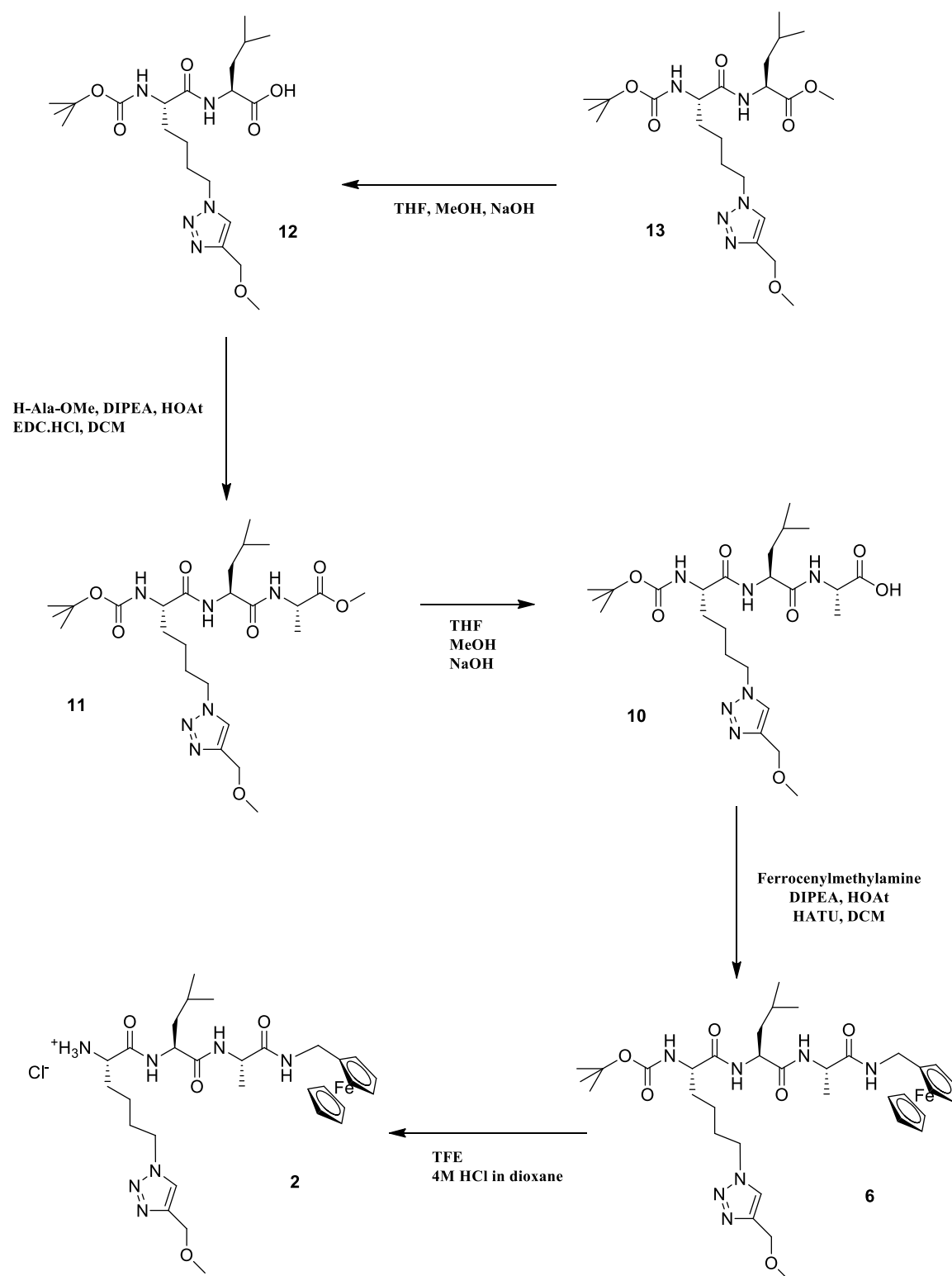
¹H NMR (600 MHz, d₆-DMSO) δ 8.69 (d, 1H, NH, $J=9.0$ Hz), δ 8.50 (d, 1H, NH, $J=9.3$ Hz), δ 8.12 – 8.06 (m, 4H, 2xNHs), δ 7.51 (s, 1H, triazoleH), δ 4.81 (ddd, 1H, C α H, $J=12.5, 9.3, 3.0$ Hz), δ 4.50 (td, 1H, C α H, $J=9.0, 6.6$ Hz), δ 4.33 (m, 2H, CH₂), δ 4.20 – 4.00 (m, 11H, Cp, CH₂), δ 3.77 (m, 1H, C α H), δ 3.07 (m, 1H, CHH), δ 2.94 (dd, 1H, CHH, $J=15.0, 12.7$ Hz), δ 1.78 – 1.30 (m, 9H, C α H azideCH₂CH₂CH₂, C α H LeuCH₂CH), δ 0.87 (m, 6H, (CH₃)₂).

¹³C NMR (150 MHz, DMSO-d₆) δ 171.0, 169.8, 167.0, 157.7, 143.1, 122.2, 85.9, 68.9, 67.4, 67.3, 67.25, 67.22, 51.5, 51.3, 50.4, 48.6, 42.1, 37.5, 30.2, 28.8, 23.9, 22.7, 22.2, 20.1.

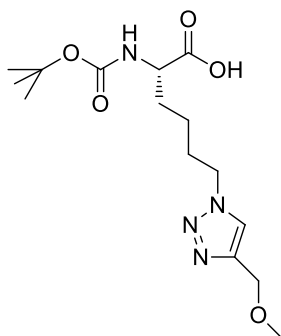
HRMS (m/z): [M]⁺ calculated for C₂₈H₄₀FeN₇O₃, 577.2463, found 577.2462.

Chapter 4

Scheme 2. The final synthetic steps for linear β -strand peptide (2)

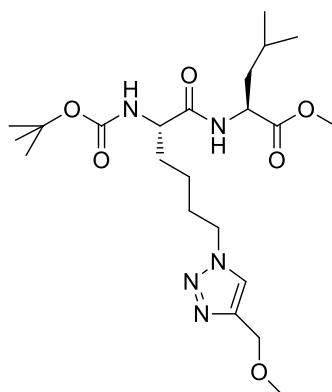


(S)-2-((tert-butoxycarbonyl)amino)-6-(4-(methoxymethyl)-1H-1,2,3-triazol-1-yl) hexanoic acid



Synthesis previously reported.^{13a}

Peptide 13



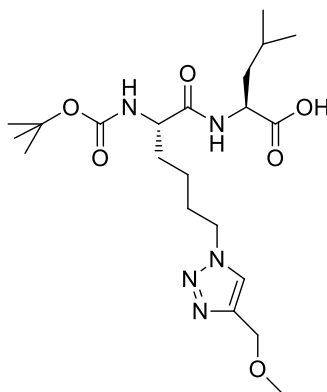
(S)-2-((tert-butoxycarbonyl)amino)-6-(4-(methoxymethyl)-1H-1,2,3-triazol-1-yl) hexanoic acid (425 mg, 1.24 mmol) and H-Leu-OMe (270 mg, 1.49 mmol) were dissolved in anhydrous DCM (10 mL) and stirred under an N₂ atmosphere. DIPEA (755 μ L, 4.34 mmol), EDC HCl (260 mg, 1.36 mmol) and HOBT.H₂O (228 mg, 1.49 mmol) were added and the mixture stirred at rt for 19 h. DCM (15 mL) and H₂O (25 mL) were added and the pH adjusted to pH 3. The organic layer was separated and washed with brine (25 mL) and dried over MgSO₄. The solvent was removed *in vacuo* to reveal a golden solid (521 mg, 90%).

Chapter 4

^1H NMR (300 MHz, d-DMSO) δ 8.13 (d, 1H, NH, $J=7.7$ Hz), δ 8.08 (s, 1H, triazoleH), δ 6.82 (d, 1H, NH, $J=8.2$ Hz), δ 4.41 (s, 2H, OCH_2), δ 4.30 (t, 2H, CH_2N_3 , $J=7.0$ Hz), δ 4.25 (m, 1H, CaH), δ 3.89 (m, 1H, CaH), δ 3.59 (s, 3H, OCH_3), δ 3.24 (s, 3H, OCH_3), δ 1.83 – 1.73 (dd, 2H, CH_2 , $J=14.6, 7.2$ Hz), δ 1.67 – 1.41 (m, 5H, CH_2 , Leu CH_2CH), δ 1.35 (s, 9H, Boc), δ 1.29 – 1.20 (m, 2H, CH_2), δ 0.84 (m, 6H, (CH_3)).

LRMS (m/z): $[\text{M} + \text{Na}]^+$ calculated for $\text{C}_{22}\text{H}_{39}\text{N}_5\text{O}_6\text{Na}$, 492.2; found 492.2.

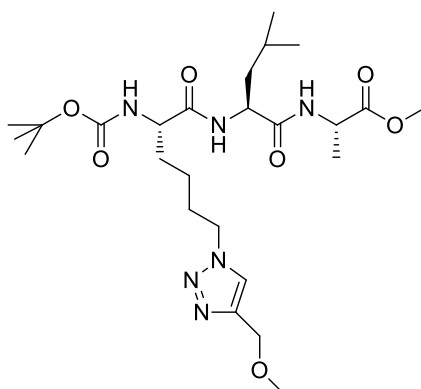
Peptide 12



Peptide **13** (500 mg, 1.06 mmol) was dissolved in THF (3.5 mL) and MeOH (1 mL). NaOH (64 mg) in H_2O (1 mL) was added and the solution stirred at rt for 16 h. The solvent was removed *in vacuo* and the residue diluted with EtOAc (25 mL) and H_2O (25 mL). The pH was adjusted to pH 2-3 and the organic layer collected, washed with brine (25 mL) and dried over MgSO_4 . The solvent was removed *in vacuo* to reveal a pale golden solid (408 mg, 85%).

^1H NMR (300 MHz, d-DMSO) δ 8.09 (s, 1H, triazoleH), δ 7.98 (d, 1H, NH, $J=8.0$ Hz), δ 6.83 (d, 1H, NH, $J=8.4$ Hz), δ 4.43 (s, 2H, OCH_2), δ 4.31 (t, 2H, CH_2N_3 , $J=6.9$ Hz), δ 4.23 (dt, 1H, CaH , $J=14.7, 7.4$ Hz), δ 3.91 (m, 1H, CaH), δ 3.26 (s, 3H, OCH_3), δ 1.84 – 1.74 (dd, 2H, CH_2 , $J=14.6, 7.3$ Hz), δ 1.70 – 1.45 (m, 5H, CH_2 , Leu CH_2CH), δ 1.37 (s, 9H, Boc), δ 1.30 – 1.21 (m, 2H, CH_2), δ 0.86 (m, 6H, (CH_3)₂).

Peptide 11

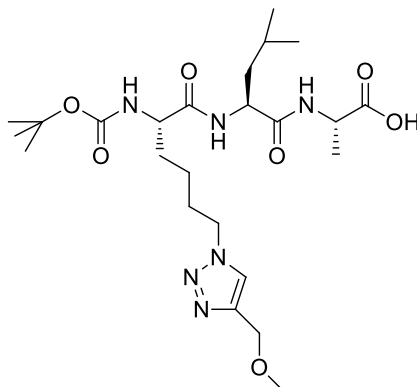


Peptide **12** (230 mg, 0.505 mmol) and H-Ala-OMe (85 mg, 0.606 mmol) were dissolved in anhydrous DCM (4 mL) and stirred under an N₂ atmosphere. DIPEA (351 μ L, 2.02 mmol), EDC HCl (106 mg, 0.555 mmol) and HOAt (76 mg, 0.555 mmol) were added and the mixture stirred at rt for 24 h. The solvent was removed *in vacuo* and the residue taken up in EtOAc (30 mL) and H₂O (30 mL). The pH was adjusted to pH 2 and the organic layer collected and washed with NaHCO₃ (30 mL), brine (30 mL) and dried over MgSO₄. The solvent was removed *in vacuo* to yield a golden oil (211 mg, 77%).

¹H NMR (300 MHz, d-DMSO) δ 8.35 (d, 1H, NH, $J=6.8$ Hz), δ 8.08 (s, 1H, triazoleH), δ 7.74 (d, 1H, NH, $J=8.3$ Hz), δ 6.89 (d, 1H, NH, $J=8.1$ Hz), δ 4.43 (s, 2H, OCH₂), δ 4.37 – 4.20 (m, 2H, 2x α H), δ 4.32 (dd, 2H, CH₂N₃, $J=13.9, 7.0$ Hz), δ 3.87 (m, 1H, α H), δ 3.60 (s, 3H, OCH₃), δ 3.25 (s, 3H, OCH₃), δ 1.83 – 1.73 (m, 2H, CH₂), δ 1.67 – 1.42 (m, 5H, CH₂, LeuCH₂CH), δ 1.36 (s, 9H, Boc), δ 1.32 – 1.22 (m, 5H, CH₂, CH₃), δ 0.86 (m, 6H, (CH₃)₂).

LRMS (m/z) : [M + Na]⁺ calculated for C₂₅H₄₄N₆O₇Na, 563.3; found 563.2.

Peptide 10

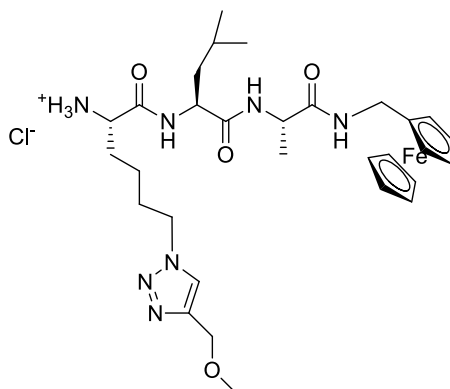


Peptide **11** (194 mg, 0.359 mmol) was dissolved in THF (1.36 mL) and MeOH (388 μ L). NaOH (22 mg, 0.54 mmol) in H₂O (388 μ L) was added and the solution stirred at rt for 18 h. The solvent was removed *in vacuo* and the residue taken up in EtOAc (20 mL) and H₂O (20 mL). The pH was adjusted to pH 2-3 and the organic layer collected, washed with brine (20 mL) and dried over MgSO₄. The solvent was removed *in vacuo* to reveal a clear solid (126 mg, 67%).

¹H NMR (300 MHz, d-DMSO) δ 8.18 (d, 1H, NH, $J=7.1$ Hz), δ 8.09 (s, 1H, triazoleH), δ 7.76 (d, 1H, NH, $J=8.3$ Hz), δ 6.91 (d, 1H, NH, $J=8.2$ Hz), δ 4.43 (s, 2H, OCH₂), δ 4.38 – 4.29 (dd, 3H, C α H, CH₂N₃, $J=13.3, 6.5$ Hz), δ 4.20 – 4.12 (m, 1H, C α H), δ 3.87 (m, 1H, C α H), δ 3.26 (s, 3H, OCH₃), δ 1.83 – 1.73 (m, 2H, CH₂), δ 1.67 – 1.42 (m, 5H, CH₂, LeuCH₂CH), δ 1.37 (s, 9H, Boc), δ 1.30 – 1.22 (m, 5H, CH₂, CH₃), δ 0.85 (m, 6H, (CH₃)₂).

LRMS (m/z) : [M]⁻ calculated for C₂₄H₄₂N₆O₇, 525.3; found 525.1.

Peptide 2



Peptide **10** (120 mg, 0.22 mmol) and ferrocenylmethylamine were dissolved in anhydrous DCM (3.8 mL) and the solution stirred under an N₂ atmosphere. DIPEA (159 μ L, 0.91 mmol), HATU (95 mg, 0.25 mmol) and HOAt (31 mg, 0.22 mmol) were added and the mixture stirred at rt for 24 h. The solvent was removed *in vacuo* and the residue taken up in EtOAc (35 mL) and H₂O (35 mL). The pH was adjusted to pH 2-3 with the addition of dilute aqueous HCl, and the organic layer collected and washed with aqueous NaHCO₃ (35 mL), brine (35 mL) and dried over MgSO₄. The solvent was removed *in vacuo* to give peptide **6** as a brown solid (152 mg), that was used in the next step without further purification.

¹H NMR (600 MHz, d₆-DMSO) δ 8.07 (s, 1H, triazoleH), δ 8.00 – 7.94 (m, 2H, 2xNH), δ 7.83 (d, 1H, NH, $J=8.2$ Hz), δ 6.90 (d, 1H, NH, $J=8.0$ Hz), δ 4.43 (s, 2H, OCH₂), δ 4.34 – 4.27 (m, 4H, 2xCaH, CH₂N₃), δ 4.20 – 3.96 (m, 11H, Cp, CH₂), δ 3.87 (m, 1H, CaH), δ 3.25 (s, 3H, OCH₃), δ 1.78 (td, 2H, CH₂, $J=12.5, 5.2$ Hz), δ 1.65 – 1.55 (td, 3H, CH₂, LeuCH₂CH, $J=13.2, 6.5$ Hz), δ 1.53 – 1.32 (m, 4H, CH₂, LeuCH₂CH), δ 1.37 (s, 9H, Boc), δ 1.31 – 1.25 (m, 3H, CH₃), δ 0.84 (m, 6H, (CH₃)₂).

¹³C NMR (150 MHz, DMSO-d₆) δ 172.4, 171.9, 170.7, 155.8, 144.1, 124.8, 123.4, 86.5, 78.5, 69.4, 68.4, 68.1, 67.4, 66.8, 66.2, 60.1, 59.3, 58.1, 55.0, 51.8, 51.5, 50.4, 49.6, 49.0, 48.6, 37.8, 28.8, 28.2, 27.6, 24.5, 22.9, 21.4, 20.9.

LRMS (m/z): [M + Na]⁺ calculated for C₃₅H₅₃FeN₇O₆Na, 746.3; found 746.2.

IR: 1643 cm⁻¹ (Amide I), 1521 cm⁻¹ (Amide II), 3292 cm⁻¹ (Amide A).

Chapter 4

Peptide **6** (130 mg, 0.18 mmol) was dissolved in TFE (4 mL) and 4M HCl in dioxane (3 mL) was added dropwise. The solution was stirred at rt for 25 min. and the solvent removed *in vacuo*. The crude product (124 mg) was re-dissolved in MeOH and purified using reverse phase HPLC to give **2** as a brown solid (30 mg, 27%).

^1H NMR (600 MHz, d_6 -DMSO) δ 8.49 (d, 1H, NH, $J=8.1$ Hz), δ 8.12 – 7.99 (m, 5H, NH), δ 8.07 (s, 1H, triazoleH), δ 4.43 (s, 2H, OCH₂), δ 4.38 (dd, 1H, C α H, $J=14.0, 8.9$ Hz), δ 4.33 – 4.29 (m, 3H, C α H, CH₂N₃), δ 4.19 – 3.93 (m, 11H, Cp, CH₂), δ 3.77 (m, 1H, C α H), δ 3.26 (s, 3H, OCH₃), δ 1.85 – 1.78 (m, 2H, CH₂), δ 1.71 (td, 2H, CH₂, $J=13.7, 7.2$ Hz), δ 1.63 (dt, 1H, LeuCH₂CH, $J=19.7, 6.5$ Hz), δ 1.51 – 1.41 (m, 2H, LeuCH₂CH), δ 1.35 – 1.28 (m, 2H, CH₂), δ 1.26 – 1.19 (m, 3H, CH₃), δ 0.88 (m, 6H, (CH₃)₂).

^{13}C NMR (150 MHz, DMSO- d_6) δ 171.4, 171.0, 168.3, 157.9, 143.7, 123.6, 68.3, 67.1, 64.9, 57.2, 51.8, 51.0, 48.9, 48.0, 40.8, 37.3, 30.6, 24.0, 23.9, 23.1, 21.4, 21.2, 18.3.

HRMS (m/z): [M]⁺ calculated for C₃₀H₄₅FeN₇O₄, 623.2882; found 623.2868.

4.6 Acknowledgements

We acknowledge the Australian Research Council (ARC) Centre of Excellence for Nanoscale BioPhotonics (CNBP) for financial support. We also acknowledge the Australian National Fabrication Facility for providing the analytical facilities used in this work. We would like to thank Ms. Katherine Moore and Prof. Joe Shapter of Flinders University, S.A., for the preparation of the SWCNT/Au electrodes used in this study and for the use of their electrochemical facilities. The computational aspects of this work were supported by an award under the National Computational Merit Allocation Scheme for JY on the National Computing Infrastructure (NCI) National Facility at the Australian National University.

4.7 References

1. Maeda, H.; Sakamoto, R.; Nishihara, H., Metal complex oligomer and polymer wires on electrodes: Tactical constructions and versatile functionalities. *Polymer* **2013**, *54* (17), 4383-4403.
2. Sek, S., Review peptides and proteins wired into the electrical circuits: An SPM-based approach. *Biopolymers* **2013**, *100* (1), 71-81.
3. Yew, S. Y.; Shekhawat, G.; Wangoo, N.; Mhaisalkar, S.; Suri, C. R.; Dravid, V. P.; Lam, Y. M., Design of single peptides for self-assembled conduction channels. *Nanotechnology* **2011**, *22* (21).
4. Maruccio, G., Molecular electronics: Protein transistors strike gold. *Nature Nanotechnology* **2012**, *7* (3), 147-8.
5. Gatto, E.; Venanzi, M., Chapter 4. Peptronics: Peptide Materials for Electron Transfer. In *Peptide Materials: From Nanostructures to Applications*, Alemán, C.; Bianco, A.; Venanzi, M., Eds. John Wiley & Sons, Ltd.: 2013.
6. Yu, J.; Zvarec, O.; Huang, D. M.; Bissett, M. A.; Scanlon, D. B.; Shapter, J. G.; Abell, A. D., Electron Transfer through α -Peptides Attached to Vertically Aligned Carbon Nanotube Arrays: A Mechanistic Transition. *Chemical Communications* **2012**, *48* (8), 1132–1134.
7. Martín, S.; Pera, G.; Ballesteros, L. M.; Hope, A. J.; Marqués-González, S.; Low, P. J.; Pérez-Murano, F.; Nichols, R. J.; Cea, P., Towards the Fabrication of the Top-Contact Electrode in Molecular Junctions by Photoreduction of a Metal Precursor. *Chemistry – A European Journal* **2014**, *20* (12), 3421-3426.
8. Xiao, X. Y.; Xu, B. Q.; Tao, N. J., Conductance titration of single-peptide molecules. *Journal of the American Chemical Society* **2004**, *126* (17), 5370-5371.
9. (a) Wu, J.-C.; Chen, C.-C.; Chen, K.-H.; Chang, Y.-C., Controlled growth of aligned α -helical-polypeptide brushes for tunable electrical conductivity. *Applied Physics Letters* **2011**, *98* (13), 133304; (b) Shlizerman, C.; Atanassov, A.; Berkovich, I.; Ashkenasy, G.; Ashkenasy, N., De Novo Designed Coiled-Coil Proteins with Variable Conformations as Components of Molecular Electronic Devices. *Journal of the American Chemical Society* **2010**, *132* (14), 5070-5076.
10. (a) Sek, S.; Swiatek, K.; Misicka, A., Electrical Behavior of Molecular Junctions Incorporating α -Helical Peptide. *The Journal of Physical Chemistry B* **2005**, *109* (49), 23121-23124; (b) Uji, H.; Morita, T.; Kimura, S., Molecular direction dependence of single-molecule conductance of a helical peptide in molecular junction. *Phys. Chem. Chem. Phys.* **2013**, *15* (3), 757-760.
11. (a) Staykov, A.; Li, X.; Tsuji, Y.; Yoshizawa, K., Current Rectification in Nitrogen- and Boron-Doped Nanographenes and Cyclophanes. *The Journal of Physical Chemistry C* **2012**, *116* (34), 18451-18459; (b) Liu Wen, C. J., Yan Cui-Xia, Li Hai-Hong, Wang Yong-Juan, Liu De-Sheng, Electronic transport properties of phenylacetylene molecular junctions. *Chin. Phys. B* **2011**, *20* (10), 107302-107302; (c) Xu, Y.; Cui, B.; Ji, G.; Li, D.; Liu, D., Effect of the orientation of nitro group on the electronic transport properties in single molecular field-effect transistors. *Phys. Chem. Chem. Phys.* **2013**, *15* (3), 832-836; (d) Benesch, C.; Rode, M. F.; Cizek, M.; Haertle, R.; Rubio-Pons, O.; Thoss, M.; Sobolewski, A. L., Switching the Conductance of a Single Molecule by Photoinduced Hydrogen Transfer. *Journal of Physical Chemistry C* **2009**, *113* (24), 10315.
12. (a) Long, Y. T.; Abu-Rhayem, E.; Kraatz, H. B., Peptide electron transfer: More questions than answers. *Chemistry-A European Journal* **2005**, *11* (18), 5186; (b) Arikuma,

- Y.; Nakayama, H.; Morita, T.; Kimura, S., Electron Hopping over 100 angstrom Along an alpha Helix. *Angewandte Chemie-International Edition* **2010**, *49* (10), 1800.
13. (a) Yu, J.; Horsley, J. R.; Moore, K. E.; Shapter, J. G.; Abell, A. D., The Effect of a Macrocyclic Constraint on Electron Transfer in Helical Peptides: A Step Towards Tunable Molecular Wires *Chemical Communications* **2014**, *50* (14), 1652; (b) Horsley, J. R.; Yu, J.; Moore, K. E.; Shapter, J. G.; Abell, A. D., Unraveling the Interplay of Backbone Rigidity and Electron Rich Side-Chains on Electron Transfer in Peptides: The Realization of Tunable Molecular Wires. *Journal of the American Chemical Society* **2014**, *136*, 12479-12488.
14. Pehere, A. D.; Sumbly, C. J.; Abell, A. D., New cylindrical peptide assemblies defined by extended parallel [small beta]-sheets. *Organic & Biomolecular Chemistry* **2013**, *11* (3), 425-429.
15. Pehere, A. D.; Abell, A. D., New beta-Strand Templates Constrained by Huisgen Cycloaddition. *Organic Letters* **2012**, *14* (5), 1330-1333.
16. Burton, N. A.; Harrison, M. J.; Hart, J. C.; Hillier, I. H.; Sheppard, D. W., Prediction of the mechanisms of enzyme-catalysed reactions using hybrid quantum mechanical molecular mechanical methods. *Faraday Discussions* **1998**, *110*, 463-475.
17. Gillespie, P.; Cicariello, J.; Olson, G. L., *Peptide Science* **1997**, *43*, 191.
18. Laviron, E., The use of linear potential sweep voltammetry and of a.c. voltammetry for the study of the surface electrochemical reaction of strongly adsorbed systems and of redox modified electrodes. *Journal of Electroanalytical Chemistry* **1979**, *100*, 263.
19. Mandal, H. S.; Kraatz, H.-B., Electron Transfer Mechanism in Helical Peptides. *The Journal of Physical Chemistry Letters* **2012**, *3* (6), 709-713.
20. Gooding, J. J.; Wibowo, R.; Liu, J. Q.; Yang, W. R.; Losic, D.; Orbons, S.; Mearns, F. J.; Shapter, J. G.; Hibbert, D. B., Protein electrochemistry using aligned carbon nanotube arrays. *Journal of the American Chemical Society* **2003**, *125* (30), 9006-9007.
21. Emanuelsson, R.; Löfås, H.; Wallner, A.; Nauroozi, D.; Baumgartner, J.; Marschner, C.; Ahuja, R.; Ott, S.; Grigoriev, A.; Ottosson, H., Configuration- and Conformation-Dependent Electronic-Structure Variations in 1,4-Disubstituted Cyclohexanes Enabled by a Carbon-to-Silicon Exchange. *Chemistry – A European Journal* **2014**, *20* (30), 9304-9311.
22. Takeda, K.; Morita, T.; Kimura, S., Effects of monolayer structures on long-range electron transfer in helical peptide monolayer. *Journal of Physical Chemistry B* **2008**, *112* (40), 12840-12850.
23. Polo, F.; Antonello, S.; Formaggio, F.; Toniolo, C.; Maran, F., Evidence against the hopping mechanism as an important electron transfer pathway for conformationally constrained oligopeptides. *Journal of the American Chemical Society* **2005**, *127* (2), 492.
24. (a) Danilov, A.; Kubatkin, S.; Kafanov, S.; Hedegård, P.; Stuhr-Hansen, N.; Moth-Poulsen, K.; Bjørnholm, T., Electronic Transport in Single Molecule Junctions: Control of the Molecule-Electrode Coupling through Intramolecular Tunneling Barriers. *Nano Letters* **2007**, *8* (1), 1-5; (b) Liu, H.; Zhao, J.; Boey, F.; Zhang, H., Asymmetric electron transport realized by decoupling between molecule and electrode. *Phys. Chem. Chem. Phys.* **2009**, *11* (44), 10323-10330.
25. Fisher, D. S.; Lee, P. A., Relation between conductivity and transmission matrix. *Physical Review B* **1981**, *23* (12), 6851-6854.
26. Staykov, A.; Nozaki, D.; Yoshizawa, K., Photoswitching of Conductivity through a Diarylperfluorocyclopentene Nanowire. *The Journal of Physical Chemistry C* **2007**, *111* (8), 3517-3521.

27. Watanabe, J.; Morita, T.; Kimura, S., Effects of dipole moment, linkers, and chromophores at side chains on long-range electron transfer through helical peptides. *Journal of Physical Chemistry B* **2005**, *109* (30), 14416.
28. Feliciano, G. T.; da Silva, A. J. R.; Reguera, G.; Artacho, E., Molecular and Electronic Structure of the Peptide Subunit of *Geobacter sulfurreducens* Conductive Phi from First Principles. *Journal of Physical Chemistry A* **2012**, *116* (30), 8023-8030.
29. Ding, W.; Negre, C. F. A.; Palma, J. L.; Durrell, A. C.; Allen, L. J.; Young, K. J.; Milot, R. L.; Schmuttenmaer, C. A.; Brudvig, G. W.; Crabtree, R. H.; Batista, V. S., Linker Rectifiers for Covalent Attachment of TransitionMetal Catalysts to Metal- Oxide Surfaces. *Chemphyschem* **2014**, *15* (6), 1138-1147.
30. (a) Beer, P. D.; Smith, D. K., Tunable bis(ferrocenyl) receptors for the solution-phase electrochemical sensing of transition-metal cations. *Journal of the Chemical Society-Dalton Transactions* **1998**, (3), 417; (b) Ossola, F.; Tomasin, P.; Benetollo, F.; Foresti, E.; Vigato, P. A., Synthesis, structure and properties of new ferrocene-containing compounds. *Inorganica Chimica Acta* **2003**, *353*, 292-300.

I hereby give permission for John Horsley to use the following papers in his PhD Thesis:

Yu, J.; Horsley, J. R.; Moore, K. E.; Shapter, J. G.; Abell, A. D. *Chemical Communications*, **2014**, *50*, 1652.

Horsley, J. R.; Yu, J.; Moore, K. E.; Shapter, J. G.; Abell, A. D. *Journal of the American Chemical Society*, **2014**, *136*, 12479.

Horsley, J. R., Yu, J., Abell, A. D. "The Correlation of Electrochemical Measurements and Molecular Junction Conductance Simulations in β -Strand Peptides" *Chemistry A European Journal*, **2015**, *21*, 5926-5933.

Horsley, J. R., Yu, J., Abell, A. D. "Understanding the Role of the Amide Bond and Electron Transfer Mechanisms in Macrocyclic Peptides" (Prepared in publication format "text in manuscript").

Signed

Date

19/6/2015

Signed

Date

19/06/2015

CHAPTER 5

Understanding the Role of the Amide Bond and Electron Transfer Mechanisms in Macrocyclic Peptides

John R. Horsley,[†] Jingxian Yu,^{*,†} and Andrew D. Abell^{*,†}

[†] ARC Centre of Excellence for Nanoscale BioPhotonics (CNBP), School of Physical Sciences, The University of Adelaide, Adelaide, SA 5005, Australia

(Prepared in publication format “text in manuscript”)

5.1 Abstract

A series of novel peptides constrained into either a 3_{10} -helical (**1** and **2**) or β -strand (**3** and **4**) conformation was synthesized. Peptides **1** and **3** are further constrained into these geometries with a side chain tether introduced by a lactam bridge, while **2** and **4** are direct linear analogues containing a terminal amide bond in their untethered side-chains. Electrochemical and theoretical studies revealed that the amide bond in the side-chain of both untethered peptides, and the amide bond in the lactam bridge of both constrained peptides does not contribute to electron transfer. This represents the first electrochemical study on a β -strand peptide constrained via a lactam-bridge. Furthermore, electron transfer was shown to proceed at significantly different rates between both linear and constrained species, with a transition in the mechanism evident from inelastic hopping to superexchange. These findings provide a more detailed understanding of the associated mechanisms that determine the efficiency of electron transfer in peptides.

5.2 Introduction

A fundamental understanding of electron transfer in peptides and proteins¹ is central not only to the elucidation of essential biological processes such as respiration and photosynthesis in living organisms, but also to the development of bio-inspired molecular electronics.² Synthetic peptides are particularly useful in this context since they can be designed to conform to specific secondary structures, such as helices and β -strands. They can be readily derivatized with 'smart' groups such as electro- or photoactive units,³ endowing the peptide scaffold with specific functionalities for applications in molecular electronics.⁴ Peptides have the capacity to self-assemble⁵ and can be functionalized along their backbone to enable precision-branching, a decisive advantage in the design of well-defined three-dimensional molecular circuitry.⁶ Revealing how electrons travel through branched-peptides is therefore crucial for understanding the electronic properties of peptide-based circuitry.⁷ However, the exploitation of peptides as electronic components requires us to first make fundamental advances in our understanding of the associated mechanisms of electron transfer.

While two main modes, superexchange and hopping⁸ are widely accepted in peptides, the precise mechanisms governing electron transfer remain in contention. This conundrum must be resolved if peptides are to be used as building blocks for complex molecular circuitry. The elastic superexchange mechanism involves direct molecule-mediated tunnelling, where the intervening bridge (peptide chain) takes on a virtual role. Here the electron transfer rate constant decreases exponentially with increasing distance between a donor and acceptor.⁹ The alternative inelastic hopping mechanism operates by using sites on the peptide chain that are coupled to each other electronically for electron transfer.¹⁰ In this case, electrons reside on the bridge for a finite time, with molecular conductance obeying ohmic behaviour with increasing distance between donor and acceptor.^{1, 11} Efficient long-range electron transfer by way of a hopping mechanism can be explained by the ordered coupling of amide groups within the backbone of a peptide.^{8c, 12} Specifically, the amide n and π orbitals are thought to provide potential hopping sites for electrons (or holes) along the peptide chain.¹³ Molecular dynamics simulations have suggested that a bi-functional model applies to the hopping mechanism, where electronic charge transfer is coupled to specific internal rotations of the amide bonds within the peptide backbone.¹⁴ These ultrafast rotations are unique to peptides and occur on the femtosecond time scale, bringing adjacent carbonyl groups into close proximity with one another. When the backbone dihedral angles reach this critical point, the energy barrier becomes negligible, allowing efficient charge transfer from one amino acid to

the next via a hopping mechanism.¹⁵ Furthermore, electron population analysis has provided clear theoretical evidence that amide groups can act as hopping sites in long-range electron transfer within the peptide backbone.^{2b, 16}

However no studies have been undertaken to investigate the role that amide bonds located in the side-chains of peptides have in electron transfer, whether in linear peptides or those constrained via a lactam bridge; nor have there been studies to investigate the mechanism(s) responsible for electron transfer in peptides constrained by a side-chain tether. We have previously shown that charge transport is significantly impeded by the introduction of a constraint linking the side-chains of peptides either via Husigen cycloaddition,¹⁷ or ring closing metathesis¹⁶ to constrain them into a well-defined helical or β -strand conformation. This additional rigidity restricts the torsional motion necessary for facile electron transfer through the peptide backbone via a hopping mechanism. Well-defined three-dimensional molecular circuitry is central to the future of electronic devices.⁶ Thus, for the promotion of peptide-based circuitry¹⁸ it is fundamental to investigate the role of the amide bond located in the side-chains of both linear and constrained systems in order to define the motive and precise course of electron transfer, together with the mechanism(s) responsible for such transference.

With this in mind we present electrochemical and theoretical studies on a series of new peptides to determine whether an amide bond in the side-bridge of a constrained peptide can either facilitate electron transfer by providing an alternative pathway (hopping site) through the bridge, or increase the backbone rigidity of the peptide so as to impede such transfer. Peptide **1** (see Figure 1) is constrained into a 3_{10} -helical conformation by linking its i to $i+3$ residues with an amide bond to form a lactam bridge, and peptide **2** (see Figure 1) is a direct linear analogue used as a control. Peptide **3** is similarly constrained into a β -strand geometry via a lactam-bridge tether, in this case linking the i to $i+2$ residues, with peptide **4** a direct linear analogue (see Figure 1). Specifically, the macrocyclic peptides (**1** and **3**) are used to define the role of the amide bond in the lactam bridge constraint in electron transfer, while the linear peptides (**2** and **4**) are used to determine the effect of the terminal amide bond in the untethered side-chain on electron transfer. Furthermore, theoretical studies are conducted in order to elucidate the mechanism(s) responsible for electron transfer in each of the linear and macrocyclic helical peptides.

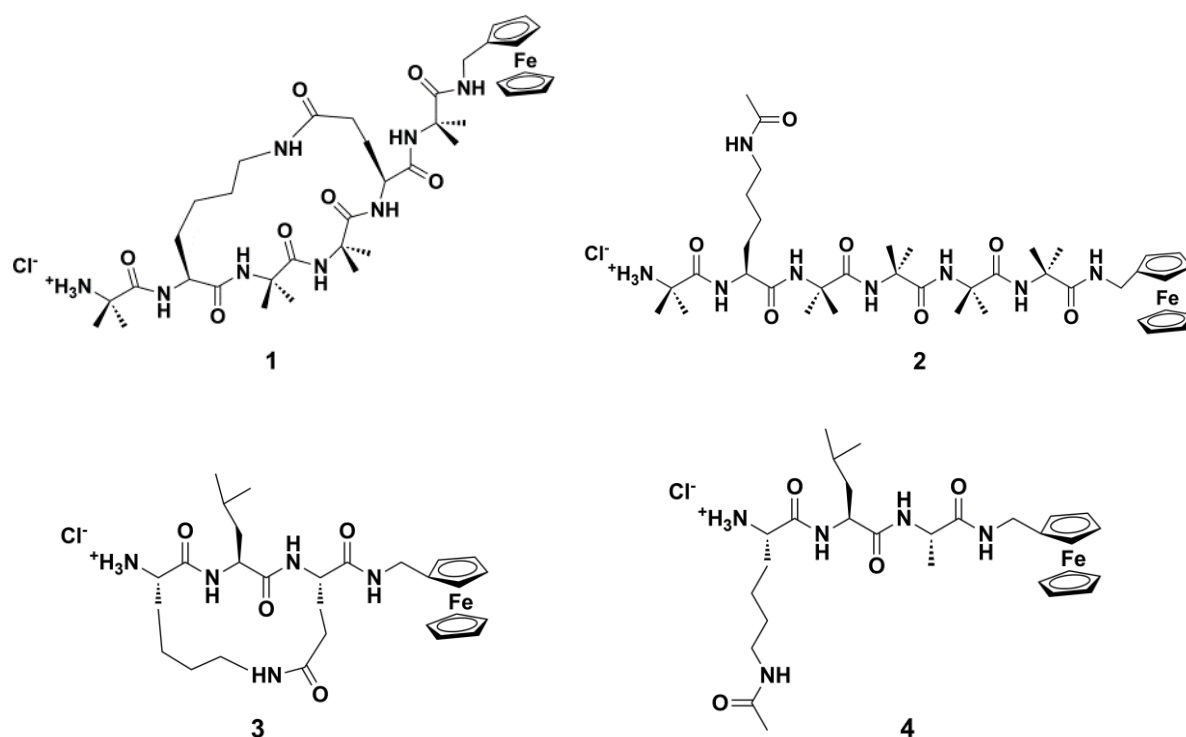


Figure 1. Synthetic peptides **1** and **2** (3_{10} -helical) and **3** and **4** (β -strand).

5.3 Results and discussion

5.3.1 Peptide design

Aib residues were incorporated into peptides **1** and **2** to establish the formation of a 3_{10} -helical secondary structure.^{17a} Peptide **1** was further rigidified into this conformation via a lactam-based tether linking the lysine and glutamic acid (*i* and *i*+3) residues. The side-chain of the lysine residue located in the *i* position of the direct linear analogue **2** was modified to contain a terminal amide bond. Peptide **3** was designed to adopt a β -strand conformation, with the lactam-based tether linking the lysine and glutamic acid (*i* and *i*+2) residues. The side-chain of the direct linear analogue **4**, located in the *i* position, was also modified to contain a terminal amide bond. Peptides **1**, **3** and **4** were synthesized using solution phase

chemistry, while the linear hexapeptide **2** was synthesized using solid phase peptide synthesis (SPPS) as detailed in the supplementary information. Each peptide (**1-4**) was purified by reverse phase HPLC prior to attachment to vertically aligned single-walled carbon nanotube array/gold (SWCNTs/Au) electrodes¹⁹ for electrochemical studies.

5.3.2 Conformational analysis of peptides

The geometries of peptides **1-4** were defined by ¹H NMR and 2D NMR spectroscopy. Specifically, *CαH* (*i*) to *NH* (*i*+1) and medium range *CαH* (*i*) to *NH* (*i*+2) ROESY correlations were observed for peptides **1** and **2**, indicative of a ₃10-helical structure.²⁰ *CαH* (*i*) to *NH* (*i*+4) interactions were not evident in these spectra, thus excluding the possibility of an α -helical structure.²¹ The conformations of **3** and **4** were confirmed to be β -strand²² based on the presence of *CαH* (*i*) to *NH* (*i*+1), *CβH* (*i*) to *NH* (*i*+1) and sequential *NH* (*i*) to *NH* (*i*+1) ROESY correlations (see Figure 2). Furthermore, ¹H NMR $J_{NH C\alpha H}$ coupling constants consistent with a β -strand conformation were observed for these peptides.²³

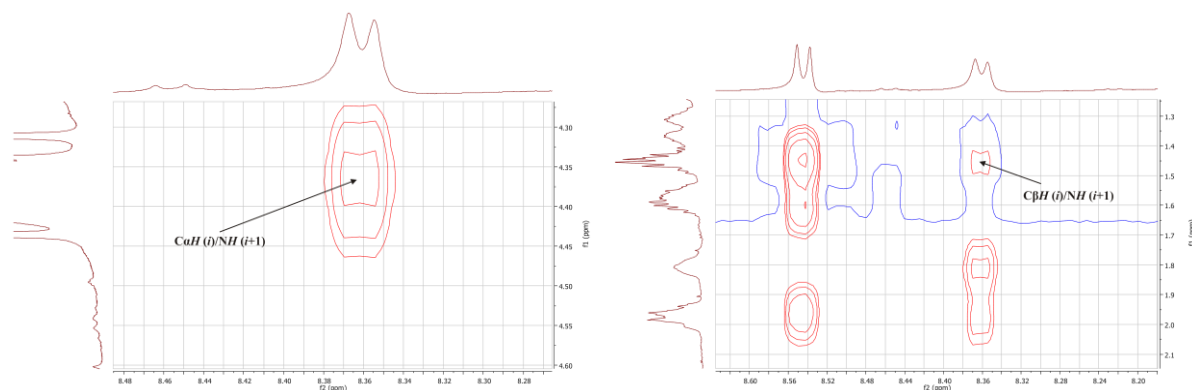


Figure 2. ROESY NMR spectra representative of peptide **3** showing *CαH* (*i*) to *NH* (*i*+1) correlations at left, and *CβH* (*i*) to *NH* (*i*+1) right, indicative of a β -strand structure.

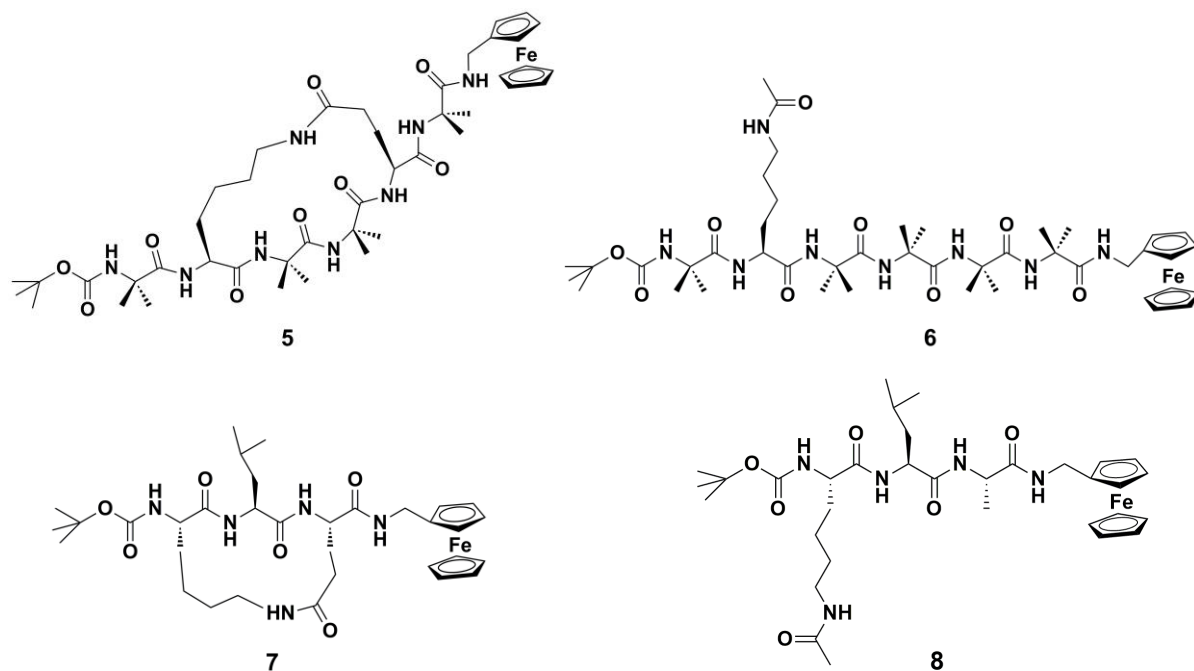


Figure 3. The lowest energy conformers of the *N*-Boc protected analogues of **1-4** (peptides **5-8**).

^1H NMR and 2D NMR spectroscopy were also used to confirm the geometry of peptides **5-8** (the *N*-Boc protected analogues of **1-4**, see Figure 3). In particular, $\text{CaH}(i)$ to $\text{NH}(i+1)$ and medium range $\text{CaH}(i)$ to $\text{NH}(i+2)$ ROESY correlations were observed for **5** and **6**, indicative of a 3_{10} -helical structure (see Figure 4). Peptides **7** and **8** were confirmed as β -strand, with $\text{CaH}(i)$ to $\text{NH}(i+1)$, $\text{C}\beta\text{H}(i)$ to $\text{NH}(i+1)$ and sequential $\text{NH}(i)$ to $\text{NH}(i+1)$ ROESY correlations evident.²² IR spectroscopy further confirmed the conformation of each of the *N*-Boc protected lactam macrocycles (**5** and **7**, see Figure 5). A strong peak at 1654 cm^{-1} representative of the Amide I band was observed for **5**, indicative of a 3_{10} -helical structure.²⁴ A strong peak at 1636 cm^{-1} with a small shoulder at 1687 cm^{-1} was found for **7**, representative of the Amide I band. Another strong peak was observed at 1525 cm^{-1} (Amide II) and a broad peak at 3289 cm^{-1} (Amide A). Each of these peaks is characteristic of a β -strand conformation.²⁵

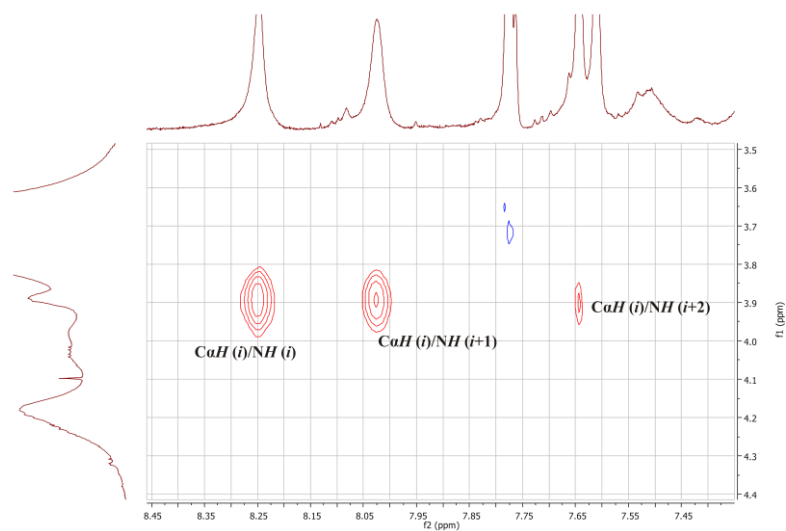


Figure 4. ROESY NMR spectrum representative of peptide **6** showing $CaH(i)$ to $NH(i+1)$ and medium range $CaH(i)$ to $NH(i+2)$ correlations indicative of a 3_{10} -helical structure.

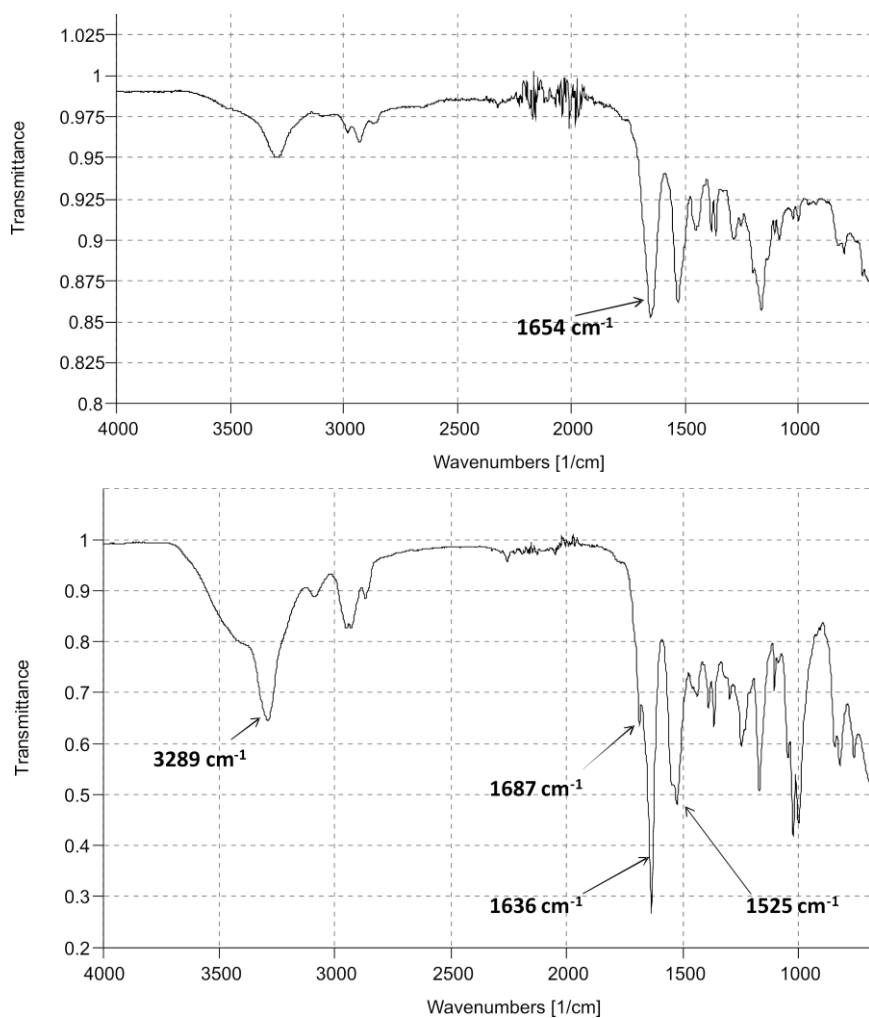


Figure 5. IR spectrum of peptide **5** (top) and peptide **7** (bottom).

Molecular modelling was used to further define the backbone geometries of peptides **5-8**. The Boc protection group was used for the respective *N*-termini as free amines are known to give rise to unrealistic electrostatic interactions, resulting in unstable lowest energy conformers.²⁶ The models indicate that the backbone lengths of peptides **5** and **6** (from first to last carbonyl carbons) are strikingly similar, differing by no more than 0.17 Å. The mean intramolecular hydrogen bond length for the macrocyclic **5** is only 0.05 Å shorter than its linear analogue **6**. The models also demonstrate that each of these peptides adopts a 3_{10} -helical conformation, with the average dihedral angles in peptide **5** deviating from an ideal 3_{10} -helix by no more than 3.7° and 4.8° for Φ and ψ respectively, and 2.2° (Φ) and 3.2° (ψ) in peptide **6** (see Table 1). The models for the two *N*-Boc protected β -strand peptides show that the macrocyclic **7** is 0.42 Å shorter than its linear analogue **8** (from first to last carbonyl carbons). All other dimensions crucial to the characterization of a β -strand conformation, such as *NH* (*i*) to *NH* (*i*+1), *CaH* (*i*) to *NH* (*i*+1) and *C β H₂* (*i*) to *NH* (*i*+1) distances, are comparable to literature values.²⁷

Table 1. Dihedral angles for all residues in the lowest energy conformers for peptides **5** and **6**.

	peptide 5		peptide 6	
	Φ	ψ	Φ	ψ
Residue 1	-64.156	-28.640	-64.329	-28.300
Residue 2	-55.638	-27.008	-56.464	-28.097
Residue 3	-52.532	-31.510	-59.037	-23.420
Residue 4	-55.092	-29.286	-55.844	-28.940
Residue 5	-70.469	-10.385	-53.315	-31.545
Residue 6	-66.630	-24.062	-66.533	-20.283
Average	-60.75	-25.14	-59.25	-26.76
Differs from ideal 3_{10} helix	3.75°	4.86°	2.25°	3.24°

Thus, the ¹H NMR and IR spectra, together with the molecular modelling data, confirm that peptides **5** and **6** share a similar 3_{10} -helical geometry, while peptides **7** and **8** share a common β -strand geometry. Ostensibly, the only structural difference between each of these peptides

(**5**, **6** and **7**, **8**) and hence their analogues (**1**, **2** and **3**, **4**), is the presence (or absence) of the lactam side-bridge constraint and the associated effect that this has on backbone rigidity.

5.3.3 Electrochemical analysis of intramolecular electron transfer

Each of the peptides **1-4** was separately attached to vertically aligned single-walled carbon nanotube array/gold (SWCNTs/Au) electrodes¹⁹ in order to study their electron transfer kinetics. Analysis of the electrochemical results for the helical peptides **1** and **2** reveals a pair of redox peaks in each cyclic voltammogram, characteristic of a one-electron oxidation/reduction reaction (Fc^+/Fc) (see Figure 6). The formal potentials (E_o) and apparent electron transfer rate constants (k_{app}) were estimated using Laviron's formalism,²⁸ and given in Table 2.

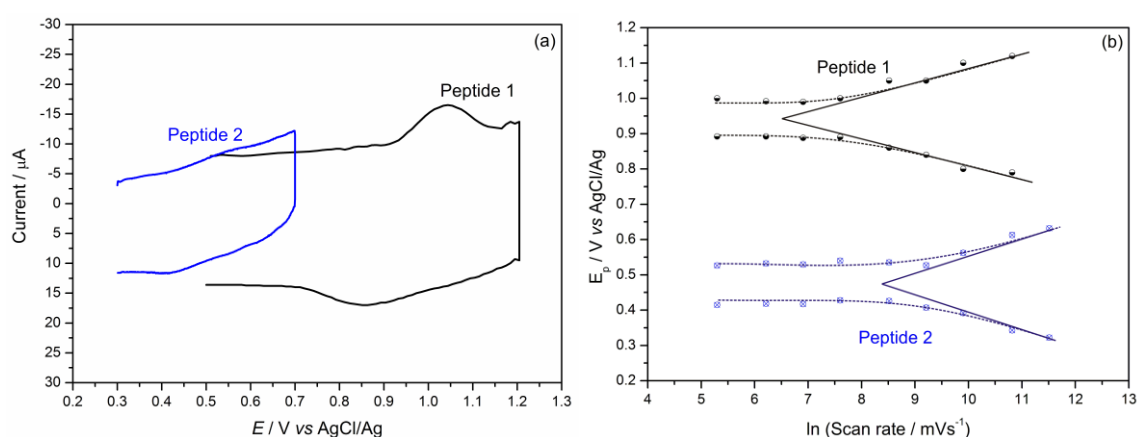


Figure 6. (a) Cyclic voltammograms for peptides **1** and **2** immobilized on SWCNTs/Au electrodes taken at 5 V s^{-1} . (b) Peak potential versus $\ln(\text{scan rate})$ for peptides **1** and **2** after background current subtraction.

Table 2. Electron transfer rate constants (k_{app}), surface concentrations and formal potentials (E_o) for the helical peptides (**1** and **2**).

Peptide	Surface concentration ($\times 10^{-10} \text{ mole.cm}^{-2}$)	E_o (V vs AgCl/Ag)	k_{app} / s^{-1}
1	4.37 ± 0.38	0.924	9.34 ± 1.58
2	2.03 ± 0.19	0.442	83.65 ± 7.64

The observed electron transfer rate constant for the macrocyclic peptide **1** was 9.34 s^{-1} , while that of the direct linear analogue **2** was almost one order of magnitude greater (83.65 s^{-1} , see Table 2). A dramatic shift to the positive in the formal potential of the constrained peptide **1** was also observed (482 mV) compared with that of the linear **2** (see Figure 6, Table 2). These electrochemical results are comparable to data from our previous studies regarding 3_{10} -helical hexapeptides, stapled in the i to $i+3$ positions either by a triazole-containing linker introduced by Huisgen cycloaddition (482 mV, see Figure 7a)^{17a} or by an alkane-containing linker (502 mV, see Figure 7b) or alkene-containing linker (465 mV, see Figure 7c) introduced by ring-closing metathesis.¹⁶

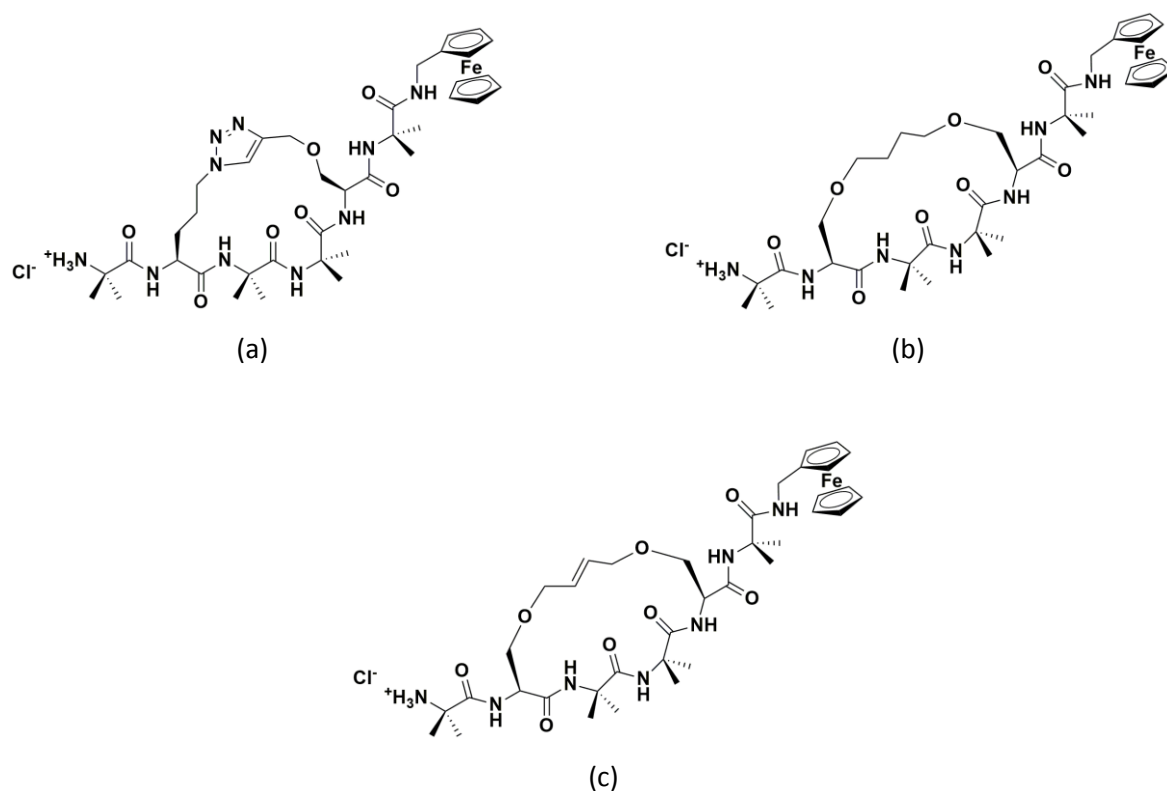


Figure 7. (a) Macrocyclic 3_{10} -helical hexapeptide with a triazole-containing side-chain linked via the i and $i+3$ residues (b) macrocyclic 3_{10} -helical hexapeptide with an alkane-containing side-chain linked via the i and $i+3$ residues and (c) macrocyclic 3_{10} -helical hexapeptide with an alkene-containing side-chain linked via the i and $i+3$ residues.

As demonstrated, peptides **1** and **2** share a common 3_{10} -helical geometry. However, the backbone of **1** is constrained and hence rigidified by the lactam-bridge, while the side-chain of **2** is untethered and thus more conformationally flexible. Such a large distinction between

the observed formal potentials of each peptide, together with the disparity in their electron transfer rate constants, is further evidence of the additional backbone rigidity imparted by the side-bridge constraint, which restricts the precise backbone torsional motions required by a hopping mechanism to facilitate intramolecular electron transfer through the peptide.^{15, 17a}

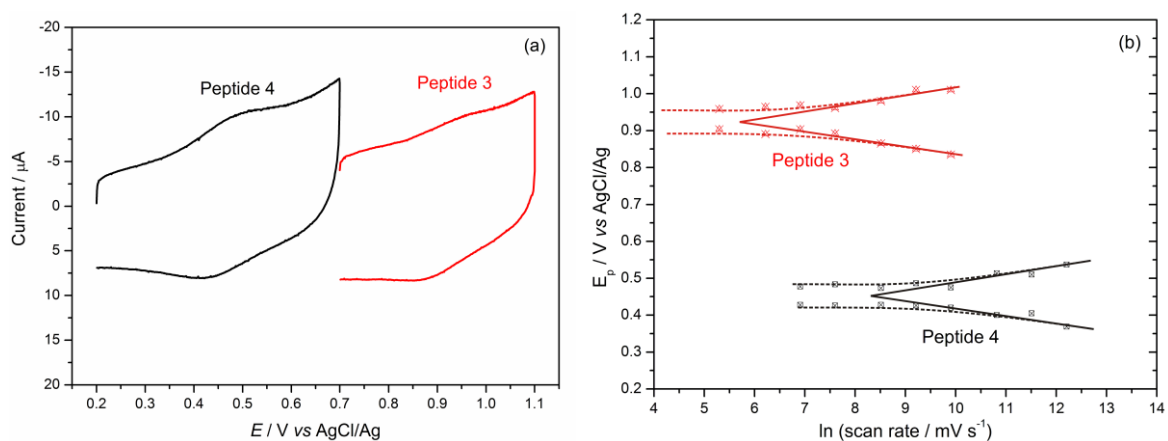


Figure 8. (a) Cyclic voltammograms for β -strand peptides **3** and **4** immobilized on SWCNTs/Au electrodes taken at 5 V s^{-1} . (b) Peak potential versus $\ln(\text{scan rate})$ for peptides **3** and **4** after background current subtraction.

Table 3. Electron transfer rate constants (k_{app}), surface concentrations and formal potentials (E_o) for the β -strand peptides **3** and **4**.

Peptide	Surface concentration ($\times 10^{-10} \text{ mole.cm}^{-2}$)	E_o (V vs AgCl/Ag)	k_{app} / s^{-1}
3	2.46 ± 0.25	0.927	5.92 ± 0.47
4	3.68 ± 0.41	0.456	86.67 ± 7.95

Peptides **3** and **4** share a common β -strand geometry, but a significant 15-fold difference was observed in their electron transfer rate constants (see Figure 8, Table 3). The shift in the formal potentials of the linear and constrained peptides was a considerable 471 mV, which is

comparable to results from our previous studies concerning β -strand tripeptides stapled in the i to $i+2$ positions (476 mV, triazole-containing side-chain, Huisgen cycloaddition, see Figure 9 a)^{17b} and (419 mV, alkane-containing side-chain, ring closing metathesis, see Figure 9 b).¹⁶

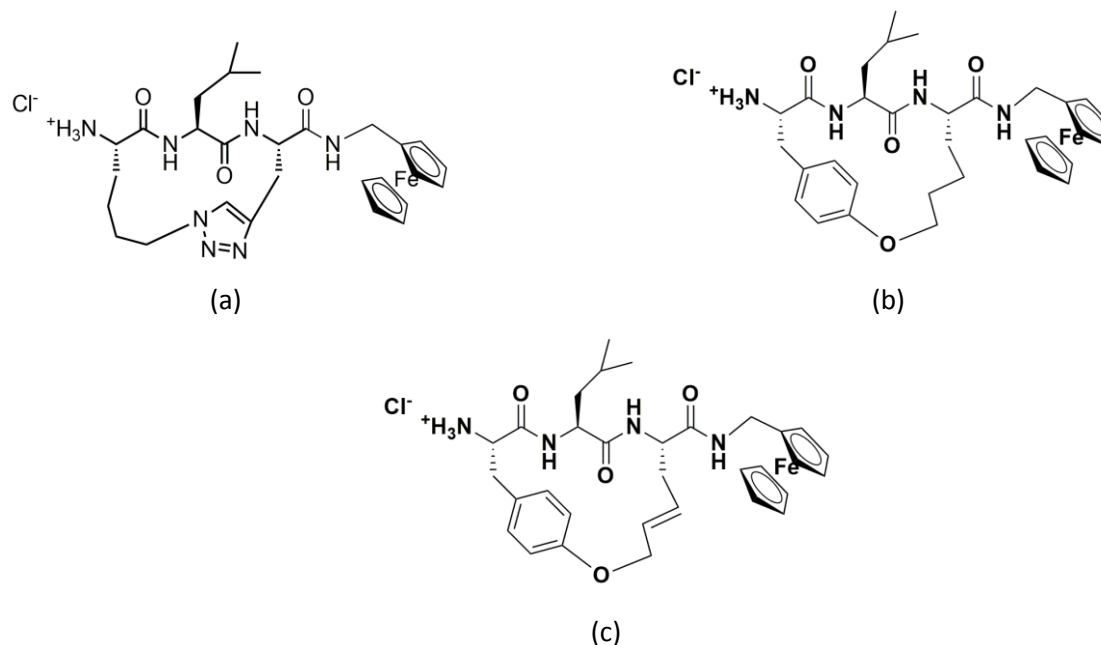


Figure 9. (a) Macrocyclic β -strand tripeptide with a triazole-containing side-chain linked via the i and $i+2$ residues (b) macrocyclic β -strand tripeptide with an alkane-containing side-chain linked via the i and $i+2$ residues and (c) macrocyclic β -strand tripeptide with an alkene-containing side-chain linked via the i and $i+2$ residues.

Indeed, the results from all our previous electrochemical studies on β -strand peptides follow a similar trend to the results from our previous electrochemical studies on 3_{10} -helical peptides, with respect to both formal potential shifts and electron transfer rate constants.¹⁶⁻¹⁷ Specifically, the 3_{10} -helical hexapeptides containing side-chains constrained either via Huisgen cycloaddition (Figure 7 a) or an alternative alkane-based tether introduced by ring closing metathesis (Figure 7 b) revealed similar electron transfer rate constants (28.1 s^{-1} and 31.8 s^{-1} respectively) each more than three times that of the 3_{10} -helical hexapeptide constrained via a lactam bridge (peptide **1**, 9.3 s^{-1}). The β -strand tripeptides with their i to $i+2$ side-chains constrained either via Huisgen cycloaddition (Figure 9 a) or an alternative alkane-based tether introduced by ring closing metathesis (Figure 9 b) also exhibited similar electron

transfer rate constants (22.5 s^{-1} and 23.6 s^{-1} respectively) each more than three times that of the β -strand tripeptide constrained via a lactam bridge (peptide **3**, 5.9 s^{-1}).

The macrocyclic peptides, **1** (helical) and **3** (β -strand), are expected to display electronic characteristics more closely resembling those of peptides containing an alkene-based tether, as the amide bond in the side-chain has a partial double bond character which renders the amide group planar, thus further rigidifying the peptide backbone. Gratifyingly, the 3_{10} -helical hexapeptide, with its side-chain constrained via an alternative alkene-based tether introduced by ring closing metathesis (Figure 7 c)¹⁶ exhibited an electron transfer rate constant (17.4 s^{-1}) only twice that of peptide **1** (9.3 s^{-1}). This tendency was also evident in the comparable β -strand tripeptides (11.7 s^{-1} Figure 9 c)¹⁶, to peptide **3**, 5.9 s^{-1}). However, the formal potential shift for each peptide constrained via a lactam bridge, relative to those cyclized via ring closing metathesis containing an alkene-based side-chain constraint, was unexpected. The formal potential shift to the positive for peptide **1**, relative to the alkene-based helical peptide (Figure 7 c) was a substantial 80 mV while the shift for peptide **3**, relative to the alkene-based β -strand peptide (Figure 9 c) was a vast 251 mV. These results clearly demonstrate that the lactam bridges in peptides **1** and **3** provide the most rigid macrocycles when compared with other forms of cyclization discussed here, with oxidation/reduction of the ferrocene moiety energetically less favourable. Hence, electrochemical evidence has demonstrated that the amide bond in the side-chain of each peptide constrained via a lactam bridge (**1** and **3**) clearly has no significant effect on the promotion of electron transfer.

A comparison was also made between the electrochemical data gleaned from the linear peptide **2** and a related linear peptide with an untethered alkene-containing side-chain in place of the amide in the '*i*' position of **2** (Figure 10 a)¹⁶ to shed light on the possible role of the amide bond as a 'stepping stone' for electron transfer.

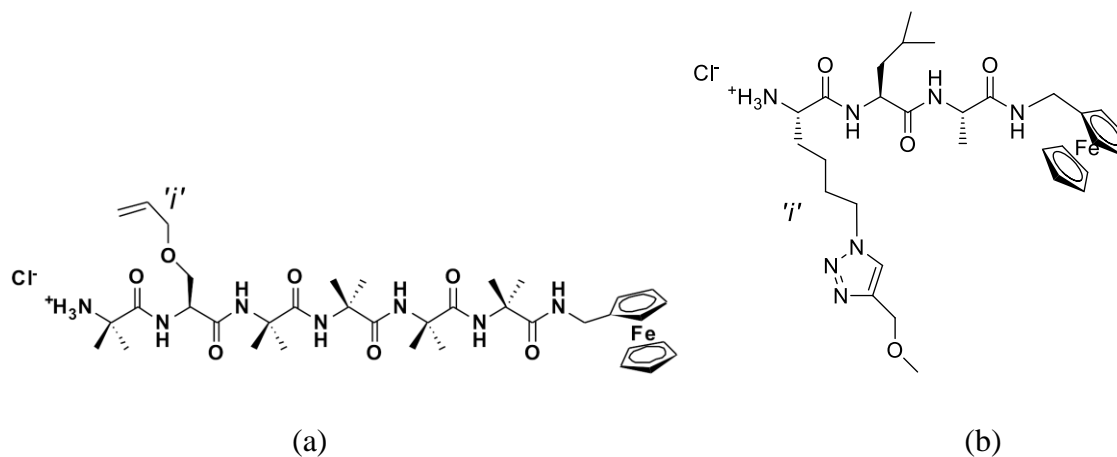


Figure 10. (a) Linear 3₁₀-helical hexapeptide with an untethered alkene-containing side-chain located on the 'i' residue (b) linear β-strand tripeptide with a triazole-containing side-chain located on the 'i' residue.

We previously demonstrated¹⁶ that the terminal alkene in the side-chain can act as a 'stepping stone' to facilitate electron transfer through the peptide, with an observed electron transfer rate constant of 260 s⁻¹, more than three times that of peptide **2** (83 s⁻¹). Furthermore, the linear peptide **4** is identical to a complementary β-strand tripeptide from a previous study (Figure 10 b)^{17b} except for the modified side-chain containing an amide bond on the 'i' residue, in place of a triazole-containing side-chain at the same location. Once again the observed electron transfer rate constants are disparate, with that of the linear peptide **4** (86 s⁻¹) significantly lower than that of the peptide with a triazole-containing side-chain (223 s⁻¹). Thus, electrochemical evidence suggests that the terminal amide bond located in the untethered side-chain of the peptide is not a candidate as a 'stepping stone' for electron transfer. However, theoretical evidence is required to confirm this premise and to determine the exact pathway for electron transfer, and this is discussed in the Computational study section.

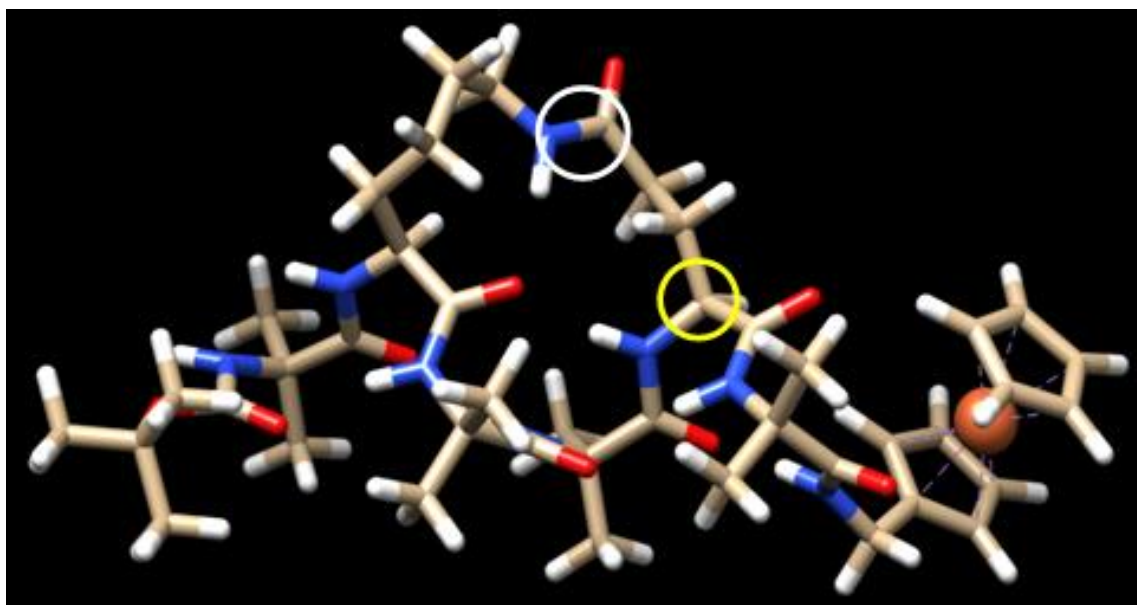


Figure 11. The lowest energy conformer for the constrained peptide **5** (analogue of **1**) with the link for the lactam macrocycle located on the *i*+3 residue (circled in yellow), showing its proximity to the amide bond in the side-bridge (circled in white).

The molecular model structure of peptide **5** (analogue of **1**, see Figure 11) discussed earlier, reveals that while the mean dihedral angles for residues 1-6 deviate from an ideal 3_{10} -helix by only 3.7° (Φ) and 4.8° (ψ), the actual angles proximal to the *i*+3 residue (**5**) differ by 13.4° (Φ) and 19.6° (ψ) respectively (see Table 1). When compared with other similar 18-membered macrocyclic 3_{10} -helical hexapeptides constrained at the *i*+3 residue by ring closing metathesis (alkane, 4.6° Φ , 10.0° ψ , Figure 7 b) and (alkene, 10.1° Φ , 16.7° ψ , Figure 7 c)¹⁶ the lactam bridge of **5** yields the largest deviation from an ideal structure at this location. The *i*+3 residue provides a link for the lactam macrocycle, thereby clearly showing the effect of the tether at this site. The resulting ‘constriction’ contributes additional rigidity to the peptide backbone, which is reflected in the high formal potential and low electron transfer rate constant.

5.3.4 Computational study of intramolecular electron transfer

Linear peptides are known to undergo electron transfer via a hopping mechanism.^{8c, 29} However, very little is known about electron transfer in constrained peptides.³⁰ Thus, Marcus theory³¹ was used in conjunction with constrained density functional theory (cDFT)³² to model the diabatic states in 3₁₀-helical models **9** and **10** (see Figures 12 and 13) in order to provide an insight into the likely electron transfer mechanism and pathway. These peptides are analogous to **1** and **2**, but with ferrocene (Fc) units located at both termini to act as electron donors and acceptors.^{17a} Diabatic states were constructed by individually localizing an overall charge of +1 on the residues, Aib1, Aib4, Aib6 and on the amide bond in the side-chain, as shown in Figures 12 and 13. The Aib4 residue represents the hopping site via the backbone pathway and the amide bond in the side-chain represents the hopping site via the side-bridge pathway. Three possible electron transfer pathways are considered in the theoretical simulation. The first is the elastic superexchange pathway involving direct electron tunnelling between Aib1 and Aib6. The other two pathways involve electrons sequentially hopping from Aib1, through either the peptide backbone (Aib4) or the amide-containing side-bridge, and terminating at Aib6. The difference in free energy (ΔG), electronic coupling constants (H_{ab}) and reorganization energies (λ) between the neighboring states along the three possible electron transfer pathways were computed from diabatic potential profiles in order to provide an insight into the overall intramolecular electron transfer dynamics. The individual electron transfer rate constant $(k_{ET})_{ij}$ from the diabatic state i to the neighbouring diabatic state j was estimated from the semi-classical Marcus theory^{31, 33} expression

$$(k_{ET})_{ij} = \frac{|H_{ab}|_{ij}^2}{\hbar} \sqrt{\frac{\pi}{\lambda_{ij} k_B T}} \exp\left(-\frac{(\Delta G_{ij} + \lambda_{ij})^2}{4\lambda_{ij} k_B T}\right)$$

where λ_{ij} is the reorganization energy from the diabatic state i to the neighbouring diabatic state j , $(H_{ab})_{ij}$ is the electronic coupling between the two states, k_B is the Boltzmann constant and ΔG_{ij} is the difference in free energy between the two states. Here the free energy difference ΔG_{ij} is approximated by the energy gap ΔE_{ij} .

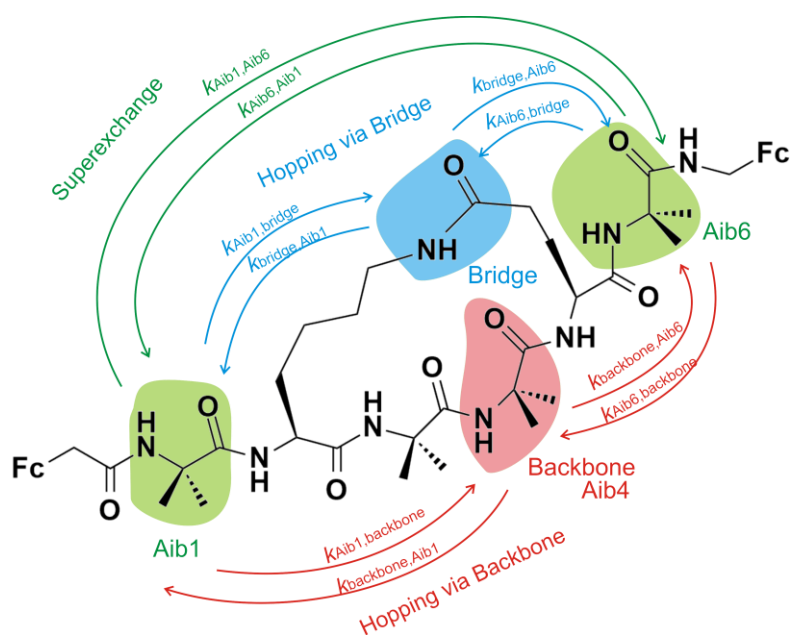


Figure 12. Constructed diabatic states for the constrained peptide **9** showing all possible electron transfer pathways.

The superexchange electron transfer rate constant in the constrained peptide **9** (see Figure 12) is represented by the forward reaction ($k_{\text{Aib1, Aib6}} = 2.28 \times 10^{11} \text{ s}^{-1}$) since the electron transfer rate in the reverse reaction is negligible ($k_{\text{Aib6, Aib1}} = 5.00 \times 10^{-1} \text{ s}^{-1}$). Hence, the overall superexchange electron transfer rate constant in peptide **9** is computed as $k_{\text{super}} = 2.28 \times 10^{11} \text{ s}^{-1}$. The overall hopping electron transfer rate constant via the backbone (Aib1 \rightleftharpoons Aib4 \rightleftharpoons Aib6) was calculated as $k_{\text{hop1}} = 2.36 \times 10^9 \text{ s}^{-1}$, using a kinetic model that assumes steady-state occupation probability for bridge sites.^{2b} For the hopping pathway through the bridge (Aib1 \rightleftharpoons Bridge \rightleftharpoons Aib6) the overall electron transfer rate constant (k_{hop2}) is exceptionally low ($1.96 \times 10^{-38} \text{ s}^{-1}$). A comparison of the three overall electron transfer rate constants (k_{super} , k_{hop1} and k_{hop2}) reveals that the superexchange pathway is the most favoured in the constrained peptide **9**, with an overall electron transfer rate constant of $2.28 \times 10^{11} \text{ s}^{-1}$.

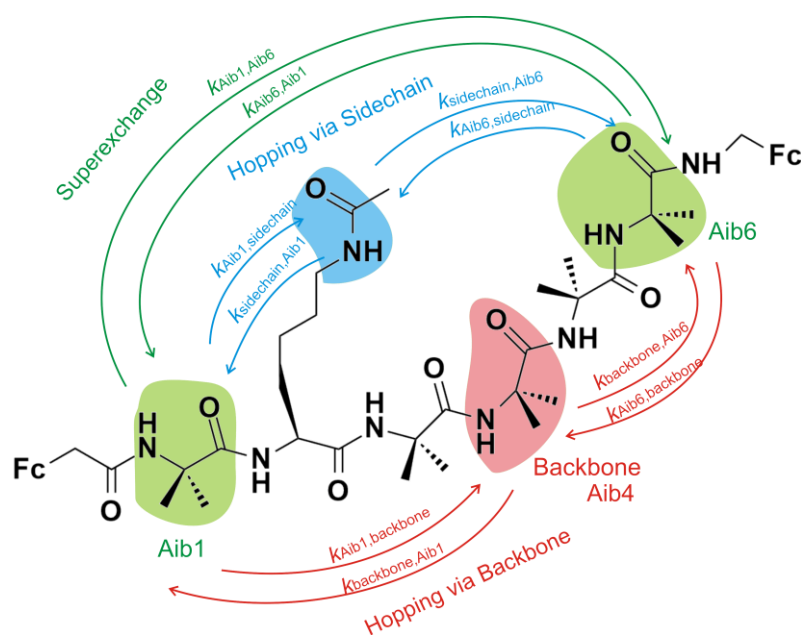


Figure 13. Constructed diabatic states for the linear peptide **10** showing all possible electron transfer pathways.

The overall superexchange electron transfer rate constant in the linear peptide **10** (see Figure 13) is dominated by the forward reaction ($k_{\text{Aib1, Aib6}} = 4.57 \times 10^{12} \text{ s}^{-1}$), since the electron transfer rate in the reverse reaction is negligible ($k_{\text{Aib6, Aib1}} = 6.77 \times 10^0 \text{ s}^{-1}$). Thus the overall superexchange electron transfer rate constant in peptide **10** is computed as $k_{\text{super}} = 4.57 \times 10^{12} \text{ s}^{-1}$. The overall hopping electron transfer rate constant via the backbone (Aib1 \rightleftharpoons Aib4 \rightleftharpoons Aib6) was calculated as $k_{\text{hop1}} = 1.00 \times 10^{15} \text{ s}^{-1}$ while the overall hopping electron transfer rate constant (k_{hop2}) through the side-chain is exceptionally low ($4.38 \times 10^{-41} \text{ s}^{-1}$). A comparison of the three overall rate constants (k_{super} , k_{hop1} and k_{hop2}) reveals that the hopping pathway via the backbone is the most favoured in the linear peptide **10**, with an overall electron transfer rate constant of $1.00 \times 10^{15} \text{ s}^{-1}$.

For the first time, we can definitively rule out the possibility of the amide bond in the side-chain tether acting as a ‘stepping stone’, as hopping through this group is prohibitive ($4.38 \times 10^{-41} \text{ s}^{-1}$). Thus, the terminal amide bond in the side-chain of the linear peptide does not

contribute to the flow of electrons through the peptide backbone. The implausibility of electron transfer through the lactam bridge of the constrained peptide is also demonstrated by the exceptionally low rate constant ($1.96 \times 10^{-38} \text{ s}^{-1}$) confirming the experimental evidence. Electron transfer through two similar 3_{10} -helical hexapeptides, each containing an amide bond in their side-chain, has not only been shown to proceed at significantly different rates, but most notably by utilizing two different mechanisms. As expected in the linear **10**, inelastic hopping along the peptide backbone is the most favoured ($1.00 \times 10^{15} \text{ s}^{-1}$) compared with the superexchange pathway ($4.57 \times 10^{12} \text{ s}^{-1}$). These findings underscore the ubiquitous nature, and importance of structural fluctuations to charge transport in peptides. Conversely, in the constrained peptide **9** the superexchange pathway is shown to be the most favoured ($2.28 \times 10^{11} \text{ s}^{-1}$) compared with hopping along the peptide backbone ($2.36 \times 10^9 \text{ s}^{-1}$). Hence, we have demonstrated for the first time that the superexchange mechanism is responsible for electron transfer through a peptide constrained via a side-chain tether. This is perhaps not surprising as the pronounced effect on the dihedral angles arising from the lactam constraint located on the $i+3$ residue (see Figure 11) is expected to further increase backbone rigidity, so reducing the torsional motion necessary for the hopping mechanism to operate. We have also shown that both mechanisms may potentially be operational in each peptide, with one mechanism favoured over the other. These findings not only add considerable weight to the belief that electron transfer utilizes both the superexchange and hopping mechanisms,³⁴ depending on such factors as the nature of the peptide architecture, they also challenge the hypothesis that the mechanism responsible for electron transfer in peptides is purely distance-dependent. These significant findings have unveiled a new approach for controlling the mechanism responsible for electron transfer in peptides, which presents a new technique for fine tuning their electronic properties. Hence this ability to judiciously change the behaviour of the system will be strategic in the design of stable building blocks for future three dimensional peptide-based circuitry.

5.4 Conclusion

In summary, a series of novel amide-containing peptides, constrained into either a well-defined 3_{10} -helical, or β -strand conformation was synthesized. Neither the terminal amide bond in the side-chain of the untethered peptides, nor the amide bond in the lactam bridge of the constrained peptides were found to contribute to electron transfer. Electrochemical and theoretical studies conducted on the 3_{10} -helical hexapeptides, one further constrained into this geometry by linking its i to $i+3$ residues with an amide bond to form a lactam bridge and the other a direct linear analogue, showed electron transfer to proceed at significantly different rates and, most notably, by utilizing two different mechanisms (inelastic hopping and superexchange). These considerable developments contribute fundamental advances to our understanding of the rates and mechanisms of electron transfer in peptides, bringing us a step closer towards our ultimate goal to design, assemble and control functional devices from the bottom up.

5.5 Acknowledgments

We acknowledge the Australian Research Council (ARC) Centre of Excellence for Nanoscale BioPhotonics (CNBP), School of Physical Sciences, The University of Adelaide, Adelaide, SA 5005, Australia, for the financial support of this work. We also acknowledge the Australian National Fabrication Facility for providing the analytical facilities used in this work. We would like to thank Ms. Katherine Moore and Prof. Joe Shapter from Flinders University, S.A., for the preparation of the SWCNT/Au electrodes used in this study and for the use of their electrochemical facilities. The computational aspects of this work were supported by an award under the National Computational Merit Allocation Scheme for JY on the National Computing Infrastructure (NCI) National Facility at the Australian National University.

5.6 Experimental methods

5.6.1 Chemicals

Fmoc-Aib-OH, Boc-Aib-OH, Fmoc-Lys(Boc)-OH, Boc-Lys(Cbz)-OH, Boc-Glu(OBzl)-OH, H-Leu-OMe, H-Ala-OMe, 1-(3-Dimethylaminopropyl)-3-ethylcarbodiimide HCl (EDC·HCl), Fmoc-OSu, 2-chlorotriyl chloride polystyrene resin, 1-hydroxy-7-azabenzotriazole (HOAt) and 2-(1H-7-azabenzotriazol-1-yl)-1,1,3,3-tetramethyl uranium hexafluorophosphate methanaminium (HATU) were purchased from GL Biochem (Shanghai) Ltd, China. Dichloromethane (DCM), diethyl ether (Et₂O), ethyl acetate (EtOAc), methanol and ethanol were purchased from Ajax Finechem Pty Ltd (Australia). Piperidine, acetonitrile, propan-2-ol, potassium carbonate, and *N,N*-dimethylformamide (DMF) were purchased from Merck, Australia. Anhydrous *N,N*-dimethylformamide (DMF), dimethyl sulfoxide (DMSO), tetrahydrofuran (THF), dioxane, 2,2,2-trifluoroethanol (TFE), trifluoroacetic acid (TFA), 4 M HCl/dioxane solution, cysteamine, methyl iodide, Pd/C and diisopropylethylamine (DIPEA) were purchased from Sigma-Aldrich, Australia. SOCl₂, CH₃COOH and NaOH were purchased from Chem Supply, Australia. Single-walled carbon nanotubes (P2-SWCNTs), purchased from Carbon Solutions Inc., USA. Ferrocenylmethylamine³⁵ was prepared as published. All solvents and reagents were used without purification unless noted.

5.6.2 High-performance liquid chromatography (HPLC)

The synthetic peptides were analyzed and purified by reverse phase HPLC, using an HP 1100 LC system equipped with a Phenomenex C18 column (250x4.6 mm) for analytical traces and a Phenomenex C18 column (250 x 21.2 mm) for purification, a photodiode array detector, and a Sedex evaporative light scattering detector. Water/TFA (100/0.1 by v/v) and ACN/TFA (100/0.08 by v/v) solutions were used as aqueous and organic buffers.

5.6.3 NMR spectroscopy

¹H NMR spectra were recorded in DMSO-d₆ or CDCl₃-d solutions using a Varian Gemini-300 NMR. ¹³C NMR and two-dimensional NMR experiments utilized COSY, ROESY, HSQC and HMBC were obtained on a Varian Inova 600 MHz spectrometer. Chemical shifts are reported in ppm (δ) using TMS (0.00 ppm) as the internal standard. Signals are reported as s (singlet), d (doublet), t (triplet) or m (multiplet).

5.6.4 Mass spectroscopy

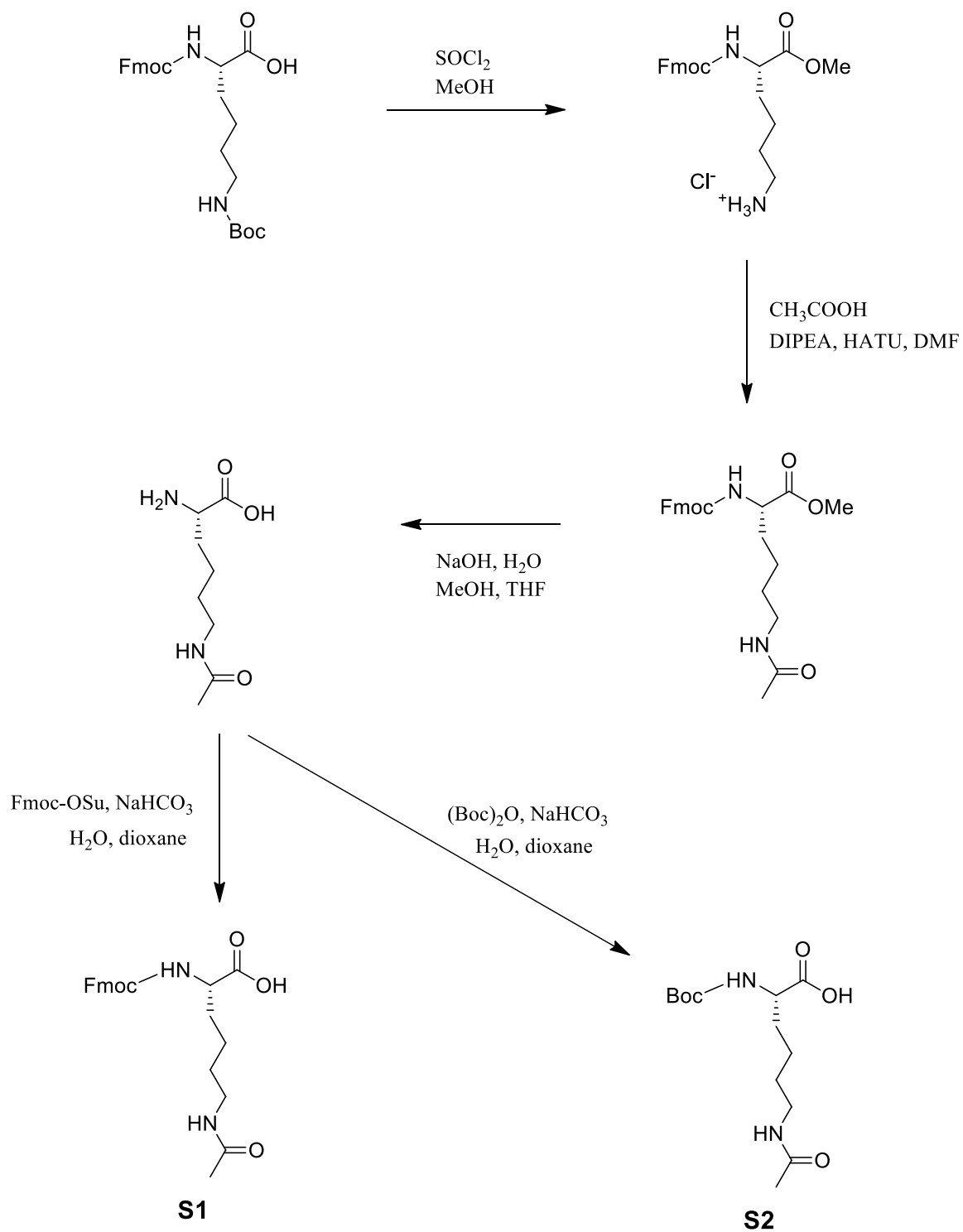
Low resolution mass spectral data were analyzed using a Finnigan MAT LCQ spectrometer with MS/MS and ESI probe, utilizing XCalibur software. High resolution mass spectral data were analyzed using an Ultimate 3000 RSL HPLC (Thermo Fisher Scientific Inc., MA) and an LTQ Orbitrap XL ETD using a flow injection method, with a flow rate of 5 $\mu\text{L}/\text{min}$. The HPLC flow is interfaced with the mass spectrometer using the Electrospray source (Thermo Fisher Scientific Inc., MA). Mass spectra were obtained over a range of $100 < m/z < 1000$. Data was analyzed using XCalibur software (Version 2.0.7, Thermo Fisher Scientific).

5.6.5 FTIR spectroscopy

Infrared spectra were collected on a Perkin Elmer Spectrum 100 FT-IR spectrometer, with attenuated total reflectance (ATR) imaging capabilities, fitted with a ZnSe crystal, with an average reading taken from 4 scans at 4 cm^{-1} resolution.

5.6.6 Peptide synthesis

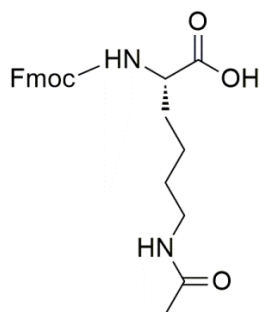
Scheme S1. The synthetic steps for building blocks S1 and S2.



Chapter 5

Fmoc-Lys(Boc)-OH (4.2 g, 8.9 mmol) was dissolved in dry methanol (40 mL, over molecular sieves) and cooled to 0 °C. Thionyl chloride (2.5 mL) was added dropwise to the solution over 5 min. The mixture was stirred at 0 °C for 30 min, then warmed to room temperature and stirred overnight. The volatiles were removed *in vacuo* to yield the intermediate Fmoc-Lys-OMe, an off-white solid (3.8 g, quant). The resulting residue and CH₃COOH (2 mL) were dissolved in anhydrous DMF (15 mL) and stirred at rt under an N₂ atmosphere. HATU (6.5 g, 17.1 mmol) and DIPEA (6 mL) were added, and the mixture stirred for 48 h. The solvent was removed and the residue taken up in EtOAc (200 mL) and H₂O (200 mL). The organic layer was separated and washed with NaHCO₃ (200 mL), brine (200 mL) and dried over Na₂SO₄. The volatiles were removed *in vacuo* to reveal a white solid (3.9 g, quant). The resulting residue was dissolved in a mixture of THF (23 mL) and methanol (16 mL). An aqueous solution of 1.6 M NaOH (9 mL) was added to the mixture, and the reaction stirred at rt for 18 h. The solvent was removed *in vacuo* and the residue redissolved in H₂O (200 mL) and Et₂O (200 mL). The aqueous layer was separated and dried over MgSO₄. The solvent was removed *in vacuo* to yield the amphoteric intermediate, an off-white solid (1.8 g, quant).

Compound S1



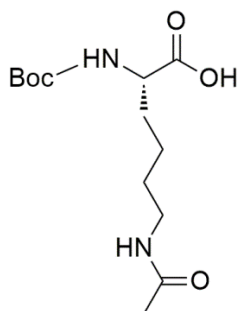
The amphoteric residue (1.8 g, 8.0 mmol) was dissolved in para-dioxane (20 mL). An aqueous solution of NaHCO₃ (2.2 g in 20 mL H₂O) was added, followed by Fmoc-OSu (2.9 g, 8.0 mmol). The reaction mixture was stirred overnight at rt and the volatiles were removed under reduced pressure. The residue was dissolved in 2.5% NaHCO₃ and washed with Et₂O (3x20 mL). The aqueous layer was then acidified to pH 4 by dropwise addition of 6 M aqueous HCl, and extracted with EtOAc (3x50 mL). The combined organic layers were washed with brine (20 mL), dried over Na₂SO₄ and the solvent removed under reduced pressure to give the product as a white solid (2.5 g, 76%).

Chapter 5

^1H NMR (300 MHz, DMSO- d_6): δ 7.88 (d, 2H, aromH), 7.81 (t, 1H, NHCH₂), 7.41 (t, 2H, aromH), 7.72 (d, 2H, aromH), 7.62 (d, 1H, NHCH), 7.46-7.28 (m, 4H, aromH), 4.32-4.16 (m, 3H, CH & CH₂ in Fmoc), 3.90 (m, 1H, NHCH), 3.06-2.96 (m, 2H, NHCH₂), 1.78 (s, 3H, CH₃), 1.64 (m, 2H, CH₂), 1.36 (m, 4H, 2xCH₂).

LRMS: $[\text{M}+\text{H}]^+$ _{calcd}=411.2, $[\text{M}+\text{H}]^+$ _{found}=411.2.

Compound S2



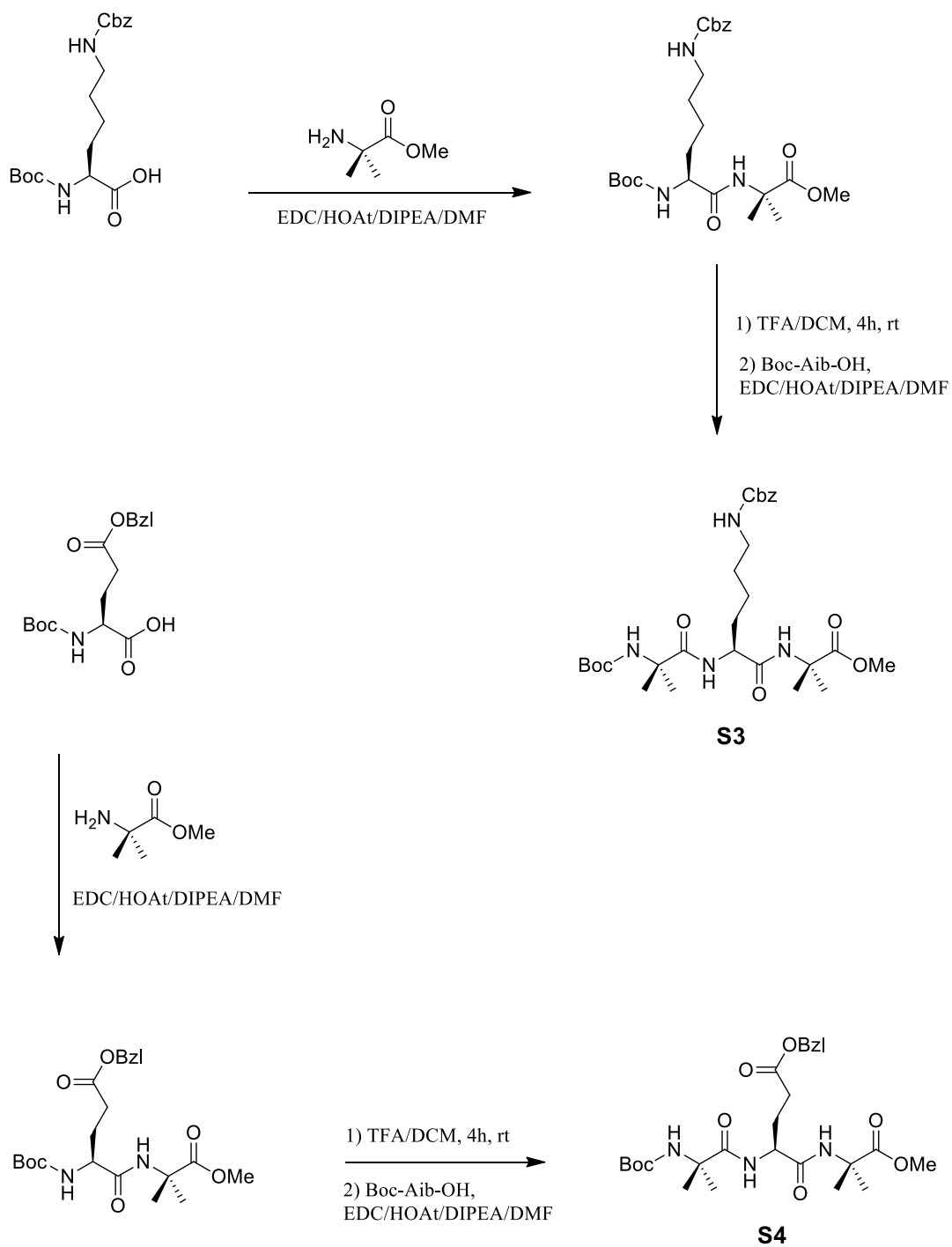
The amphoteric intermediate (3.9 g, 17 mmol) and NaHCO₃ (2.8 g, 34 mmol) were dissolved in water (60 mL). A solution of (Boc)₂O (5.6 g in 60 mL para-dioxane) was added. The reaction mixture was stirred overnight at rt and the volatiles were removed under reduced pressure. The residue was redissolved in H₂O (200 mL) and EtOAc (200 mL). The aqueous layer was acidified to pH 3 by dropwise addition of 6 M aqueous HCl and extracted with EtOAc (3x100 mL). The combined organic layers were washed with brine (50 mL), dried over Na₂SO₄ and the solvent removed under reduced pressure to give the product as a white solid (4.4 g, 89%).

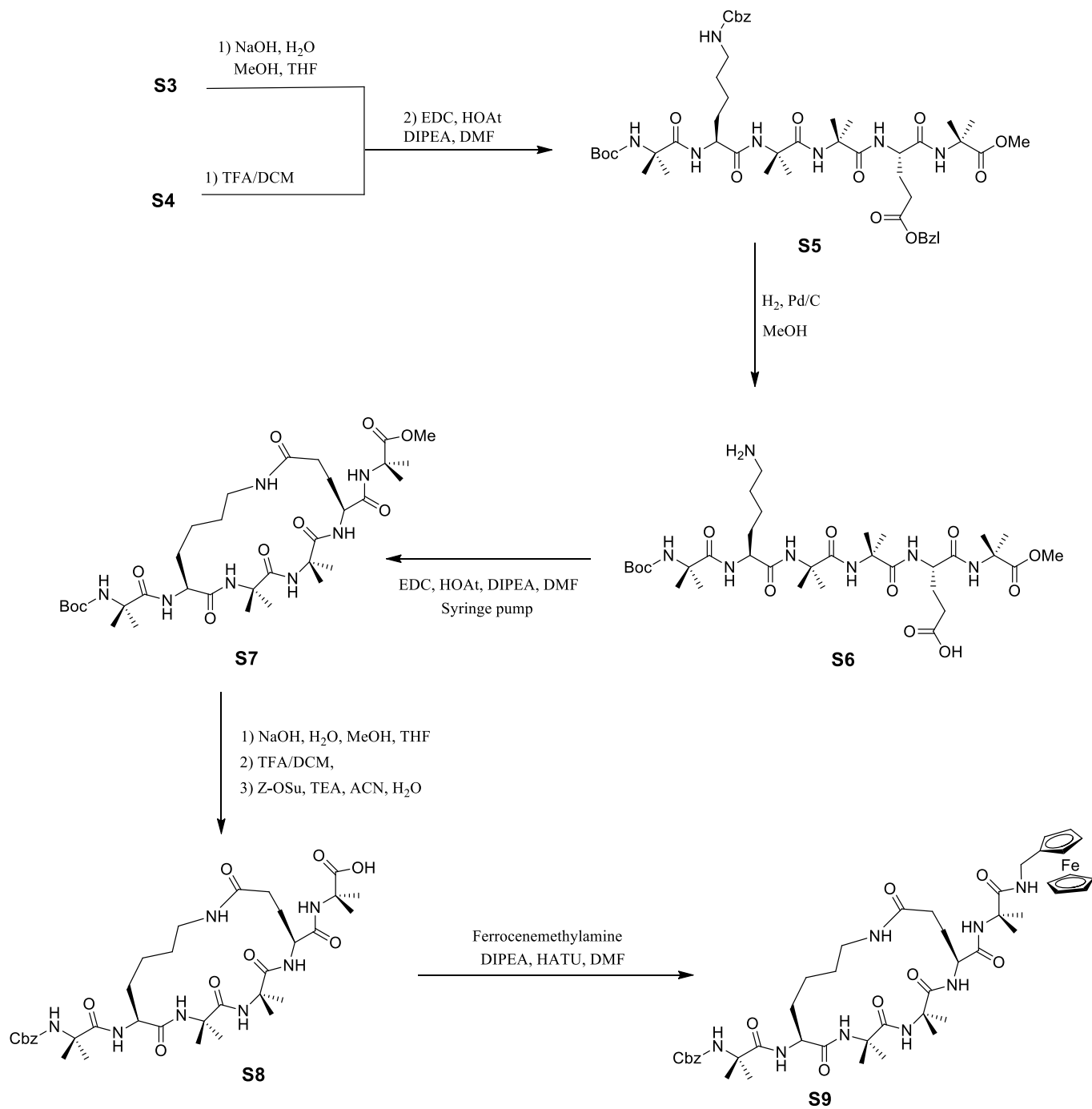
^1H NMR (300 MHz, DMSO- d_6): δ 7.78(t, 1H, NHCH₂), 7.05 (d, 1H, NHCH), 3.80 (m, 1H, NHCH), 3.06-2.92 (m, 2H, NHCH₂), 1.76 (s, 3H, CH₃), 1.58 (m, 2H, CH₂), 1.40-1.20 (m, 13H, Boc, 2xCH₂).

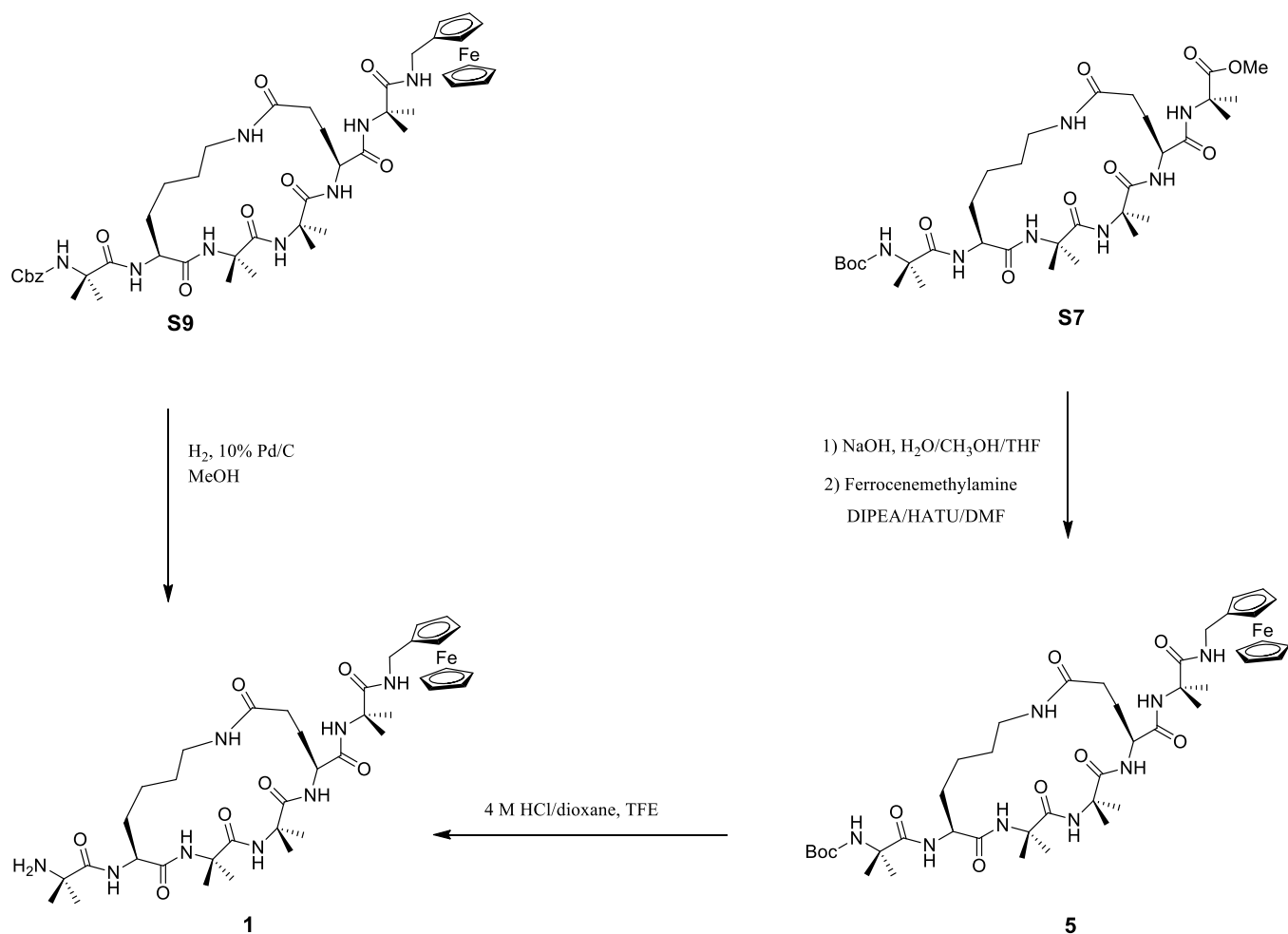
LRMS: $[\text{M}+\text{H}]^+$ _{calcd}=289.2, $[\text{M}+\text{H}]^+$ _{found}=289.2.

Chapter 5

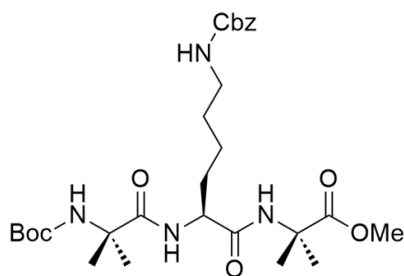
Scheme S2. The final synthetic steps for lactam-bridged 3₁₀-helical peptides.



Scheme S2. The final synthetic steps for lactam-bridged 3₁₀-helical peptides (continued).

Scheme S2. The final synthetic steps for lactam-bridged 3₁₀-helical peptides (continued).

Compound S3

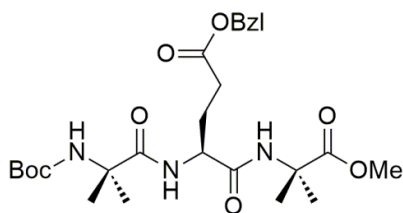


Boc-Lys(Cbz)-OH (1.6 g, 4.4 mmol) and HCl·H₂N-Aib-OMe (880 mg, 4.4 mmol) were dissolved in anhydrous DMF (28 mL) and stirred at rt under an N₂ atmosphere. HOAt (780 mg, 5.7 mmol), EDC·HCl (1.1 g, 5.7 mmol) and DIPEA (3.5 mL, 20 mmol) were added, and the mixture stirred for 26 h. The solvent was removed *in vacuo* and the residue taken up in EtOAc (200 mL) and H₂O (200 mL). The organic layer was separated and washed with NaHCO₃ (200 mL), brine (200 mL) and dried over Na₂SO₄. The solvent was removed *in vacuo* and the crude product was purified by column chromatography (EtOAc: petroleum ether 50:50 by v/v) to reveal a white solid, Boc-Lys(Cbz)-Aib-OMe, (1.70 g, 81%).

The resulting compound was dissolved in DCM (10 mL) and TFA (10 mL), added dropwise. The reaction was stirred at rt for 3 h, and the solvent removed *in vacuo* to reveal a brown oil. The oil and Boc-Aib-OH (880 mg, 4.4 mmol) were dissolved in anhydrous DMF (25 mL) and stirred at rt under an N₂ atmosphere. HOAt (884 mg, 6.5 mmol), EDC·HCl (1.2 g, 6.5 mmol) and DIPEA (3.5 mL, 20 mmol) were added, and the mixture stirred for 40 h. The solvent was removed *in vacuo* and the residue taken up in EtOAc (200 mL) and H₂O (200 mL). The organic layer was separated and washed with NaHCO₃ (200 mL), brine (200 mL) and dried over Na₂SO₄. The solvent was removed *in vacuo* and the crude product was purified by column chromatography (EtOAc: petroleum ether 70:30 by v/v) to yield the product, a white solid (1.98 g, 80%).

¹H NMR (300 MHz, DMSO-d₆): δ 8.04 (s, 1H, NH), 7.35-7.25 (m, 6H, NH, benzene), 7.16 (t, 1H, NHCH₂), 7.08 (br s, 1H, NH), 4.96 (s, 2H, OCH₂), 4.09 (m, 1H, CαH), 3.51 (s, 3H, OCH₃), 2.92 (m, 2H, NHCH₂), 1.76 (s, 3H, COCH₃), 1.65-1.45 (m, 2H, CH₂), 1.40-1.10 (m, 25H, 2xCH₂, Boc, 4xCH₃).

LRMS: [M+H]⁺_{calcd}=565.3, [M+H]⁺_{found}=565.3.

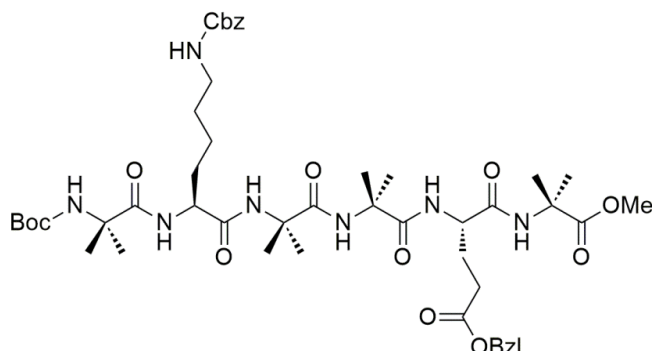
Compound **S4**

Boc-Glu(OBzl)-OH (1.7 g, 5.0 mmol) and HCl·H₂N-Aib-OMe (1.0 g, 5.0 mmol) were dissolved in anhydrous DMF (28 mL) and stirred at rt under an N₂ atmosphere. HOAt (884 mg, 6.5 mmol), EDC·HCl (1.2 g, 6.5 mmol) and DIPEA (3.5 mL, 20 mmol) were added, and the mixture stirred for 26 h. The solvent was removed *in vacuo* and the residue taken up in EtOAc (200 mL) and H₂O (200 mL). The organic layer was separated and washed with NaHCO₃ (200 mL), brine (200 mL) and dried over Na₂SO₄. The solvent was removed *in vacuo* and the crude product was purified by column chromatography (EtOAc: petroleum ether 50:50 by v/v) to reveal a white solid, Boc-Glu(OBzl)-Aib-OMe, (1.98 g, 92%).

Boc-Glu(OBzl)-Aib-OMe (453 mg, 1.0 mmol) was dissolved in DCM (5 mL) and TFA (5 mL) added dropwise. The reaction was stirred at rt for 3 h. The solvent was removed *in vacuo* to reveal a brown oil. The resulting oil and Boc-Aib-OH (210 mg, 1.0 mmol) were dissolved in anhydrous DMF (2 mL) and stirred at rt under an N₂ atmosphere. HOBt (207 mg, 1.3 mmol), EDC·HCl (260 mg, 1.3 mmol) and DIPEA (0.75 mL, 4.2 mmol) were added, and the mixture stirred for 40 h. The solvent was removed *in vacuo* and the residue taken up in EtOAc (50 mL) and H₂O (50 mL). The organic layer was separated and washed with NaHCO₃ (50 mL), brine (50 mL) and dried over Na₂SO₄. The solvent was removed *in vacuo* and the crude product was purified by column chromatography (EtOAc: petroleum ether 70:30 by v/v) to yield the product, a white solid (430 mg, 80%).

¹H NMR (300 MHz, DMSO-d₆): δ 8.15 (s, 1H, NH), 7.50 (d, 1H, NH, *J*=6.0 Hz), 7.42-7.25 (m, 5H, benzene), 7.16 (s, 1H, NH), 5.08 (s, 2H, OCH₂), 4.17 (m, 1H, CaH), 3.52 (s, 3H, OCH₃), 2.35 (t, 2H, CH₂), 1.98 (m, 1H, CHH), 1.83 (m, 1H, CHH), 1.45-1.20 (m, 12H, 4xCH₃).

LRMS: [M+H]⁺_{calcd}=522.3, [M+H]⁺_{found}=522.3.

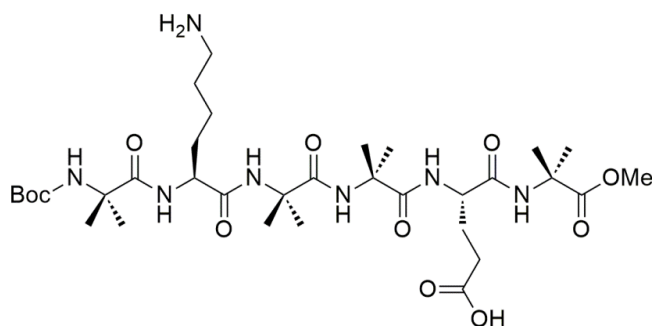
Compound **S5**

Compound **S3** (2.2 g, 4.0 mmol) was dissolved in THF (12 mL) and methanol (8 mL). An aqueous solution of 1.6 M NaOH (4 mL) was added and the reaction stirred at rt for 18 h. The solvent was removed *in vacuo* and the residue redissolved in EtOAc (200 mL) and H₂O (200 mL). The pH was adjusted to pH 3 and the organic layer separated and washed with brine (200 mL), and dried over MgSO₄. The solvent was removed *in vacuo* to reveal a white solid (2.3 g).

Compound **S4** (2.1 g, 4.0 mmol) was dissolved in DCM (5 mL) and TFA (5 mL) added dropwise. The reaction was stirred at rt for 3 h. The solvent was removed *in vacuo* to reveal a brown oil. The resulting oil and the (hydrolysed) compound **S3** (2.3 g) were dissolved in anhydrous DMF (28 mL) and stirred at rt under an N₂ atmosphere. HOAt (707 mg, 5.2 mmol), EDC·HCl (1.0 g, 5.2 mmol) and DIPEA (2.8 mL, 16 mmol) were added, and the mixture stirred for 40 h. The solvent was removed and the residue taken up in EtOAc (200 mL) and H₂O (200 mL). The organic layer was separated and washed with NaHCO₃ (200 mL), brine (200 mL) and dried over Na₂SO₄. The solvent was removed *in vacuo* and the crude product was purified by column chromatography (EtOAc: petroleum ether 90:10 by v/v) to yield a white solid (2.1 g, 55%).

¹H NMR (300 MHz, DMSO-d₆): δ 8.32-8.06 (m, 2H, 2xNH), 7.93-7.14 (m, 15H, 5xNH, 2x benzene), 5.06 (s, 2H, OCH₂), 4.98 (s, 2H, OCH₂), 4.05 (m, 1H, CαH), 3.94-3.67 (m, 1H, CαH), 3.53 (s, 3H, OCH₃), 2.95 (m, 2H, CH₂NH), 2.44 (m, 2H, CH₂), 2.14-1.22 (m, 41H, 4xCH₂, 8xCH₃, Boc).

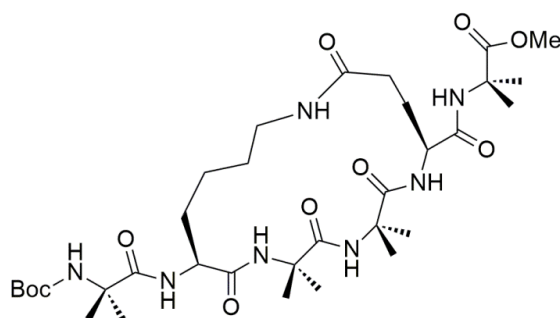
LRMS: [M+H]⁺_{calcd}=954.5, [M+H]⁺_{found}=954.5.

Compound **S6**

Compound **S5** (1.7 g, 1.8 mmol) was dissolved in dry methanol (20 mL, over molecular sieves). Pd/C (15% w/w, 260 mg) was added and the mixture stirred. A hydrogen balloon was fitted under vacuum and the solution stirred at rt for a further 18 h. The solution was filtered through celite and washed with methanol (3x 20 mL), and the solvent removed *in vacuo* to yield a white solid (1.3 g, 95%).

^1H NMR (300 MHz, DMSO- d_6): δ 8.60 (br s, 1H, NH), 8.29 (br s, 1H, NH), 8.19 (br s, 1H, NH), 7.65 (br s, 1H, NH), 7.56 (br s, 1H, NH), 7.47 (br s, 1H, NH), 3.90 (m, 1H, CaH), 3.74 (m, 1H, CaH), 3.55 (s, 3H, OCH₃), 2.75-1.52 (m, 12H, 6xCH₂), 1.41-1.30 (m, 24H, 8xCH₃), 1.34 (s, 9H, Boc).

LRMS: $[\text{M}+\text{H}]^+$ _{calcd}=730.4, $[\text{M}+\text{H}]^+$ _{found}=730.4.

Compound **S7**

Chapter 5

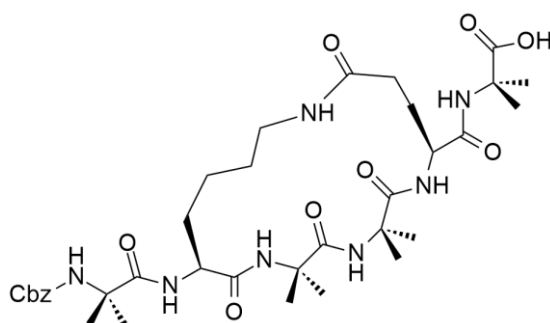
EDC·HCl (815 mg, 4.3 mmol), HOBt (576 mg, 4.3 mmol) and DIPEA (1.5 mL) were dissolved in anhydrous DMF (255 mL) and the solution stirred at rt under an N₂ atmosphere. Compound **S6** (622 mg, 0.85 mmol) was dissolved in anhydrous DMF (25 mL) and, using a syringe pump, added to the solution containing the coupling agents at the rate of 20 μL/min, and stirred for 68 h. The solvent was removed *in vacuo* and the residue taken up in EtOAc (100 mL) and H₂O (100 mL). The pH was adjusted to pH 3, the organic layer separated and washed with NaHCO₃ (100 mL), brine (100 mL) and dried over Na₂SO₄. The solvent was removed *in vacuo* to give the crude product, which was purified using reverse phase HPLC, to yield a white solid (90 mg, 15%).

¹H NMR (600 MHz, DMSO-d₆): δ 8.33 (br s, 1H, NH), 8.04 (br s, 1H, NH), 7.79-7.70 (m, 2H, 2x NH), 7.63 (m, 1H, NH), 7.53 (s, 1H, NH), 7.45 (d, 1H, NH, *J*=8.0 Hz), 3.80-3.73 (m, 2H, 2x CaH), 3.54 (s, 3H, OCH₃), 3.07 (m, 1H, CHHNH), 2.90 (m, 1H, CHHNH), 2.15-1.22 (m, 10 H, 5x CH₂), 1.41-1.27 (m, 24H, (CH₃)₈), 1.34 (s, 9H, Boc).

¹³C NMR (150 MHz, DMSO-d₆): δ 175.6, 174.8, 174.7, 174.6, 172.9, 171.6, 171.5, 158.7, 158.5, 79.3, 79.2, 56.7, 56.6, 56.2, 55.3, 55.2, 52.1, 40.3, 28.6, 26.0, 25.2, 25.1.

LRMS: [M+H]⁺_{calcd}=712.4, [M+H]⁺_{found}=712.4.

Compound **S8**



Compound **S7** (380 mg, 0.5 mmol) was dissolved in THF (3.8 mL) and H₂O (3.8 mL). NaOH (85 mg) was added and the reaction stirred at rt for 2 h. The reaction was quenched by 1M HCl (2 mL). The solvent was removed *in vacuo* to reveal a white solid (514 mg). The resulting intermediate (190 mg, 0.3 mmol) was dissolved in DCM (5 mL) and TFA (2 mL)

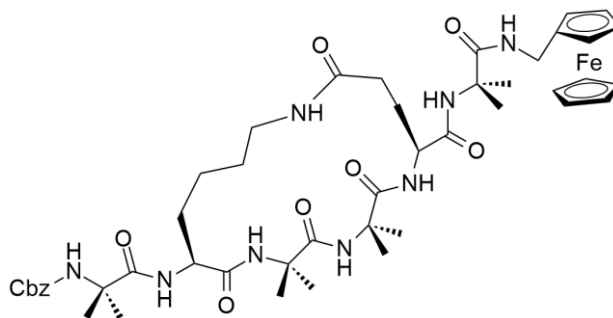
added dropwise. The reaction was stirred at rt overnight. The solvent was removed *in vacuo* to reveal a brown oil (350 mg).

The resulting oil (350 mg) and triethylamine (150 μ L) were dissolved in a mixture of water (5 mL) and acetonitrile (3 mL). A solution of Z-OSu (82 mg) in acetonitrile (2 mL) was added. The reaction mixture was stirred overnight at rt, after which the volatiles were removed under reduced pressure. The residue was redissolved in MeOH (5 mL), and purified using reverse phase HPLC to yield a white solid (120 mg).

^1H NMR (600 MHz, DMSO- d_6): δ 8.01 (d, 1H, NH), 7.79 (s, 1H, NH), 7.77 (m, 1H, NH), 7.71 (t, 1H, NH), 7.61 (d, 1H, NH), 7.58 (s, 1H, NH), 7.40 (s, 1H, NH). 7.38-7.26 (m, 5H, aromH), 5.05 (dd, 2H, Cbz CH_2), 4.12 (m, 1H, CaH), 3.72 (m, 1H, CaH), 3.06 (m, 2H, CH_2NH), 2.04 (m, 1H, CHHCO), 1.92 (m, 1H, CHHCO), 1.85 (m, 1H, CHHCO), 1.54 (m, 1H, CHHCO), 1.48-1.09 (m, 26H, CH_2 , 8x CH_3), 1.22 (m, 2H, CH_2).

LRMS: $[\text{M}+\text{H}]^+$ _{calcd}=732.4, $[\text{M}+\text{H}]^+$ _{found}=732.4.

Compound S9



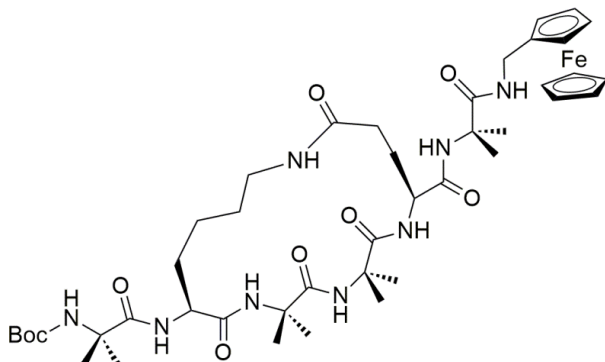
Compound **S8** (120 mg, 0.16 mmol) and ferrocenylmethylamine (60 mg, 0.27 mmol) were dissolved in anhydrous DMF (2 mL) and stirred at rt under an N_2 atmosphere. EDC·HCl (67 mg), HOAt (50 mg) and DIPEA (200 μ L) were added, and the mixture stirred for 36 h. The solvent was removed and the residue redissolved in MeOH (15 mL) and purified using reverse phase HPLC to yield a sandy brown solid (90 mg).

^1H NMR (600 MHz, DMSO- d_6): δ 8.05 (d, 1H, NH), 7.84 (d, 1H, NH), 7.82 (s, 1H, NH), 7.78 (s, 1H, NH), 7.74 (s, 1H, NH), 7.72 (t, 1H, NH), 7.44 (s, 1H, NH), 7.39-7.28 (m, 5H, aromH), 7.26 (t, 1H, NH), 5.06 (dd, 2H, CH_2), 4.25-3.90 (m, 12H, Cp, CH_2Fc , CaH), 3.70

(m, 1H, C α H), 3.18 (m, 2H, CH₂CH₂NH), 1.99 (m, 2H, CHHCO), 1.85 (m, 1H, CHHCO), 1.54 (m, 1H, CHHCO), 1.48-1.19 (m, 28H, 2x CH₂, 8x CH₃).

LRMS: [M+H]⁺_{calcd}=929.9, [M+H]⁺_{found}=929.9.

Peptide 5



Compound **S7** (125 mg, 0.17 mmol) was dissolved in THF (1.25 mL) and H₂O (1.5 mL). An aqueous solution of 1.6 M NaOH (352 μ L) was added and the reaction stirred at rt for 2 h. The solvent was removed *in vacuo* to reveal a white solid (157 mg, quant). The resulting intermediate (122 mg, 0.17 mmol) and ferrocenylmethylamine (75 mg, 0.35 mmol) were dissolved in anhydrous DMF (3.4 mL) and stirred at rt under an N₂ atmosphere. EDC·HCl (37 mg, 0.19 mmol), HOAt (24 mg, 0.17 mmol) and DIPEA (122 μ L) were added, and the mixture stirred for 36 h. The solvent was removed *in vacuo* and the residue redissolved in MeOH (15 mL), and purified using reverse phase HPLC to yield a sandy brown solid (40 mg, 29%).

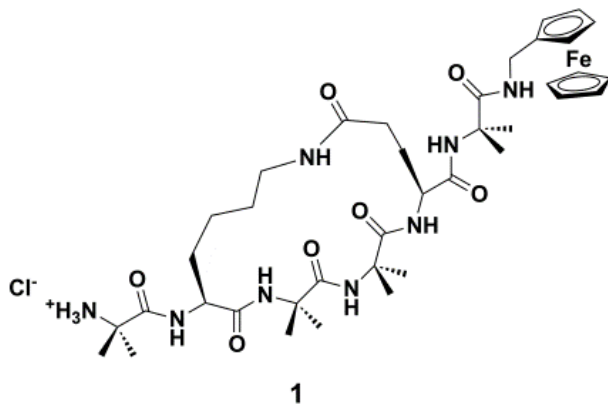
¹H NMR (600 MHz, DMSO-d₆): δ 8.16 (br s, 1H, NH), 7.96 (s, 1H, NH), 7.86 (d, 1H, NH, *J*=3.9 Hz), 7.82 (s, 1H, NH), 7.70 (t, 1H, NH, *J*=12.0 Hz), 7.46 (s, 1H, NH), 7.35 (s, 1H, NH), 7.27 (br s, 1H, NH), 4.25-4.02 (m, 9H, Cp), 3.99-3.90 (m, 3H, CH₂Fc, C α H), 3.71 (m, 1H, C α H), 3.18 (m, 1H, CHHNH), 2.96 (m, 1H, CHHNH), 2.15-1.37 (m, 10H, 5xCH₂), 1.44-1.29 (m, 24H, 8X CH₃), 1.34 (s, 9H, Boc).

¹³C NMR (150 MHz, DMSO-d₆): 175.83, 175.37, 174.89, 173.61, 171.07, 170.75, 155.31, 86.55, 78.79, 68.66, 68.34, 66.99, 66.97, 66.92, 56.35, 56.29, 56.02, 55.70, 53.63, 38.12,

37.82, 33.63, 31.26, 31.02, 29.40, 28.97, 28.86, 28.66, 28.50, 28.19, 25.48, 24.55, 24.26, 22.96, 22.06.

HRMS: $[M]^+$ $_{\text{calcd}}=894.4302$, $[M]^+$ $_{\text{found}}=894.4303$.

Peptide 1

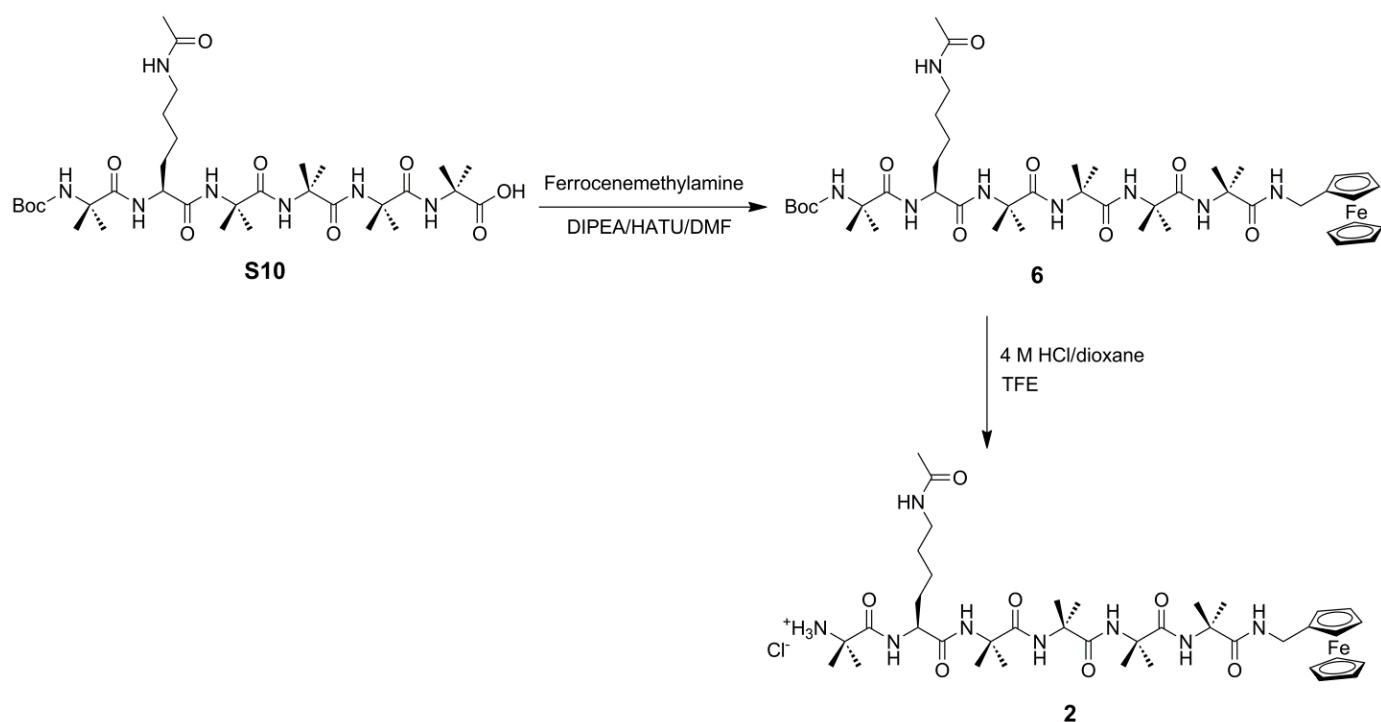


Peptide **5** (5 mg, 0.006 mmol) was dissolved in TFE (600 μ L) and 4M HCl in dioxane (200 μ L) added. The reaction was stirred at rt for 25 min. The solvent was removed *in vacuo* to reveal a light brown solid (5 mg, quant). The crude product was purified using reverse phase HPLC to yield a sandy brown solid (2 mg, 45%).

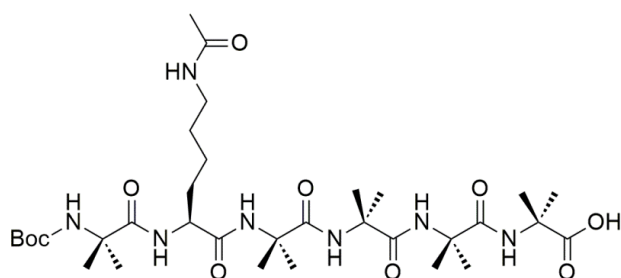
¹H NMR (600 MHz, DMSO-*d*₆): δ 8.30 (s, 1H, NH), 8.08 (s, 1H, NH), 7.75 (d, 1H, NH), 7.72 (m, 1H, NH), 7.54 (s, 1H, NH), 7.49 (m, 1H, NH), 7.33 (s, 1H, NH), 7.18 (t, 1H, NH), 4.25-3.90 (m, 12H, Cp, CH₂Fc, C α H), 3.85 (m, 1H, C α H), 3.04-2.90 (m, 2H, CH₂NH), 2.30-1.80 (m, 4H, 4x CHH), 1.80-1.10 (m, 28H, 8xCH₃, 2xCH₂).

¹³C NMR (150 MHz, DMSO-*d*₆): 173.66, 172.51, 172.26, 171.96, 169.20, 166.27, 149.91, 144.91, 105.60, 100.89, 85.08, 84.44, 78.30, 77.34, 68.80, 67.45, 68.34, 66.99, 66.97, 66.92, 56.38, 56.02, 55.70, 53.68, 44.99, 43.47, 38.72, 31.50, 29.46, 28.95, 28.53, 24.89.

HRMS (*m/z*): $[M]^+$ $_{\text{calcd}}=794.3778$, $_{\text{found}}=794.3778$.

Scheme S3. The final synthetic steps for linear 3₁₀-helical peptides.

Compound S10



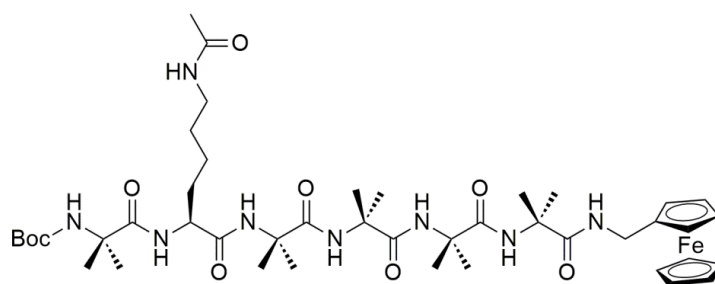
Fmoc-Aib-OH loaded 2-chlorotrityl chloride resin^{8c} (2.0 g, typically 0.5 mmol/g of resin) was transferred into a sintered funnel fitted with a Teflon stopcock, and then rinsed with DCM (2x20 mL). After air drying, the Fmoc group was removed by reaction with a solution of 25% piperidine in DMF (20 mL) for 30 min, followed by washing successively with DCM (3x20 mL), DMF (3 x 20 mL) and finally DCM (3 x 20 mL). To a solution of Fmoc-Aib-OH (1.00

g, 2 equiv) in DMF (4 mL) was added a 0.5 M solution of HATU in DMF (2 mL) followed by DIPEA (1.2 mL, 4-fold excess) and the resulting solution was added to the deprotected resin. The mixture was left for 2 h, with occasional stirring. The resin was isolated by filtration and rinsed successively with DCM (3 x 50 mL), DMF (3 x 50 mL), and finally DCM (3 x 50 mL). The sequence was repeated twice to ensure complete coupling. Using this protocol, the tetrapeptide (Aib₄) was produced by sequential additions of Fmoc-Aib-OH. The peptide was then coupled with the building block **S1** to yield the appropriate pentapeptide. In the last cycle, Boc-Aib-OH was capped to the pentapeptide. The resulting hexapeptide was cleaved from the resin with 2% TFA / DCM (v/v). The crude products were purified by reverse phase HPLC.

¹H NMR (300 MHz, DMSO-d₆): δ 8.22 (s, 1H, NH), 8.08 (s, 1H, NH), 7.78 (t, 1H, NHCH₂), 7.56 (s, 1H, NH), 7.32-7.20 (m, 3H, 3xNH), 3.85 (m, 1H, NHCH), 2.95 (m, 2H, NHCH₂), 1.75 (s, 3H, COCH₃), 1.68 (m, 2H, CH₂), 1.50-1.20 (m, 43H, 2xCH₂, Boc, 10xCH₃).

LRMS: [M+H]⁺_{calcd}=714.4, [M+H]⁺_{found}=714.4.

Peptide 6



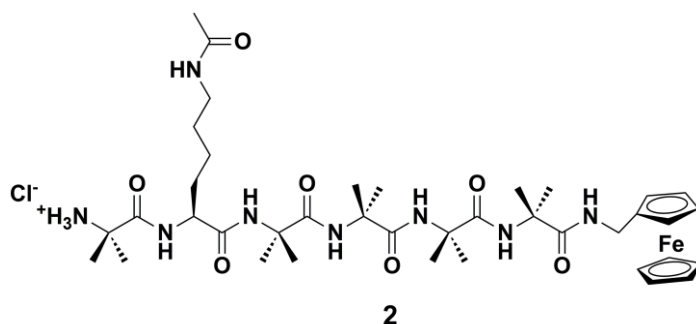
Peptide **S10** (410 mg, 0.6 mmol) and ferrocenylmethylamine (140 mg, 0.6 mmol) were dissolved in anhydrous DMF (8 mL). DIPEA (400 μL, 4 equiv), HOAt (160 mg, 2 equiv) and HATU (430 mg, 2equiv) were added. The reaction mixture was stirred overnight under an N₂ atmosphere at rt. The solvent was removed *in vacuo* and the peptide purified using reverse phase HPLC.

^1H NMR (300 MHz, DMSO- d_6): δ 8.21 (s, 1H, NH), 7.99 (s, 1H, NH), 7.73 (t, 1H, NHCH₂), 7.61 (s, 1H, NH), 7.57 (s, 1H, NH), 7.47 (br s, 1H, NH), 7.28 (s, 1H, NH), 7.20 (s, 1H, NH), 4.31-3.40 (m, 12H, Cp, CaH, CH₂Fc), 2.95 (m, 2H, NHCH₂), 1.76 (s, 3H, COCH₃), 1.68 (m, 2H, CH₂), 1.45-1.20 (m, 43H, 2xCH₂, Boc, 10xCH₃).

^{13}C NMR (150 MHz, DMSO- d_6): 175.59, 175.09, 175.08, 174.98, 174.82, 174.41, 173.73, 173.41, 172.80, 168.93, 158.29, 154.93, 78.59, 68.33, 66.94, 56.14, 56.03, 56.02, 55.63, 54.25, 42.69, 42.66, 42.62, 40.04, 38.24, 37.73, 35.12, 29.66, 28.91, 28.14, 25.39, 24.91, 24.70, 22.64, 22.57. .

MS: $[\text{M}+\text{H}]^+$ _{calcd}=911.5, $[\text{M}+\text{H}]^+$ _{found}=911.5.

Peptide 2



Peptide **6** (100 mg, 0.11 mmol) was dissolved in TFE (1.5 mL) and 4M HCl in dioxane (500 μL) added. The reaction was stirred at rt for 25 min. The solvent was removed *in vacuo* and the crude product was purified using reverse phase HPLC to yield a sandy brown solid (24 mg, 27%).

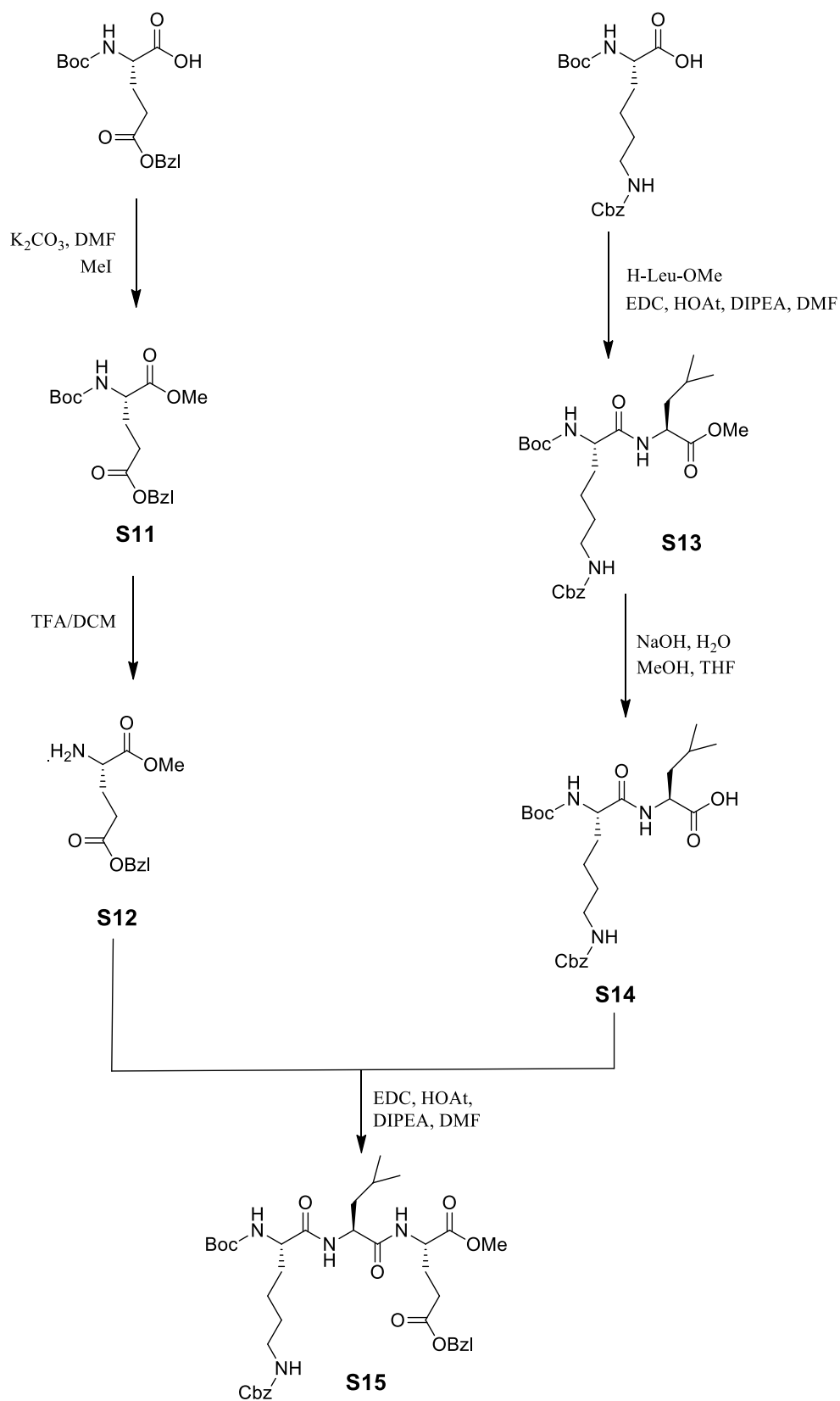
^1H NMR (600 MHz, DMSO- d_6): δ 8.51 (s, 1H, NH), 8.13 (s, 1H, NH), 8.10 (s, 3H, NH₃), 7.84 (t, 1H, NHCH₂), 7.68 (s, 1H, NH), 7.63 (s, 1H, NH), 7.43 (m, 1H, NH), 7.34 (br s, 1H, NH), 4.55-3.50 (m, 12H, Cp, CaH, CH₂), 3.02 (m, 2H, NHCH₂), 1.76 (s, 3H, COCH₃), 1.68 (m, 2H, CH₂), 1.45-1.20 (m, 34H, 2xCH₂, 10xCH₃).

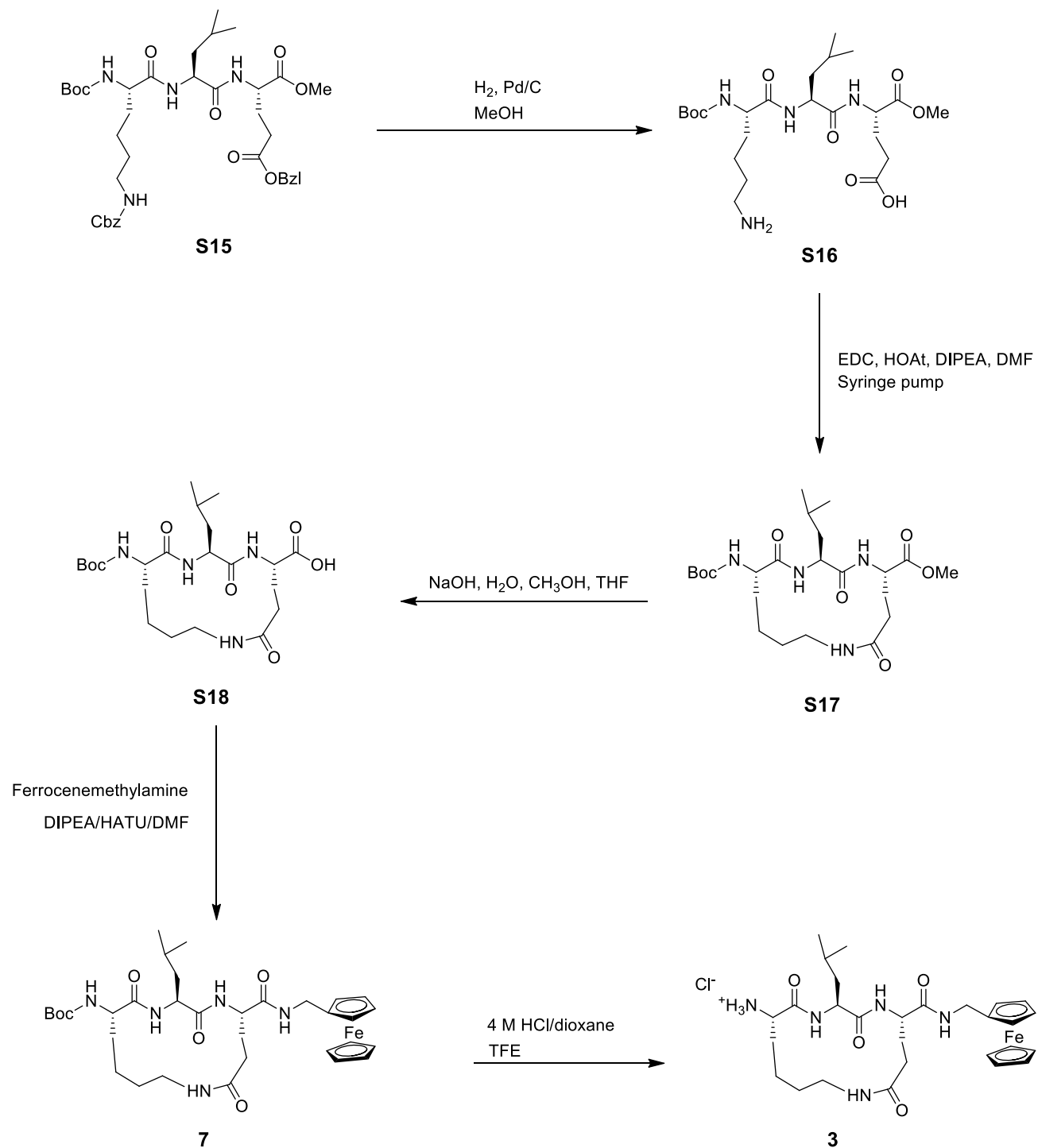
^{13}C NMR (150 MHz, DMSO- d_6): δ 174.81, 174.35, 173.74, 173.47, 172.21, 171.81, 169.00, 128.89, 127.25, 121.35, 119.99, 109.72, 68.41, 66.90, 56.31, 56.10, 56.01, 55.93, 55.79,

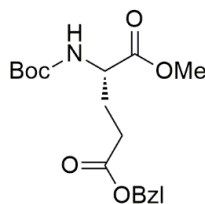
Chapter 5

53.26, 40.03, 38.30, 37.69, 30.45, 29.14, 28.87, 26.00, 25.38, 25.10, 24.97, 24.50, 24.20, 23.50, 23.37, 23.24, 22.60.

HRMS: $[M]^+$ $_{\text{calcd}}=811.4164$, $_{\text{found}}=811.4162$.

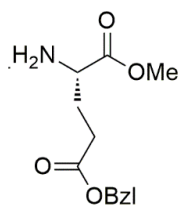
Scheme S4. The final synthetic steps for lactam-bridged β -strand peptides.

Scheme S4. The final synthetic steps for lactam-bridged β -strand peptides (continued).

Compound **S11**

K_2CO_3 (982 mg, 7.1 mmol) was suspended in anhydrous DMF (20 mL). Boc-Glu(OBzl)-OH (2.0 g, 5.9 mmol) was added, followed by MeI (1.0 g, 7.1 mmol, 443 μL). The reaction was stirred at rt under an N_2 atmosphere for 18 h. The solvent was removed *in vacuo* and the residue taken up in EtOAc (200 mL) and H_2O (200 mL). The pH was adjusted to pH 3-4 and the organic layer separated and washed with brine (200 mL) and dried over NaSO_4 . The solvent was removed *in vacuo* to reveal a golden oil (1.8 g, 86%).

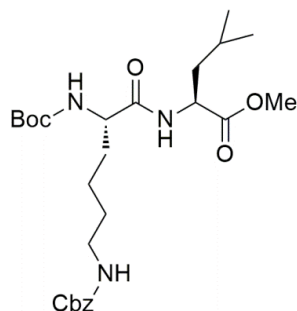
^1H NMR (300 MHz, DMSO-d_6): δ 7.40-7.30 (m, 6H, benzene, NH), δ 5.09 (s, 2H, OCH_2), δ 4.06-3.98 (m, 1H, $\text{C}\alpha\text{H}$), δ 3.61 (s, 3H, OCH_3), δ 2.45 (dd, 2H, CH_2 , $J=9.8, 5.8$ Hz), δ 2.01-1.74 (m, 2H, CH_2), δ 1.37 (s, 9H, Boc).

Compound **S12**

Compound **S11** (877 mg, 2.5 mmol) was dissolved in DCM (5 mL). TFA (5 mL) was added dropwise and the reaction stirred at rt for 3 h. The solvent was removed *in vacuo* to reveal a golden oil (1.2 g, quant).

^1H NMR (300 MHz, DMSO-d_6): δ 8.44 (br s, 3H, NH), 7.37 (m, 5H, benzene), 5.11 (s, 2H, OCH_2), 4.10 (br s, 1H, $\text{C}\alpha\text{H}$), 3.72 (s, 3H, OCH_3), 2.56 (m, 2H, CH_2), 2.04 (m, 2H, CH_2).

Compound S13

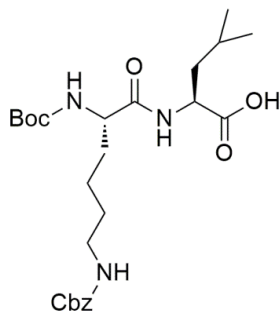


Boc-Lys(Z)-OH (1.0 g, 2.6 mmol) and HCl·H₂N-Leu-OMe (572 mg, 3.2 mmol) were dissolved in anhydrous DCM (20 mL) and stirred at rt under an N₂ atmosphere. Anhydrous DIPEA (1.6 mL), EDC·HCl (552 mg, 2.9 mmol) and HOAt (393 mg, 2.9 mmol) were added and the solution stirred for 36 h. DCM (30 mL) and H₂O (50 mL) were added and the pH adjusted to pH 2-3. The organic layer was separated and washed with brine (50 mL) and dried over MgSO₄. The solvent was removed *in vacuo* to yield a clear oil (1.1 g, 81%).

¹H NMR (300 MHz, DMSO-d₆): δ 8.11 (d, 1H, NH, *J*=7.6 Hz), 7.40-7.30 (m, 5H, benzene), 7.23 (t, 1H, NH, *J*=10.5 Hz), 6.79 (d, 1H, NH, *J*=8.1 Hz), 5.00 (s, 2H, OCH₂), 4.33-4.26 (m, 1H, CαH), 3.90 (m, 1H, CαH), 3.60 (s, 3H, OCH₃), 2.97 (d, 2H, CH₂NH, *J*=5.9 Hz), 1.70-1.22 (m, 9H, 4xCH₂, CH), 1.37 (s, 9H, Boc), 0.90-0.82 (m, 6H, 2xCH₃ Leu).

LRMS: [M+Na]⁺_{calcd}=530.2, [M+Na]⁺_{found}=530.2.

Compound S14



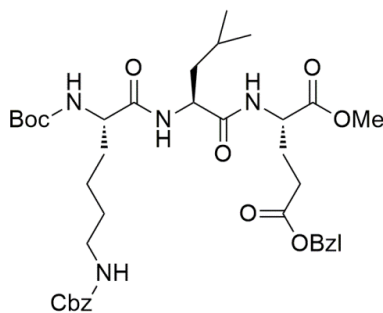
Chapter 5

Compound **S13** (1.1 g, 2.1 mmol) was dissolved in THF (8.4 mL) and methanol (2.1 mL). NaOH (125 mg, 3.1 mmol) was dissolved in H₂O (2.1 mL) and added to the solution and stirred at rt for 24 h. The THF was removed *in vacuo* and EtOAc (50 mL) and H₂O (50 mL) added. The pH was adjusted to pH 2-3, the organic layer separated and washed with brine (50 mL) and dried over MgSO₄. The solvent was removed *in vacuo* to yield a clear solid (904 mg, 87%).

¹H NMR (300 MHz, DMSO-d₆): δ 7.93 (d, 1H, NH, *J*=7.7 Hz), 7.40-7.30 (m, 5H, benzene), 7.23 (t, 1H, NH, *J*=10.2 Hz), 6.79 (d, 1H, NH, *J*=8.4 Hz), 5.00 (s, 2H, OCH₂), 4.22 (dd, 1H, CαH, *J*=14.2, 8.4 Hz), 3.89 (m, 1H, CαH), 2.96 (d, 2H, CH₂NH, *J*=5.6 Hz), 1.70-1.22 (m, 9H, 4xCH₂, CH), 1.37 (s, 9H, Boc), 0.90-0.82 (m, 6H, 2xCH₃ Leu).

LRMS: [M+Na]⁺_{calcd}=516.2, [M+Na]⁺_{found}=516.2.

Compound **S15**

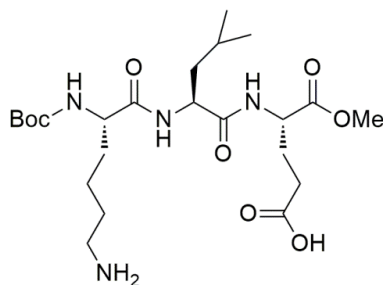


Compound **S12** (627 mg, 2.5 mmol) and compound **S14** (1.12 g, 2.3 mmol) were dissolved in anhydrous DCM (42 mL) and stirred at rt under an N₂ atmosphere. Anhydrous DIPEA (1.6 mL), HATU (949 mg, 2.5 mmol) and HOAt (308 mg, 2.3 mmol) were added and the solution stirred for 42 h. DCM (60 mL) and H₂O (100 mL) were added and the pH adjusted to pH 3. The organic layer was separated and washed with brine (100 mL) and dried over MgSO₄. The solvent was removed *in vacuo* to reveal a white solid, which was purified by column chromatography on silica gel (70/30 EtOAc/PE), yielding (785 mg, 48%).

^1H NMR (300 MHz, DMSO- d_6): δ 8.31 (d, 1H, NH, $J=7.2$ Hz), 7.77 (d, 1H, NH, $J=7.9$ Hz), 7.40-7.30 (m, 10H, 2x benzene), 7.23 (t, 1H, NH, $J=9.0$ Hz), 6.87 (d, 1H, NH, $J=8.0$ Hz), 5.09 (s, 2H, OCH₂), 4.99 (s, 2H, OCH₂), 4.30 (dd, 2H, 2x C α H, $J=13.5, 6.2$ Hz), 3.89-3.82 (m, 1H, C α H), 3.59 (s, 3H, OCH₃), 2.99-2.91 (m, 2H, CH₂NH), 2.43 (t, 2H, CH₂, $J=7.5$ Hz), 2.07-1.22 (m, 11H, 5x CH₂, CH), 1.36 (s, 9H, Boc), 0.89-0.82 (m, 6H, (CH₃)₂ Leu).

LRMS: $[\text{M}+\text{Na}]^+$ $_{\text{calcd}}=749.3$, $[\text{M}+\text{Na}]^+$ $_{\text{found}}=749.3$.

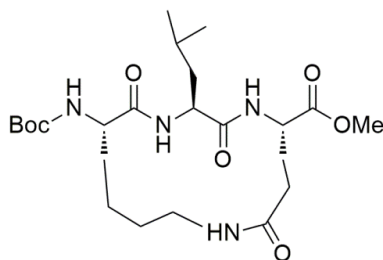
Compound S16



Compound **S15** (464 mg, 0.64 mmol) was dissolved in dry methanol (10 mL, over molecular sieves) and stirred at rt under an N₂ atmosphere for 10 min. Pd/C (15% w/w, 70 mg) was added. A hydrogen balloon was fitted under vacuum and the solution stirred at rt for a further 24 h. The solution was filtered through celite and washed with methanol (3x20 mL) and the solvent removed *in vacuo* to yield a white solid (232 mg, 72%).

^1H NMR (600 MHz, DMSO- d_6): δ 8.89 (d, 1H, NH, $J=6.5$ Hz), 8.02 (d, 1H, NH, $J=8.5$ Hz), 6.78 (d, 1H, NH, $J=8.0$ Hz), 4.33 (dd, 1H, C α H, $J=14.4, 9.0$ Hz), 4.23 (t, 1H, C α H, $J=9.8$ Hz), 3.95 (m, 1H, C α H), 3.58 (s, 3H, OCH₃), 2.03-1.26 (m, 15H, 7x CH₂, CH), 1.36 (s, 9H, Boc), 0.87-0.81 (m, 6H, 2xCH₃ Leu).

LRMS: $[\text{M}+\text{Na}]^+$ $_{\text{calcd}}=525.3$, $[\text{M}+\text{Na}]^+$ $_{\text{found}}=525.3$.

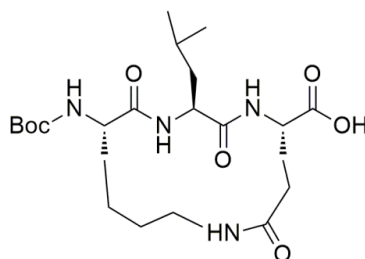
Compound **S17**

Compound **S16** (127 mg, 0.25 mmol) was suspended in anhydrous DMF (26 mL) and anhydrous THF (20 mL) and sonicated. EDC·HCl (238 mg, 1.25 mmol), HOAt (170 mg, 1.25 mmol) and DIPEA (435 μ L) were dissolved in a mixture of anhydrous DMF (15 mL) and anhydrous THF (8 mL) and the solution stirred at rt under an N_2 atmosphere. The **S16**/DMF/THF mixture was placed into a syringe pump and added to the coupling reagents at the rate of 30 μ L/min, and stirred for 48 h. The crude product was purified using reverse phase HPLC to yield a white solid (39 mg, 31%).

1H NMR (600 MHz, DMSO- d_6): δ 8.25 (d, 1H, NH, $J=7.4$ Hz), 8.06 (d, 1H, NH, $J=8.2$ Hz), 7.42 (m, 1H, NH), 6.43 (d, 1H, NH, $J=7.3$ Hz), 4.43 (m, 1H, C α H), 4.34 (m, 1H, C α H), 4.05 (m, 1H, C α H), 3.60 (s, 3H, OCH $_3$), 3.32 (m, 1H, CHHNH), 2.71 (m, 1H, CHHNH), 2.28-1.04 (m, 13H, 6x CH $_2$, CH), 1.36 (s, 9H, Boc), 0.90-0.84 (m, 6H, 2xCH $_3$ Leu).

^{13}C NMR (150 MHz, DMSO- d_6): δ 172.4, 172.1, 171.4, 170.7, 158.0, 154.5, 77.8, 53.2, 51.7, 50.8, 50.4, 48.5, 41.0, 36.9, 31.4, 28.4, 28.1, 27.9, 25.5, 24.6, 23.9, 23.8, 21.7.

LRMS: $[M+Na]^+$ $_{calcd}=507.2$, $[M+Na]^+$ $_{found}=507.2$.

Compound **S18**

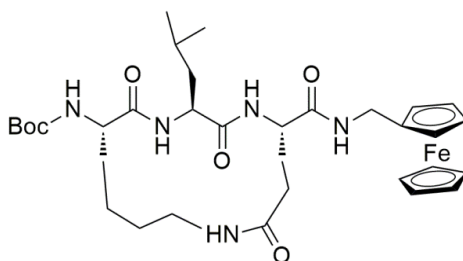
Compound **S17** (125 mg, 0.26 mmol) was dissolved in THF (2.6 mL) and methanol (750 μ L). NaOH (15 mg, 0.39 mmol) was dissolved in H $_2$ O (250 μ L) and added to the acid, and the

reaction stirred at rt for 17 h. The solvent was removed *in vacuo* and the residue redissolved in EtOAc (25 mL) and H₂O (25 mL). The pH was adjusted to pH 2 and the organic layer separated and washed with brine (25 mL) and dried over MgSO₄. The solvent was removed *in vacuo* to reveal a white solid (95 mg, 78%).

¹H NMR (500 MHz, DMSO-d₆): δ 8.15-8.01 (m, 2H, 2x NH), 7.37 (br s, 1H, NH), 6.43 (d, 1H, NH, *J*=7.1 Hz), 4.37-4.29 (m, 2H, 2x CαH), 4.06 (dd, 1H, CαH, *J*=14.1, 7.1 Hz), 3.30 (m, 1H, CHHNH), 2.73 (m, 1H, CHHNH), 2.28-1.06 (m, 13H, 6x CH₂, CH), 1.36 (s, 9H, Boc), 0.89-0.83 (m, 6H, 2xCH₃ Leu).

LRMS: [M+Na]⁺_{calcd}=493.2, [M+Na]⁺_{found}=493.2.

Peptide 7



Compound **S18** (95 mg, 0.20 mmol) and ferrocenylmethylamine (48 mg, 0.22 mmol) were dissolved in anhydrous DMF (4 mL) and stirred at rt under an N₂ atmosphere. HATU (84 mg, 0.22 mmol), HOBt (27 mg, 0.20 mmol) and DIPEA (140 μL) were added, and the mixture stirred for 48 h. The solvent was removed *in vacuo* and the residue taken up in EtOAc (25 mL) and H₂O (25 mL). The pH was adjusted to pH 3 and the organic layer separated and washed with NaHCO₃ (25 mL), brine (25 mL) and dried over Na₂SO₄. The solvent was removed *in vacuo* to yield a brown solid (98 mg, 73%).

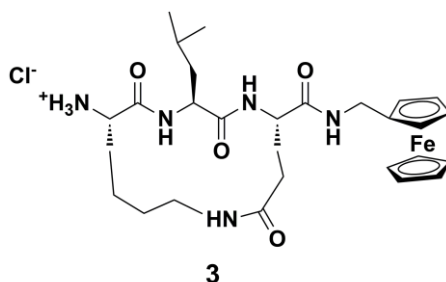
¹H NMR (600 MHz, DMSO-d₆): δ 8.24-8.19 (m, 2H, 2x NH), 7.63 (t, 1H, NH, *J*=5.8 Hz), 7.49 (br s, 1H, NH), 6.37 (d, 1H, NH, *J*=7.4 Hz), 4.32 (m, 1H, CαH), 4.20 (m, 1H, CαH), 4.18-4.05 (m, 9H, Cp), 4.09 (m, 1H, CαH), 3.98 (d, 2H, CH₂Fc, *J*=5.7 Hz), 3.32 (m, 1H, CHHNH), 2.75 (m, 1H, CHHNH), 2.28-1.01 (m, 13H, 6xCH₂, CH), 1.36 (s, 9H, Boc), 0.89-0.83 (m, 6H, 2xCH₃ Leu).

Chapter 5

^{13}C NMR (150 MHz, DMSO- d_6): δ 172.8, 172.3, 172.0, 170.9, 155.0, 86.3, 78.3, 73.4, 70.7, 69.8, 69.3, 69.2, 68.8, 68.7, 67.98, 67.93, 67.6, 67.5, 60.1, 53.5, 52.4, 52.2, 46.3, 40.9, 38.0, 31.5, 30.7, 28.5, 26.3, 24.4, 23.3, 22.2.

LRMS: $[\text{M}+\text{Na}]^+$ $_{\text{calcd}}=690.3$, $[\text{M}+\text{Na}]^+$ $_{\text{found}}=690.3$.

Peptide 3



Peptide **7** (86 mg, 0.13 mmol) was dissolved in TFE (2 mL) and 4M HCl in dioxane (1 mL) added dropwise. The reaction was stirred at rt for 25 min. The solvent was removed *in vacuo* to reveal a brown solid. The crude product was purified using reverse phase HPLC to yield a sandy brown solid (15 mg, 21%).

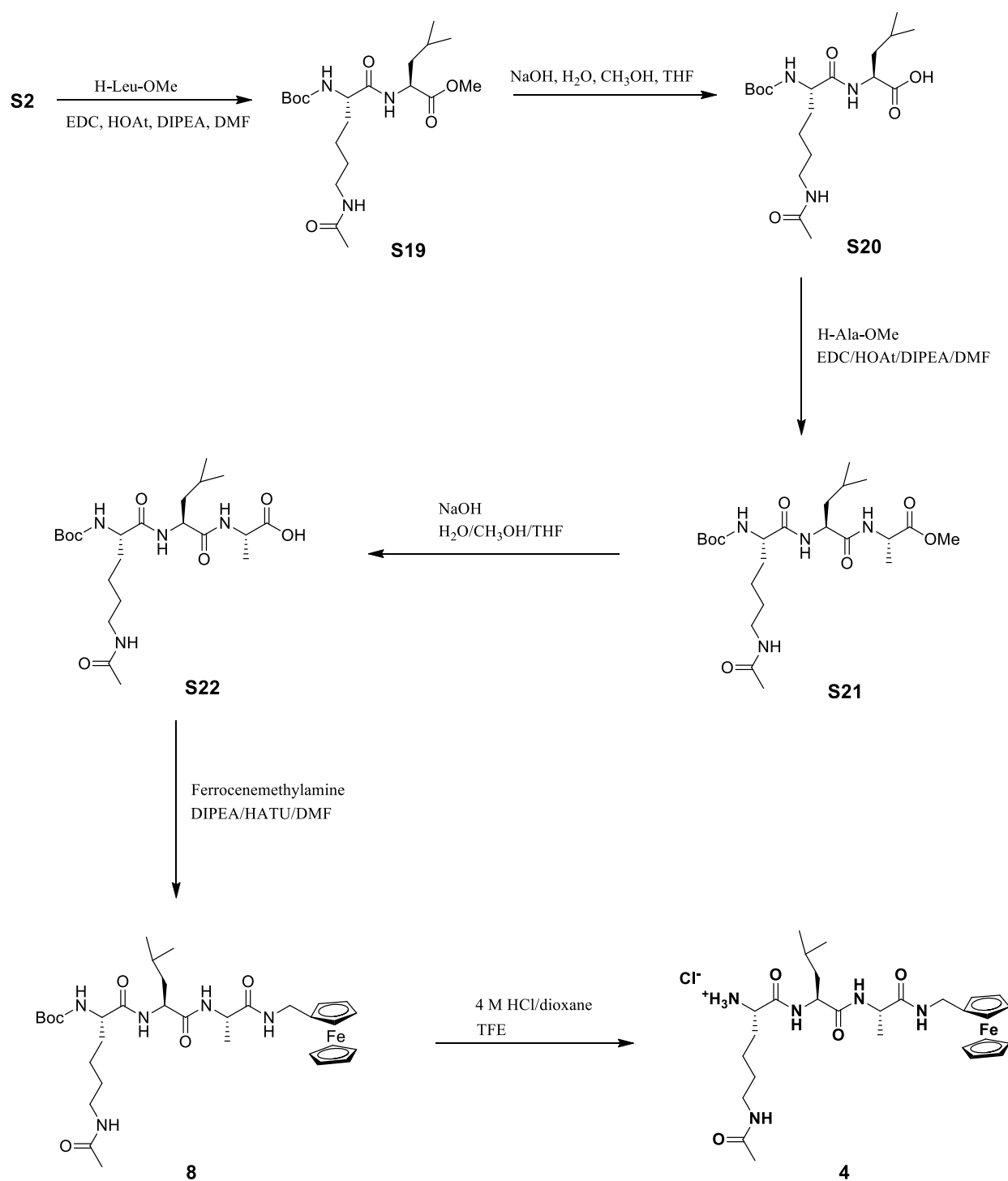
^1H NMR (600 MHz, DMSO- d_6): δ 8.54 (d, 1H, NH, $J=7.9$ Hz), 8.36 (d, 1H, NH, $J=7.6$ Hz), 8.07 (br s, 3H, NH), 7.79 (br s, 1H, NH), 7.55 (m, 1H, NH), 4.41 – 4.34 (m, 2H, 2x $\text{C}\alpha\text{H}$), 4.19-3.93 (m, 9H, Cp), 4.07 (br s, 2H, CH_2Fc), 3.88 (br s, 1H, $\text{C}\alpha\text{H}$), 3.28 (m, 1H, CHHNH), 2.79 (m, 1H, CHHNH), 2.32-1.05 (m, 13H, 6x CH_2 , CH), 0.90-0.87 (m, 6H, $(\text{CH}_3)_2$ Leu.).

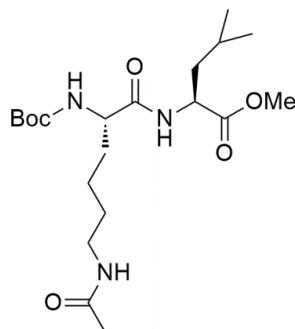
^{13}C NMR (150 MHz, DMSO- d_6): δ 171.63, 171.29, 170.68, 168.36, 157.88, 70.92, 69.38, 68.92, 68.37, 67.33, 67.14, 51.81, 51.77, 51.58, 45.45, 41.49, 40.04, 37.45, 36.69, 30.19, 28.76, 25.20, 24.26, 23.98, 22.99, 22.63, 21.86, 19.50.

HRMS: (m/z): $[\text{M}+\text{H}]^+$ $_{\text{calcd}}=568.2586$, $_{\text{found}}=568.2582$.

Chapter 5

Scheme S5. The final synthetic steps for linear β -strand peptides.

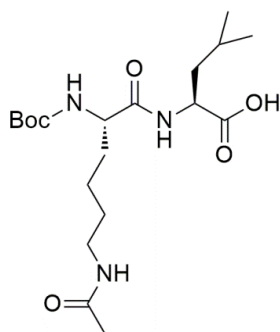


Compound **S19**

Compound **S2** (367 mg, 1.3 mmol) was dissolved in anhydrous DCM (10 mL). H-Leu-OMe (275 mg, 1.5 mmol) was added and stirred at rt under an N₂ atmosphere. Anhydrous DIPEA (883 μ L) was added, followed by EDC·HCl (267 mg, 1.4 mmol) and HOAt (173 mg, 1.3 mmol) and the reaction mixture stirred for 24 h. DCM (20 mL) and H₂O (30 mL) were added and the pH adjusted to pH 2-3. The organic layer was collected, washed with brine (30 mL) and dried over MgSO₄. The solvent was removed *in vacuo* to yield a pale golden oil (373 mg, 71%).

¹H NMR (300 MHz, d-DMSO) δ 8.12 (d, 1H, NH, $J=7.6$ Hz), δ 7.79 (br s, 1H, NH), δ 6.80 (d, 1H, NH, $J=8.2$ Hz), δ 4.29 (m, 1H, CaH), δ 3.89 (m, 1H, CaH), δ 3.60 (s, 3H, OCH₃), δ 3.02 – 2.85 (m, 2H, CH₂NH), δ 1.78 (s, 3H, CH₃), δ 1.66 – 1.23 (m, 9H, 4xCH₂, CH), δ 1.37 (s, 9H, Boc), δ 0.90 – 0.81 (m, 6H, (CH₃)₂Leu).

LRMS: [M+Na]⁺_{calcd}=438.2, [M+Na]⁺_{found}=438.2.

Compound **S20**

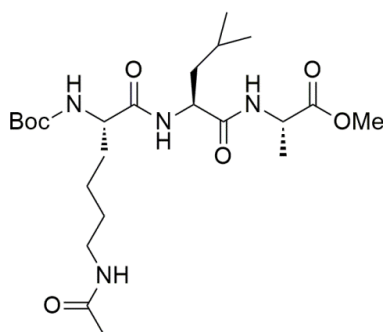
Chapter 5

Compound **S19** (357 mg, 0.9 mmol) was dissolved in THF (2.5 mL) and methanol (714 μ L) and the mixture stirred at rt. NaOH (52 mg, 1.3 mmol) was dissolved in H₂O (714 μ L) and this solution was added to the acid and stirred at rt for 31 h. The THF was removed *in vacuo* and the residue dissolved in EtOAc (25 mL) and H₂O (25 mL). The pH was adjusted to pH 2-3 and the organic layer collected and washed with brine (25 mL) and dried over MgSO₄. The solvent was removed *in vacuo* to reveal a clear solid (294 mg, 85%).

¹H NMR (300 MHz, DMSO-d₆): δ 7.94 (d, 1H, NH, $J=7.8$ Hz), 7.77 (t, 1H, NH, $J=9.0$ Hz), 6.79 (d, 1H, NH, $J=8.3$ Hz), 4.22 (dd, 1H, C α H, $J=13.9, 8.3$ Hz), 3.88 (m, 1H, C α H), 3.00-2.85 (m, 2H, CH₂NH), 1.77 (s, 3H, CH₃), 1.70-1.23 (m, 9H, 4xCH₂, CH), 1.36 (s, 9H, Boc), 0.89-0.81 (m, 6H, 2xCH₃Leu).

LRMS: [M+Na]⁺_{calcd}=400.2, [M+Na]⁺_{found}=400.2.

Compound **S21**



Compound **S20** (275 mg, 0.69 mmol) and HCl·H₂N-Ala-OMe (105 mg, 0.76 mmol) were dissolved in anhydrous DMF (11.5 mL) and stirred at rt under an N₂ atmosphere. Anhydrous DIPEA (477 μ L), HATU (287 mg, 0.76 mmol) and HOAt (93 mg, 0.69 mmol) were added and the reaction stirred for 25 h. The solvent was removed *in vacuo* and the residue dissolved in EtOAc (50 mL) and H₂O (50 mL). The pH was adjusted to pH 3 and the organic layer washed with NaHCO₃ (50 mL) and brine (50 mL) and dried over MgSO₄. The solvent was removed *in vacuo* to yield a pale golden oil (265 mg, 79%).

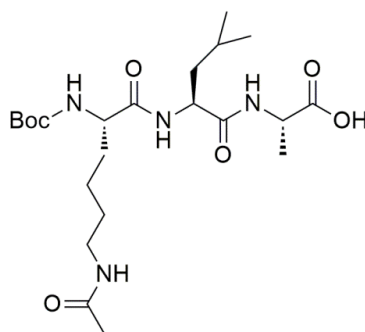
¹H NMR (300 MHz, DMSO-d₆): δ 8.36 (d, 1H, NH, $J=6.8$ Hz), 7.77 (t, 1H, NH, $J=9.0$ Hz), 7.72 (d, 1H, NH, $J=8.2$ Hz), 6.87 (d, 1H, NH, $J=8.1$ Hz), 4.35 (m, 1H, C α H), 4.23 (m, 1H,

Chapter 5

$\text{C}\alpha\text{H}$), 3.87 (m, 1H, $\text{C}\alpha\text{H}$), 3.60 (s, 3H, OCH_3), 3.03-2.90 (m, 2H, CH_2NH), 1.77 (s, 3H, CH_3), 1.70-1.34 (m, 9H, $4\times\text{CH}_2$, CH), 1.37 (s, 9H, Boc), 1.27 (d, 3H, CH_3 , Ala, $J=7.3$ Hz), 0.89-0.81 (m, 6H, $2\times\text{CH}_3\text{Leu}$).

LRMS: $[\text{M}+\text{Na}]^+_{\text{calcd}}=509.3$, $[\text{M}+\text{Na}]^+_{\text{found}}=509.3$.

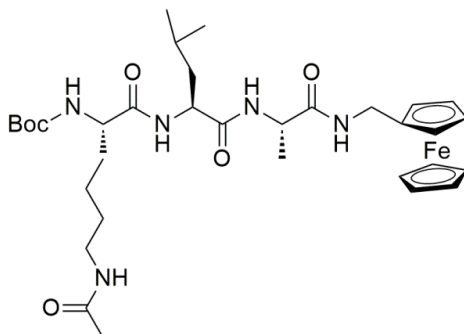
Compound S22



Compound **S21** (246 mg, 0.5 mmol) was dissolved in THF (1.7 mL) and methanol (492 μL), and the mixture stirred. NaOH (30 mg, 0.75 mmol) was dissolved in H_2O (492 μL) and this solution was added to the acid and stirred at rt for 27 h. The THF was removed *in vacuo* and the residue dissolved in EtOAc (35 mL) and H_2O (35 mL). The pH was adjusted to pH 2 and the organic layer collected and washed with brine (35 mL) and dried over MgSO_4 . The solvent was removed *in vacuo* to reveal a clear oil (189 mg, 79%).

^1H NMR (300 MHz, DMSO-d_6): δ 8.19 (d, 1H, NH , $J=7.0$ Hz), 7.78 (t, 1H, NH , $J=9.9$ Hz), 7.72 (d, 1H, NH , $J=8.3$ Hz), 6.88 (d, 1H, NH , $J=8.1$ Hz), 4.35 (m, 1H, $\text{C}\alpha\text{H}$), 4.16 (m, 1H, $\text{C}\alpha\text{H}$), 3.86 (m, 1H, $\text{C}\alpha\text{H}$), 3.03-2.83 (m, 2H, CH_2NH), 1.77 (s, 3H, CH_3), 1.70-1.34 (m, 9H, $4\times\text{CH}_2$, CH), 1.37 (s, 9H, Boc), 1.25 (d, 3H, CH_3Ala , $J=7.3$ Hz), 0.89-0.82 (m, 6H, $2\times\text{CH}_3\text{Leu}$).

LRMS: $[\text{M}+\text{Na}]^+_{\text{calcd}}=495.2$, $[\text{M}+\text{Na}]^+_{\text{found}}=495.2$.

Peptide **8**

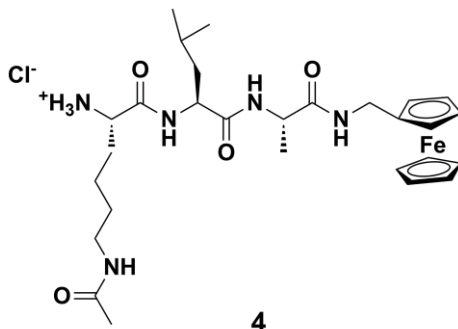
Compound **S22** (164 mg, 0.35 mmol) and ferrocenylmethylamine (82 mg, 0.38 mmol) were dissolved in anhydrous DMF (5.8 mL) and stirred at rt under an N₂ atmosphere. Anhydrous DIPEA (242 μL), HATU (145 mg, 0.38 mmol) and HOAt (47 mg, 0.35 mmol) were added and the reaction stirred for 66 h. The solvent was removed *in vacuo* and the residue dissolved in EtOAc (35 mL) and H₂O (35 mL). The pH was adjusted to pH 2 and the organic layer washed with NaHCO₃ (35 mL) and brine (35 mL) and dried over MgSO₄. The solvent was removed *in vacuo* to yield a brown solid (192 mg, 83%).

¹H NMR (300 MHz, DMSO-d₆): δ 8.05-7.95 (m, 2H, 2xNH), 7.86-7.76 (m, 2H, 2xNH), 6.93 (d, 1H, NH, *J*=7.5 Hz), 4.35-3.82 (m, 14H, CH₂Fc, Cp, 3xCαH), 3.02-2.92 (m, 2H, CH₂NH), 1.77 (s, 3H, CH₃), 1.70-1.34 (m, 9H, 4xCH₂, CH), 1.37 (s, 9H, Boc), 1.22 (d, 3H, CH₃ Ala, *J*= 8.1 Hz), 0.89-0.82 (m, 6H, (CH₃)₂ Leu).

¹³C NMR (150 MHz, DMSO-d₆): 172.1, 171.5, 171.4, 168.5, 155.3, 123.1, 122.6, 115.5, 86.0, 78.0, 77.3, 68.9, 68.35, 68.30, 67.5, 67.3, 54.4, 50.7, 48.0, 40.8, 38.6, 37.4, 31.5, 31.3, 30.6, 28.8, 28.2, 28.1, 23.9, 23.1, 22.6, 21.4.

LRMS: [M+Na]⁺_{calcd}=692.3, [M+Na]⁺_{found}=692.3.

Peptide 4



Peptide **8** (120 mg, 0.18 mmol) was dissolved in TFE (4 mL) and 4M HCl in dioxane (3 mL) added dropwise. The solution was stirred for 25 min, the solvent removed *in vacuo* and the residue washed with MeOH (2x10 mL). The crude product was purified using reverse phase HPLC to yield a sandy brown solid (25 mg, 25%).

^1H NMR (600 MHz, DMSO- d_6): δ 8.48 (d, 1H, NH, $J=8.1$ Hz), 8.16 (d, 1H, NH, $J=7.3$ Hz), 8.07 (m, 3H, NH), 8.01 (br s, 1H, NH), 7.77 (t, 1H, NH, $J=5.4$ Hz), 4.39 (dd, 1H, C α H, $J=14.1, 8.8$ Hz), 4.31 (m, 1H, C α H), δ 4.20-3.94 (m, 11H, Cp, CH $_2$ Fc), 3.76 (m, 1H, C α H), 2.99 (dd, 2H, CH $_2$ NH, $J=13.1, 6.8$ Hz), 1.78 (s, 3H, CH $_3$), 1.71-1.61 (m, 3H, CH $_2$, CH), 1.49-1.45 (m, 2H, CH $_2$), 1.39-1.35 (dd, 2H, CH $_2$, $J=14.3, 7.1$ Hz), 1.32-1.26 (dt, 2H, CH $_2$, $J=14.9, 7.2$ Hz), 1.22 (d, 3H, CH $_3$, $J=6.3$ Hz), 0.90-0.86 (m, 6H, (CH $_3$) $_2$ Leu).

^{13}C NMR (150 MHz, DMSO- d_6): δ 171.8, 171.5, 169.3, 168.8, 158.3, 71.3, 69.8, 69.3, 68.8, 67.8, 67.5, 52.4, 51.5, 48.5, 41.2, 38.6, 37.8, 31.3, 24.4, 23.5, 23.0, 21.9, 18.8.

HRMS: $[\text{M}+\text{H}]^+$ $_{\text{calcd}}=570.2737$; $_{\text{found}}=570.2743$.

5.7 References

1. Long, Y. T.; Abu-Rhayem, E.; Kraatz, H. B., Peptide electron transfer: More questions than answers. *Chemistry-A European Journal* **2005**, *11* (18), 5186.
2. (a) Maruccio, G.; Biasco, A.; Visconti, P.; Bramanti, A.; Pompa, P. P.; Calabi, F.; Cingolani, R.; Rinaldi, R.; Corni, S.; Di Felice, R.; Molinari, E.; Verbeet, M. R.; Canters, G. W., Towards protein field-effect transistors: Report and model of prototype. *Advanced Materials* **2005**, *17* (7), 816-+; (b) Yu, J.; Huang, D. M.; Shapter, J. G.; Abell, A. D., Electrochemical and Computational Studies on Intramolecular Dissociative Electron Transfer in beta-Peptides. *Journal of Physical Chemistry C* **2012**, *116* (50), 26608-26617.
3. Lowik, D. W. P. M.; Leunissen, E. H. P.; van den Heuvel, M.; Hansen, M. B.; van Hest, J. C. M., Stimulus responsive peptide based materials. *Chemical Society Reviews* **2010**, *39* (9), 3394-3412.
4. (a) Sek, S., Review peptides and proteins wired into the electrical circuits: An SPM-based approach. *Biopolymers* **2013**, *100* (1), 71-81; (b) Yasutomi, S.; Morita, T.; Imanishi, Y.; Kimura, S., A molecular photodiode system that can switch photocurrent direction. *Science* **2004**, *304* (5679), 1944-1947; (c) Korpany, K. V.; Langat, P.; Kim, D. M.; Edelman, N.; Cooper, D. R.; Nadeau, J.; Blum, A. S., Conductance Switching in the Photoswitchable Protein Dronpa. *Journal of the American Chemical Society* **2012**, *134* (39), 16119-16122.
5. Mandal, D.; Shirazi, A. N.; Parang, K., Self-assembly of peptides to nanostructures. *Organic & Biomolecular Chemistry* **2014**, *12* (22), 3544-3561.
6. Maruccio, G., Molecular electronics: Protein transistors strike gold. *Nature Nanotechnology* **2012**, *7* (3), 147-8.
7. Sakamoto, R.; Katagiri, S.; Maeda, H.; Nishimori, Y.; Miyashita, S.; Nishihara, H., Electron Transport Dynamics in Redox-Molecule-Terminated Branched Oligomer Wires on Au(111). *Journal of the American Chemical Society* **2014**.
8. (a) Malak, R. A.; Gao, Z. N.; Wishart, J. F.; Isied, S. S., Long-range electron transfer across peptide bridges: The transition from electron superexchange to hopping. *Journal of the American Chemical Society* **2004**, *126* (43), 13888; (b) Mandal, H. S.; Kraatz, H.-B., Electron Transfer Mechanism in Helical Peptides. *The Journal of Physical Chemistry Letters* **2012**, *3* (6), 709-713; (c) Yu, J.; Zvarec, O.; Huang, D. M.; Bissett, M. A.; Scanlon, D. B.; Shapter, J. G.; Abell, A. D., Electron Transfer through α -Peptides Attached to Vertically Aligned Carbon Nanotube Arrays: A Mechanistic Transition. *Chemical Communications* **2012**, *48* (8), 1132-1134.
9. Wenger, O. S., How Donor-Bridge-Acceptor Energetics Influence Electron Tunneling Dynamics and Their Distance Dependences. *Accounts of Chemical Research* **2011**, *44* (1), 25.
10. Watanabe, J.; Morita, T.; Kimura, S., Effects of dipole moment, linkers, and chromophores at side chains on long-range electron transfer through helical peptides. *Journal of Physical Chemistry B* **2005**, *109* (30), 14416.
11. Cordes, M.; Giese, B., Electron transfer in peptides and proteins. *Chemical Society Reviews* **2009**, *38* (4), 892-901.
12. Lauz, M.; Eckhardt, S.; Fromm, K. M.; Giese, B., The influence of dipole moments on the mechanism of electron transfer through helical peptides. *Phys. Chem. Chem. Phys.* **2012**, *14* (40), 13785-13788.
13. Gatto, E.; Venanzi, M., Chapter 4. Peptonics: Peptide Materials for Electron Transfer. In *Peptide Materials: From Nanostructures to Applications*, Alemán, C.; Bianco, A.; Venanzi, M., Eds. John Wiley & Sons, Ltd.: 2013.

14. Schlag, E. W.; Lin, S. H.; Weinkauf, R.; Rentzepis, P. M., Dynamical principles in biological processes. *Proceedings of the National Academy of Sciences of the United States of America* **1998**, *95* (4), 1358-1362.
15. Schlag, E. W.; Sheu, S. Y.; Yang, D. Y.; Selzle, H. L.; Lin, S. H., Distal charge transport in peptides. *Angewandte Chemie-International Edition* **2007**, *46* (18), 3196-3210.
16. Horsley, J. R.; Yu, J.; Moore, K. E.; Shapter, J. G.; Abell, A. D., Unraveling the Interplay of Backbone Rigidity and Electron Rich Side-Chains on Electron Transfer in Peptides: The Realization of Tunable Molecular Wires. *Journal of the American Chemical Society* **2014**, *136*, 12479-12488.
17. (a) Yu, J.; Horsley, J. R.; Moore, K. E.; Shapter, J. G.; Abell, A. D., The Effect of a Macrocyclic Constraint on Electron Transfer in Helical Peptides: A Step Towards Tunable Molecular Wires *Chemical Communications* **2014**, *50* (14), 1652; (b) Horsley, J. R. Y., J. Abell, A.D., The Correlation of Electrochemical Measurements and Molecular Junction Conductance Simulations in β -Strand Peptides. *Chemistry A European Journal* **2015**, Accepted 26 January 2015.
18. (a) Xiao, X. Y.; Xu, B. Q.; Tao, N. J., Conductance titration of single-peptide molecules. *Journal of the American Chemical Society* **2004**, *126* (17), 5370-5371; (b) Yew, S. Y.; Shekhawat, G.; Wangoo, N.; Mhaisalkar, S.; Suri, C. R.; Dravid, V. P.; Lam, Y. M., Design of single peptides for self-assembled conduction channels. *Nanotechnology* **2011**, *22* (21).
19. Gooding, J. J.; Wibowo, R.; Liu, J. Q.; Yang, W. R.; Losic, D.; Orbons, S.; Mearns, F. J.; Shapter, J. G.; Hibbert, D. B., Protein electrochemistry using aligned carbon nanotube arrays. *Journal of the American Chemical Society* **2003**, *125* (30), 9006-9007.
20. Wüthrich, K., *NMR of proteins and nucleic acids*. Wiley: 1986.
21. Biron, Z.; Khare, S.; Samson, A. O.; Hayek, Y.; Naider, F.; Anglister, J., A monomeric 3(10)-helix is formed in water by a 13-residue peptide representing the neutralizing determinant of HIV-1 on gp41. *Biochemistry* **2002**, *41* (42), 12687-12696.
22. Pehere, A. D.; Abell, A. D., New beta-Strand Templates Constrained by Huisgen Cycloaddition. *Organic Letters* **2012**, *14* (5), 1330-1333.
23. Fernando, S. R. L.; Kozlov, G. V.; Ogawa, M. Y., Distance dependence of electron transfer along artificial beta-strands at 298 and 77 K. *Inorganic Chemistry* **1998**, *37* (8), 1900-1905.
24. Lakhani, A.; Roy, A.; De Poli, M.; Nakaema, M.; Formaggio, F.; Toniolo, C.; Keiderling, T. A., Experimental and Theoretical Spectroscopic Study of 3(10)-Helical Peptides Using Isotopic Labeling to Evaluate Vibrational Coupling. *Journal of Physical Chemistry B* **2011**, *115* (19), 6252-6264.
25. (a) Pehere, A. D.; Sumbly, C. J.; Abell, A. D., New cylindrical peptide assemblies defined by extended parallel [small beta]-sheets. *Organic & Biomolecular Chemistry* **2013**, *11* (3), 425-429; (b) Zhuang, W.; Hayashi, T.; Mukamel, S., Coherent Multidimensional Vibrational Spectroscopy of Biomolecules: Concepts, Simulations, and Challenges. *Angewandte Chemie-International Edition* **2009**, *48* (21), 3750-3781.
26. Burton, N. A.; Harrison, M. J.; Hart, J. C.; Hillier, I. H.; Sheppard, D. W., Prediction of the mechanisms of enzyme-catalysed reactions using hybrid quantum mechanical molecular mechanical methods. *Faraday Discussions* **1998**, *110*, 463-475.
27. Gillespie, P.; Cicariello, J.; Olson, G. L., *Peptide Science* **1997**, *43*, 191.
28. Laviron, E., The use of linear potential sweep voltammetry and of a.c. voltammetry for the study of the surface electrochemical reaction of strongly adsorbed systems and of redox modified electrodes. *Journal of Electroanalytical Chemistry* **1979**, *100*, 263.

29. Arikuma, Y.; Nakayama, H.; Morita, T.; Kimura, S., Electron Hopping over 100 angstrom Along an alpha Helix. *Angewandte Chemie-International Edition* **2010**, *49* (10), 1800.
30. Sasaki, H.; Makino, M.; Sisido, M.; Smith, T. A.; Ghiggino, K. P., Photoinduced electron transfer on beta-sheet cyclic peptides. *Journal of Physical Chemistry B* **2001**, *105* (42), 10416-10423.
31. Marcus, R. A., Chemical and Electrochemical Electron-Transfer Theory. *Annual Review of Physical Chemistry* **1964**, *15*, 155-196.
32. Van Voorhis, T.; Kowalczyk, T.; Kaduk, B.; Wang, L. P.; Cheng, C. L.; Wu, Q., The Diabatic Picture of Electron Transfer, Reaction Barriers, and Molecular Dynamics. *Annual Review of Physical Chemistry, Vol 61* **2010**, *61*, 149-170.
33. (a) Marcus, R. A.; Sutin, N., Electron Transfers In Chemistry And Biology. *Biochimica Et Biophysica Acta* **1985**, *811* (3), 265-322; (b) Wu, Q.; Van Voorhis, T., Direct calculation of electron transfer parameters through constrained density functional theory. *Journal of Physical Chemistry A* **2006**, *110* (29), 9212-9218.
34. Petrov, E. G.; Shevchenko, Y. V.; May, V., On the length dependence of bridge-mediated electron transfer reactions. *Chemical Physics* **2003**, *288* (2-3), 269-279.
35. (a) Beer, P. D.; Smith, D. K., Tunable bis(ferrocenyl) receptors for the solution-phase electrochemical sensing of transition-metal cations. *Journal of the Chemical Society-Dalton Transactions* **1998**, (3), 417; (b) Ossola, F.; Tomasin, P.; Benetollo, F.; Foresti, E.; Vigato, P. A., Synthesis, structure and properties of new ferrocene-containing compounds. *Inorganica Chimica Acta* **2003**, *353*, 292-300.